SCIENCE • TECHNOLOGY • RESEARCH HIGHLIGHTS • VISIONS

Dissertation
85

Sulfur based abatement of PCDD/F and alkali chlorides production during fluidized bed combustion of solid recovered fuel

Cyril Jose E. Bajamundi

VTT

VTT SCIENCE 85

Sulfur based abatement of PCDD/F and alkali chlorides production during fluidized bed combustion of solid recovered fuel

Cyril Jose E. Bajamundi

Thesis for the degree of Doctor of Philosophy to be presented with due permission for public examination and criticism in KEM1, at University of Jyväskylä, on the 13.May,2015 at 12:00.

ISBN 978-951-38-8244-0 (Soft back ed.)
ISBN 978-951-38-8245-7 (URL: http://www.vtt.fi/publications/index.jsp)

VTT Science 85

ISSN-L 2242-119X
ISSN 2242-119X (Print)
ISSN 2242-1203 (Online)

JULKAISIJA – UTGIVARE – PUBLISHER

Teknologian tutkimuskeskus VTT Oy
PL 1000 (Tekniikantie 4 A, Espoo)
02044 VTT
Puh. 020 722 111, faksi 020 722 7001

Teknologiska forskningscentralen VTT Ab
PB 1000 (Teknikvägen 4 A, Esbo)
FI-02044 VTT
Tfn +358 20 722 111, telefax +358 20 722 7001

VTT Technical Research Centre of Finland Ltd
P.O. Box 1000 (Tekniikantie 4 A, Espoo)
FI-02044 VTT, Finland
Tel. +358 20 722 111, fax +358 20 722 7001

Cover image: Artist's view of the interactions of key ash and aerosol forming and trace elements during waste firing in a BFB boiler. By David Gonzales and Cyril Bajamundi.

Grano Oy, Kuopio 2015

Preface

As the world population grows, waste production grows as well. Over the years energy recovery from waste is considered to be one of the suitable options to meet this increase in demand for proper waste management. This work is focused on addressing two among several challenges that are associated with combustion of fuel mixture with high or advanced energy-share SRF, namely PCDD/F formation and Cl-induced corrosion. Through a combination of an experimental campaign, thermodynamic equilibrium modeling, and physical and chemical characterization, this thesis seeks to present robust solutions that are practicable and can readily be applied in bubbling fluidized bed combustion systems.

My journey to Finland started when I saw an online advertisement in the corner of an email which stated “PhD position – ash and aerosol forming elements in waste and biomass, Jyväskylä, Finland.” I told myself “Wow! Finland! Snow!” Right then and there I applied and by 17th May, 2011 I had received a letter confirming my selection. I arrived in Finland on the 1st September, 2011 without any idea about PCDD/F formation, waste combustion, and chlorine induced corrosion; but I did come with a sponge-like mind ready to absorb whatever experiences and technical knowledge might come my way.

A great share of new knowledge and experiences came from the time, effort, guidance and resources graciously shared by a triumvirate of Finnish experts – Dr. Pasi Vainikka at VTT, Prof. Jukka Konttinen at JyU, and M.Sc. Merja Hedman at Valmet Power Oy. I am truly grateful to them, and in return, they can rest assured that my pursuit for scientific and technical knowledge will not end with the publication of this dissertation.

Several more people offered their help and much needed support. Irina Hyytiäinen, Janni Silvennoinen, Teemu Heinanen, Kirsi Korpijärvi, Manu Lahtinen, Wantana Klysubun and Heino Kuuluvainen were instrumental in building the articles included in this work. Marko Räsänen, Juho Kauppinen, Teemu Soini, Matti Ranta-Korpi, Hannu Salo and Nasrullah Muhammad aided in data and sample collection. The staff of BL8 at SLRI in Thailand, and Prof. Nurak Grisdanurak, Dr. Pummarin Khamdahsag, Dr. Pongtanawat Khemthong, Prof. James Penner-Hahn and Dr. Bruce Ravel helped in my adventure with XANES. Janne Paaso, Maunu Toivainen, Pekka Teppola, Prof. Tommi Kärkäinen took time to answer my queries on PLS regression.

At VTT, Martti Mäkipää, Janne Kärki, Jouni Hämälainen, Jani Lehto, Päivi Sarja, Tuula Rastela, Seija Laukkanen, Marita Hokkanen, Sanna Idström, and Tuija Meriläinen all ensured that all the practicalities whether small or big were taken care of. I thank also Martti Aho, Kaisu Loikkanen and of course Raili and Pekka Taipale for all the help and the much enjoyed warm company and conversations.

Major funding and support allowed me to stay in Finland and carry out this work – the OSER project, Valmet Power, Foster Wheeler, the European Regional Development Fund, and RECOMBIO project TREN/FP7EN/239530. Stora Enso Oyj at Anjalankoski shared many data for my work. Rest assured your investment in this foreigner will bring a return one way or another.

To my Filipino friends spread all over the world for keeping in touch, and sometimes providing technical assistance. I am grateful too to the Filipino community of Jyväskylä for welcoming me to your homes, for letting me join much enjoyed get-togethers and for letting me play with your little babies.

Maria Chiarria, Morena and Rodolfo – you have been my constant source of encouragement and strength. Your support is unwavering and your presence is resolute against miles of physical separation. I am evermore grateful.

And to the source of all of these… to You I return always.

Cyril Jose E. Bajamundi
13:07 27.8.2014
Jyäskylä, Finland

*"Nothing in the world can take the place of persistence. Talent will not; nothing is more common than unsuccessful men with talent. Genius will not; unrewarded genius is almost a proverb. Education will not; the world is full of educated derelicts. Persistence and determination alone are omnipotent. The slogan **Press On!** has solved and always will solve the problems of the human race."*
— Calvin Coolidge

Academic dissertation

Supervisor	Prof. Jukka Konttinen Department of Chemistry, Renewable Natural Resources and Chemistry of Living Environment, POB 35, FI-40014, University of Jyväskylä, Finland
	Dr. Pasi Vainikka VTT Technical Research Centre of Finland Ltd Tuotantokatu 2, Lappeenranta P.O.Box 17021, FI-53851 Lappeenranta, Finland
Reviewers	Dr. Sonja Enestam Valmet Technologies Oy P.O. Box 109, Lentokentänkatu 11 FI-33101 Tampere, Finland
	Dr. Maria Zevenhoven Åbo Akademi Process Chemistry Centre c/o Combustion and Materials Chemistry Biskopsgatan 8, FI-20500 Åbo, Finland
Opponent	Prof. Lars-Erik Åmand Department of Energy and Environment Chalmers University of Technology Gothenburg, Sweden

List of publications

This thesis is based on the following original publications which are referred to in the text as Papers I–V. The publications are reproduced with kind permission from the publishers.

I Bajamundi, C.J.E., Vainikka, P, Hedman, M., Hyytiäinen, I., Silvennoinen, J., Heinanen, T., Taipale, R., & Konttinen, J. 2014. Towards controlling PCDD/F production in a multi-fuel fired BFB boiler using two sulfur addition strategies. Part I: Experimental campaign and results. Fuel 134, pp. 677–687.

II Bajamundi, C.J.E., Vainikka, P., Hedman, M., & Konttinen, J. 2014. Towards controlling PCDD/F production in a multi-fuel fired BFB boiler using two sulfur addition strategies. Part II: Thermodynamic analysis. Fuel 134, pp. 688–697.

III Bajamundi, C.J.E , Vainikka, P., Hyytiäinen, I., Korpijärvi, K, Lahtinen, M., Klysubun, W., & Konttinen, J. 2014. Towards controlling PCDD/F production in a multi-fuel fired BFB boiler using two sulfur addition strategies. Part III: Cu speciation in the fly ash. Fuel 132, pp. 178–186.

IV Bajamundi, C.J.E., Vainikka, P., Hedman, M., Silvennoinen, J., Heinanen, T., Taipale, R., & Konttinen, J. Searching for a robust anti-corrosion measure to combust high SRF-energy-share fuel. – Submitted to Fuel for publication.

V Kuuluvainen, H., Karjalainen, P., Bajamundi, C.J.E., Maunula, J., Vainikka, P., Roppo, J., Keskinen, J., & Rönkkö, T. 2014. Physical properties of aerosol particles measured from a bubbling fluidized bed boiler. Fuel 139, pp. 144–153.

Author's contributions

I. Bajamundi co-planned the experimental work, collected fly ash samples, prepared samples for analysis, analyzed the results collected during the campaign and wrote the manuscript.

II. Bajamundi developed the staged-equilibrium modeling platform, performed the simulations and wrote the manuscript.

III. Bajamundi planned the characterization experiments, performed majority of the characterization and data analyses except for the XRD which was done by Lahtinen, and wrote the manuscript except for the section of XRD results which was authored by Lahtinen.

IV. Bajamundi developed the systematic analysis of the data collected, performed all data analysis, performed thermodynamic calculations, and wrote the manuscript.

V. Bajamundi performed a critical analysis of chemical properties of the aerosol collected in the DLPI which were used to explain the changes in the physical properties measured by H. Kuuluvainen and P. Karjalainen, and wrote the chemical interpretation of results presented in Section 3.1 of the paper.

Contents

List of symbols and abbreviations

APR	Active/Passive Ratio, molar ratio of active and passive copper species
BAEF	Bottom ash entrainment factor, fraction of the condensed phase formed in the reducing zone and entrained to the oxidizing zones.
BAFAR	Bottom ash / fly ash ratio, mass ratio, mass ratio of bottom ash and fly ash calculated by the equilibrium model
BFB	Bubbling fluidized bed
C&IW	Commercial and industrial waste
c.v.	Coefficient of variance, is a standardized measure of dispersion of a probability distribution or frequency distribution. It is defined as the ratio of the standard deviation to the mea
DLPI	Dekati low pressure impactor
DMA	Differential particle analyzer
d_p	Particle diameter (majority mass based except for Fig 38. and 42)
ELPI	Electrical low pressure impactor
ESP	Electrostatic precipitator
FTIR	Fourier transform infrared spectroscopy
GCP	Good combustion practices
ICP-MS	Inductively coupled plasma - mass spectrometry
λ	Air-to-fuel ratio, mole of air supplied per mole of air required to fully combust C,H in the fuel
LCF	Linear combination fitting
LUVO	Air preheater
M	Alkalis (Sodium, Potassium)

Me	Metal
MLR	Multiple linear regression
$\mu(E)$	Normalized absorption
OLEn	Object linking and embedding
PBDD/F	Polybrominated dibenzo-p-dioxins/ dibenzofuran
PCDD/F	Polychlorinated dibenzo-p-dioxins/ dibenzofuran
PLS	Partial least squares regression
PXDD/F	Polychlorinated-brominated dibenzo-p-dioxins/ dibenzofuran
RDF	Refuse derived fuel
RMSECV	Root mean square error of cross-validation
SEM	Scanning electron microscope
SH	Superheater
SMPS	Scanning mobility particle sizer
SRF	Solid recovered fuel
SDD	Steady-state detection
TEQ	Toxicity equivalence quantity
WtE	Waste-to-energy
WID	Waste incineration directive
X	Matrix of predictors
XAS	X-ray absorption spectroscopy
XANES	X-ray absorption near edge structure
XPS	X-ray photoelectron spectroscopy
XRD	X-ray diffraction
XRF	X-ray fluorescence spectroscopy
Y	Matrix of response

1. Introduction

In 2008 the Finnish Government approved the National Waste Plan for 2016 with the main aim of stabilizing the amount of municipal waste production and ensuring that the trend will be downwards by the year 2016. The specific target is to arrive at a situation where around 50% of all municipal waste is recycled as material, 30% is energy recovered and not more than 20% sent to landfill [1]. By 2016, at least 70% of all construction and renovation waste will be used as material and energy source. The plan estimates the required incineration capacity (incineration and co-incineration plants) for energy recovery to be between 700 000 and 750 000 tonnes. This is to be accomplished by increasing and promoting the use of non-recyclable waste as fuel in co-incineration plants, provided that such capacity is available in a given region or area (Section 4.3 of [1]).

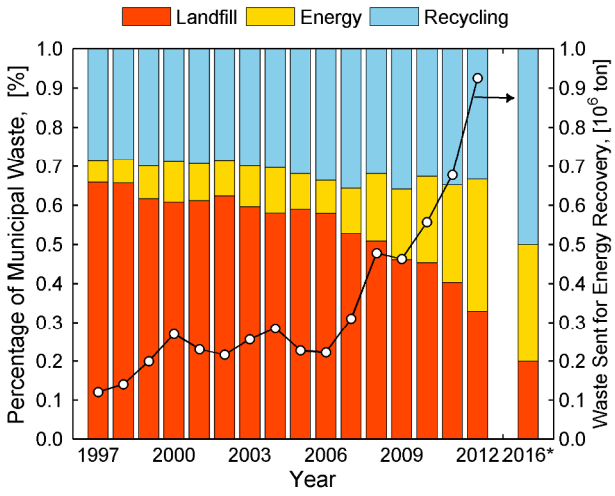

Figure 1. Fifteen year history of treatment of municipal solid waste in Finland and the 2016 target, data from [2].

The Finnish National Waste Plan for 2016 is in line with the 2008 European Union Directive on Waste Management which sets the order of priority on waste prevention and management as follows: prevention, preparing for re-use, recycling, other recovery, e.g. energy recovery, and disposal [3].

The effect of the plan is clearly reflected in the historical data on the treatment of municipal waste (see Figure 1). In 2012, 67% of the waste is energy-recovered or recycled, while 33% is still being sent to landfill. In the same year the amount of waste sent for energy recovery is 5.7 times that of 1997 and 1.9 times that of 2008 when the plan was approved.

1.1 Waste-to-energy technologies and technical challenges

In Western European countries, at least 35% and in some cases up to 80% of the residential waste is disposed of through incineration [4]. Northern European countries are highly reliant on mass-burn incineration coupled with energy generation [4]. Mass burning of heterogeneous waste which requires little or no pretreatment in a moving grate incinerator is the widely used and tested technology for treatment of waste coupled with energy recovery [5]. Over the past decade, there has been increasing interest and experience in the use of fluidized bed technologies to handle preprocessed waste. European experience in fluidized/bed incineration comes from several plants where refuse derived fuels, RDF, is incinerated with other fuels[6]. Meanwhile, Rogoff and Screve in their book published in 2011 reports that in the United States the use of fluidized beds to incinerate municipal solid waste is in the research and development stage [6]. The table below lists some of the major advantages and disadvantages of these two technologies.

Table 1. Comparison of two waste incineration technologies, adopted from [5].

Incinerator Technology	Advantages	Disadvantages
Moving Grate	• No need for prior sorting or shredding. • The technology is widely used and thoroughly tested for waste incineration and meets the demands for technical performance • It can accommodate large variations in waste composition and calorific value. • Allows for an overall thermal efficiency of up to 85 percent. • Each furnace can be built with a capacity of up to 1,200 t/day.	• Capital and maintenance costs are relatively high.

Fluidized Bed	• Relatively low capital and maintenance cost due to simple design concept. • Allows thermal efficiency of up to 90%. • Suitable for wide range of fuel and mixtures of fuel and can handle liquid or solid waste either in combination or separately.	• Not a common nor thoroughly tested technology for MSW incineration. • Relatively strict demands on size and composition of waste, which usually requires thorough pre-treatment.

The first challenge and perhaps the principal restrictive constraint on the performance of waste-to-energy systems is the issue of Cl-induced corrosion of heat exchange surfaces, especially the superheaters (SH). Corrosion is said to follow the active oxidation mechanism [7], where alkali chlorides in superheater deposits act as key agents of corrosion [8–11]. Alkali chlorides may come from the fuel or be produced during the combustion of the fuel [8,12–14]. The net reaction for the metal, Me (Fe, Cr, Ni) is described in (1) and with little consumption of chlorides [7,15].

$$4Me_{(s)} + 3O_{2(g)} \rightleftharpoons 2Me_2O_{3(s)} \quad (1)$$

A minute amount of chlorine in the deposit is enough to initiate corrosion at typical superheater temperatures ca. 480 ~ 500°C. For example, a mixture of alkali sulfate and chloride containing 0.3 wt.% Cl has been shown to corrode 10CrMo9-10 (at 450–600 °C) and T91 (at 575–600°C) steel grade [16].

Corrosion is further enhanced by the presence of a molten phase on the surface of the steel. The rate of corrosion is faster in this case because (a) liquid phase reactions are faster than solid – solid reactions and (b) the liquid phase provides an electrolyte or pathway of ionic charge transfer for the electrochemical attack [15].

Recently the presence of lead and zinc chlorides has been shown to increase the risk of corrosion at low metal temperature (230–450 °C) during combustion of recovered waste wood; this makes the economizers among other heat transfer areas susceptible to chlorine induced corrosion [17–19].

Another issue related to waste co-firing is emission of heavy metals and organic pollutants. The main source of heavy metals is the commercial and industrial waste (C&IW) used as raw materials for producing the fuel. Vainikka et al. have studied some of the key trace elements (Ba, Br, Co, Cr, Pb, Sb, Sn, Zn, and Fe) found in the fuel of an 80MW bubbling fluidized bed boiler (BFB) combusting solid recovered fuel (SRF) [20]. They concluded that these elements came mainly from additives, stabilizers, dyes, colorants and flame retardants used in the production of paper and plastics – which are the main components of the SRF [21]. After

combustion these elements can end up in the bottom ash, fly ash and flue gas depending on their speciation and degree of volatilization (Se, Hg, Pb, Cd are volatile; As volatility of Cu, Ni and Zn is influenced by temperature, air/fuel ratio and Cl/metal ratio) [22–24].

One particular element of interest is copper. Studies have shown that Cu, among other metals present in the fly ash, plays an important role in the production of dioxins and furans (PCDD/F) in the post combustion zones of waste-to-energy (WtE) systems [25,26]. Because of this, together with poor public perception, WtE facilities are still seen as *dioxin factories* [27].

This stigma remains even with efficient post combustion cleaning strategies and strict regulations. In EU member states, an emission limit of 0.1 ng/Nm^3 (O_2 content 6%) on polychlorinated dibenzo-p-dioxins (PCDDs) and dibenzofuran (PCDFs) are strictly imposed by the Waste Incineration Directive (WID) [28]. The limit is applicable to stationary and mobile technical equipment partially or fully utilizing waste as fuel and converting it to energy via thermal processes, e.g. combustion, gasification, and pyrolysis. WID is enacted to avoid trans-boundary emission movements from states with less stringent environmental standards, and for the protection of the public and environment.

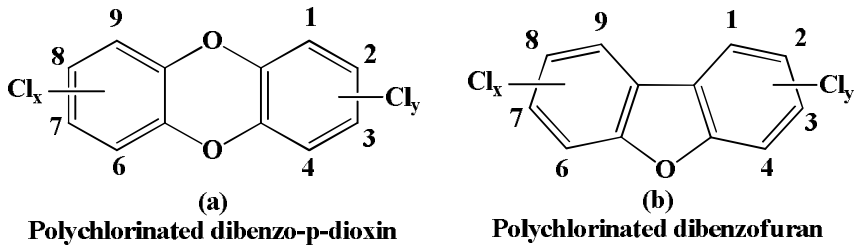

Figure 2. Molecular structures of PCDD/F showing the position for chlorination. There are 75 PCDD and 135 PCDF congeners distinguished by the position and number of chlorine atoms attached to the benzene ring [29].

PCDD/Fs are planar, aromatic, and chlorinated organic compounds. In a dioxin molecule two oxygen atoms bond the two benzene rings while for a furan, a single oxygen atom bonds the two rings (Figure 2). Dioxins and furans with the same number of chlorine atoms constitute a homologue group or isomers. Tetra- to octachlorinated homologues are considered in calculating the toxicity equivalence quantity or TEQ [30].

Figure 3 shows the yearly emission of PCDD/F in Finland from 2006 to 2012 reported by the Finnish Environment Institute (SKYE) [31]. These values are significantly lower (c.a. 60%) than the emission reported from year 1990 to 2005. On

average around 52% of the yearly dioxin emission comes from the energy sector which includes public energy and heat sector [31,32]. Around 23% of the yearly emissions come from industrial processes which include, for example, the metal, iron and steel sectors. Methonen et al. reports that any significant decrease in air emission in Finland may not be expected; the estimated emission reduction is around 20–30% for metallurgy, power production and waste incineration [32]. Therefore the need to develop means to improve current emission levels or at least to keep to them is especially relevant if more and more waste is to be energy recovered: see Figure 1.

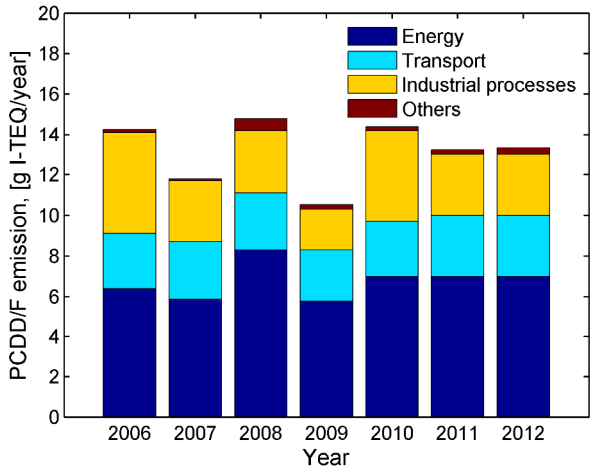

Figure 3. Finnish dioxin and furans total air emissions during the period 2006–2012. Data from SKYE [31].

Ash melting, slagging, severe bed agglomeration, and de-fluidization in fluidized bed boiler could also occur during multi-fuel firing [33–35]. However it is beyond the scope of this work.

1.2 Interaction of fuel key components linking PCDD/F and Cl -induced corrosion

Figure 4 attempts to summarize interactions of key fuel components in the bubbling fluidized bed boiler (BFB) which can promote or inhibit PCDD/F production and Cl-induced corrosion. The same figure also presents the system boundary or scope of this thesis.

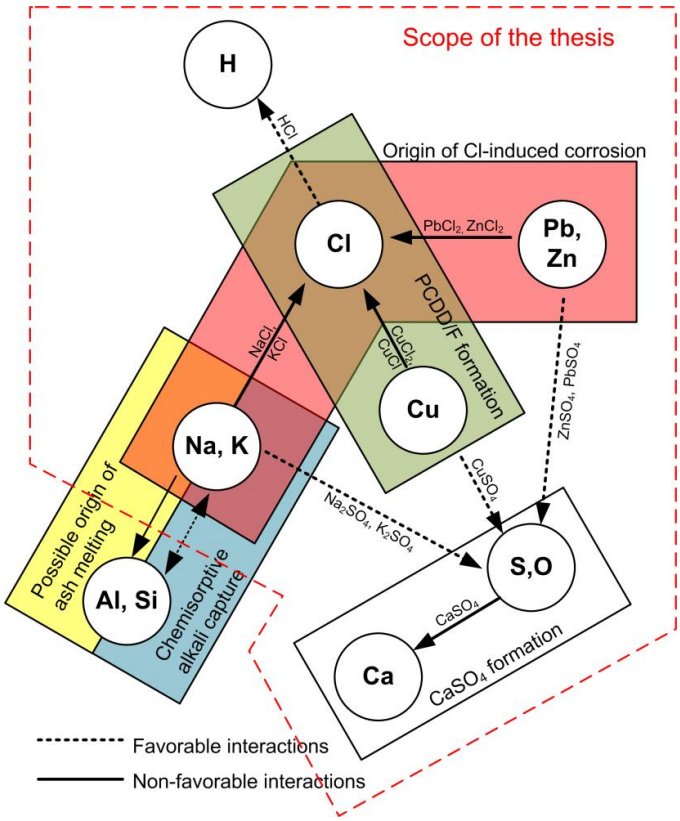

Figure 4. Simplified interactions of key ash and aerosol forming and trace elements during waste firing in a BFB boiler. A nearly similar diagram appears in [11]. Favorable interactions reduce the availability of alkali and copper chlorides in the boiler. Non-favorable interaction causes alkali chloride formation and/or ash melting and PCDD/F formation.

The interaction of (Na, K) – Cl and (Pb, Zn) – Cl promote the deposition of risky forms of chlorine in the superheater and economizers. The interaction of Cu – Cl in the post combustion zones of the BFB boiler is favorable for the formation of dioxins and furans. Meanwhile the interaction of the alkalis with Al and Si, depending on mode of occurrence, may help promote ash melting or may undergo chemisorption to capture alkalis. Depending on the relative abundance of these elements, these non-favorable interactions can cause corrosion in the superheater, ash melting (mostly in the bed) and PCDD/F formation to occur simultaneously or one at a time.

The presence of S can alter the chemistry inside the BFB boiler to favor the formation of alkali and trace-metal sulfates. This interaction reduces the risk of

chlorine induced corrosion, provided that the sulfation takes place in the proper phase, and the formation of PCDD/F. Sulfation of alkali chlorides allows the interaction H – Cl to happen. In a typical boiler, the concentration of $HCl_{(g)}$ in the flue gas around the superheater area rarely exceeds 1000 ppmv, so the risk of severe gas phase corrosion attack is negligible [15]. Sulfation of Pb and Zn chlorides is also thermodynamically favorable, but due to severe kinetic restrictions, the extent of reaction is low [36].

A more detailed description of the theories relevant to these interactions is found in Chapter 2.

1.3 Objective of this work

The literature is rich with studies focused on the corrosion [7–10,12–15,22,37] and PCDD/F formation and abatement [26,29,38–47] during combustion of waste derived fuels. These studies also vary in scale (bench scale, pilot scale, full scale), methods (modeling or computational, experimental approach) and combustion system (grate incinerator, fluidized bed technology). However, because of the limited application of fluidized bed technology to waste-to-energy (see Section 1.1) studies simultaneously discussing PCDD/F production and corrosion in fluidized bed technologies are limited. Furthermore, the PCDD/F production during combustion of fuel mixtures containing high or advanced (50 to 100%) energy shares of solid recovered fuel or other waste derived fuels in fluidized bed system is less, unlike in grate firing systems. For example in the recent study of Åmand and Kassman for the combustion of waste fuel and biomass in a 12MWth circulating fluidized bed boiler, the share of SRF in the fuel mixture is only around 20% [48].

This work seeks to find method/s that can simultaneously reduce alkali chloride formation and PCDD/F production during combustion of fuel mixtures containing high or advanced (50 to 70%) energy-share of solid recovered fuel in a large scale bubbling fluidized boiler. The scale of the system is chosen in line with the Finnish National Waste Plan for 2016. Systems such as the one employed in this work are expected to be able to absorb the required capacity brought about by the execution of the waste plan.

PCDD/F production in WtE systems is a function of several factors. The focus of Papers I–III is to examine one of these factors – Cu speciation. Using staged equilibrium modelling, the changes in speciation of Cu from fuel feeding to the post combustion zone is modelled and examined against the levels of PCDD/F measured. This approach seeks to find an empirical relationship between Cu speciation and the levels of PCDD/F measured. In addition, S based additive and fuel substitution strategies used to minimize Cl-induced corrosion are tested for their influence in reducing PCDD/F production.

In the aspect of Cl-induced corrosion (Papers IV–V), the focus is to (1) understand the risk of high temperature corrosion associated from firing fuel mixtures

with SRF e-% from 50 to 70% and (2) evaluate currently available corrosion mitigation measures – sulfur addition and peat combustion – to find a robust solution to counter the previously mentioned constraint. We define a robust solution as a procedure whose anti-corrosion performance is highly insensitive to the quality of the fuel being fired. Aerosol samples collected before the superheater are used to determine the corrosivity of the gas. Deposits collected in the superheater region are used to examine the extent of Cl deposition. The correlation between conditions around the superheater (gas temp, aerosol composition) and Cl concentration in the deposits is analyzed using partial least squares, PLS regression. PLS is a simple approach that can allow quantification of the effect of a certain factor, e.g. temperature to a response, e.g. Cl concentration.

1.4 Structure of the thesis

In Chapter 1, a general introduction and rationale for this work is presented to familiarize the reader with the scope and boundaries of the study.

In Chapter 2, pertinent theories on PCDD/F production and chlorine induced corrosion are discussed. In addition abatement measures and their corresponding mechanism of action are presented.

In Chapter 3, the experimental system, sampling techniques, and data analysis procedures used are presented.

From here, the discussions will focus on the results of PCDD/F measurements and related results (Chapter 4), and on Cl deposition studies during the firing of fuel mixtures with advanced energy-share SRF and related results (Chapter 5).

The main body of the thesis ends with a conclusion section which summarizes key findings and recommendations.

2. Pertinent theories

The chemistry governing the production of dioxins and furans and Cl-induced corrosion is presented in this chapter. In addition, the mechanism of action of key technologies employed to inhibit the process are also discussed.

2.1 Production and abatement of polychlorinated dibenzo-p-dioxins (PCDDs) and dibenzofuran (PCDFs)

2.1.1 Production

Temperature governs the type of product (dioxin or furan) and the mechanism of production. In a survey by Everaert and Baeyens of 42 thermal processes (MSWI, combustor, etc.) they concluded that temperature is the major controlling role in PCDD/F production irrespective of the type of thermal process considered [43]. This is also supported by lab scale experiments performed by Wikström which concluded that overall the most significant parameter for the rate of formation of PCDD/Fs is the reaction temperature [49].

Pyrosynthesis or precursor formation was first suggested as a formation mechanism; it occurs between 300 and 600°C. This gas phase mechanism requires chemically similar intermediates (e.g. chlorobenzene, chlorophenols and polychlorinated biphenyls [50]) to undergo self-condensation (coupling of molecules or radical intermediates), cyclization of intermediates [29,41], and chlorination/dechlorination reactions. The last step is remarkably enhanced on a Cu(II)O surface either via the Eley-Rideal or Langmuir-Hinshelwood mechanism, as suggested in the simulated catalytic tests performed by Lommincki et al. [42]. Precursor formation commonly yields more dioxins than furans and has a signature ratio of [51]:

$$\frac{\sum \text{PCDDF}}{\sum \text{PCDD}} < 1 \qquad (2)$$

In parallel a *de novo* mechanism was also under investigation; early experiments showed that this happens in the temperature range of 200 to 400°C [43]. It is a heterogeneous reaction, catalyzed by metals (e.g., Cu, Zn, Mg, Y and Ti [52]) in the incineration fly ash [44,53], and is thought to occur in the post combustion zones of WtE facilities. *De novo* mechanism requires carbon molecules contained in fly ashes to react with oxygen and chlorine, and has a characteristic signature of [43,54]:

$$\frac{\sum \text{PCDDF}}{\sum \text{PCDD}} > 1 \tag{3}$$

The availability of chlorine is important and can either be sourced from the carbon matrix of partially combusted fuel such as soot [55], or produced from the metal-catalyzed Deacon reaction of $HCl_{(g)}$ and $O_{2(g)}$ (see (4)) [56] .

$$2HCl_{(g)} + \frac{1}{2}O_{2(g)} \rightleftharpoons Cl_{2(g)} + H_2O_{(g)} \tag{4}$$

Gullet showed that this reaction is promoted by Cu (as CuO) and leads to an increase in the concentration of tetra- to octachlorinated homologues. It was also reported that a strong peak of formation occurs at 400°C for all the PCDD congeners [45,56].

Copper is the most important catalyst responsible for the synthesis of PCDD/F in incineration systems [29,54,56,57]. In the BFB, Cu undergoes several chemical transformations such as sulfidation in the splash zone, oxidation in the O_2-rich stages, and chlorination in the cold zones of the boiler. The non-volatile fraction of Cu in the fuel leaves the boiler as part of the bottom ash, mostly as Cu^0, Cu^I or Cu^{II} [58]. The rest of the Cu is volatilized or entrained in flue gas and, depending on speciation, Cu can be a catalyst for the *de novo* reaction: see Figure 5.

Using in-situ X-ray absorption techniques, Takaoka and co-worker observed the transformation of Cu from 200°C to 400°C and the production of PCDD/F [25,26,59]. At 200°C, the majority of copper exists as Cu^I or Cu^0. The rate of chlorination reaction of carbon is so slow and few dioxins are formed. At around 300–400°C Cu undergoes oxidation and chlorination-forming oxychlorides. Additional HCl, Cl_2, KCl present in the surrounding gas may react with oxychlorides to form $CuCl_2$ or $CuCl_2 \cdot 2H_2O$. Cupric species can then chlorinate carbon in the ash and form dioxin/furan or compounds of similar structures. In parallel, oxychlorides and O_2 react to form copper oxide. CuO aides in the cleavage of carbon matrices in the ash and can enhance carbon gasification [60], a necessary step in PCDD/F formation. Figure 5 summarizes the Cu-catalyzed production of PCDD/F mentioned above.

In the 1990's studies on the influence of combustion [61–63] and post-combustion conditions [64,65] reinforced the role that poor combustion efficiency

plays in PCDD/F production. Poor combustion is conducive for forming chemically similar precursors that eventually react to form PCDD/Fs. In addition, understanding of dioxin's behavior in the gas cleaning equipment was developed. Memory effects due to the absorption-desorption of dioxins and furans were reported [66]; this can increase the concentration of PCDD/F after the wet scrubber. Memory effects refers to the slow desorption of dioxin or its precursor to the flue gas which increases the dioxin concentration at stack, resulting in a lower dioxin removal efficiency than expected [67]. The effect of corona discharge in the electrostatic precipitator (ESP) on PCDD formation was explored. Corona discharge in the ESP can cause an increase of O and OH radicals which in turn may increase the concentration of chlorophenoxyl radicals [68].

2.1.2 Abatement of the catalytic activity of copper by interaction with sulfur

Sulfur present as SO_2 depletes the Cl_2 levels through the homogeneous gas phase reaction, thereby inhibiting the aromatic substitution reactions necessary for PCDD/F production [46]:

$$Cl_{2(g)} + SO_{2(g)} + H_2O_{(g)} \rightleftharpoons 2HCl_{(g)} + SO_{3(g)} \quad (5)$$

Raghunathan et al. noted that during SO_2 injection, in a gas mixture of 500ppm Cl_2, 10% O_2 and 3% H_2O at 400°C, the exit HCl concentration is considerably higher than during times when injection was halted. In addition SO_2 can heterogeneously poison $CuCl_2$ [69], a *de novo* catalyst, via the reaction

$$SO_{2(g)} + CuCl_{2(s)} + H_2O_{(g)} + \frac{1}{2}O_{2(g)} \rightleftharpoons CuSO_{4(s)} + 2HCl_{(g)} \quad (6)$$

The Gibbs free energy of this reaction at 300°C equals -116 kJ mol^{-1}, which suggests its thermodynamic feasibility and the considerable probability of its occurrence [69]. SO_2 can also sulfate another active Cu species in the ash via [70,71]:

$$SO_{2(g)} + 2CuCl_{(s)} + O_{2(g)} \rightarrow CuSO_{4(s)} + CuCl_{2(s)} \quad (7)$$

$$2CuOCl_{(s)} + \frac{1}{2}O_2 + 2SO_{2(g)} + H_2O_{(g)} \rightarrow 2CuSO_{4(s)} + 2HCl_{(g)} \quad (8)$$

These studies show that Cu is an active *de novo* catalyst when it is present as chloride (Cu – Cl), oxide (Cu – O) and oxychloride (Cu – O – Cl), while $CuSO_4$ is

inactive or passive. Figure 5 summarizes the production and abatement reactions mentioned above.

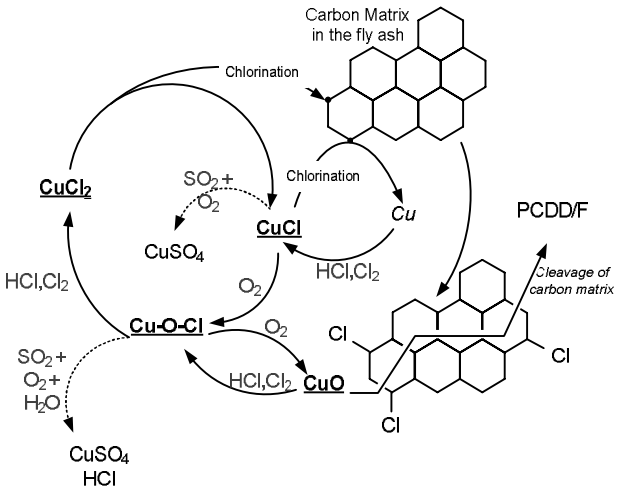

Figure 5. Reactions of copper and the production of PCDD/F. Regular arrows represent active pathways towards PCDD/F production, while broken arrows represent poisoning. The main oxychlorination cycle is adopted from [25] and the poisoning reactions are from [71] and [70].

Ogawa et al. investigated the PCDD/Fs inhibition rates during addition of gaseous SO_2, coal high in sulfur, and coal with a sulfur agent; they concluded that the mode of addition affects the dioxin inhibition [72]. Hunsinger et al. performed a pilot plant campaign to assess the optimum conditions to support PCDD/F inhibition via S addition in their TAMARA municipal solid waste incinerator [47]. Their results emphasize two important process conditions for successful utilization of S as a potential inhibitor:

- Only by maintaining a sufficient concentration of SO_2 (relative to HCl) in the flue gas will there be a lower PCDD/F formation. Thus they proposed a recycling technique for the sulfur to remain in the system while avoiding excessive use of additives.
- The ratio of HCl: SO_2 (both measured as mg/Nm^3) should be 1:1.

In addition, good combustion practices (GCP) were adopted to ensure minimization of PCDD/F production. In the EU, the following GCP are imposed [28]:

- Total organic carbon, TOC, content of the slag and bottom ashes should be less than 3%.
- The combustion gas should be kept, after injection of the combustion air, to a temperature of 850°C and be maintained there for at least 2 seconds.

- Continuous measurement should be taken of CO, total dust, TOC, HCl, HF, NOx and SO_2.
- At least two measurements should be made per year of heavy metals, dioxins and furans; or one measurement at least every three months to be carried out for the first 12 months of operation.

2.2 Chlorine-induced corrosion and corrosion reduction by sulfation

The general accepted model of chlorine induced corrosion in oxidizing/chloridizing atmospheres is the active oxidation mechanism. In this model, chlorine is formed by Deacon reaction from HCl on top of the oxide scale of the oxidized metal, see (4) or by the reaction of solid alkali chlorides (MCl, M = K, Na) with the oxide scale [73].

$$2MCl_{(s)} + Fe_2O_{3(s)} + \frac{1}{2}O_{2(g)} \rightleftharpoons M_2Fe_2O_{4(s)} + Cl_{2(g)} \quad (9)$$

Chlorine can diffuse to the metal/scale interface and react with the metal to form solid metal chlorides ($MeCl_2$, Me = [Fe, Cr, Ni]). There it gets oxidized and gaseous metal chloride species are released. At typical superheater metal temperature (c.a. 300 to ~500°C), the vapor pressure of the metal chloride is high enough to drive the vaporization:

$$Me_{(s)} + Cl_{2(g)} \rightarrow MeCl_{2(s)} \rightarrow MeCl_{2(g)} \quad (10)$$

Volatile ferrous chloride diffuses to regions of high O_2 partial pressure, becomes oxidized and releases $Cl_{2(g)}$ to begin the cycle anew [7,15]:

$$2MeCl_{2(g)} + 2H_2O_{(g)} + \frac{1}{2}O_{2(g)} \rightarrow Me_2O_{3(s)} + 4HCl_{(g)} \quad (11)$$

$$2MeCl_{2(g)} + \frac{3}{2}O_{2(g)} \rightarrow Me_2O_{3(s)} + 2Cl_{2(g)} \quad (12)$$

The net reaction is given by (1) and is summarized in Figure 6.

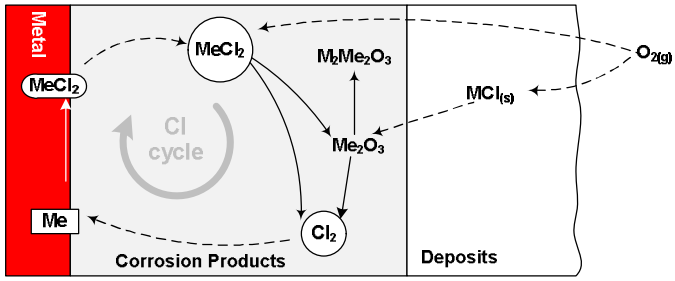

Figure 6. Chlorine induced active oxidation corrosion.

Several methods are available for corrosion mitigation. Making sure that the waste derived fuel such as SRF is of good quality with low Cl content is the first line of defense. This can be done by ensuring minimal contamination of chlorinated plastics such as polyvinylchloride (PVC) and salt-containing food residues. However residual chlorine is always present in the SRF, so in-situ solutions are still employed in actual operation.

One method to address Cl-induced corrosion is by alkali capture. The method prevents the formation of alkali chlorides and subsequent deposition by trapping the alkalis in the matrix of reactive aluminosilicates and aluminosilicate-containing additives such as kaolinite and bauxite [74]. The chemisorption process follows,

$$2MCl + H_2O + Al_2O_3 \cdot xSiO_2 \rightarrow M_2O \cdot Al_2O_3 \cdot xSiO_2 + 2HCl \quad (13)$$

where M = Na, K [75].

Peat ash addition has also been shown to significantly affect the chlorine content in the aerosols due to the interaction of K with the peat ash resulting in the reduced volatilization of the alkali [76]. Co-firing of peat can also lower the amount of alkali chlorides provided that the aluminosilicates present is “reactive”. Sludge is also a possible alkali-capture agent [77].

Sulfation of alkali chlorides is another popular method to address chlorine induced corrosion in waste fired boilers [78,79]. Sulfation can happen in-flight or through intra-particle sulfation – a reaction between SO_2 and the alkali chlorides in the deposits. Both of these reactions produce $HCl_{(g)}$ via the reaction

$$2MCl_{(s,g)} + SO_{2(g)} + \frac{1}{2}O_2 + H_2O_{(g)} \rightarrow M_2SO_{4(s)} + 2HCl_{(g)} \quad (14)$$

where M is Na or K [80].

The sulfation reaction above can further be enhanced if the reactant SO_2 is substituted with SO_3. However in typical boiler conditions the partial pressure of SO_2 is much higher than SO_3. To supply the necessary SO_3, Kassman et al. used

ammonium sulfate [81] while Aho et al. used ferric sulfate to carry out alkali sulfation in power plant boilers [78,82]. Thermal decomposition of ferric sulfate is estimated to produce 1.2 moles of SO_3 and 1.8 moles of SO_2 [83]. $Fe_2(SO_4)_{3(aq)}$ - can easily be sprayed near the superheater region which guarantees high local SO_3 concentration to allow successful alkali sulfation. SO_3 reacts with the alkali chloride as follows:

$$2MCl_{(s)} + SO_{3(g)} + H_2O_{(g)} \rightarrow M_2SO_{4(s)} + 2HCl_{(g)} \quad (15)$$

where M is Na or K [78]. The equilibrium constant for (15) at 800°C is 2.997×10^4, a slight improvement from that of (14) which is 2.711×10^4.

Inflight sulfation using SO_2 and SO_3 is kinetically governed and follow a complex chemistry [83,84]. One manifestation of this condition is the growth in the peak size of the fine aerosol fractions collected during sulfur addition tests [85].

Sulfation of alkali chlorides in the deposit or intra-particle sulfation is also possible. The general schematic of intraparticle sulfation is shown in Figure 7.

When all of the gaseous reactants required are present the main product is alkali sulfate and $HCl_{(g)}$. HCl formation is possible especially if (14) happens near the flue gas and deposit interface [7] where O_2 partial pressure is high. A great deal of generated $HCl_{(g)}$ escapes to the free gas stream [86], but there will be a remainder that can diffuse to the metal/scale interface or be oxidized to form $Cl_{2(g)}$. A more problematic scenario occurs when intra-particle sulfation proceeds without H_2O and produce $Cl_{2(g)}$ directly via the reaction

$$2MCl_{(s)} + SO_{2(g)} + O_2 \longrightarrow M_2SO_{4(s)} + Cl_{2(g)} \quad (16)$$

where M is Na or K. The generated chlorine can very easily push itself through the oxide layer by cracking, grain boundary grooving and fissuring [7]. Both (14) and (16) therefore increase the proximity of $HCl_{(g)}$ and/or $Cl_{2(g)}$ to the metal/scale interface, thus increasing the risk of Cl-induced corrosion. After sulfation, the corrosion mechanism is similar to that of the one described earlier [15].

Meanwhile the presence of Ca in the BFB system may reduce the efficiency of alkali chloride sulfation and favor the production of $CaSO_{4(s)}$ [82]. Ca species can be sulfated as follows [87]

$$CaO_{(s)} + SO_{2(g)} + \frac{1}{2}O_{2(g)} \rightarrow CaSO_{4(s)} \quad (17)$$

$$K_{eq,800^\circ C} = 9.031 \times 10^9$$

$$CaCO_{3(s)} + SO_{2(g)} + \frac{1}{2}O_{2(g)} \rightarrow CaSO_{4(s)} + CO_{2(g)} \qquad (18)$$

$$K_{eq,800^\circ C} = 2.019 \times 10^{9}$$

The equilibrium constant[1] at 800°C for these two reactions is higher than the sulfation of KCl described in (14).

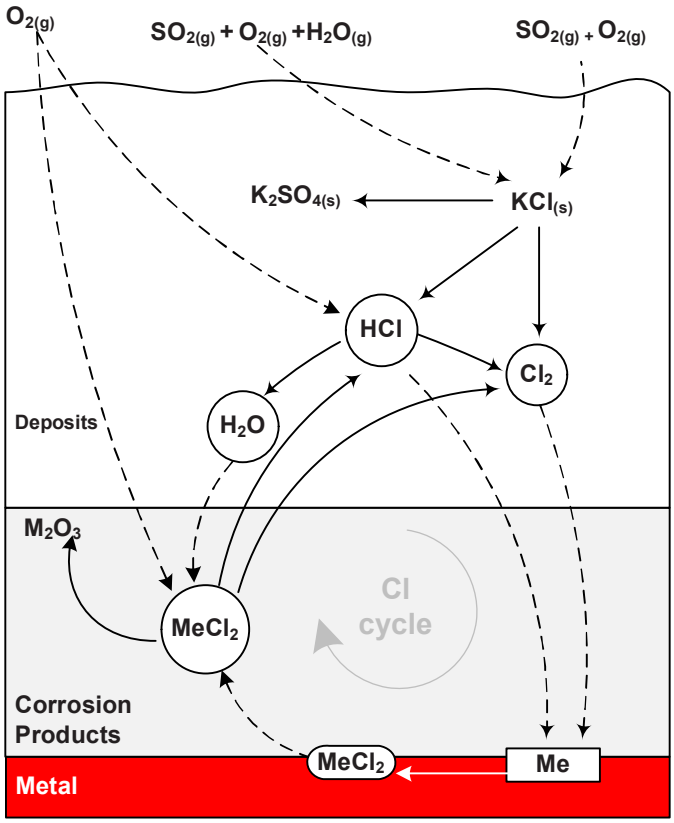

Figure 7. Mechanism of intra-particle sulfation of KCl and the subsequent attack of the metal, adopted from the discussion in [15].

[1] Estimated using FactSage® Reaction module at standard state conditions.

3. Experimental procedures and modeling

This chapter presents the boiler system employed in the test for all the papers covered in this work, fuels, sampling procedures, analyses, and modeling and/or regression strategies.

3.1 Bubbling fluidized bed boiler and the WtE facility

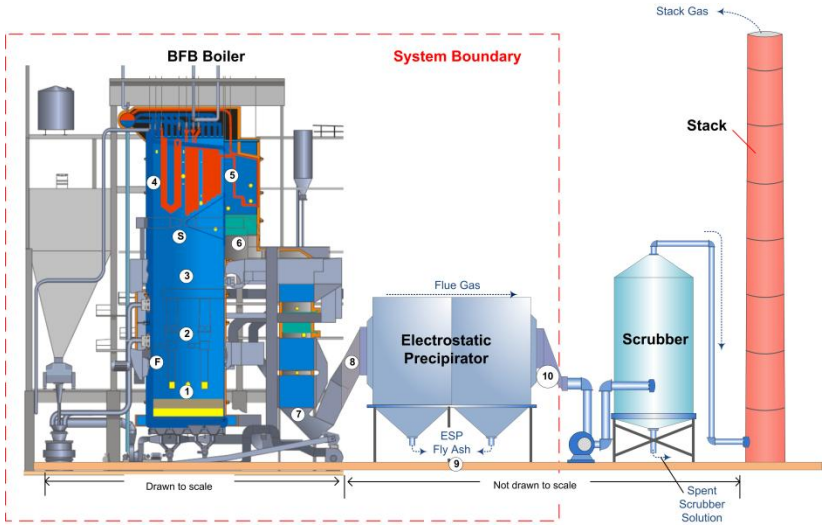

Figure 8. Stora-Enso Anjalankoski bubbling fluidized bed boiler and flue gas cleaning devices. The system boundary for this thesis is shown. Key locations in the boiler: (1) above the bed, splash zone; (2) downstream from the secondary air just before the tertiary air; (3) downstream from the tertiary air to just below the bullnose; (4) before the superheater; (5) after the superheater or backpass; (6) after the economizer; (7) after LUVO; (8) before the electrostatic precipitator; (9) ESP fly ash collection point; (10) after ESP; (F) fuel feeding; (S) sulfate injection. Used with permission from Valmet Power and Stora Enso.

Figure 8 shows Stora Enso's Anjalankoski waste-to-energy facility where all experiments and data collection were carried out. This facility was originally commissioned as a pulverized fuel (PF) boiler with a grate for bark co-combustion in 1971 and has undergone retrofitting to become a BFB in 1995 for SRF−bark−sludge co-incineration.

By the year 2000, sludge thermal drier was installed increasing the dry matter content of sludge being fired to about 90%. This paved the way for increasing the amount of SRF in the fuel mix. In 2008, a bed retrofit was made increasing its capacity from 87MWth to 148MWth. The facility maintains two gas cleaning devices – an electrostatic precipitator and a wet scrubber.

During the test campaign the boiler was operating at a mean load of 90 MW_{th}. Possible hotspots for PCDD/F formation are the economizers and the preheater or LUVO. Flue gases enter the economizer on average at ~ 430°C and exit at 340°C, while at the air preheater the flue gases enter on average at ~ 260°C and leave at ~ 185°C.

The ESP consists of two parallel lines in the flue gas flow direction, both with two sequential fields being maintained at approximately 185–190°C during the test runs. This temperature setting was fixed to decrease the likelihood of generating more dioxins and furans in the ESP.

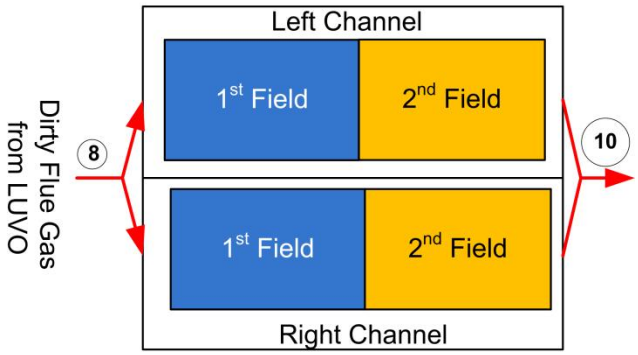

Figure 9. Flow of flue gas in the ESP channels and consequent fields. Point (8) and (10) after ESP are shown and follows the designation of points in Figure 8.

For Papers I–III, the study is limited to the boiler and the electrostatic precipitator; therefore the levels reported in this work cannot be considered as the actual PCDD/F emissions of the facility.

3.2 General description of the fuels

The BFB facility uses Scandinavian spruce bark, dried paper mill sludge and solid recovered fuel (SRF). The bark comes from the debarking process of the paper

mill adjacent to the boiler and the sludge is from the wastewater treatment facility of the same mill. This sludge is rich in calcium from paper fillers and coating used during the paper manufacturing. The wastewater treatment facility uses around 30–40 kg of iron(III) sulfate per ton of dry sludge as flocculants and aluminum(III) sulfate for pH control [88].

The SRF used in the study is collected from offices, wholesale businesses, and small to middle scale industries in southern Finland [89]. PVC based packaging plastics have been excluded during the collection and preparation of the SRF. In the SRF plant, materials are homogenized to 50–100 mm particle size and magnetic materials are separated. SRF is transported to the facility in wrapped bales or fluffs [88].

Peat used in fuel substitution studies is mined in Finland with sulfur content of c.a. 0.2%. It is introduced to the fuel mixer before the boiler, together with bark (fuel mixture composition is in Table 3).

3.3 Materials and methods for Papers I to III

The main focus of Papers I to III is to study PCDD/F production in the BFB system and find ways to control it. This subsection presents key information pertinent to these papers.

3.3.1 Boiler condition

It is necessary to ensure that the system where all data collection and experiment is made is operating at steady state. Before any data collection is made, there is a period allotted to allow the BFB to reach steady state condition.

The process conditions extracted from the boiler's instrumentation are shown in Figure 10. Together with a steady-state detection (SDD) algorithm developed by Kelly and Hedengren [90], we used these process data to assess whether the BFB was running at steady state. The term steady state implies that the process is operating around some stable point or within some stationary region where it must be assumed that the accumulation or rate-of-change of material, energy, and momentum is statistically insignificant [90]. A probability of 0.90 or greater indicates that the process is at a steady state. The probabilities for the process data used for this analysis (see Figure 10) are all within the cut-off indicating that the BFB is running at a steady state or at least stationary during each test case.

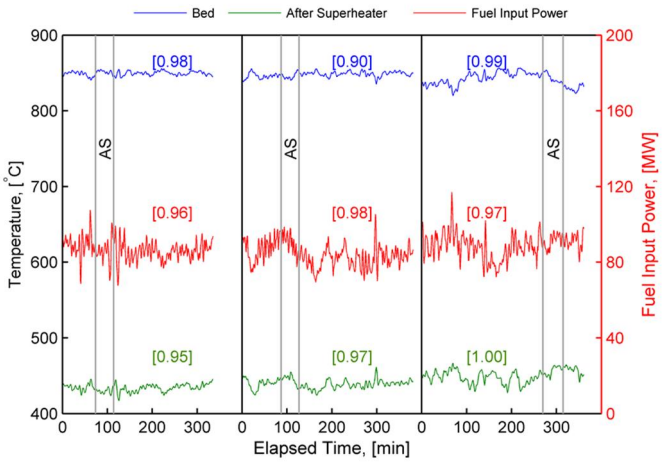

Figure 10. Process data extracted from the boiler's instrumentation. Fuel input power does not include the power input from the sludge. AS indicates when aerosol sampling was taken. The numbers inside the square bracket indicate the probability that the process is at steady state using a steady-state detection algorithm [90].

3.3.2 Fuel proportion and composition

The proportions, in percentage energy share, of the fuels fired are given in Table 2. Fuel mixtures containing SRF – Bark for Case 1 and 2, and SRF – Peat for Case 3 are fed to the boiler through the chutes in the left and right walls, see F in Figure 8. Sludge is fed separately to the boiler from the thermal drying plant via pneumatic transport lines.

Table 2. Fuel proportion and S-pellet addition in the study. Note that the fuel mixture comprises SRF-Bark and SRF-Peat.

Case	%Energy Share				S-pellet added?
	SRF	Bark	Sludge	Peat	
1	50	44	6	0	No
2	50	44	6	0	Yes*
3	60	0	6	34	No

* Ratio of mass flow rate (kg/s) S-pellet/fuel is around 0.001.

Each test case run lasted for six hours. However for Case 2 the sulfur addition started the night before the actual test run to ensure that the system had been

saturated with sulfur prior to the actual data collection. This is to follow the recommendation that only by maintaining the level of S in the boiler is dioxin and furan production effectively combated [47].

The properties and the composition of the fuels fired in the boiler are found in Table 3. Because SRF has a large energy share, the majority of the elements found in the fuel mixture can be traced from it. This is true for example for minor components, sodium, potassium and chlorine, and for trace components copper, zinc and lead. Variation in the composition of the fuel mixture can also be traced directly to the SRF, with possible exceptions of Si and Al, since these elements are abundant in the peat. For the trace components, variability is high for Cr, Cu, Ni and Sb, as clearly seen in the values in the same table. This variation can be traced to the sources of these elements in the actual collected waste used to prepare the SRF. To name a few, Cu can come from brass, plastic catalyst and colorant, and copper wire, Cr can come from the impregnating agent found in CCA wood, Sb from fire retardant additives [88] and Ni can come from discarded electronics and additives in paint and plastics [91].

The concentration of Br in the fuel is low compared to Cl. Thus the amount of PBDD/F or PXDD/F that can be produced may be less compared to PCDD/F. Substantial PBDD/F formation in thermal treatment processes (e.g. pyrolysis at 800°C with polyvinyl chloride [92], pilot scale combustion reactor [93] and pilot incineration plant[94]) has been reported in the literature. However these studies have used either fuels with equal molar amounts of Br and Cl [93] or a fixed proportion of the halogens in the fuel to reach a required gas phase concentration [94], or performed the test at pyrolytic conditions [92]. None of these proportions or conditions is applicable in this study.

In addition, chemical fractionation was performed to estimate the mode of occurrence of Na, K, Al and Si in the pure fuel. Increasingly aggressive solvents were used to leach out these elements, (a) H_2O for alkali sulfates, carbonates, and chlorides, (b) acetic acid (HOAc) for organically bound fractions, and (c) HCl for carbonates and sulfates of alkaline earth and other metals [13]. The rest are silicates and minerals. The analysis was done by an accredited laboratory. However, the advanced role of this procedure in this study is not emphasized [95] and the results are used only to explain the partitioning behavior of K, Na, Al, and Si calculated by the staged equilibrium model.

3.3.3 Aerosol sampling

Aerosol samples were collected from the right wall of the backpass zone indicated by (5) in Figure 8 using the Dekati Low Pressure Impactor (DLPI). Each sampling interval runs for 40 minutes and the schedule is shown in Figure 10. The impactor deposits were digested with water or strong acid for five days and subjected to ultrasonic mixing prior to extraction.

Table 3. Properties of fuel mixture and sludge used in the study. Analyses were carried out according to the appropriate CEN/Ts, ASTM and ISO methods.

Parameter/Component	Fuel Mixture			Sludge
	Case 1	Case 2	Case 3	
Gross heating Value (MJ/kg, d)	23.02	21.78	19.59	20.2
Net heating Value (MJ/kg, d)	21.51	20.35	18.38	18.92
Net heating Value (MJ/kg, a.r.)	9.84	8.45	8.99	4.29
Moisture content (wt. %, a.r.)	48.7	52.2	45.1	68.5
Major components (wt.%, d.)				
C	52.5	51.2	46	49.3
H	7	6.6	5.6	5.9
N	0.63	0.56	0.76	1.81
S	0.12	0.21	0.41	0.5
O (calculated)	36.04	37.26	37.64	38.54
Minor components (mg/kg, d)				
Cl	3300	2900	2800	200
Na	1800	1700	3300	2300
K	1500	1700	4600	970
Ca	18500	18400	15100	14100
Mg	1000	1500	1700	840
P	430	390	290	1800
Al	3900	3000	11100	5700
Si	4100	8600	47300	11400
Fe	1200	1700	6300	830
Trace components (mg/kg, d)				
Mn	200	280	120	1100
Zn	200	170	260	82
Br	10	10	20	30
Cr	17	56	340	7.3
Cu	26	26	670	13
Ni	3.8	11	150	1.9
Sb	5.9	4	140	0.5
Cd	0.24	0.24	0.46	0.25
Co	2.7	0.43	4.8	0.5
Pb	43	48	32	3.2
Sn	6.2	18	4.7	0.56
V	2.9	3.5	12	1.8

The concentrations of water soluble Na, K and Ca were measured using ICP-MS. For Cl, SO_4 and Br, ion chromatography was used, and for the acid soluble Cu, ICP-MS was employed. A detailed discussion on the schematic and subsequent analysis of aerosol samples was provided in [96]. For this work, the aerosol concentration of Ca, Na, K, Cl, and S (represented as sulfate) and Br are from the water soluble fractions while that of Cu is from the acid soluble fraction.

Gas properties and composition are collected at the same time and point using GASMET Fourier transform infrared spectroscopy.

3.3.4 Dioxin/Furan measurements in the flue gas path (Paper I)

Sampling and analysis of dioxin and furan in the flue gas path were done by Pöyry Oy, an accredited laboratory in Finland. Sample collection, clean up, extraction and measurements are governed by the CSN EN 1948: Stationary source emissions – determination mass concentration of PCDDs/PCDFs and dioxin like PCBs Part 1–3. Sampling locations are situated before and after the electrostatic precipitator (see 8 and 10, respectively in Figure 8) in order to determine the dioxin/furan in-boiler production and assess if further production takes place in the ESP. For toxicity purposes only the homologues with four or more chlorine atoms are considered; thus only these homologues are reported in this study. All concentrations are based on I-TEQ at a 6% O_2 (101.3 kPa and 273 K) dilution factor.

3.3.5 ESP fly ash sampling and analyses (Papers I and III)

The fly ash was collected in the pneumatic transport lines below the fields of the ESP – see (9) in Figure 8 – using a tube sampler made from a steel pipe. For each test case, five sampling periods lasting for about four minutes, sufficient for the sampler to be filled, were performed. Each sample was cooled before being bagged into a clean and sealed container. During the experimental runs, the volume of the fly ash collected in the 1st field of the ESP is approximately four times of that collected in the 2nd field.

For the analysis of the PCDD/F composition and concentration in the ESP fly ash, Paper I, the composite sample for each test case was prepared according to the following procedure.

First, for each channel, 4 parts by volume of ashes collected from the 1st field and 1 part by volume of ashes collected from the 2nd field were mixed (dubbed as channel-mixture). Then equal mass portions of channel-mixtures from the left and right channels were combined (dubbed as sampling-mixture). Finally, five equal mass portions of sampling-mixtures were then combined to make up the composite fly ash sample for each test case.

Analysis of PCDD/F concentration in the ESP fly ash was done by Eurofins GfA Lab Service GmbH in Germany. This laboratory uses an internal method and is accredited to perform this test. The concentration of Cu and S was analyzed by Labtium Ltd. in Espoo, Finland using the XRF technique.

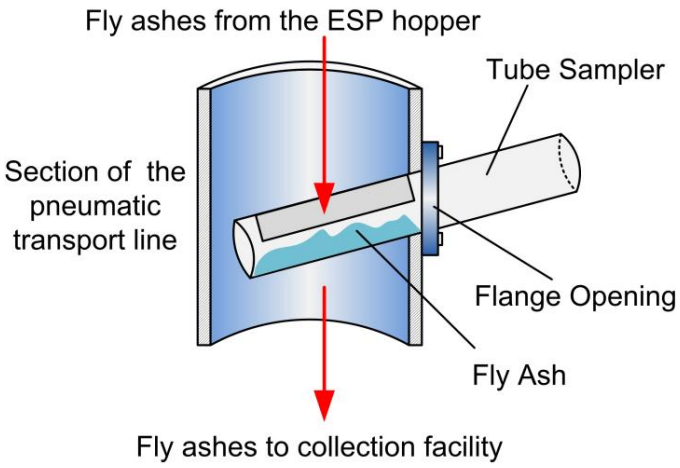

Figure 11. Schematic for fly ash collection in the pneumatic transport line below the ESP hopper (see in Figure 8) using a tube sampler.

For the ESP fly ash characterization and composition tests, Paper III, the fly ashes collected in the first and second fields were not combined. It was anticipated that the chemical and physical properties of these two ashes may be different [97]. The composite sample was made by combining equal mass portions of ash samples from each sampling period for each field. In total six composite samples were prepared and analyzed for this study – 3 samples from the 1st field, and 3 samples from the 2nd field. By visual inspection the first field captures the coarse fly ashes while the second collects the much finer fly ashes.

3.3.6 Physical and chemical properties of the ESP fly ash (Paper III)

The concentration of major ash forming and trace elements in the fly ash were determined using X-ray fluorescence spectroscopy (XRF) without prior treatment except for size reduction using a ceramic ball mill. Micrographs were also taken using a scanning electron microscope (SEM) to examine the morphology of fly ash samples. X-ray powder diffraction data was measured using PANalytical X´Pert PRO alpha 1 diffractometer in Bragg–Brentano geometry using Johansson mono-chromator to produce Cu Kα1 radiation (1.5406 Å; 45kV, 30mA). The diffraction

intensities were recorded by an X´Celerator detector using continuous scanning mode in 2θ-range of 4-100° with a step size of 0.017° and counting times of 800s per step. Data processing and semi-quantitative search-match identification of the crystalline phases were made by X´Pert HighScore Plus v. 2.2d program using the ICDD-PDF4+ (release 2012) powder diffraction database reference retrieval source. The semi-quantitative information was acquired by the reference intensity ratio method (RIR) included in the program.

3.3.7 Speciation of copper (Paper III)

Copper has a central role in the production of PCDD/F: see Section 2.1. In Paper III, we wanted to examine changes in the speciation of Cu brought about by changing the fuel and the S-based additive introduced to the boiler.

Several methods are currently available for the speciation of elements found in fly ashes, but due to the complex mixture of elements present in these ashes most of these methods are applicable only to specific element constituents and at a given concentration.

A sensitive element-specific and non-destructive technique based on X-ray absorption is used in this work. X-ray absorption spectroscopy (XAS) is a method for investigating the local structural environment of elements. XAS is divided into X-ray absorption near edge structure (XANES) analysis which provides information primarily about the oxidation state of the absorbing element and its local geometry, and X-ray absorption fine structure (EXAFS) analysis which provides information about atomic coordination (type and number of neighboring atoms and inter-atomic distance).

XANES spectra of the fly ash samples were collected at BL8 of the Synchrotron Light Research Institute in Thailand [98]. The photon energy of the synchrotron X-rays was scanned by a Ge(220) double crystal in the *K*-edge XANES region of copper. The photon energy was calibrated against the *K*-edge of Cu foil at 8979 ± 0.3 eV. Prior to analysis, all samples were finely ground and deposited in polyimide tape. Due to the low Cu concentration, all fly ash samples were scanned in the fluorescence mode. The incident photon intensity, I_O, was monitored by a 10 cm ion chamber filled with Ar (76 mbar), while the fluorescence signal, I_F, was measured using a 13-element Ge detector. Absorption is given by I_F/I_O. On the other hand the *K*-edge XANES spectra of the pure standards (Cu foil, Cu_2O, CuCl, CuO, $CuCl_2$, $CuBr_2$, and $CuSO_4$) were collected using the transmission mode due to high Cu concentration. The intensity of the incident x-ray beam, I_O, and the transmitted x-ray beam, I_t, were monitored by a 10 cm long ion chamber (with Ar at 76 mbar) and a 40 cm long ion chamber (with Ar at 413 mbar) respectively. Absorption is defined as $\ln(I_O/I_t)$. Each XANES spectrum is an average of two or more scans.

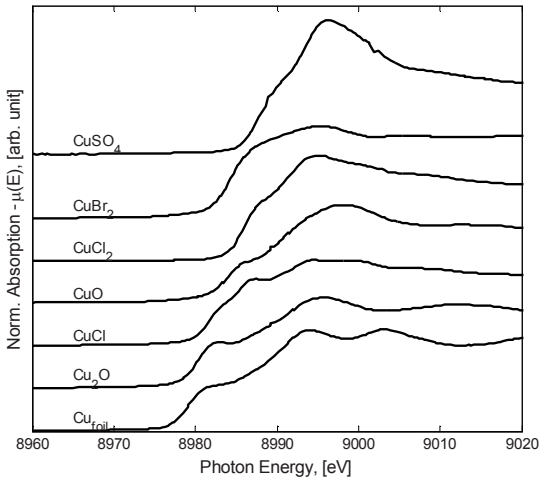

Figure 12. Cu K-edge XANES spectra of the model or reference compounds used in LCF.

Data analysis for the spectra was performed in ATHENA a XAS data processing software [99]. Spectra were normalized using the MBACK algorithm developed by Penner-Hahn and co-workers [100]. Linear combination fitting (LCF) was used to perform a semi-quantitative compositional analysis of the chemical species of Cu in the ESP fly ash. LCF assumes that the spectrum of a given sample is a linear combination of known spectra from "model compounds" or references. The selection of reference Cu compounds (see Figure 12) was based on the thermodynamic modeling results in Paper II, and similar studies on PCDD/F production using XAS as a method for Cu speciation [25,59,101–104]. This selection strategy limits the number of reference compounds used, so it is possible that other Cu compounds were present in the sample but were not accounted for.

The fitting space is the normalized absorption, $\mu(E)$, at the range of -20 to 30 eV around the absorption edge. The misfit (R-factor) is given by

$$\text{R-factor} = \frac{\sum(\text{data-fitted})^2}{\sum \text{data}^2} \tag{19}$$

The coefficients obtained from linear combination fitting of the XANES spectra indicate mole percentage of the respective references used [25].

3.3.8 Chemical Equilibrium Modeling

Chemical equilibrium calculations have been used to analyze systems such as combustion [105–107], gasification [108], cement kiln chemistry [109] and several others [110]. The flexibility of the computation approach and the rapid growth in computing power enabled systematic calculation of multi-phase multi-component equilibrium systems. Equilibrium calculations give accurate results in high temperature applications because the assumptions of the calculations are met. One assumption is rapid reaction which essentially renders the reaction to approach equilibrium. This assumption is true for high temperature systems. The quality of the database used in the simulation also greatly determines the output of equilibrium calculation. Talonen used five commercial databases (HSC, FACT,SGTE, IVTANTHERMO and JANAF) to study the behavior of 12 heavy metals regulated in the WID and noted significant variation in this thermodynamic databases [111]. The algorithm for performing Gibbs minimization also affects the outcome of the result. For example, HSC handles only pure substances while FactSage can handle both pure and solution databases. In addition the, applicability of thermodynamic equilibrium modeling can be limited by local temperature gradients, physical processes such as adsorption and capillary condensation, non-ideal mixing behavior between different ash forming elements and the mode of occurrence of components in the fuel which dictates its release or retention rate [19,112]. However, clever and carefully designed methodologies can produce valuable information about overall stabilities and speciation trends [8].

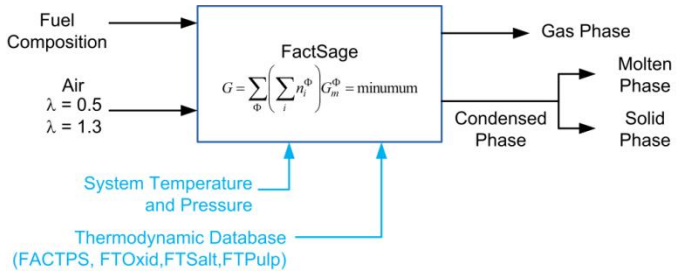

Figure 13. Diagram showing the implementation of global equilibrium modeling in FactSage.

In the field of combustion, applications include the study of the behavior of fuel components during combustion [113], multi-fuel combustion strategies [8,77], alkali chemistry related to combustion [114,115], bed agglomeration [116–118] and the fate of trace elements [22,119–121]. The systems mentioned above may contain multi-components and multi-phases, so it is necessary to employ numerical method to solve the minimization of the Gibbs energy of the system in equilibrium [122]. For such system, the minimization equilibrium condition is written as

$$G = \sum_{\Phi} \left(\sum_{i} n_i^{\Phi} \right) G_m^{\Phi} = \text{minimum} \tag{20}$$

Here G_m^{Φ} is the molar internal Gibbs energy of the phase Φ, and n_i^{Φ} are the mole numbers of the phase constituent i of this phase. Thus the inner sum refers to the respective phase amounts, and the outer sum runs over all phases [122].

Global Gibbs minimization is implemented in FactSage 6.3.1 (for Paper II) and 4 (for Paper IV) and the schematic of procedure is shown in Figure 13.

In practice, the role of reaction kinetics is equally important. This makes simulations of large-scale systems challenging when using straightforward global equilibrium calculation alone. Dividing large processes into simpler subsystems or stages may add value to the calculation. Sandelin and Backman used this approach to analyze the behavior of trace elements in a coal-fired power plant [112]. They concluded that their modeling results agree with full scale measurements and the overall chemistry was predicted with satisfaction.

Staged equilibrium calculation can be done on several platforms. For example, ChemSheet combines MS Excel with the multi-phase multi-component calculation capability of FactSage [123]. Aspen Plus is also available and has been widely used in the field of chemical engineering [124,125].

In this work the macro processing module of FactSage is employed. Since the macros are already available in the FactSage distribution, additional software is no longer required. Macro commands enable the user to run the subprogram *Equilib* in the background and execute commands stored in a macro [126].

The main motivation for the use of this platform is to take advantage of the integrated database and computing facility in FactSage, and to develop an Excel-based user interface as a process model for the boiler used in this study.

3.3.9 Staged-equilibrium process model implementation

The main purpose of performing a staged-equilibrium process model is to develop an understanding of how Cu speciation evolves inside the BFB and how it influences the PCDD/F production. Using this information, the model will also be used to perform scenario analyses to examine how PCDD/F production is affected by lowering the Cu concentration during peat co-combustion, and increasing the sludge energy share.

The process model uses Microsoft Excel and FactSage 6.3.1; and the structure of data flow is shown in Figure 14. The Excel worksheet contains all the local conditions, the mass and composition of the input/output streams for each stage (or equilibrium reactor). The worksheet also stores all equilibrium calculation results, and calculates the mass balance in the reactor network.

A command button in the worksheet can launch a batch file that prompts the macro facility of FactSage to accept the process information, launch the *Equilib* subprogram, initialize and perform equilibrium calculation, and finally return the calculation results back to the interface. Data are exchanged from Excel to FactSage and vice-versa via Object Linking and Embedding (OLE).

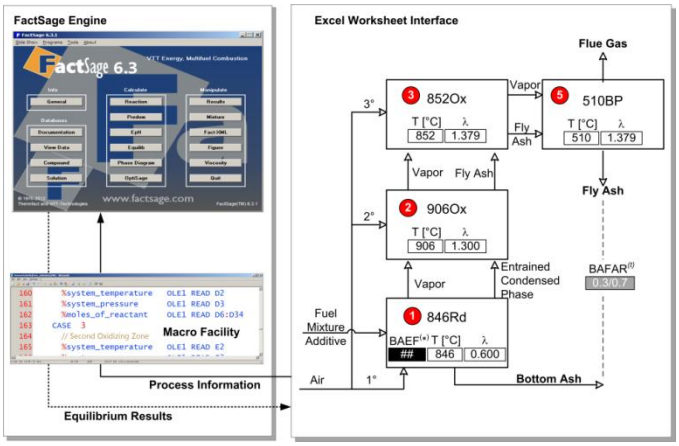

Figure 14. Data flow structure between FactSage's equilibrium calculation engine and the staged equilibrium process model in Excel. The local temperature and air/fuel ratio, λ , are shown in the box inside each equilibrium reactor. The asterisk (*) denotes an adjustable parameter while (t) denotes a target parameter. The number in the red circle corresponds to the section of the boiler described by the stage and the location is presented in Figure 8.

The process model is made up of four stages, each representing a certain region in the BFB: see Figure 8 and Figure 14. Each stage is an adiabatic system operated at atmospheric pressure. Through this approach, the model approximates to local conditions prevailing in key zones of the BFB.

The first stage, 846Rd, represents the splash zone. 846Rd takes in all the fuel mixture (plus the additive for Case 2) and the primary air. After performing equilibrium calculation, a fraction of the condensed phase (pure and solid solutions) is entrained together with the vapor to the next reactor, and the remainder is drawn out as bottom ash. The amount of entrained-condensed phase is controlled by the adjustable parameter bottom ash entrainment factor (BAEF) which is applied equally to all the condensed phase constituents (or species) formed in 846Rd.

The presence of this stage offers an advantage over global equilibrium calculations. The 846Rd allows the removal of some fractions of elements that are expected to be enriched in the bottom ash. For example, Lundholm et al. reported that around 40 to 70% of Cu was retained in the bottom ash when burning chro-

mate copper arsenate (CCA)-preserved wood with or without the addition of peat [120]. This changed the amount of copper downstream of the boiler. The 846Rd meets this expectation and allows the partitioning of the element to be estimated. In the model, an element can partition between the bottom ash, fly ash, and flue gas stream.

The next stage, 906Ox, the first oxidation stage, takes in the secondary air and the vapor plus the entrained condensed phase from 846Rd. After equilibrium has been calculated, all of the vapor and condensed phase (now called fly ash) are passed to the 3rd stage as input. The 906Ox simulates what happens to the components of the fuel mixture as they move from a reducing to an oxidizing atmosphere.

The third stage, 852Ox, the second oxidation stage, takes in the tertiary air and the results of the calculation in 906Ox. The air to fuel ratio (λ) at this stage is 1.379 and represents the final λ for the boiler during the test cases.

The last stage, 510BP, represents the backpass and accepts all the masses from 852Ox. This is the coldest among the four and is assumed to govern the total amount of fly ashes produced for each test case. This stage has two output streams: Flue Gas and Fly Ash.

Once the total amount of fly ash has been calculated, the Bottom/Fly Ash Ratio, BAFAR, is evaluated and compared against the target value of 0.3/0.7. The macro uses a simple bisection algorithm to meet the target BAFAR by iterating the adjustable parameter BAEF. The actual value of BAFAR is not exactly known because of the difficulty of measuring the flow of the bottom and fly ash for the test cases. The current value is based on historical estimates collected from the plant.

The thermodynamic database includes 181 gaseous and 337 pure solid species from the FactPS, FToxid, FTsalt and FTpulp database. Solution species from FToxid and FTsalt are likewise included. For each case and equilibrium stage, preliminary runs and post calculations of activities are made to ensure that no pure species that should be included in the thermodynamic database are left out in the simulation. Nitrogen is assumed to exist as $N_{2(g)}$ [19], and the mass and activity limits are 1 nanogram and 1×10^{-3} respectively.

3.4 Materials and methods for Papers IV and V

The main focus of Papers IV to V is to study Cl deposition in the superheater brought about by shifting the energy share of the SRF from the base load of 50 e-% to 70 e%. This subsection presents key experimental methods pertinent to these papers.

3.4.1 Test schemes and boiler conditions

Nine tests constitute this part which is summarized in Figure 15. Test points I to V are assessment phase tests while VI to IX are performance analysis tests. During the assessment stage we study the associated corrosion risk for firing the base case fuel of the BFB – Fuel 1 and the effect of three anti-corrosion measures: elemental S-addition (II), sulfate injection (III) and peat co-firing (IV). During V the amount of SRF is 60 e-%, an intermediate value between the base fuel and the target fuel. Promising anti-corrosion measures from the assessment stage are applied to the target fuel (70 e-%) in the performance analysis test (VI to IX).

The duration of the test vary from a minimum of 1.3 h (IV) to 8.5 h (V) because other parameters outside the scope of this study are also measured and required longer test time. There is a period prior to each test point allotted to allow the BFB to reach steady state condition. All the necessary data gathering presented in this work have been collected at a relatively constant time span and at steady state operation.

Figure 16(a) shows the temperature profile of the BFB; all data are from the BFB's online instrumentation. Each location has a corresponding boxplot that shows the variation of temperature during the test in the said location. No outlier temperature was recorded.

Figure 16(b) shows the boiler load and steam power during the duration of the study. The mean boiler load is 94 ± 3 MW and steam power is 80 ± 2 MW, giving a boiler efficiency of around 85%. The wet gas O_2 concentration is also shown in the figure with a mean of 8.82 ± 0.13% and corresponds to an air/fuel ratio of around 1.3.

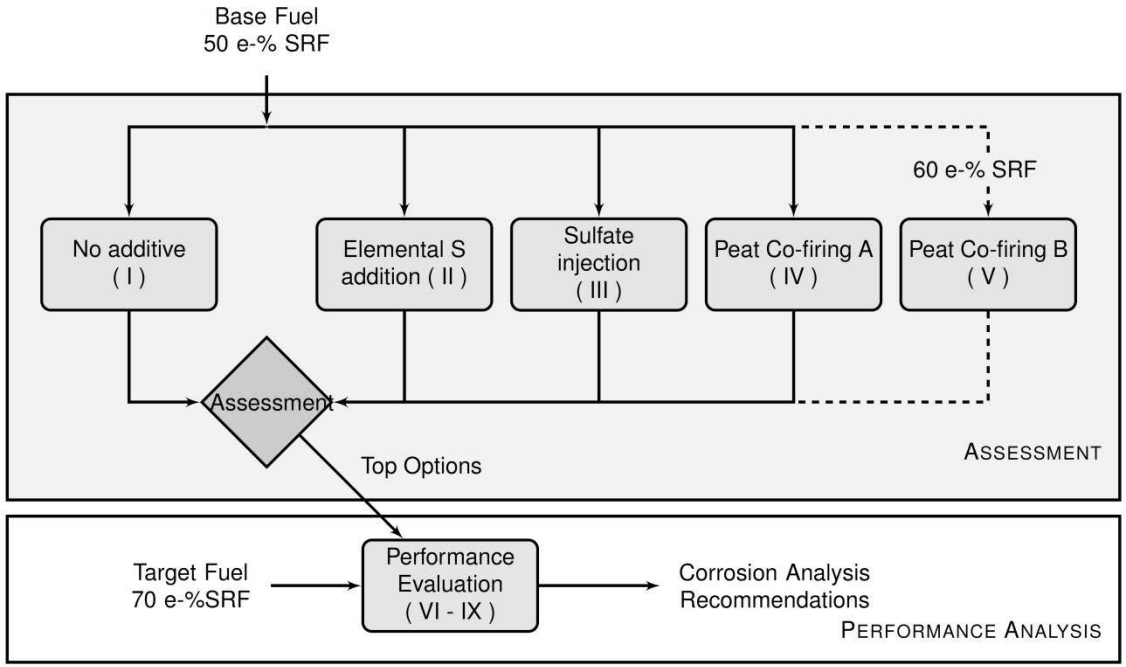

Figure 15. Schema of tests.

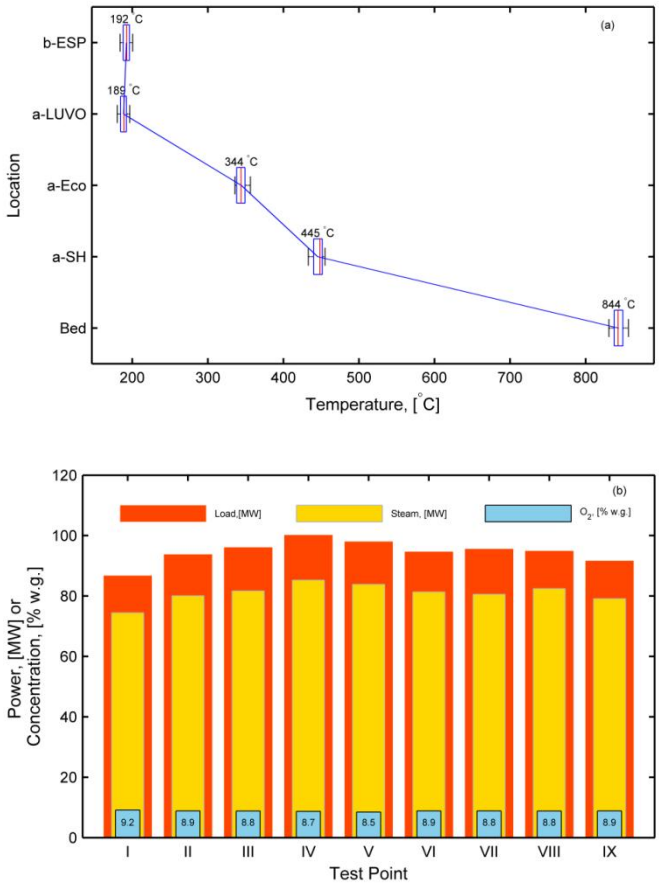

Figure 16. (a) Boxplot of flue gas temperatures at key locations in the boiler: bed; after superheater, a-SH; after economizer, a-Eco; after LUVO, a-LUVO; before ESP, b-ESP. Mean temperature is annotated. (b) Fuel load, steam power and O_2 concentration in the wet flue gas.

3.4.2 Fuels

Table 4 lists the recipe of pure fuels used to prepare the fuel mixture. F1 to F3 are for the assessment phase (see Figure 15) and F4 is the target mixture for the performance analysis test (see Figure 15). The ultimate analysis of the pure fuel used in the study is in Table 5. Test point V used sludge 1 and SRF 1 because it was performed a week earlier compared to the rest of the test.

The gross calorific value (mean = 21 ± 0.7 MW/kg, d) and the concentration of C, H, O in the pure fuels do not vary significantly.

Variation of minor and trace components is high. The range of the coefficient of variation (standard deviation/mean) for the concentration of minor element is 0.41–1.51 while for the trace element 0.75–2.34. For the minor elements, the concentration of Cl, Ca, Mg and Ti is highest in SRF relative to the other fuels. The concentration of S, Na, Al and Si is comparable for the sludge and SRF. Peat and bark have low concentrations of minor elements compared to the other two fuels. For the trace elements, the concentration of Zn, Sn, Sb, As, Pb, Cr, Co, Cu, Ni and V is highest in the SRF. In the fuel mixture, increasing the proportion of SRF increases the concentration of these elements.

Table 4. Fuel mixture showing the pure fuel components used and their corresponding energy share.

Fuel Components	**Energy Share, [%]**			
	F 1	**F 2**	**F 3**	**F 4**
SRF	50	50	60	70
Bark	44	10	-	24
Sludge	6	6	6	6
Peat	-	34	34	-
Test point	I, II, II, III	IV	V	VI - IX

Table 5. Properties of the pure fuel. Analyses were carried out according to appropriate CEN/Ts, ASTM and ISO methods.

Properties	Units	Fuel					
		Sludge 1[a,b]	Sludge 2[a,c]	SFR 1[b]	SFR 2[c]	Peat[d]	Bark[d]
Gross calorific value	MJ/kg, d	20.20	20.19	21.86	22.26	21.56	20.39
Net calorific value	MJ/kg, d	18.92	18.91	20.39	20.80	20.34	19.06
Ash content (815°C)	wt%, d	7.6	6.7	12.3	10.7	3.1	1.7
Ash content (550°C)	wt%, d	8.0	6.9	14.0	12.3	3.2	2.2
Volatile matter	wt%, d	73.5	74.8	75.0	75.8	69.6	77.9
Total moisture	wt%	68.5	67.9	45.5	45.0	49.8	63.5
Major Components	wt%, d						
C		49.3	49.3	50.6	50.6	54.3	51.8
H		5.9	5.9	6.8	6.8	5.6	6.1
N		1.81	1.81	0.61	0.74	1.16	<0.3
S		5	4.9	4.7	4.6	1.8	0.2
O (calculated)		34.5	35.6	27.5	29.1	35.6	39.6
Minor Components	mg/kg, d						
Cl		200	160	3700	7000	250	90
Br		30	20	50	30	20	<10
Ca		14100	11100	24400	23600	3600	5600
Mg		840	620	2400	2900	830	630
Na		2300	1800	2300	2100	440	400
K		970	820	2100	1800	600	1600
P		1800	1600	440	160	340	430
Mn		1100	1200	110	84	62	260
Fe		830	630	4400	2300	2900	330
Al		5700	5400	7000	5400	2200	420
Si		11400	10400	17500	12300	5600	1500
Ti		91	78	1800	1800	94	32
Trace Elements	mg/kg, d						
Zn		82	63	180	230	9.6	65
Sn		0.56	0.63	11	26	<0.5	<0.5
Cd		0.25	0.21	0.3	0.76	0.09	0.24
Tl		<0.5	<0.5	<0.5	<0.5	<0.5	<0.5
Hg		0.26	0.49	0.08	0.1	<0.05	<0.05
Sb		<0.5	0.57	42	150	<0.5	<0.5
As		0.92	0.78	16	20	1.1	<0.5
Pb		3.2	2.8	42	68	2.9	0.59
Cr		7.3	5	51	53	3.2	3.2
Co		<0.5	<0.5	8.7	3.7	0.74	<0.5
Cu		13	9	80	3200	2.5	12
Ni		1.9	0.69	20	12	0.77	<0.5
V		1.8	1.4	13	11	2.7	<0.5

a. Wet sludge collected before the thermal drying plant.

b. Used for test point V.

c. Used for all test points except test point V.

d. Used for all test points.

3.4.3 Sampling techniques

To examine the risk of corrosion to the superheater, we collected flue gas composition and condition, aerosol composition, and deposits near the vicinity of the secondary superheater, indicated by point 4 in Figure 8. During the performance stage, additional aerosol samples were made at the back pass (point 5 in Figure 8) to assess for possible risk of corrosion in the economizer and air preheater. Corrosion at these heat exchange surfaces is associated with lead and zinc chloride deposition.

Gas properties and composition were collected using GASMET Fourier transform infrared spectroscopy. Aerosol sampling was made using Dekati Low Pressure Impactor (DLPI), each sampling lasting for 40 minutes: see dashed region in Figure 17. The impactor deposits were digested with water for five days and subjected to ultrasonic mixing prior to extraction. The method employed is similar to the discussions in Section 3.3.3 with the addition of Si and Al.

Deposits were collected using an air-cooled probe (38 mm diameter, 1.9 m long with 1.4 m in contact with the flue gases) and equipped with a detachable metal ring. The temperature of metal ring facing the wind side is held at around 500°C and the flue gas temperature is c.a. 700°C. Deposits were sampled at three locations along the circumference: on the side facing the flow (wind), 30–40° (side) and 180° (lee). The deposits were placed on copper tape strip and sent to SEM/EDS for analysis. Each sampling lasted for 2 hours. Additional features of the sampling procedure are found in [35].

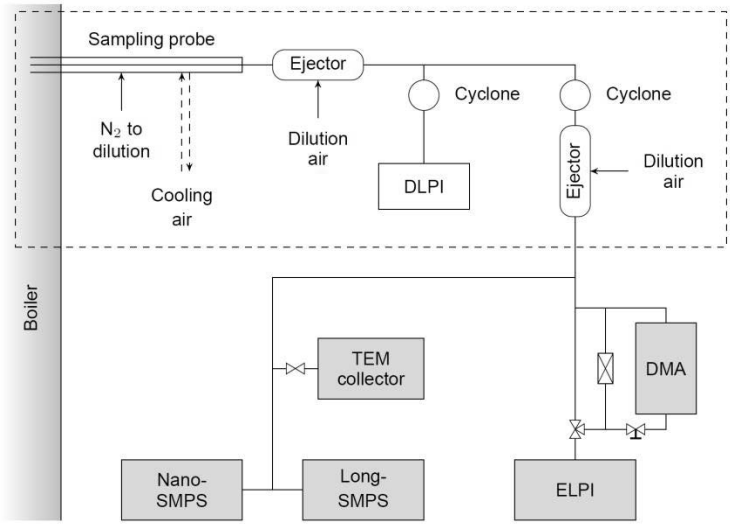

Figure 17. Schematic diagram of the particle size distribution sampling system. The system enclosed by the dashed line is similar to the DLPI system used to sample aerosols for chemical analysis (from Paper V).

The particle size distribution of fine particles was measured using two parallel scanning mobility particle sizers (SMPS) enabling the measurement of high resolution aerosol particle size distribution. The Nano-SMPS is used for measuring particles in the size range of 3–65 nm, and the Long-SMPS are for particles falling in the 10–422 nm size range. In addition, TEM collector and an ELPI-differential particle analyzer (DMA) system are installed.

3.4.4 Relating flue gas conditions and risk of corrosion

The quality of the flue gas arriving in the superheater has a significant impact on the risk of corrosion. Modeling of the arrival of corrosive species to critical heat exchange areas such as the superheater is in various state of development. Zhou et al. divides the ash deposition models as: empirical indices models, mechanistic models, and computational fluid dynamics (CFD) models [127]. The objective of these models is to examine the importance of a given parameter e.g. temperature to a certain response. However, process data from large scale combustion systems are often plentiful and collinear. Collinearity makes the use of process data as predictors challenging for classical multiple linear regression (MLR) because MLR requires a full rank for the matrix of predictor variables [128].

To solve the issue of multi-collinearity, partial least squares (PLS) regression is used to relate flue gas conditions and the quality of the superheater deposits. PLS regression is a method that generalizes MLR and is particularly useful in dealing with collinear predictors. The goals of PLS regression and MLR are similar, being to predict the response (**Y**) given a set of predictors (**X**). A more detailed and exhaustive explanation on the method is found in [129].

We implemented PLS regression using the PLS_Toolbox installed in Matlab 2014a [130].

4. Experimental results – Production and abatement of PCDD/F (Paper I to III)

PCDD/F production in WtE systems is a function of several factors. The focus of this work is to examine one of these factors – the dynamics of copper in the BFB boiler and its effect on the production of PCDD/F in the said system. This chapter presents the results and discussion of Papers I to III.

4.1 Levels of SO_2 and HCl in the backpass[2]

Hunsinger et al. prescribe that only maintained levels of SO_2 (relative to HCl) are required to lower PCDD/F production in their grate incinerator. The ratio of HCl to SO_2 (both measured as mg/Nm^3) equal to 1:1 should be maintained [47]. We used this ratio as a guide to set the dosing level of S in the BFB boiler. The concentration of SO_2 and HCl during the three test cases is presented in Figure 18.

Sulfur addition increased the SO_2 concentration in the flue gas from 20 $\pm$ 8 mg/Nm^3 for Case 1 to 400 $\pm$ 80 mg/Nm^3 and 400 $\pm$ 100 mg/Nm^3 for Cases 2 and 3, respectively. The SO_2 concentration was stable for Case 1 and 2, but in Case 3 a slight increase was noted from 3:00 pm onwards. The latter can be the result of variations in the S content of the peat. In terms of stability, the use of sulfur pellets is better as compared to peat. In the long run, the stability of the SO_2 concentration is important for effectively reducing the PCDD/F production [47].

The concentration of HCl in the flue gas likewise increased from 200 $\pm$ 20 mg/Nm^3 to 300 $\pm$ 30 mg/Nm^3 for S-pellet addition and to 320 $\pm$ 30 mg/Nm^3 for peat co-combustion. Such an increase occurred even though the concentration of Cl in the fuel decreased (Table 2). This observation is similar to what Raghunathan and co-workers observed [46] and suggests a possible occurrence of a reaction (5) which decreases the amount of $Cl_{2(g)}$ in the flue gas. Sulfation of alkali chlorides and oxidation of S pellets could also be responsible for this increase in SO_2 concentration.

[2] Numerical figures in the second and third paragraph have been adjusted to correct significant figures.

The required HCl/SO_2 ratio of 1/1 [47] was not reached. However the ratios for Case 2 and 3 are near, at 0.745 and 0.703 respectively (see annotated values in Figure 18). The value of ratio for both cases is greater than 1, which suggests over addition of sulfur to the BFB; this was made to ensure a sufficient amount of S is available for sulfation and saturation of S in boiler deposits.

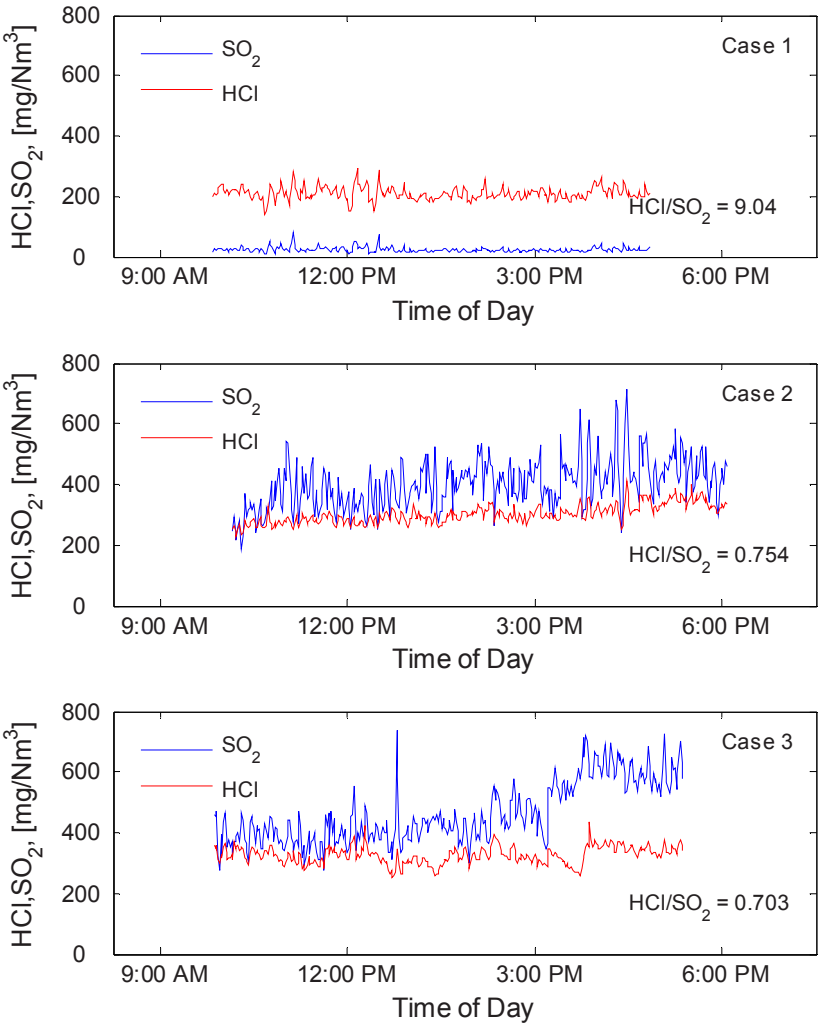

Figure 18. Levels of SO_2 and HCl in the backpass for the three test cases as measured by the FTIR.

4.2 Aerosols

For all the impactor results, fine particles found in the region of $d_p < 1.6\ \mu m$ were once in vapor form. Due to supersaturation, in the gas phase, they have undergone homogeneous nucleation and coagulation. Particles found in the region of $d_p > 1.6\ \mu m$ represent coarse particles that are mostly non-volatile fragments of the fuel or ash, and/or entrained particles [131,132].

4.2.1 Main aerosol forming elements

For Case 1, the aerosols are mostly Na, K and Cl, with slight amounts of SO_4 (Figure 20 on p. 55). In the fine particle mode, the molar ratio Cl/(Na + K) = 0.95 indicates that the alkalis present are mostly alkali chloride with some alkali sulfate. This is similar to aerosol data collected near the superheater region of other boilers firing the waste derived fuels [13,81] without the aid of anti-corrosion additives. The coarse particle fraction showed a significant amount of water soluble Ca, possibly as $CaSO_4$. The formation of $CaCl_2$ is less likely since some Na and K are also present in this fraction.

In Case 2 the fine particle fraction is composed of Na, K, and Cl with more SO_4 present. The molar ratio Cl/(Na + K) = 0.61 indicates that more of the alkalis present can now be found as alkali sulfates. The sulfation of the alkalis can proceed via reaction (15) [77,78,133]. The same reaction holds for the homogeneous sulfation of gaseous alkali chlorides, $MCl_{(g)}$. The required SO_3 in reaction (15) could have come directly from the oxidation of sulfur from the fuel, alkali sulfation, or from reaction (5). The latter is possible because of the increase in HCl resulting in co-production of SO_3 (see Figure 18).

Sulfation requires sufficient time and results in particle growth [78,134]. Kassman and co-worker report growth in fine particle size from 0.1 μm to 0.4 μm in a reference case test for S- addition [85]. Such growth is seen when Cases 1 and 2 are compared, as the peak concentration shifted from 0.09–0.26 μm to 0.26–0.6 μm. The increase of SO_4 and peak shift suggest successful alkali sulfation.

For Case 3, the size distribution is still bi-modal but the peak in the coarse particle range is now higher than in the fine particle range. In the coarse particle range, significant amounts of Ca and Cl are present with fewer alkalis, less than half of Case 1). This suggests the presence of $CaCl_2$, $CaSO_4$ and some alkali chlorides or sulfates. In the fine particle range, the total amount of Na and K (0.91 mmol/Nm^3) is almost half of that in the two other cases (1.56 mmol/Nm^3 for Case 1 and 1.72 mmol/Nm^3 for Case 2); even though the concentration of Na and K in the fuel mixture for Case 3 is almost twice that in the two other cases: see Table 3. Three probable reasons can explain this observation. First, the difference in the mode of occurrence of Na and K in the fuel mixture used in Case 3 relative to the

two other cases. Second, sulfation via reaction (15) might have occurred because of the presence of SO_4 in the aerosol, with SO_3 being sourced again from reaction (5). Third, chemisorption of alkali aluminosilicates. which converts gaseous alkali chloride to water-insoluble alkali-aluminosilicate [77].

The chemical fractionation results (Figure 19) suggest that the decrease of alkalis in the aerosols for Case 3 is most likely the result of the mode of occurrence of Na and K in the fuel. With peat substituting bark in the fuel mixture for Case 3, the total amount of alkalis increased. However these alkalis are “less reactive” and are bound to the aluminosilicates in the peat [135] which lowers the amount of Na and K in the flue gas. Less reactive alkalis are nonreactive alkali compounds that do not appear to participate significantly in the ash chemistry of fluidized bed systems [135]. The SO_4 in the aerosol could likewise be explained by the reaction (15). Through this line of reasoning, the contribution of chemisorption is limited.

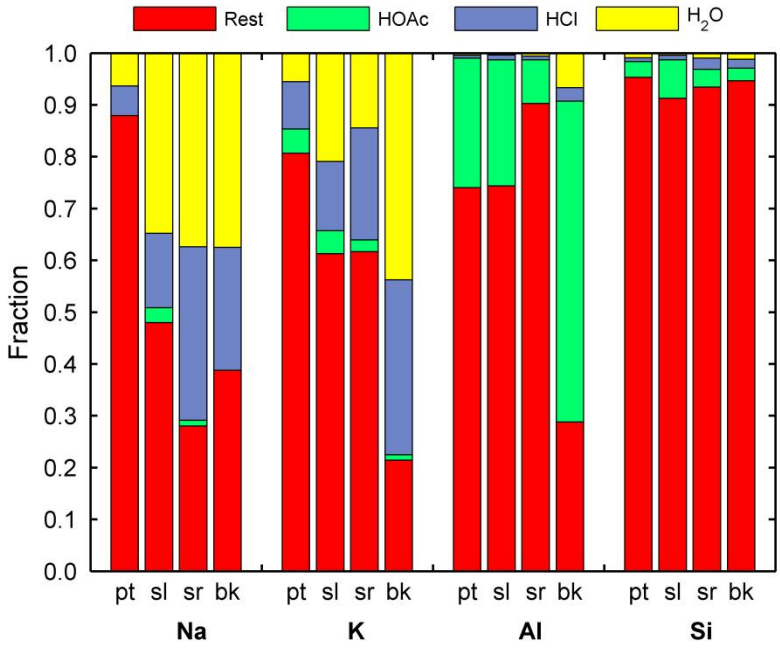

Figure 19. Chemical fractionation of the pure fuels used in the tests – peat (pt), sludge (sl), SRF (sr) and bark (bk).

4.2.2 Copper and bromine in the aerosol

For all the test cases, copper in the fine particle range suggests volatilization of this element. Cases 1 and 2 have cumulative concentrations of 0.036 mmol/Nm^3 and 0.041 mmol/Nm^3 of Cu respectively. However, Case 3 exhibits the least amount of Cu, 0.023 mmol/Nm^3, in the fine particle range even if the concentration of Cu in the fuel mixture is highest, at 670 mg/kg, d. For this case, copper might have been present in a less volatile form (e.g. metallic copper and solid oxides) and has remained in the coarse fly ashes or been retained as part of the fragments of the fuel being entrained in the flue gas.

A shift in the peak in the fine particle range, from 0.09–0.26 μm to 0.26–0.6 μm, from Case 1 to 2 suggests the possibility of $CuSO_4$ formation. Copper existing as $CuCl_{(g)}$ or $CuCl_{2(s)}$ could be sulfated via reaction (15) and (6) respectively. In addition, free $Cl_{2(g)}$ can react with $CuO_{(s)}$ forming a product that can also be sulfated via the two step reaction postulated by Ryan et al. [71]:

$$2CuO_{(s)} + Cl_{2(g)} \rightleftharpoons 2CuOCl_{(s)} \qquad (21)$$

followed by (8).

Takaoka et al. have reported the presence of similar forms of copper oxychloride species using advanced X-ray techniques [25]; this supports the possibility of $CuO_{(s)}$ sulfation.

The occurrence of sulfation is further supported by the increase in the S concentration in the ESP fly ash from 1.44 mg/kg to 2.03 mg/kg for Cases 1 and 2 respectively (Table 6). These two values can easily be compared since the dilution effect of having too much ash is not very significant between these two cases.

Bromine is mostly found in the fine particle fraction and could have existed possibly as (K, Na)$Br_{(g)}$ and $CuBr_{3(g)}$ [14,88]. When Br is present it can compete with Cl for available Cu, which reduces the amount of active *de novo* catalyst such as $CuCl_2$. With respect to PCDD/F formation, it is clear that $CuCl_2$ is an important catalyst either for direct chlorination or as a provider of Cl_2 [93]. On the other hand the catalytic effects of Cu-Br compounds in PCDD/F formation have not been intensively investigated [94].

Table 6. Concentration of selected elements in the fly ash.

Element	Concentration, [mg/kg a.r.]		
	Case 1	Case 2	Case 3
K	2.05	2.05	1.69
Al	10.06	8.26	7.09
Si	17.58	19.73	22.39
Cl	1.61	0.60	0.40
S	1.44	2.03	1.09
Cu	0.26	0.23	0.18

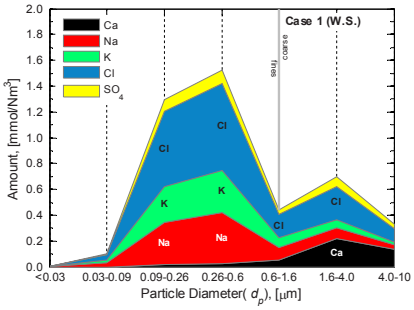

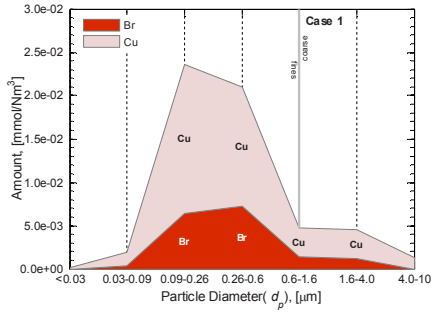

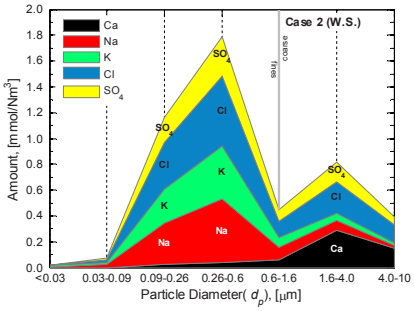

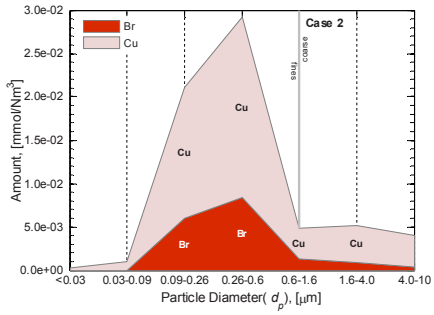

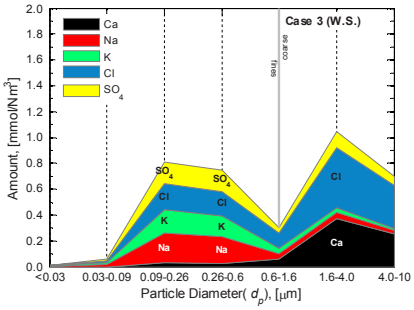

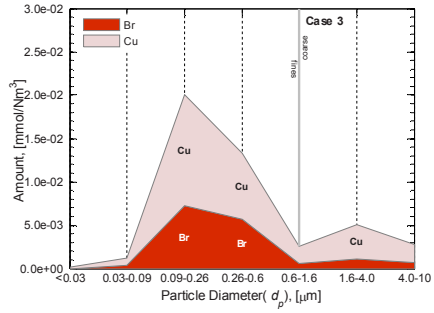

Figure 20. Composition of select water soluble ash and aerosol forming elements collected at the backpass of the BFB boiler.

Figure 21. Concentration of Cu and Br in the aerosols collected at the backpass. Data for copper are based on acid soluble fraction, while data for Br comes from the water soluble fraction.

4.3 PCDD and PCDF production and removal

4.3.1 Total concentrations at different sampling points

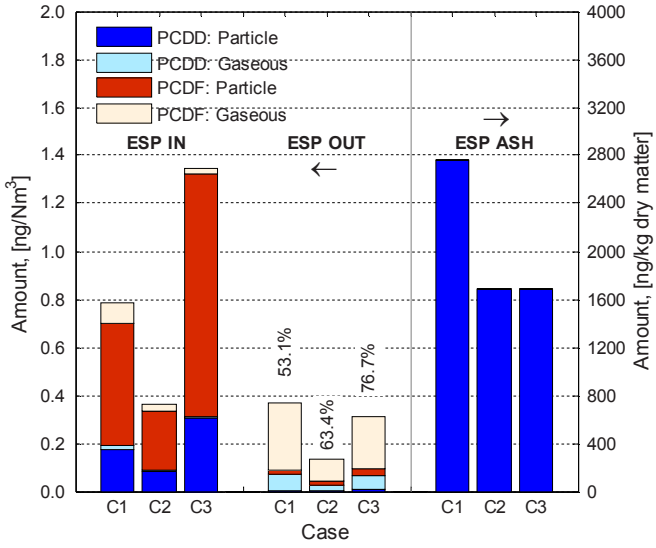

Figure 22. Total levels of PCDD/F in the flue gas path (ESP IN and OUT) and ESP Fly Ash. The values above the bars for ESP OUT are the percentage removals of PCDD/F in the flue gas path.

The total concentration of PCDD/F around the ESP is found in Figure 22. At the ESP inlet, the concentration of PCDD/F is 0.786 ng/Nm^3 for Case 1. Adding sulfur pellets (Case 2) reduced the concentration to 0.363 ng/Nm^3 while co-firing of peat (Case 3) increased the concentration to 1.345 ng/Nm^3. The PCDD/F production did not follow the concentration of Cl in the fuel.

After the ESP, the concentration of PCDD/F for Case 2 is the lowest at 0.133 ng/Nm^3, while Case 1 and 3 have 0.369 ng/Nm^3 and 0.313 ng/Nm^3 respectively. These values show that the ESP is effective in reducing the concentration of these compounds in the flue gas path. But phase redistribution has occurred along the flue gas path; PCDD/F are particle bound in the inlet and they leave the ESP in the gaseous phase (especially furan). This particle to gas phase redistribution is typical in many ESPs [136–139].

As for the ESP fly ash, the concentration in Case 1 is highest compared to the levels for Cases 2 and 3, which are almost comparable. For Case 1, poor sulfation of Cu may have prolonged the existence of active Cu species and have led to

successive chlorination and/or synthesis. This can happen even if the temperature is below the optimum temperature window of 200–400°C [140]. For Case 2, additional chlorination may have occurred but because of effective Cu sulfation, the PCDD/F levels in the fly ash remained low. Meanwhile, the low concentration in Case 3 could simply be the result of dilution. While we cannot exactly quantify the total amount of fly ash for each test, the particle loading data from the aerosol sampling may support this dilution hypothesis (see Figure 23). Case 3 has the highest particle loading in the coarse size range and indicates that there is more fly ash during this case. A high tendency of peat to produce fly ashes when fired has been reported in the literature [141].

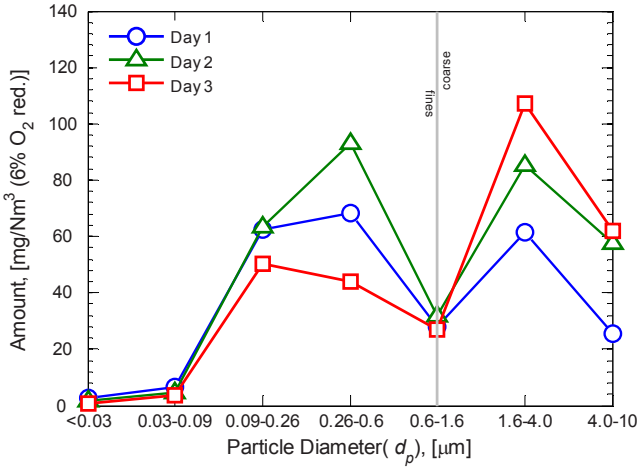

Figure 23. Particle loading at different size fractions in the backpass from the impactor measurements.

4.3.2 Homologue distribution in the flue gas path

PCDD/F homologue distribution can give information on the dominant mechanism of PCDD/F formation and help explain the trends noted above. For all the test cases the ratio Σ_{PCDF} / Σ_{PCDD} > 1 (see Figure 24); this points to the *de novo* mechanism as the dominant means of production [43,54]. The conditions from the backpass to the LUVO are suited for this mechanism; the flue gas is cooling to the right temperature window, the residence time requirement is met (order of seconds, 2.9 sec at 340°C [54]) and the deposition of carbon rich ash can occur.

Dioxin and furan concentrations are highest for the lighter homologues, penta-chlorinated dibenzo-p-dioxins (5D) and penta-chlorinated dibenzofuran (5F). The phase distribution favors species to be bound to particles. This suggests that the key ingredients for *de novo* synthesis are present in the active fly ash.

The difference between the levels of production between Cases 1 and 2 can be explained by the deactivation of the key *de novo* catalyst, Cu. With the introduction of S-pellets, effective conversion of copper oxides and chlorides to sulfates may have been possible, as supported by the aerosol data in Figure 21. Metal sulfates, unlike metal chlorides or oxides, are not likely to promote the formation of PCDD/F [71]. In addition, the availability of free $Cl_{2\ (g)}$, an active ingredient for PCDD/F formation, may have decreased in Case 2, as discussed in Section 4.1.

The high concentration of PCDD/F for Case 3 is a result of high ash loading in the flue gas and low Cu volatilization. These two situations enhanced the possibility for Cu (in the form of oxide and oxychloride [25]) to remain in the ash and act as a catalyst for cracking carbon matrices to form structurally related material [29]. Cu may also have easily aided in the shuttling of $O_{2\ (g)}$ and $Cl_{2\ (g)}$ to the active fly ash surface, thus adding to its effectiveness as a catalyst for chlorination. In addition, particles can serve as effective and porous support where Cu, Cl, and partially burned or unburned carbon can adsorb. These observations benefit the in-flight PCDD/F production via *de novo* mechanism.

For all the test cases the homologue distribution patterns of PCDD/F in the outlet of the ESP are almost similar to patterns at the ESP inlet; dioxin and furan concentration peaks are seen at the lighter homologues, penta-chlorinated dibenzo-p-dioxins (5D) and penta-chlorinated dibenzofuran (5F), respectively. This is an indication that the succeeding reaction or chlorination may not have occurred in the ESP flue gas path. The ESP was operated at a temperature 10°C below the temperature window for *de novo* synthesis [43,54,138] preventing subsequent reactions in the flue gas path.

Also the phase distribution of PCDD/F at the ESP flue gas path outlet now favors gaseous dioxins and furans. Changes in the concentrations of PCDD/F homologues between the two phases are found in Figure 25. The gas phase removal is negative, indicating vaporization or repartitioning of PCDD/F from the particle to the gas phase [51],[54]. Vaporization can be affected by temperature [142], particle density and size distribution [144].

The increase in the gaseous furans is higher than that of dioxins. Factors affecting these are (a) original amount – there are more furans than dioxins to begin with, therefore if both are vaporized the change in furan should be higher, (b) the vapor pressure of furans is slightly higher than that of dioxins. For instance at 25°C the vapor pressure of 1,2,3,4-tetrachloro dibenzofuran is 1.223×10^{-4} Pa while for 2,3,7,8-tetrachloro dibenzo-p-dioxin is 1.044×10^{-4} Pa [145].

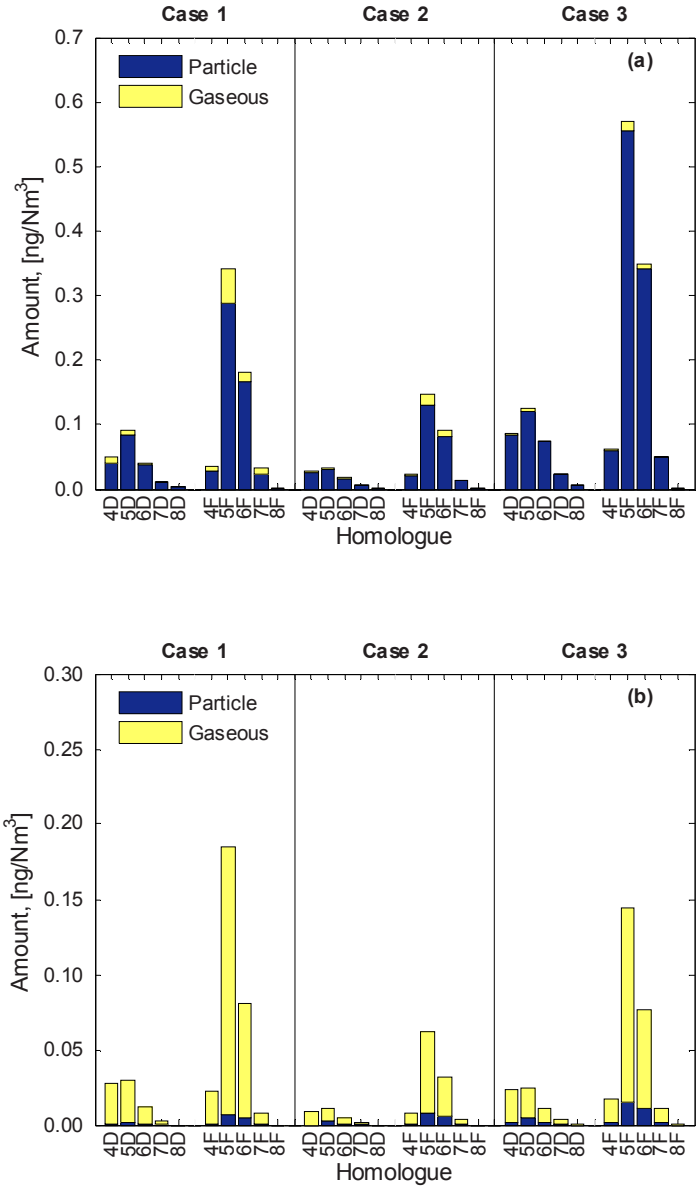

Figure 24. Flue gas path homologue distribution patterns of toxic PCDD/F in (a) ESP IN (b) ESP OUT.

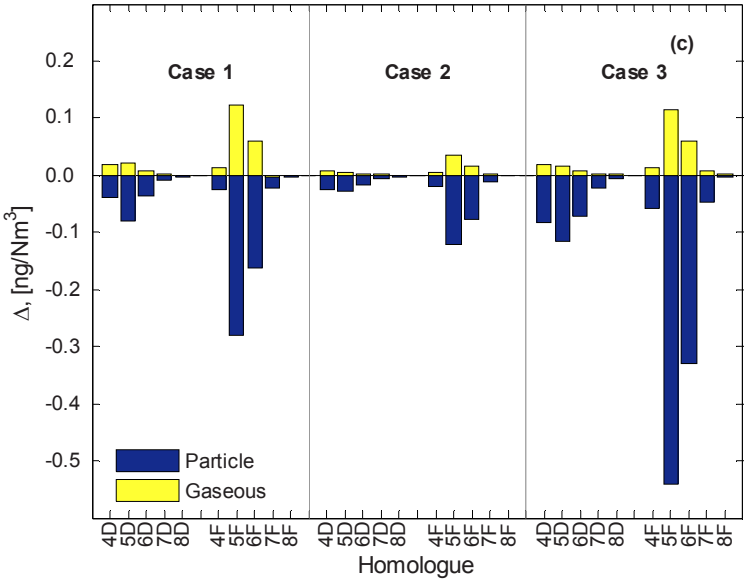

Figure 25. Changes in particle bound and gaseous concentration of PCDD/F or the removal homologue distribution.

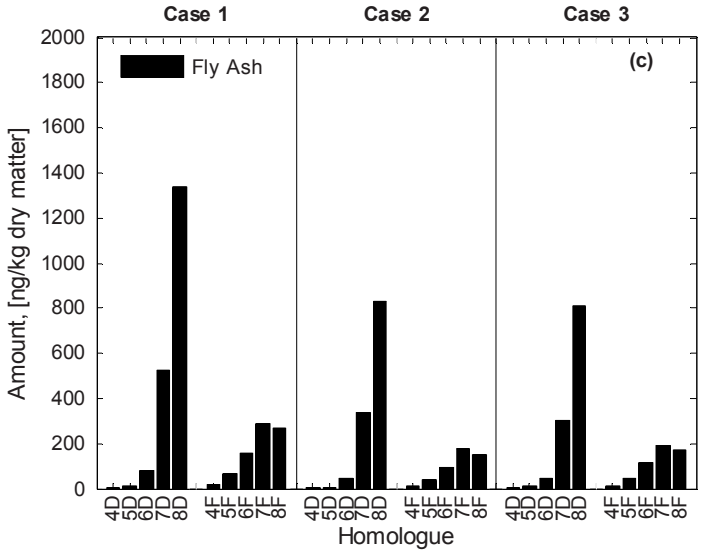

Figure 26. ESP fly ash homologue distribution patterns of toxic PCDD/F.

4.3.3 Homologue distribution in the ESP fly ash

In comparison to the homologue distribution in Figure 24, the distribution for the ESP fly ash peaks at higher chlorinated dioxins and furans: see Figure 26. Heavier homologues, octa-chlorinated dibenzo-p-dioxins (8D) and hepta-chlorinated dibenzofuran (7F), are dominant. In addition the $\Sigma_{PCDF} / \Sigma_{PCDD} < 1$, indicating subsequent chlorination or production in the fly ash. This implies that particle bound PCDD/F and catalysts such as copper and chlorine found in carbon matrices are still active. These reactions however may require longer time and therefore have not contributed additional PCDD/Fs in the flue gas path. Furthermore, ageing of the sample may also have contributed to this shift in the distribution patterns.

4.4 Staged-equilibrium process modeling results

This subsection presents the results of the process model discussed in Section 3.3.8. The purpose of the model is to explain the behavior of major aerosol forming elements as well as Cu and Br, and use these understandings to explain the levels of PCDD/F presented earlier.

4.4.1 Coarse particle loading

The coarse size fraction measured in the backpass indicates that Case 3 gave the highest amount of coarse particle loading, while Case 1 registered the least: see Figure 23 or Table 7.

The amount of particles entrained in 846Rd follows the trend mentioned above (see Table 7)**.** The model estimates that the amounts of particles entrained for Case 1 (17.12 g/kg fuel fed) and Case 2 (18.36 g/kg fuel fed) are nearly equal. This is expected because the fuel mixtures for these two cases are similar. In both cases, the change in the amount at the condensed phase between 846Rd to 510BP is large, at 35.21% and 42.21% respectively. This suggests that the fly ashes are not fragments of the original fuel but are formed from the condensation of some species in the flue gas moving from the splash zone to the backpass.

Table 7. Coarse particle loading measured by DLPI and the entrained condensed phase in 846Rd and 510BP. The coarse particle loading corresponds to aerosols within the size range of 1.6–10 μm .

Case	Coarse particle loading	Entrained Condensed Phase in 846Rd	Fly ash in 510BP	% increase in condensed phase between 846Rd to 510BP
	[mg/Nm^3]	[g/kg fuel fed]	[g/kg fuel fed]	
1	87.1	17.12	23.15	35.21
2	142.8	18.36	26.12	42.21
3	168.9	60.87	67.30	10.58

Case 3 has the highest amount of condensed phase entrained in 846Rd, 60.87 g/kg fuel fed. However it has the lowest change in the amount of condensed phase between 846Rd to 510BP, 10.58%. This indicates that majority of the fly ash is carried over from the splash zone. These observations are consistent with reports on peat co-combustion combustion [118,135,146]. Peat is rich in alumino-silicates and other ash forming compounds. Nonvolatile fuel fragments are usually formed in the lower part of the boiler and are entrained in the fluidizing air. These results also agree with the chemical fractional results presented in Figure 19.

4.4.2 Main aerosol forming elements

The partitioning of aerosol-forming elements between the bottom ash, fly ash and flue gas is calculated for the subsystem 846Rd-852Ox (SS) and the whole system 846Rd-510BP (WS) are shown in Figure 27 (a) and (b) respectively.

For SS, the model predicts that the partitioning of Na and K in the fly ash increased from Case 1 to Case 2. For Case 1, the alkalis are mostly present in the flue gas as KCl and NaCl; some are present as sulfates. For Case 2, Na_2SO_4 and K_2SO_4 were formed together with $KAlSi_2O_6$ and $NaAlSiO_4$. Formation of alkali sulfate in the model supports the occurrence of sulfation detected in the experiments. Meanwhile the calculated alkali-aluminosilicate is the result of the two-fold increase in Si content of the fuel mixture for Case 2.

However, the partitioning evaluated for WS failed to show the trends of experimental results because alkalis are mostly present as solid compounds (salts and silicates). One could no longer detect the expected increase in the partitioning of alkalis in the fly ash resulting from sulfation.

For Case 3, the model suggest that around 30% of the alkalis in the fuel partitioned to the bottom ash. This was true for SS and WS. For all the stages, 98% of Na and K were present as $KAlSi_2O_6$ and $NaAlSi_3O_8$ respectively. This agrees with

the results of (1) chemical fractionation that shows that the majority of the alkalis are “less reactive” and (2) aerosol samples that suggest alkalis are less volatile during SRF-peat-sludge combustion.

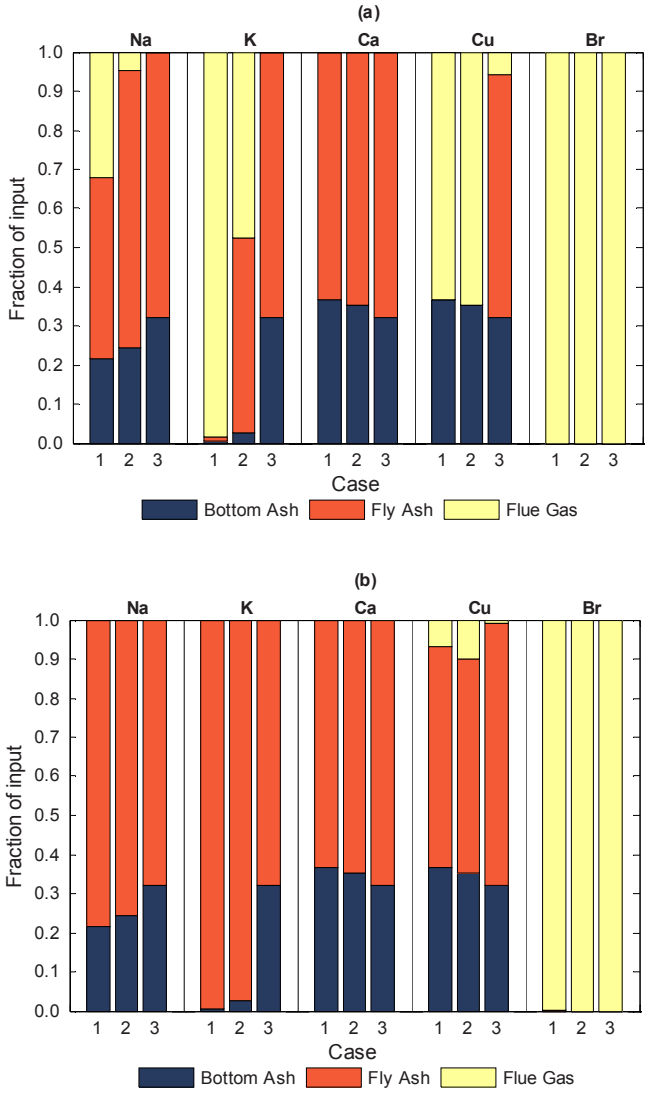

Figure 27. Partitioning of aerosol forming elements in the bottom ash, fly ash and flue gas at (a) 852Ox and (b) 510BP.

Calcium found in the DLPI was mostly in the coarse particle fraction. This suggests that few gaseous Ca species formed during the tests. In the model, Ca parti-

tioned between the bottom and fly ash alone. For all cases, gaseous species of calcium were not detected.

The results above show that the subsystem 846Rd-852Ox (SS) can more closely predict the results of the aerosol measurements. On the other hand, 846Rd-510BP (WS) overestimates condensation of the alkalis in the backpass. The current model cannot handle the influence of kinetics and other transport limitations at 510 °C (temperature of 510BP). This is the reason for the overestimation.

In the current model, no attempt was made to account for these kinetic and transport limitations. We assume that reactions after the introduction of the tertiary air may have been frozen, meaning succeeding reactions are halted, [147] due to the phenomena cited above, and the properties of such a “frozen” system were reflected in the aerosol samples.

4.4.3 Copper and bromine

Cu and Br in the aerosols were mostly found in the fine particle fraction, <0.03–1.6 μm. This indicates the presence of gaseous Cu and Br species for all the test cases. It was also established that Cu was least volatile for Case 3.

Similar to the main aerosol forming element, the partitioning of Cu and Br evaluated for WS overestimated condensation (Figure 27b). On the other hand, SS shows the expected partitioning of Cu and Br. In Figure 27a, the amount of Cu existing in the flue gas fraction is small in Case 3 as compared to that of Cases 1 and 2, supporting the findings of the aerosol sampling. Meanwhile, all Br partitioned to the flue gas.

Analysis of equilibrium species calculated by the model for these two elements reveals their dominant mode of occurrence at a given stage in the boiler: see Figure 28. First, Cu exists as Cu_2S(s3) at the reducing zone and becomes CuCl(g) (for Case 1 to 3) and CuO(s) (for Case 3 alone) as it transitions from 846Rd to 906Ox. The formation of CuO(s) after secondary air injection is unique to Case 3 and explains the apparent decrease in volatility of copper as measured by the DLPI.

Most of the bromine exists as KBr(g) and NaBr(g) in the splash zone for Cases 1 and 2, while HBr(g) for Case 3. The latter is explained by the high amount of Si and Al if the fuel mixture used in the calculation for Case 3, without the necessary reactivity restrictions for Si and Al the model does not favor formation of alkali bromide because the alkalis are bound to Si and Al. At 906Ox and 852Ox the amount of alkali chlorides decreased to favor formation of other gaseous bromine species: $CuBr_3$ for Case 1, HBr(g) and $CuBr_3$(g) for Case 2 and Br(g) and $CuBr_3$(g) for Case 3. As flue gas cools Br competes with Cl for Cu to form $CuBr_3$ (g). In Figure 28 (a) and (b), the concentration CuCl(g) decreases as $CuBr_3$(g) are formed in 852Ox.

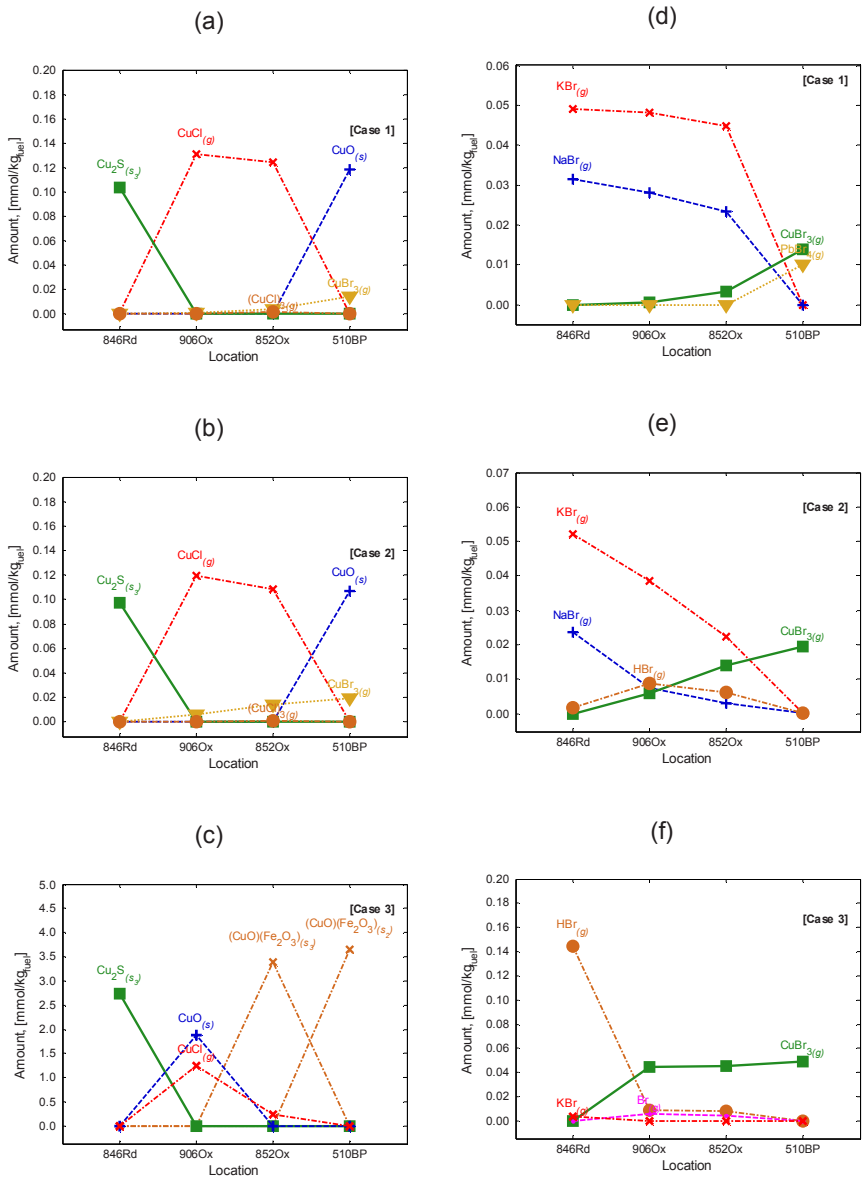

Figure 28. Top species of Cu (a-c) and Br (d-f) at different stages in the BFB boiler as predicted by the staged equilibrium process model.

4.4.4 $CuSO_4$ formation

Formation of $CuSO_4$ was not detected even at 510Ox where the temperature is lower than the decomposition temperature of $CuSO_4$ (572–678°C) [148]. The presence of significant amounts of Ca in the fuel mixture led to the capture of most of the sulfur in the system. This is because the formation $CaSO_4$ is more thermodynamically favorable than $CuSO_4$. At 825°C the phase stability diagram in Figure 29a indicates that the partial pressure of SO_2 should be greater than 0.1 to support the formation of copper sulfate as $(CuO)(CuSO_4)_{(s)}$. The levels required for this formation may not be practical or feasible with the current boiler set-up. On the other hand Figure 29b predicts that at 510°C formation of $CuSO_4$ is feasible even at slightly lower concentrations of SO_2. Overestimation of $CaSO_4$ formed using the current modeling approach may explain why formation of $CuSO_4$ was not detected by the model.

Harriot et al. and Gullet et al. have shown that adsorption of sulfur compound on copper surfaces is possible leading to the subsequent formation of $CuSO_4$ [148,149]. However their studies also reveal that the formation of $CuSO_4$ requires longer residence time (in the order of minutes) and is therefore kinetically governed.

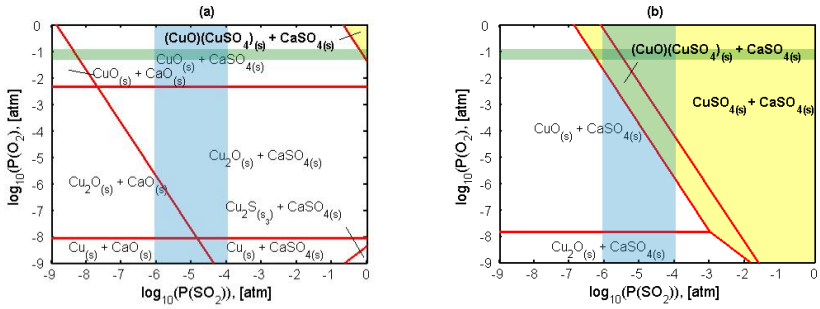

Figure 29. Phase stability diagram of Cu-Ca-S-O system at (a) 825°C and (b) 510°C at 1 atm pressure, 0 < Ca/(Cu+Ca) < 1. Diagrams are generated in FactSage 6.3.1. The shaded region in yellow corresponds to a concentration favorable for $CuSO_4$ formation. The region shades in blue and green corresponds to the approximate SO_2 and O_2 levels measured in BP.

4.4.5 Active and passive species of Cu

Figure 5 (page 24) shows chlorides, oxide, and oxychlorides of Cu are active catalysts in the formation of PCDD/F. Their role can either be as a chlorinating agent, as a catalyst in the cleavage of carbon matrices, or both. Meanwhile, $CuSO_4$ is the deactivated form of the *de novo* catalyst. In addition, Section 4.4.3

showed that the formation of Cu-Br compounds is in competition with Cl for available Cu thereby reducing the formation of copper chloride. Compared to Cu-Cl, an accepted mechanism for the catalytic role of Cu-Br species focused on the formation of PCDD/F alone is not yet available [93,150].

With these observations, we can define the empirical molar active/passive species ratio (APR) as:

$$APR = \left[\frac{(Cu\text{-}Cl) + (Cu\text{-}O) + (Cu\text{-}O\text{-}Cl) + Cu}{CuSO_4 + (Cu\text{-}Br) + Cu} \right] \quad (22)$$

$CuSO_4$ is still included, to indicate that it is part of the passive form of copper with respect to the *de novo* reaction. Metallic copper is present both in the numerator and denominator because it can be chlorinated to become CuCl (active) or as the left-over product of the chlorination (passive) of the carbon matrix.

This ratio is evaluated from the results at 852Ox and 510BP. APR was not evaluated in 846Rd because of the reducing condition at this stage which is different from the oxygen-rich atmosphere of the post combustion zone. Similarly APR was not evaluated in 906Ox because this is still far from the post combustion conditions and the oxidant (air) introduction is not yet complete.

Table 8. APR evaluated at 852Ox and 510BP and the production of PCDD/F in the ESP inlet. R^2 is the square of the Pearson product moment correlation coefficient evaluated through data points PCDD/F at ESP inlet and APR.

Case	PCDD/F at ESP inlet [ng/Nm^3]	APR [unitless]	
		852Ox	510BP
1	0.786	37.459	8.481
2	0.363	7.764	5.497
3	1.345	80.270	74.151
R^2		0.99	0.84

The APRs evaluated at 852Ox and 510BP are found in Table 8. Both APRs have correlation with the PCDD/F levels measured in the ESP inlet. The correlation coefficient is higher for the APR evaluated at 852Ox. This is explained by the earlier observations that 852Ox gives a better picture of what is happening in the backpass as compared to 510BP.

APR increases with PCDD/F at the ESP inlet. This agrees with the nature of the *de novo* mechanism. More active copper species should result in increased PCDD/F formation.

4.4.6 Scenario analysis: Peat-SRF-sludge with low Cu content

To test whether the overly excessive Cu concentration for Case 3 significantly affects PCDD/F production, the concentration of Cu for the fuel mixture is reduced from 670 mg/kg to 26 mg/kg dry solids. The latter is the concentration of Cu in the fuel mixture for Case 1. The concentration of the rest of the elements in the fuel is similar to Case 3.

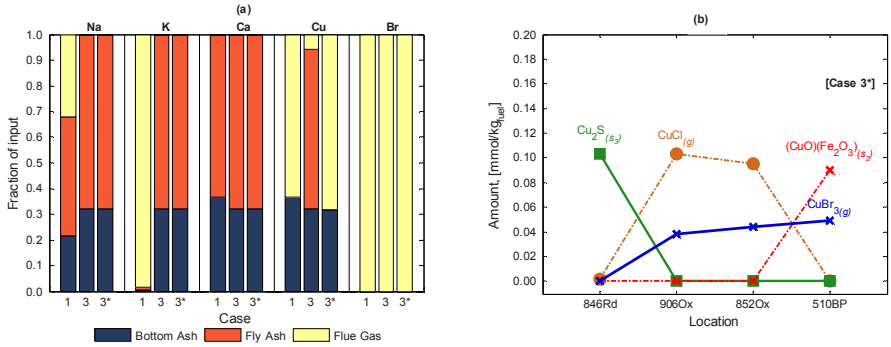

Figure 30. (a) Partitioning of aerosol forming elements in the bottom ash, fly ash and flue gas at 852Ox showing Case 1, 3 and 3*. (b) Top species of copper for peat-SRF-sludge combustion and reduced Cu concentration.

Figure 30a compares the partitioning of the alkalis Ca, Cu, and Br for the scenario being studied (Case 3*) and the two original cases (Case 1 & 3). A decrease of Cu concentration in the fuel does not affect the alkalis, Ca, and Br. On the other hand there was a remarkable increase in the fraction of Cu being volatilized for Case 3*. Cu is present as $Cu_2S_{(s)}$ in the reducing zone and becomes $CuCl_{(g)}$ as it transitions to the first oxidizing zone. As the gas cools, $CuBr_{3(g)}$ and $(CuO)(Fe_2O_3)_{(s2)}$ are formed. However $CuO_{(s)}$ did not form at 906Ox as it did in Case 3.

For the peat co-firing with low Cu content, the APR at 852Ox is 2.195 mol/mol. This APR corresponds to the PCDD/F concentration estimate of 0.30 $\pm$ 0.013 ng/Nm^3. This level is near the value reported for Case 2, indicating that the peat addition strategy may also help in PCDD/F abatement under the strict premise that the concentration of Cu in the fuel is kept as low as possible.

4.4.7 Scenario analysis: SRF-bark-sludge + S-pellet (Case 2) at varying sludge energy share

Increasing the portion of sludge in the fuel mixture can reduce the concentration of several trace elements in the fuel mixture. For this part, the energy share of sludge

is varied according to the proportions in Table 9; note that the SRF/bark energy share ratio is maintained.

Table 9. Energy share simulated at varying sludge energy share and constant SRF/Bark energy share ratio.

Case	SRF	Bark	Sludge	S- pellet
2L	51.60	45.40	3	YES
2	50.00	44.00	6	YES
2H	46.81	41.19	12	YES

The partitioning of key elements for this sensitivity analysis is shown in Figure 31a. Variation in the sludge energy share did not affect the partitioning of Cu, Br and Ca. This is because the speciation of these elements did not vary significantly at the proportions evaluated. As sludge energy share increases, Al and Si concentration increase as well, leading to the enrichment of Na in the bottom ash due to the formation of $NaAlSiO_4$. This resulted in the increase of available Cl for K, causing this alkali to be slightly more volatile at the splash zone.

K is captured by “reactive” Si and Al from the sludge, in the succeeding stages. This could explain why even if K is volatile in the splash zone for Case 2H, the fraction of K in the gas phase (flue gas) is slightly smaller. Alkali capture during sludge co-combustion has been reported by Vanio et al. [13].

The partitioning of Cu did not change with an increase sludge share, though its concentration has been reduced due to dilution. Also, since Br concentration is higher in the sludge, increasing the sludge share led to the passivation of Cu because more $CuBr_{3(g)}$ is formed. Formation of $CuBr_{3(g)}$ decreased APR and the calculated PCDD/F concentration (see Figure 31b). In actual practice, S in sludge may also help enhance $CuSO_4$ formation and further reduce PCDD/F production [48].

This sensitivity analysis presents a possible situation where both alkali chloride deposition at the superheaters and PCDD/F production are reduced due to the synergistic effects of low trace element concentration, alkali capture of Si and Al from the sludge, and sulfation of alkalis and Cu.

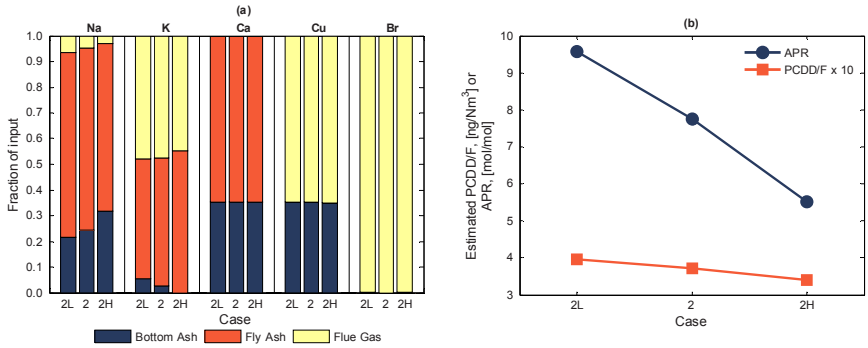

Figure 31. Effects of varying sludge energy share: (a) Partitioning of aerosol forming elements in the bottom ash, fly ash and flue gas at 852Ox; (b) Variation of APR and the estimated PCDD/F. All plots are from the 852Ox stage.

At this point, both S-pellet addition and peat-SRF-sludge co-firing are seen as possible PCDD/F abatement strategies, provided that the amount of Cu in the latter strategy is kept as minimal as possible. In actual practice, peat-SRF-sludge co-firing may still be inferior with S-pellet addition because of the high share of SRF and variability of the concentrations of trace elements in the SRF. In the succeeding sections, the formation of $CuSO_4$ is experimentally investigated using advanced X-ray absorption techniques to settle which strategy can lead to more successful sulfation.

4.5 Elemental analysis and morphology of the ESP fly ash

The concentrations of major and trace elements in the ash samples are found in Table 10. In general, the concentration of main ash forming elements Si, Ca, Al, and Fe, which are referred to as ash matrix forming elements [151], is higher in the samples collected in the first field as compared to the second field of the ESP. The first field of the ESP is designed to capture the coarse particles which are usually fragments or inert components of the fuel or fuel mixture being fired in the boiler [97]. This field is also designed to capture entrained bed materials.

The next group is the salt-forming group consisting of K, Cl, and S. The definition of “salt” is somewhat inaccurate, but here we refer to it to as low melting point water soluble fractions in contrast to the high melting point inert and insoluble oxides [76]. In general, the concentration of the salts is higher in the second field which collects fine particle fractions of the fly ash entrained in the flue gas.

Table 10. Major and trace elements in the ESP fly ashes.

Element (mg/kg a.r.)	Field 1			Field 2		
	Case 1	Case 2	Case 3	Case 1	Case 2	Case 3
Si	111000	108000	164000	69000	78000	101000
Ca	210000	224000	158000	274000	249000	200000
Al	49000	37000	38000	42000	35000	35000
Fe	21000	27000	41000	19000	27000	44000
K	24000	24000	18000	38000	31000	20000
Cl	30000	13000	6000	90000	23000	19000
S	44000	81000	36000	72000	103000	61000
P	6000	5800	3600	6800	7200	4200
Cu	3400	3700	2100	5700	4200	3200
Zn	4100	4300	2500	7700	5700	4400
Cr	380	380	310	480	370	520
Pb	530	510	320	1720	960	790

The fine ESP fly ash fraction is the end product of the complex process of aerosol formation and growth. In the post combustion zone of the BFB boiler, vapor species with a saturation ratio (S_∞) greater than unity start to condense and eventually form particles. S_∞ is the partial pressure of the vapor in the flue gas over the saturation vapor pressure. These particles grow further by condensation on pre-existing particles or via chemical reactions. In addition, particles can collide with each other and form larger particles or coagulate [152]. Agglomerates formed from primary particles tend to partly coalesce together, from fractal-life aggregates to compact spherical structures, via the process called multiparticle sintering [153].

In both fields, the concentrations of K in Case 1 and 2 are comparable, while Case 3 has the lowest. This trend is also true for Cl. These observations agree with earlier findings that the alkalis have poor “reactivity” and volatility during peat co-firing. As a result K may have partitioned to the bottom ash. Without the alkalis, the majority of Cl in the fuel formed $HCl_{(g)}$ and remained in the flue gas.

For the samples collected in the first field, the concentration of S for Case 2 is 1.84 times that of Case 1; this nearly corresponds to the increase in S content of the fuel mixture in Case 1 to Case 2 (see Table 3 on page 34). In the second field, the concentration of S for Case 2 is 1.43 times that of Case 1. These observations indicate the possibility that (1) S was non-volatile and stayed in the ash, or (2) S volatilized, reacted with Ca, alkalis and perhaps even Cu, and condensed back as part of the fly ash. The first possibility is less likely to happen because $SO_{2(g)}$ measured at the backpass for Case 2 is almost 17.5 times that of Case 1 (see Figure 18 in page 51) and the aerosol samples have shown indications that sul-

fation has occurred during S-pellet addition (see Section 4.2). Meanwhile, in both fields S concentration for Case 3 is only 4/5 of S concentration in Case 1 even if the S in the fuel mixture for Case 3 is around 3.42 times that of Case 1.

The trance element group (Cu, Zn, Cr, and Pb) exhibits a similar behavior to the salt-forming group. These elements are enriched in the fine fly ash particles collected in the second field as compared to the coarse particles of the first field. These elements volatilize and leave the fuel in the reducing zones of the boiler either as pure element, or sulfide, or chlorides, or oxides (for Cr) [22] and then condense in the post combustion zones of the boiler [18] and form fine particles in the fly ash. The presence of Cu in the fine fly ashes collected in the second field is important in understanding PCDD/Fs formation.

The morphology of the fly ashes collected in the first field is much coarser and larger relative to the ones collected in the second field (see Figure 32). For the cases with SRF-bark-sludge (Cases 1 and 2) the large particles are a combination of spherical and unstructured morphologies. For SRF-sludge-peat firing (Case 3), large irregular shaped particles have been found together with some slightly smaller spherical particles. These irregularly shaped particles may have been fragments of the peat being used. There are reports in the literature that inert silicate-rich structures in fuels, though possibly subject to fragmentation, retain their morphology even after being subjected to harsh combustion conditions [154].

On the other hand, the morphology of the fly ashes collected in the second field of the ESP is more homogeneous and composed of fine clusters of spherical particles. A higher degree of magnification reveals the detail of these clusters (Figure 32e).

4.6 Crystalline compounds in the ESP fly ash

The relative mass fractions of phases identified by XRD are found in Table 11. Based on the semi-quantitative search-match analysis, the samples collected for both fields are composed primarily of SiO_2 (quartz), $CaSO_4$ (anhydrite), $CaCO_3$ (calcite), various alkali and alkaline earth metal containing tectoalumosilicates $(Na,Ca,K)Al(Si,Al)_3O_8$ (e.g. albeite, microcline, anorthite) and $Ca_2(Mg,Al)Al(Si,Al)O_7$ (e.g. gehlenite and melilite). Present in minor to trace amounts are phases like NaCl (halite), KCl (sylvite), $Ca(OH)_2$ (portlandite), MgO (periclase), Fe_2O_3 (hematite), Al (aluminum), and TiO_2 (rutile). However, due to the complexity of the diffraction patterns, the presence or absence of trace amounts of K_2SO_4 (arcanite), Na_2SO_4 (thenardite) and/or $KNaSO_4$ (aphthitalite) cannot easily be ruled out.

In the same table, the species detected by the thermodynamic model are also indicated. Not all phases detected by XRD are also detected by the model especially albite, gehlenite and microcline for Case 1 and 2.

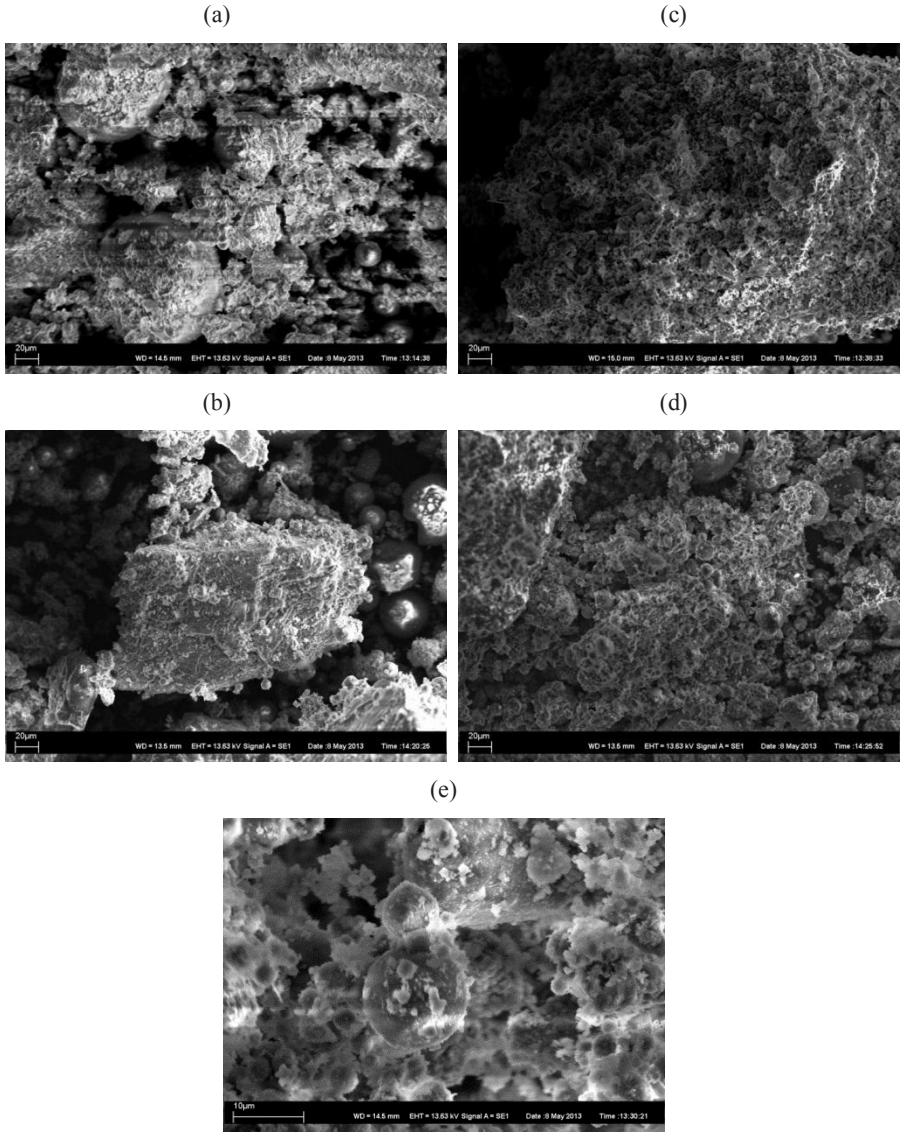

Figure 32. SEM micrographs of the ESP fly ash. (a)–(b) are for the fly ashes collected at the first field, while (c)–(d) are from the second field. The first row is for the SRF-Bark-Sludge (Case 1 and 2) firing while the second row is for the case of SRF-Sludge-Peat firing (Case 3). (e) is from Case 2 fly ash collected at the second field of the ESP. (a)-(d) are taken at 1000x magnification while (e) is taken at 6000x magnification.

For all test cases, the mass fraction of quartz is higher for the samples from the first field as compared to the second field. The impact of peat co-firing to the fly ash is clearly demonstrated by the increase of the relative mass fraction of quartz in the samples collected for Case 3. Furthermore, elevated fractions of $(K,Na)AlSi_3O_8$ (microcline) in samples for Case 3 support poor reactivity and volatility of the alkalis during peat co-firing. Microcline found in fly ashes are formed during combustion [95] or are present as small fractions of original fuel such as peat [155]. This led to a decrease of NaCl (halite) and KCl (sylvite) in Case 3 (vs. Case 1) for samples collected at the second field.

Both sulfur addition strategies reduced halite and sylvite in the sample collected at the second field. For Case 2 this can be the result of sulfation of alkali chlorides. For Case 3, it can be the result of the presence of stable microcline in the fuel mixture which did not allow halite and sylvite to form. In addition, the presence of $(Na, Ca, K)Al(Si,Al)_3O_8$ (albite) in the sample was also detected. Albite is formed from the capture of Na salts at around 576°C by aluminosilicates and by subsequent crystallization [95].

Due to the presence of high amounts of Ca in the fuel mixture, especially for Cases 1 and 2, formation of $CaSO_4$ (anhydrite) was possible. In fact anhydrite is always present in appreciable amounts for all test cases and sampling locations. Anhydrite can be formed by sulfation of $CaO_{(s)}$ released from the organic fraction of the fuel [95].

Table 11. Relative mass fraction of crystalline compounds identified by XRD and thermodynamic model. x means that the species has been detected in the condensed phase at the 3rd and/or 4th stage of the staged equilibrium model

Phase	First Field			Second Field			Thermodynamic Model		
	Case 1	Case 2	Case 3	Case 1	Case 2	Case 3	Case 1	Case 2	Case 3
SiO_2 (quartz)	22	29	38	8	16	25	*x*		*x*
$CaSO_4$ (anhydrite)	14	13	4	32	21	11	*x*	*x*	*x*
$CaCO_3$ (calcite)	7	4	3	24	10	8	*x*		
NaCl (halite)	1	1	1	7	3	2	*x*	*x*	
KCl (sylvite)	1	-	-	4	-	1	*x*	*x*	
$Ca(OH)_2$ (portlandite)	1	1	1	2	2	2			
MgO (periclase)	1	1	-	2	2	1	*x*	*x*	
Fe_2O_3 (hematite)	2	1	1	3	2	3	*x*		*x*
Al (metallic)	3	1	1	1	2	1			
$(Na,Ca,K)Al(Si,Al)_3O_8$ (albite)	18	23	21	2	24	23			*x*
$Ca_2(Mg,Al)Al(Si, Al)O_7$ (gehlenite)	8	6	4	13	13	9			
$(K,Na)AlSi_3O_8$ (microcline)	14	14	19	-	1	12			*x*
$K_2Ca_2(SO4)_3$ (langbeinite)	6	5	5	-	-	-			
TiO_2 (rutile)	2	1	2	2	4	2			

These differences in chemical composition and morphology are indications that the histories of the fly ashes collected in the ESP fields are different. Ashes col-

lected in the first field are composed primarily of large and relatively inert oxides originating from the fuel or from products of attrition or from fragmentation of bed material, while those that were collected at the second field can be traced from the condensation, heterogeneous nucleation or sintering of aerosol-forming elements.

4.7 Cu speciation via Cu K-edge XANES

The purpose of this Cu speciation is to (a) to detect the presence of $CuSO_4$ which is the target compound and the main reason why sulfur was added to the fuel mixture being burned; (b) to assess whether the active/passive ratio, APR, defined above can still correlate with the levels of PCDD/F produced in the post combustion zones of the boiler. The comparison between the original and fitted spectra is found in Figure 33 and the numerical results of LCF are found in Table 12.

Formation of $CuSO_4$ for all the test cases has been confirmed by the results of LCF. Even for the case where no S was added, $CuSO_4$ formation was detected; this is probably the result of having sludge in the fuel mixture. In this study the concentration of S is 0.5 wt.% d.s. in the sludge. Addition of sludge during combustion of SRF has been reported to also contribute in the inhibition of PCDD/F formation as it can also be a sulfur rich source [48]. The additional S may aid the poisoning of active Cu compounds. In the second ESP field, adding S-pellet led to a higher $CuSO_4$ mole fraction relative to peat co-combustion, which exhibited the smallest fraction. Other studies using the same technique have also detected $CuSO_4$ in the fine particles collected in a BFB fired with MSW [58].

The fly ash collected at the first and second field for Case 1 registered a high sum of $CuCl_2$ and CuCl mole fractions. Chlorinated copper is expected to be high in Case 1 because measures to induce or enhance sulfation have not yet been implemented. Gaseous $CuCl_2$ and CuCl leaving the furnace can condense in the post combustion zone and be collected in the fine particle fraction of the ESP fly ash. Eventually, the presence of Cu-Cl together with Cu-O species may further increase the degree of chlorination of the PCDD/F residing in the ESP fly ash. This explains why the degree of chlorination and concentration of PCDD/F in the ESP fly ash is the highest for Case 1.

Likewise the high value of the combined mole fraction of Cu_2O and CuO in both fields also supports the observation that Cu was least volatile for Case 3. LCF reveals that the combined mole fraction of these two compounds in the second field is around 0.331 for Case 3, higher than the 0.300 and 0.309 for Cases 1 and 2 respectively. Cu_2O and CuO are nonvolatile species of copper under typical BFB boiler conditions where the temperature rarely exceeds 1000°C.

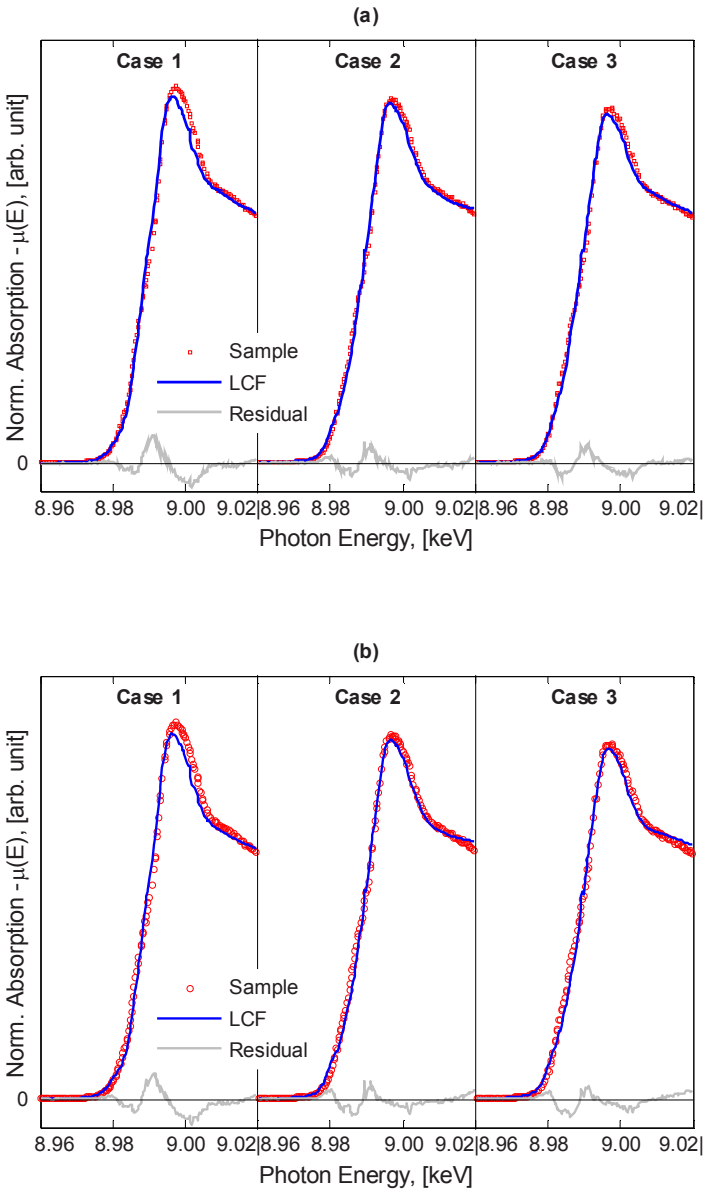

Figure 33. Fly ash sample spectra and LCF results of Cu K-edge Xanes spectra and the residual. (a) is for the samples from the first field and (b) is for the samples from the second field of the electrostatic precipitator.

Table 12. Result of the linear combination fitting of ESP fly ashes. R-factor is defined in (19).

Standards	First Field			Second Field		
	Case 1	Case 2	Case 3	Case 1	Case 2	Case 3
Cu_2O	0.021 ± 0.042	0.057 ± 0.031	0.163 ± 0.039	0.000 ± 0.053	0.000 ± 0.035	0.065 ± 0.036
$CuBr_2$	0.000 ± 0.048	0.000 ± 0.040	0.000 ± 0.052	0.000 ± 0.060	0.000 ± 0.039	0.000 ± 0.041
$CuCl_2$	0.120 ± 0.055	0.000 ± 0.039	0.000 ± 0.050	0.219 ± 0.068	0.037 ± 0.044	0.120 ± 0.046
CuCl	0.118 ± 0.044	0.201 ± 0.046	0.227 ± 0.059	0.040 ± 0.057	0.115 ± 0.037	0.164 ± 0.038
CuO	0.230 ± 0.044	0.307 ± 0.038	0.212 ± 0.048	0.300 ± 0.059	0.309 ± 0.039	0.266 ± 0.040
$CuSO_4$	0.273 ± 0.028	0.216 ± 0.020	0.116 ± 0.025	0.359 ± 0.035	0.359 ± 0.023	0.287 ± 0.023
Cu foil	0.239 ± 0.108	0.218 ± 0.093	0.282 ± 0.117	0.082 ± 0.140	0.181 ± 0.090	0.098 ± 0.096
R-factor	0.0044	0.0019	0.0032	0.0064	0.0030	0.0037
Active*	0.728 ± 0.143	0.783 ± 0.121	0.884 ± 0.153	0.641 ± 0.184	0.642 ± 0.119	0.713 ± 0.125
Passive**	0.512 ± 0.121	0.434 ± 0.103	0.398 ± 0.130	0.441 ± 0.156	0.540 ± 0.101	0.385 ± 0.107
Active/Passive Ratio	1.422 ± 0.437	1.804 ± 0.512	2.221 ± 0.824	1.454 ± 0.663	1.189 ± 0.313	1.852 ± 0.608

* [Cu_2O + $CuCl_2$ + CuCl + CuO+ Cu]

** [$CuSO_4$+ $CuBr_2$ + Cu]

The values of the APR are found in the last row of Table 12 and are plotted against the PCDD/F levels measured at the ESP inlet in Figure 34a. There is no correlation between the APR evaluated in the first field and the PCDD/F concentration. On the other hand APR evaluated in the second field is linearly varies with the PCDD/F levels. This observation is expected since the histories of these two fly ashes are different, as discussed above. The empirical equation was originally developed to take into account the transformation of Cu species existing in the vapor and in the condensed phases in the boiler. Since fly ashes in the first field do not possess this history, the equation's applicability is limited in contrast to the fly ashes collected from the second field. It may also be irrelevant to evaluate APR in the fly ashes from the first field since large fly ash particles have been shown to contain less PCDD/F in respect to the finer ones [156].

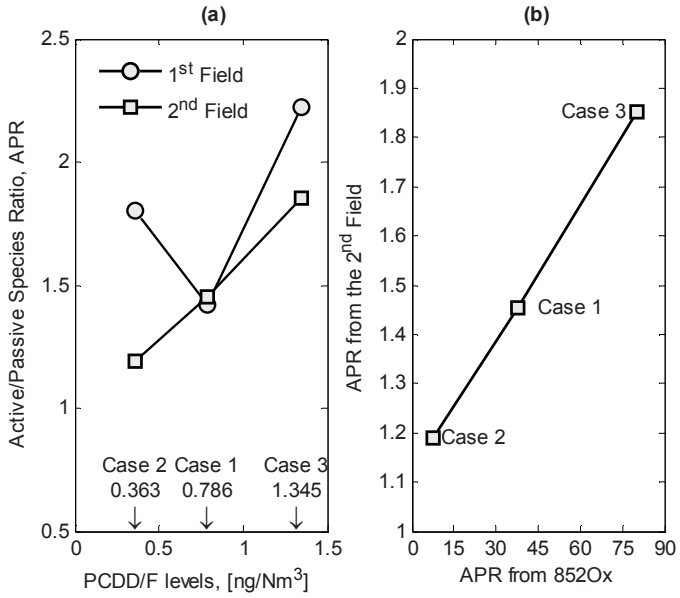

Figure 34. (a) Variation of the calculated APR vs PCDD/F levels measured at the ESP inlet. (b) Comparison between the APR evaluated the 852Ox and second ESP field. Line connecting the points indicate the established trend.

In Sections 4.4.1–3, the APR evaluated at the equilibrium reactor mimicking the region just after tertiary air addition (T = 852°C, λ = 1.379, coded as 852Ox), was able to explain the behavior of aerosol-forming elements and correlated with the PCDD/F levels measured at the ESP inlet. In Figure 34b the APR for the second field is plotted against the APR evaluated at 850Ox. The values of APR at 850Ox are higher than that of APR for the second field; however, there still exists some degree of linear correlation between the two. The difference in magnitude is due to

factors such as the limitation of the thermodynamic equilibrium modeling and the fact that the conditions at 852Ox are very different from those of the ESP. Therefore, while the active/passive species ratio is highly empirical and might be very specific to the conditions prevailing in this study, APR highlights the role of the modes of occurrences of Cu on PCDD/F production.

5. Experimental results – Anti-corrosion measure to combust high SRF-energy-share fuel (Paper IV & V)

The results and implications of the data collected during the assessment stage (see Section 3.4.1 or Figure 15) are first presented. Thereafter the performance stage follows.

5.1 Concentration of key components in the resulting fuel mix

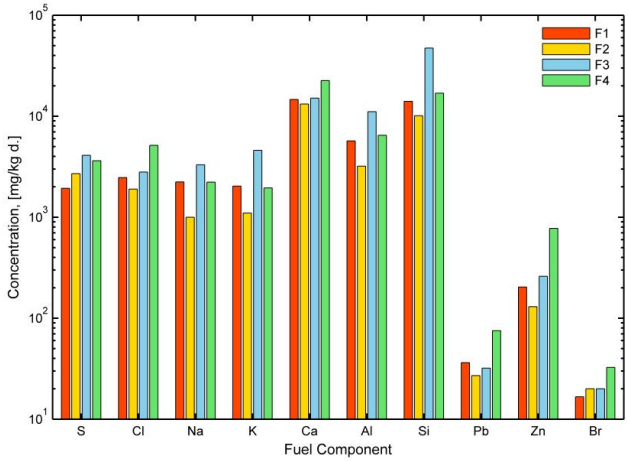

Figure 35. Resulting concentration of key fuel components in the fuel mixture defined in Table 4.

Figure 35 shows the mean concentration of key fuel components of the fuel mixture fired during the tests. Sulfur content is lowest for F1; partial and full substitu-

tion of bark by peat/SRF increases the S content in F2 & F3. The target fuel, F4, also has high S concentration. Chlorine concentration is highest in the target fuel, a direct result of increasing the proportion of the SRF in the fuel mixture.

Na, K, Al and Si registered high concentration in F3, a finding which is probably the result of increased concentration of these elements in the type of SRF used – SRF 1 (see Table 4 and Table 5). Ca, Br, Zn and Pb concentration is highest in F4, resulting in increasing the energy share of the SRF.

In general, moving from the base fuel to the target fuel recipe (mixture with 70 e-% SRF) increases the concentration of chlorine and trace elements in the fuel mixture. There is also an increase in S which may help lessen the risk of corrosion. This increase in S may be countered however by a corresponding increase of Ca concentration in the target fuel (see Figure 4 for the summary of key fuel components interaction).

5.2 Aerosols arriving in the superheater region

5.2.1 Effect of peat substitution

Aerosol samples collected for firing F1 and F3 are shown in Figure 36. Both exhibits a bimodal particle size distribution, though for firing F1 the peak of the fine particle is more pronounced compared to the coarse particle. For F3, the peak height is almost equal for both size fractions. The peak in the coarse particle may have come from fragments of the peat used. The presence of Si in the coarse fraction of Figure 36 may support this claim.

The elements comprising the fine aerosol fraction are similar, namely K, Na, Cl and SO_4. However, the concentration of these K, Na and Cl is higher for firing F1. The mode of occurrence of the alkalis may be “less reactive” during firing of F3 and could have resulted in the decrease of volatile K, Na and Cl.

Analysis of the particle size distribution of the aerosols arriving at the superheater region shows the same observations as above. Figure 37 shows the size distribution of fine particles arriving at the superheater. Mode 1 particles are composed of ultra-fine particles with a peak at around 20 nm ($0.02\,\mu m$) while Mode 2 is composed of fine particles with a peak at around 100 nm ($0.1\,\mu m$). The peak of Mode 1 particles for F1 is highest, while the peaks for F2 and F3 are nearly equal and the lowest among the fuels tested. This supports the earlier chemical observation that presence of reactive and volatile Na and K chloride is reduced during peat substitution (F2 and F3).

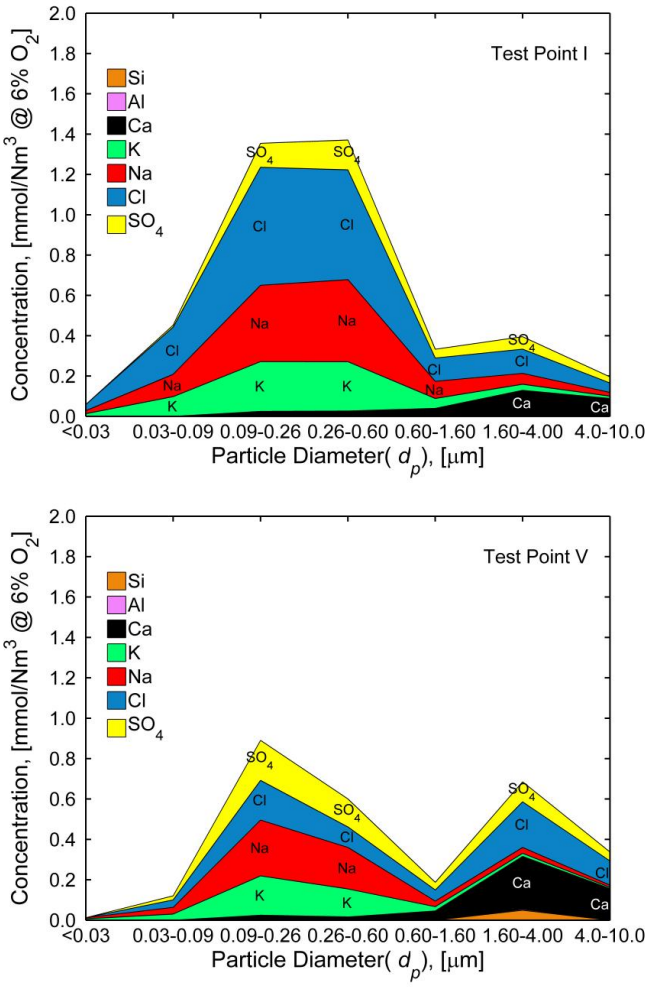

Figure 36. Composition and size distribution of aerosols collected before the SH during Test point I and Test point V.

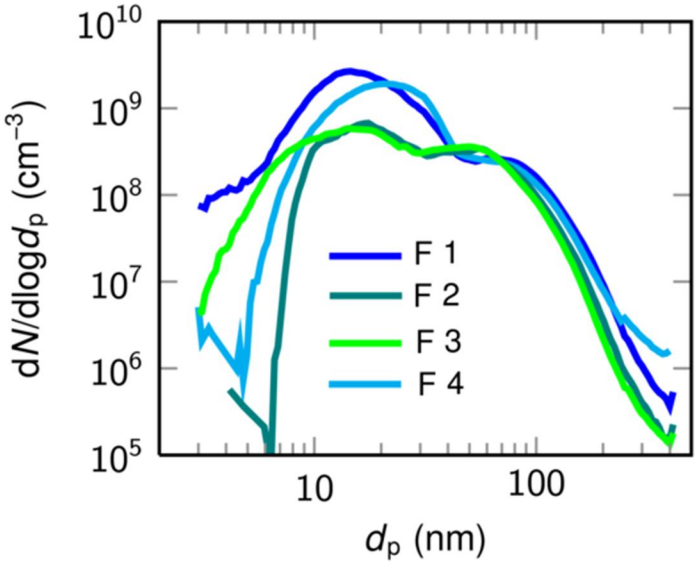

Figure 37. Particle size distribution of the fuel mixtures collected before the SH (from Paper V).

5.2.2 Assessment of anti-corrosion measures to aerosol quality

To assess the performance of the anti-corrosion measures, we take the sum of the concentration of Na+K, Cl, and SO_4 in the fine particle fraction of the DLPI samples and plot them in Figure 38. We have chosen only these elements because of their central role in active corrosion and mitigation (see Figure 4). Pb and Zn were not included because the measured concentration is low and have low condensation temperature.

The aerosol in I is rich Cl, and the proportion of Na+K and Cl is almost near that of the alkali chloride – MCl. Upon addition of elemental sulfur the fraction of Cl is decreased to more than half (see red and dashed arrow connecting points I and II in Figure 38) and is accompanied by an increase in the proportion of SO_4. Although not shown here, the peak of the fine particle fraction shifted from 0.09–0.26 μm to 0.26–0.60 μm, an indication of alkali chloride sulfation [85].

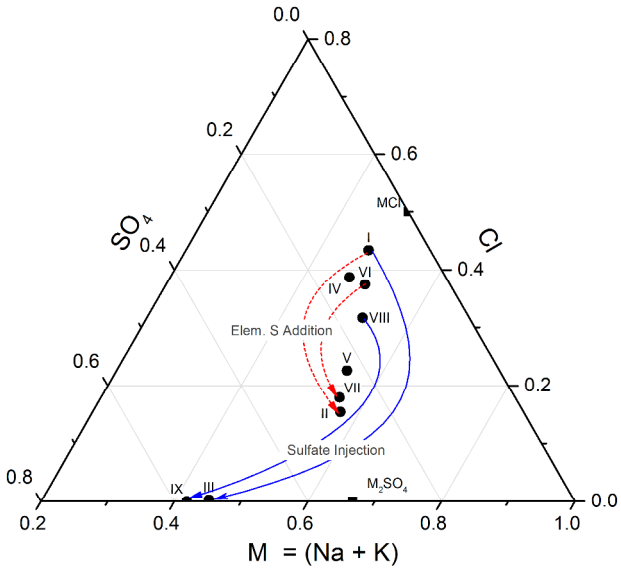

Figure 38. Summary of composition of the fine particle fraction of the aerosols collected before the SH. Points are labelled according to test points.

When the sulfate solution is injected, III, the aerosol is virtually free of Cl. Na+K and SO_4 dominate the fine aerosol fraction (see the solid arrow connecting points I and III in Figure 38). The peak of the fine particle is at 0.26–0.60 μm and there is enough SO_4 to ensure the formation of $(Na, K)_2SO_4$. The risk of fire side corrosion is much lower for III compared to I and II based on the aerosol composition data.

When peat is added in the fuel mixture to partially substitute bark (Fuel 2 and IV), the proportion of the elements of interest is not very far from those collected during I. When bark is not used in the fuel mixture (Fuel 3 and V) the proportion of Cl in the aerosol is reduced. However this decrease is not solely attributable to the absence of bark, but more likely to the difference in the quality of the SRF used. Test point V is using an SRF with a Cl content of 3700 mg/kg, d., which is almost half of the Cl content of the SRF for the other tests (see Table 5). For both IV and V, the peak in the fine particle fraction has remained in the 0.09–0.26 μm range. These observations suggest that peat co-firing is not a robust method to combat Cl-induced corrosion, because the concentration of Cl in the resulting aerosol is more tied to the quality of the SRF than to the corrosion mitigating power of peat.

5.3 Flue gas

Variations in the fuel mixture and application of corrosion mitigating measures do not significantly vary the parameters listed in Table 13 except of the SO_2, HCl and CO concentrations.

Test point I registered the least concentration of SO_2 in the flue gas. Without the necessary SO_2, alkali chlorides persist and are detected in the aerosol samples. At this condition the risk of corrosion is high. Upon the addition of S-pellets (II) a tenfold increase in SO_2 concentration is measured, with a corresponding increase in HCl concentration (~1.2×). These observations, in conjunction with the changes in the quality of the aerosols noted earlier, suggest the progress of (14) and/or (15), and even (5).

Sulfate injection (III) resulted in an increase in SO_2 concentration (~3.4×), with an accompanying increase in HCl concentration comparable to II, ~1.18×. Together with the aerosol results, these observations suggest that sulfate injection is able to wipe out alkali chloride via (14) and/or (15). However the contribution of (15) is more significant for III compared to II because sulfate was injected in the strategic position, ensuring high local concentration of SO_3 just below the bullnose: see point S in Figure 8.

When peat partially substituted bark (IV), SO_2 concentration is similar to III, but the increase in HCl concentration is lower than II and III. The Cl concentration is least for F2 – the fuel fired in IV – but this is not seen as the primary reason for the small increase measured for HCl. Aerosol data in Figure 38 suggest that the conversion of (Na,K)Cl to $(Na,K)_2SO_4$, which produces HCl, did not happen appreciably during IV compared to II and III.

Total substitution of bark with peat/SRF (V, fuel F3) likewise increased SO_2 concentration, by c.a. 6×, with an increase in HCl concentration (~1.19×). HCl could have been produced via (14) or at the lower part of the BFB, i.e. splash zone. The latter is also likely because Na and K might have been bound with the Al, Si in F3 making them *less* reactive. Without reactive alkalis, Cl preferred to interact with H forming HCl.

Using global equilibrium calculations, we simulated the combustion during III, IV and V in FactSage 6.4 to estimate the fraction of Cl_{fuel} that formed HCl in the splash zone. In Figure 39, test points IV and V both have Cl_{fuel} to HCl conversion higher than 0.6, with V having higher conversion than IV. However for III, Cl_{fuel} to HCl conversion is below 0.6. This supports the results in Section 5.2.2 that the increase in HCl measured for III is a result of successful alkali sulfation via (14) and more importantly (15); while HCl measured during V is the result of H-Cl interaction in the lower part of the BFB.

Table 13. Properties of the flue gas in the superheater region during the assessment stage. All data expect for temp after SH is from the FTIR. The coefficient of variation c.v. (standard deviation/mean) is also shown.

Property	Unit	Test Points Assessment Stage					
		I	II	III	IV	V	*c.v.(I-V)*
Temperature before SH	°C	701	701	701	n.d.	634	*0.05*
Temperature after SH[a]	°C	441	449	455	433	438	*0.02*
H_2O	vol-%	17.0	17.3	17.5	14.7	16.0	*0.07*
O_2	vol-% dry	8.1	8.3	8.4	8.8	9.2	*0.05*
CO_2	vol-% 6%O_2 dry	6.0	5.9	5.8	5.9	5.7	*0.02*
CO	mg/Nm^3 6% O_2 dry	0.0	0.0	0.0	0.0	0.3	*2.24*
SO_2	mg/Nm^3 6% O_2 dry	54.8	598.9	185.1	185.0	333.6	*0.77*
HCl	mg/Nm^3 6% O_2 dry	175.7	225.8	208.2	185.5	210.1	*0.10*

n.d. : no data available

a.: From the BFB's online instrumentation

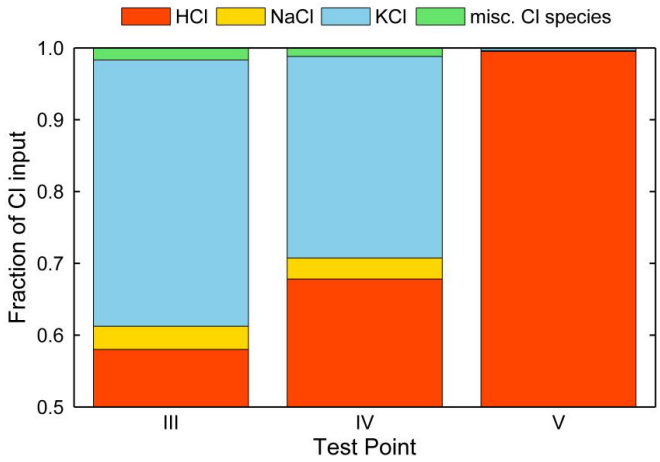

Figure 39. Conversion of Cl to HCl, alkali chlorides and misc. Cl species estimated using FactSage 6.4. The temperature is 840°C and λ = 0.6, these are the average condition at the splash zone in the boiler.

5.4 Quality of the deposits

Table 14 shows the concentration of select components of the deposits. Among the components listed Ca and S registered the highest concentration; this indicates abundance of $CaSO_4$ in the deposits. The concentration of Cl and Fe (the latter may also be occasionally come from the ring itself) has high variation during the assessment stage, with the coefficient of variation or c.v. of 0.99 and 1.52 respectively. For Na and K the variation is low, with c.v. of 0.35 for both elements.

The concentration of Cl is consistently lowest during sulfate injection (III), on average at 0.1 wt.%. The test for sulfur addition (II) and peat co-firing (V) both registered an average Cl concentration of 0.4 wt.%. These Cl concentration is significantly lower than the Cl concentration measured for the base test (I) which is on average 6.1 wt%. The average is taken from the concentration of the element in the wind, side and lee positions.

In the fine particle fraction of the aerosols, the Cl content is virtually zero during III but we detect the presence of Cl in the deposits. This suggests that other size fractions and factors can contribute to chlorine deposition.

Test point III registered the highest concentration of Fe in the deposit, 5.4 wt.%, six times its concentration during I. This result is consistent with the decomposition of $Fe_2(SO_4)_{3(aq)}$ which produces Fe_2O_3 [83]. Due to the proximity of sulfate injection to the superheater, the oxide can later be deposited in the superheater region. The risk associated with ash melting is low even at this condition. Using the composition at the wind position, the thermodynamic equilibrium calculation estimates the molten fraction of the deposit to be below 1% in the temperature range 500–800°C. The risk of ash melting is low because the deposit has plenty of $CaSO_4$ (T_{melt} = 1459°C).

5.5 Assessment phase output

The results above from the analysis of aerosol composition, flue gas condition, and deposit suggest that sulfate injection is able to significantly reduce the risk of Cl-induced corrosion. With sulfate injection, a strategic location can be chosen to ensure maximum effect of the additive. Sulfate injection yields the lowest Cl concentration in the deposit and in the fine particle fraction.

Peat co-firing and elemental S addition are also able to bring down the concentration of Cl in the aerosol and deposits. However since the performance of peat co-firing is dependent on the nature of the SRF being combusted (see paragraph 3 in Section 5.2.2), we see this strategy as less robust compared to S-pellet addition.

In the performance analysis stage, elemental S addition and sulfate injection are tested. Test points VI and VIII fire the target fuel alone, while VII and IX are for S addition and sulfate injection test respectively. VI serves as a reference test for VII, while VIII is the reference for IX.

Table 14. Selected components of the deposits. No data is available for test point IV. Concentration of Fe presented below may partly come from the ring.

Component	Test Points							
	Assessment				Performance Analysis			
	I	II	III	V	VI	VII	VIII	IX
Wind, wt%								
Ca	22.0	18.7	17.1	11.8	26.2	20.2	22.7	13.4
S	11.9	11.3	14.6	8.9	12.4	13.7	12.7	15.5
Fe	1.0	0.5	5.3	3.1	0.9	0.7	1.2	8.5
Cl	4.5	0.7	0.2	0.2	3.1	1.9	2.1	0.2
Na	4.2	3.9	3.5	3.3	2.0	3.5	2.7	3.0
K	4.3	3.8	4.5	5.7	1.9	2.2	1.9	4.5
Side, wt%								
Ca	15.0	7.4	11.6	9.5	20.6	10.5	0.5	9.4
S	11.3	13.0	16.4	5.9	11.2	6.8	4.3	17.4
Fe	0.9	0.4	7.3	1.6	1.1	0.3	8.6	9.8
Cl	6.8	0.3	0.1	0.5	4.5	0.7	6.6	0.1
Na	2.4	8.3	5.2	3.9	2.5	4.8	0.2	3.9
K	3.6	10.6	7.0	9.6	3.7	8.8	1.6	6.8
Lee, wt%								
Ca	19.6	12.8	14.7	12.2	15.0	15.0	13.1	10.1
S	13.6	13.6	16.0	4.9	11.1	12.4	10.5	14.7
Fe	0.6	0.6	3.6	1.6	1.8	1.0	1.4	2.8
Cl	7.0	0.3	0.1	0.5	7.8	1.5	6.5	0.1
Na	4.5	6.9	6.0	4.1	6.2	5.6	6.5	4.9
K	6.4	9.1	5.2	6.6	7.0	7.0	7.8	4.7

5.6 Combustion of the target fuel – performance stage

The composition of the aerosols before the superheater during firing of the target fuel (F4 and VI) is shown in Figure 40. Even though Cl is highest in F4, the risk of corrosion when firing this fuel is not enhanced. In fact in Figure 38 the fraction of Cl in the Na+K /SO_4 / Cl system decreases from the base fuel (I) to the target fuel (VI and VIII). In addition, the average concentration of Cl in the deposits is 5.1

wt.% for VI and VIII, lower than the 6.1 wt.% measured for I. A possible explanation for these measurements is the increase in S_{fuel} from F1 to F4. The flue gas concentration of SO_2in VI and VIII (see Table 15) are 2.5× and 4.5× that of I respectively, which may provide the necessary sulfur to achieve alkali sulfation even without the additives. Due to increased Zn and Pb in F4, it is also probable that some Cl's formed zinc and/or lead chlorides [37] which partly lowers the amount of condensable Cl in the superheater region.

Elemental S addition to the target fuel (VII) improves the quality of the aerosols and deposits in terms of preventing alkali chloride induced corrosion. In the aerosols, the fraction of Cl is lowered similar to II (see Figure 38). The flue gas registered the highest SO_2 concentration (see Table 15) with an accompanying increase in HCl concentration. However the Cl content in the deposit is on average 1.4 wt.%, c.a. 26% of its reference test (VI) (see Table 14).

Sulfate injection during combustion of the target fuel (IX) yields an aerosol with composition similar to III. The aerosol is virtually free of Cl and the deposit has an average Cl concentration of 0.1 wt.% which is c.a. 2.6 % of its reference case (VIII). Similar to III, the deposit is also rich in Fe with mean concentration of 7 wt.%. For all tests in the performance analysis phase, Ca and S have the highest concentration in the deposits.

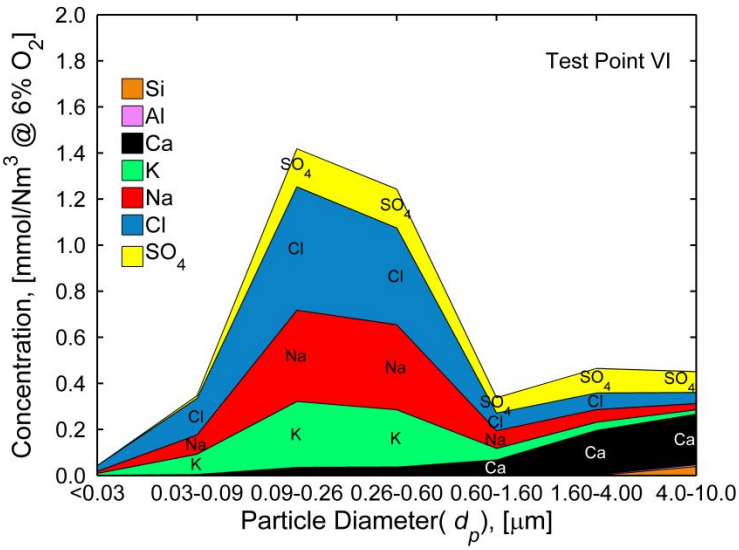

Figure 40. Composition and size distribution of aerosols collected before the SH during firing of the target fuel (test point VI).

Table 15. Properties of the flue gas in the superheater region during the performance analysis stage. All data expect for temp after SH is from the FTIR. The coefficient of variation c.v. (standard deviation/mean) is also shown

Property	Unit	Test Points Performance Analysis Stage				
		VI	VII	VIII	IX	*c.v.(VI-IX)*
Temperature before SH	°C	739	739	751	751	*0.01*
Temperature after SH[a]	°C	440	448	453	451	*0.01*
H_2O	vol-%	17.4	16.7	17.5	19.9	*0.08*
O_2	vol-% dry	8.0	8.3	8.4	8.1	*0.02*
CO_2	vol-% 6%O_2 dry	6.1	6.1	6.1	6.2	*0.01*
CO	mg/Nm^3 6% O_2 dry	0.0	0.1	0.2	0.2	*0.85*
SO_2	mg/Nm^3 6% O_2 dry	138.2	758.0	247.0	480.6	*0.68*
HCl	mg/Nm^3 6% O_2 dry	198.5	278.6	226.8	313.0	*0.20*

n.d. : no data available

a.: From the BFB's online instrumentation

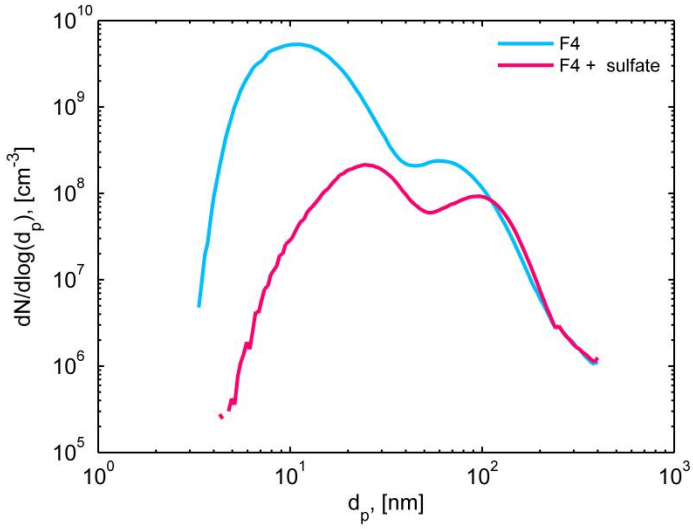

Figure 41. Particle size distribution changes during sulfate injection and firing of F4 (from Paper V).

The impact of sulfate injection to F4 is also visible in the particle size distribution of aerosols collected in the SH region. It can be seen in Figure 41 that sulfate injection affects both the concentration (particle count) and distribution modes. The concentrations for Mode 1 and 2 particles are both reduced when sulfate is injected during combustion of F4. There is also a corresponding shift in peak position for both particle modes; we again attribute this shift in peak position to the possible occurrence of alkali chloride sulfation.

The aerosol at the back pass (point 5 in Figure 8) collected during IX is composed mainly of Na, K and SO_4. Trace elements Pb and Zn are present at very low concentration.

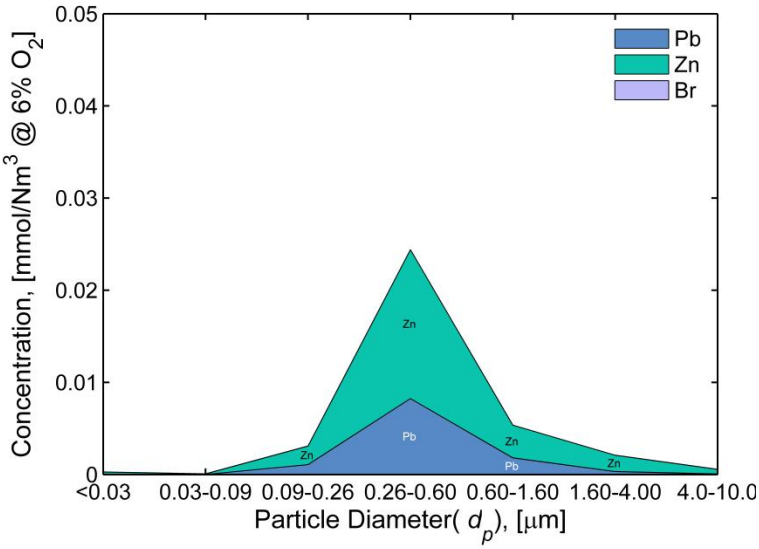

Figure 42. Composition and size distribution of trace elements after the SH during IX.

These results suggest that elemental S and sulfate injection are both robust means of reducing the corrosion risk associated with combustion of high SRF share fuel mixture. Even though there are variations in the quality of the SRF used between I, II, III and VI–IX, both procedures were able to provide consistent trends in aerosol and deposit composition as well as flue gas conditions. However in terms of ensuring that the superheater deposit is Cl free, the performance of sulfate injection is superior to sulfur addition.

5.7 Factors affecting Cl concentration in the deposits

The fuel composition and anti-corrosion measures tested are able to affect the composition of the aerosols and the deposits. The concentration of the Cl in the deposit is never totally reduced to zero, however, even if the concentration of alkali chlorides in the aerosols is virtually negligible. In order to know what other factors should be considered in order for Cl deposition to be understood effectively, the relationship of flue gas and fine aerosol properties and the concentration of Cl in the wind side deposit collected before the superheater were examined (point 4 in Figure 8).

Partial least squares regression is used to examine the contribution of the 14 variables found in the abscissa of Figure 43. The PLS regression model was used, because there was no systematic way of including or excluding variable/s to create a set of non-collinear estimators. The predictive power of this model is not expected to be high due to the limited number of test point, and consequently extrapolation of the results is not advised.

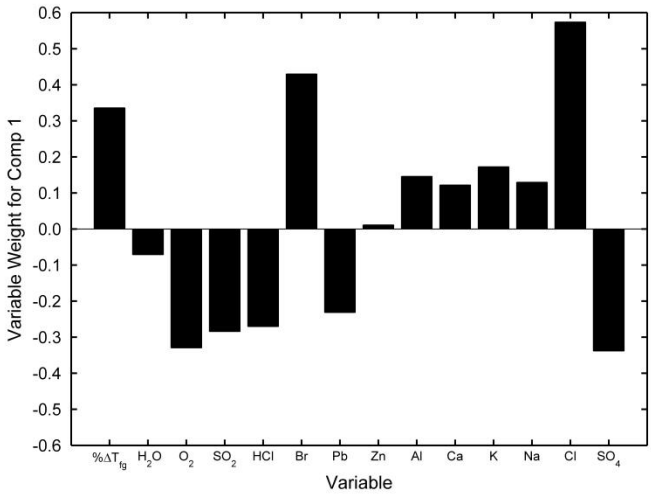

Figure 43. Weights of variables tested to component 1 of the PLS regression model for the wind side superheater deposits.

$\%\Delta T_{fg}$ is the percent decrease in flue gas temperature traversing the superheaters. H_2O, O_2, SO_2 and HCl are the concentrations of components of the flue gas (see Table 13 and Table 15), and the rest are concentrations of the components of the aerosol. Since the units of these variables vary, normalization by mean center-

ing was performed first. The mean centered data forms the matrix of predictors **X** and the wind side Cl-concentration is the response **Y**.

Cross validation step suggests the use of three components or x-scores in the PLS regression model. Using a 3-component PLS regression model the calculated R^2 is 0.94, see Figure 44. The first component of the regression captures 82.29% of the variance and the weight of the original variables in this component is found in Figure 43.

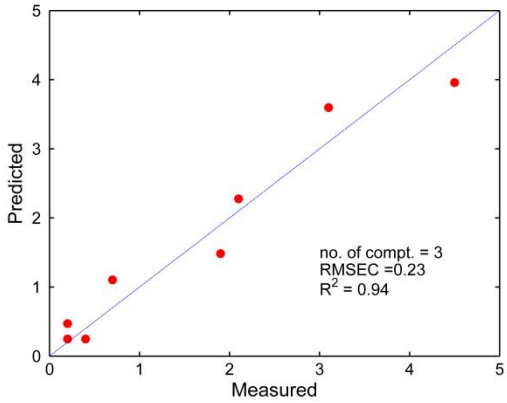

Figure 44. Parity plot between predicted concentration and measured wind side Cl concentration, in wt.%.

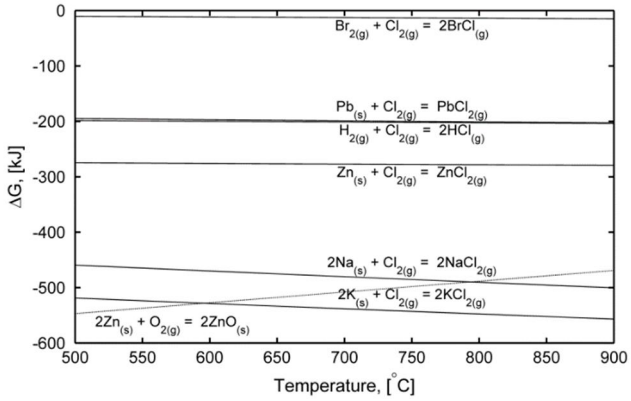

Figure 45. Stability of chlorine containing compounds and ZnO. Calculated using FactSage 6.4® Reaction module at standard state conditions.

The decrease in the temperature of the flue gas passing through the superheaters, and the Cl and Br content in the aerosol have high positive effects on Cl-

deposition. An increase in Cl content in the aerosol plus a large decrease in flue gas temperature enhances Cl-deposition in the superheater because of saturation.

On the other hand, the positive effect of Br is probably linked to the formation of BrCl [157,158]. Formation of bromine chloride is thermodynamically feasible at typical boiler conditions, but it is less stable compared to other chloride salts (see Figure 45). Na and K also contribute positively to Cl-deposition via formation of alkali chlorides. These chloride salts may then condense to enhance deposition in the superheater. Ca and Al also positively affect Cl-deposition via formation of chlorides or the capture the sulfates by forming aluminum or calcium sulfate instead of alkali sulfates.

Meanwhile, O_2, SO_2 and HCl reduce Cl-deposition through alkali sulfation. O_2 and SO_2 are reactants to (14) and (15) which help convert condensable Cl to HCl. HCl is not expected to condense in the superheater, thereby reducing Cl-deposition. O_2, SO_2 and HCl are also reactants in the intra-particle sulfation of the alkali chlorides. Intra-particle sulfation localized in the periphery of the deposits results in the loss of Cl to the flue gas as HCl [86], even if some Cl can still diffuse towards the metal.

The concentrations of SO_4 and Pb in the aerosol also have negative weights in the 1st component of the PLS regression model. Having more SO_4 in the aerosol increases the likelihood that (14) and/or (15) take place and the amount of condensable Cl is reduced. The presence of Pb in the water-soluble aerosol samples may indicate the presence of $PbCl_2$ which reduce the amount of condensable Cl in the superheater region. Zn meanwhile has a low effect on Cl deposition because the formation of ZnO is more favored than $ZnCl_2$ (see Figure 45). These interpretations agree with Enestam's estimates that in the superheater region Pb is predominantly $PbCl_{2(g)}$ while Zn can exist mostly as $ZnO_{(s)}$ and some as $ZnCl_{2(g)}$ [37].

6. Conclusion

The *de novo* mechanism is the dominant means of production of PCDD/F in the multi-fuel fired BFB facility. Aerosol samples suggest that sulfur pellets were able to convert copper chlorides or oxides to sulfate. On the other hand, during co-firing of peat, Cu was less volatile and ash loading in the flue gas was high; this led to a significant increase in PCDD/F. The staged-equilibrium process model indicates that during peat addition excessive Cu in the fuel mixture favors the formation of $CuO_{(s)}$, a key *de novo* catalyst. The same modeling approach also showed that synergistic effects of increasing sludge share and sulfur pellet addition can promote abatement of PCDD/F production and promote alkali capture. This can be explained by trace element dilution, alkali capture of Si and Al from the sludge, and additional S available for sulfation reactions. Furthermore, the modeling approach also allowed the introduction of the empirical active/passive species ratio or APR which correlated to the levels of PCDD/F measured at the ESP inlet.

Characterization and chemical analysis of the ESP fly ash reveals that the formation histories of the fly ashes collected in the ESP fields. Coarse fly ashes are products of attrition and fragmentation of the non-volatilized fuel components and bed material while fine fly ashes are formed from secondary gas/solid reaction (e.g. alkali aluminosilicate capture, sulfation) and salts that have been in the gas phase in the boiler and have condensed and agglomerated while traveling with the cooling flue gases.

Based on XANES analysis, the presence of more Cu-Cl species in Case 1 led to a slightly higher PCDD/F concentration, relative to Case 2. This has implications also in the possible additional chlorination of particle-bound PCDD/Fs of the ESP fly ashes. The combined presence of Cu-Cl and Cu-O promoted subsequent chlorination of PCDD/F in the ESP fly ash in Case 1.

As for Case 3, linear combination fitting of XANES spectra showed the significant presence of Cu-O in the fine ESP fly ashes suggesting that Cu was indeed the least volatile and that it could have effectively shuttled Cl to the carbon matrices, as is required for the inflight *de novo* formation of PCDD/F. Moreover, the mole fraction of the $CuSO_4$ fraction is smallest in Case 3, suggesting poor sulfation of Cu. XANES analysis also corrects the limitations of the staged equilibrium

models at low temperature conditions, as it was able to show that $CuSO_4$ did form, and it validates the correlation between APR and PCDD/F production.

In the flue gas path, most of the PCDD/F leaving the post combustion zones is particle bound. Phase redistribution or volatilization occurred in the ESP and resulted in an increase in gaseous PCDD/F leaving the device. This phase redistribution did not however affect the overall decrease of the PCDD/F concentration in the flue gas traversing the ESP.

There is evidence pointing to some reactions in the ESP fly ash because the homologue distribution pattern is different from the pattern in the flue gas path and the ratio of furans and dioxins is different. The trend in the PCDD/F concentration in the ash has been affected by dilution and the amount of active Cu in the ash.

Based on these results it can be concluded that adding S-pellet to the fuel mixture is more suitable than peat co-firing because it accomplishes the required extent of Cu sulfation. Furthermore, the increased particle loading in peat co-combustion may be detrimental in PCDD/F abatement since this can house unburned organic carbon matrices – an important ingredient in *de novo* synthesis. In addition, keeping the concentration of Cu as low as possible is key to for PCDD/F abatement. This is because oxychlorination can happen and promote PCDD/F production if sulfur is unable to fully convert Cu-Cl and Cu-O species to $CuSO_4$.

In this two stage study to assess chlorine-deposition in the superheater during firing of a fuel mixture containing 50, 60 and 70 e.-% share SRF, it is noted that the increase in SRF share increase Cl and trace elements in the fuel.

In the assessment stage, sulfur addition and sulfate injection exhibited robust performance against the agents of active corrosion by partially or fully reducing the concentration of alkali chlorides. Peat co-firing can also reduce alkali chlorides but its action is dependent on the quality of the fuel mixture used.

During firing of the target fuel (70 e.-% share of SRF), sulfur addition and sulfate injection are able to lower the concentration of alkali chlorides in the aerosol and in the deposits at the superheater. Sulfate injection ensures however that the concentration of Cl in the aerosol and in the deposits is minimal. With these observations it can be conclude that sulfate injection is a robust strategy for combating Cl-induced corrosion of the superheater.

The quality of the flue gas and the aerosol has a strong impact on the quality of the deposits. During firing of high e.-% share SRF, Cl content of the aerosol has the highest positive impact on Cl deposition. Therefore any corrosion mitigating measure must be able to reduce Cl concentration in the aerosols to as low a level as is technically and economically possible.

This work showed two problems associated with combustion of high or advanced energy-share SRF fuel mixture – PCDD/F formation and Cl-induced corrosion. Both can be dealt with appropriately by the addition of sulfur based additive that can induce the sulfation of Cu, for dioxin and furan production, alkalis, and for Cl-induced corrosion.

Future work should focus on optimizing the treatment levels of the sulfur based additive to improve cost effectiveness. In addition, sulfate injection should also be tested (dose and point of injection) for its PCDD/F abatement.

References

[1] 2009, Towards a recycling society – The National Waste Plan for 2016, Ministry of the Environment, Helsinki.

[2] Official Statistics of Finland (OSF), Waste statistics [e-publication].ISSN=2323-5314. 2011, Appendix table 1. Municipal waste in 2011, tonnes . Helsinki: Statistics Finland [referred: 28.2.2013]. [Online]. Available: http://www.stat.fi/til/jate/2011/jate_2011_2012-11-20_tau_001_en.html. [Accessed: 28-Feb-2013].

[3] 2008, Directive 2008/98/EC of the European Parliament and the Council of 19 November 2008 on waste and repealing certain Directives., Off. J. Eur., pp. 3–30.

[4] Solid Waste Management Sourcebook/2.3 Topic d: Incineration [Online]. Available: http://www.unep.or.jp/ietc/ESTdir/Pub/MSW/RO/Europe/Topic_d.asp. [Accessed: 08-Jan-2015].

[5] 1999, The World Bank, Municipal Solid Waste Incineration, Washington D.C.

[6] Rogoff, M. J., and Screve, F., 2011, Waste-to-Energy, Elsevier.

[7] Grabke, H. J., Reese, E., and Spiegel, M., 1995, The Effects of Chloride, Hydrogen Chloride and Sulfur Dioxide in the Oxidataion of Steels Below Deposits, Corros. Sci., **37**(7), pp. 1023–1043.

[8] Becidan, M., Sørum, L., and Lindberg, D., 2010, Impact of Municipal Solid Waste (MSW) Quality on the Behavior of Alkali Metals and Trace Elements during Combustion: A Thermodynamic Equilibrium Analysis, Energy & Fuels, **24**(6), pp. 3446–3455.

[9] Becidan, M., Sørum, L., Frandsen, F., and Pedersen, A. J., 2009, Corrosion in waste-fired boilers: A thermodynamic study, Fuel, **88**(4), pp. 595–604.

[10] Jappe Frandsen, F., 2005, Utilizing biomass and waste for power production—a decade of contributing to the understanding, interpretation and analysis of deposits and corrosion products, Fuel, **84**(10), pp. 1277–1294.

[11] Otsuka, N., 2008, A thermodynamic approach on vapor-condensation of corrosive salts from flue gas on boiler tubes in waste incinerators, Corros. Sci., **50**(6), pp. 1627–1636.

[12] Tillman, D. A., Dao, D., and Miller, B., 2008, Chlorine in Solid Fuels Fired in Pulverized Fuel Biolers - Sources, Forms, Reactions and Consequences: a Literature Review, Energy & Fuels, **23**, pp. 3379–3391.

[13] Vainio, E., Yrjas, P., Zevenhoven, M., Brink, A., Laurén, T., Hupa, M., Kajolinna, T., and Vesala, H., 2013, The fate of chlorine, sulfur, and potassium during co-combustion of bark, sludge, and solid recovered fuel in an industrial scale BFB boiler, Fuel Process. Technol., **105**, pp. 59–68.

[14] Vainikka, P., Bankiewicz, D., Frantsi, A., Silvennoinen, J., Hannula, J., Yrjas, P., and Hupa, M., 2011, High temperature corrosion of boiler waterwalls induced by chlorides and bromides. Part 1: Occurrence of the corrosive ash forming elements in a fluidised bed boiler co-firing solid recovered fuel, Fuel, **90**(5), pp. 2055–2063.

[15] Nielsen, H. P., Frandsen, F. J., Dam-Johansen, K., and Baxter, L. L., 2000, The implications of chlorine-associated corrosion on the operation of biomass-fired boilers, Prog. Energy Combust. Sci., **26**, pp. 283–298.

[16] Skrifvars, B.-J., Backman, R., Hupa, M., Salmenoja, K., and Vakkilainen, E., 2008, Corrosion of superheater steel materials under alkali salt deposits Part 1: The effect of salt deposit composition and temperature, Corros. Sci., **50**(5), pp. 1274–1282.

[17] Enestam, S., Boman, C., Niemi, J., Bostr, D., Backman, R., and Kari, M., 2011, Occurrence of Zinc and Lead in Aerosols and Deposits in the Fluidized-Bed Combustion of Recovered Waste Wood . Part 1 : Samples from Boilers, pp. 1396–1404.

[18] Enestam, S., Mäkelä, K., Backman, R., and Hupa, M., 2011, Occurrence of Zinc and Lead in Aerosols and Deposits in the Fluidized-Bed Combustion of Recovered Waste Wood. Part 2: Thermodynamic Considerations, Energy & Fuels, **25**(5), pp. 1970–1977.

[19] Bankiewicz, D., Vainikka, P., Lindberg, D., Frantsi, A., Silvennoinen, J., Yrjas, P., and Hupa, M., 2012, High temperature corrosion of boiler waterwalls induced by chlorides and bromides – Part 2: Lab-scale corrosion tests and thermodynamic equilibrium modeling of ash and gaseous species, Fuel, **94**, pp. 240–250.

[20] Vainikka, P., Lindberg, D., Moilanen, A., Ollila, H., Tiainen, M., Silvennoinen, J., and Hupa, M., 2013, Trace elements found in the fuel and in-furnace fine particles collected from 80MW BFB combusting solid recovered fuel, Fuel Process. Technol., **105**, pp. 202–211.

[21] Nasrullah, M., Vainikka, P., Hannula, J., Hurme, M., and Kärki, J., 2014, Mass, energy and material balances of SRF production process. Part 1: SRF produced from commercial and industrial waste., Waste Manag., p. http://www.ncbi.nlm.nih.gov/pubmed/24735992.

[22] Sørum, L., Frandsen, F. J., and Hustad, J. E., 2003, On the fate of heavy metals in municipal solid waste combustion Part I: devolatilisation of heavy metals on the grate, Fuel, **82**(18), pp. 2273–2283.

[23] Toledo, J. M., Corella, J., and Corella, L. M., 2005, The partitioning of heavy metals in incineration of sludges and waste in a bubbling fluidized bed 2. Interpretation of results with a conceptual model., J. Hazard. Mater., **126**(1-3), pp. 158–68.

[24] Miller, B. B., Kandiyoti, R., and Dugwell, D. R., 2002, Trace Element Emissions from Co-combustion of Secondary Fuels with Coal : A Comparison of Bench-Scale Experimental Data with Predictions of a Thermodynamic Equilibrium Model, Energy & Fuels, (3), pp. 956–963.

[25] Takaoka, M., Shiono, A., Nishimura, K., Yamamoto, T., Uruga, T., Takeda, N., Tanaka, T., Oshita, K., Matsumoto, T., and Harada, H., 2005, Dynamic change of copper in fly ash during de novo synthesis of dioxins., Environ. Sci. Technol., **39**(15), pp. 5878–84.

[26] Fujimori, T., Tanino, Y., Takaoka, M., and Morisawa, S., 2010, Chlorination mechanism of carbon during dioxin formation using Cl-K near-edge X-ray-absorption fine structure., Anal. Sci., **26**(11), pp. 1119–25.

[27] Buekens, A., and Cen, K., 2011, Waste incineration, PVC, and dioxins, J. Mater. Cycles Waste Manag., **13**(3), pp. 190–197.

[28] 2000, Directive 2000/76/EC of the European Parliament and the Council of December 4, 2000 on the incineration of waste., Off. J. Eur. Communities, p. L 332/91–111.

[29] Altarawneh, M., Dlugogorski, B. Z., Kennedy, E. M., and Mackie, J. C., 2009, Mechanisms for formation, chlorination, dechlorination and destruction of polychlorinated dibenzo-p-dioxins and dibenzofurans (PCDD/Fs), Prog. Energy Combust. Sci., **35**(3), pp. 245–274.

[30] EnvironmentAustralia, 1999, Incineration and Dioxins Review of Formation Processes, consultancy report prepared by Environmental and Safety Services for Environment Australia, Canberra.

[31] Finnish Environmental Institute, Air pollutant emissions in Finland [Online]. Available: http://www.ymparisto.fi/en-US/Maps_and_statistics/Air_pollutant_emissions/Air_pollutant_emissions_in_Finland(9739).

[32] Mehtonen, J., Munne, P., and Verta, M., 2012, Work package 4: Identification of sources and estimation of inputs/impacts on the Baltic Sea, Summary Report Finland, Helsinki.

[33] Dunnu, G., Maier, J., and Scheffknecht, G., 2010, Ash fusibility and compositional data of solid recovered fuels, Fuel, **89**(7), pp. 1534–1540.

[34] Kupka, T., Mancini, M., Irmer, M., and Weber, R., 2008, Investigation of ash deposit formation during co-firing of coal with sewage sludge, saw-dust and refuse derived fuel, Fuel, **87**(12), pp. 2824–2837.

[35] Silvennoinen, J., and Hedman, M., 2013, Co-firing of agricultural fuels in a full-scale fluidized bed boiler, Fuel Process. Technol., **105**, pp. 11–19.

[36] Jones, F., Tran, H., Lindberg, D., Zhao, L., and Hupa, M., 2013, Thermal Stability of Zinc Compounds, Energy & Fuels, **27**(10), pp. 5663–5669.

[37] Enestam, S., 2011, Corrosivity of hot flue gases in the fluidized bed combustion of recovered waste wood, Åbo Akademi University.

[38] Wielgosin, G., 2011, The Reduction of Dioxin Emissions from the Processes of Heat and Power Generation, J. Air Waste Manage. Assoc., **61**(May), pp. 511–526.

[39] Chandler, A. J., 2007,
Review of Dioxins and Furans from Incineration In Support of a Canada-wide Standard Review.

[40] Hutzinger, O., Choudhry, G. G., Chittim, B. G., Johnston, L. E., and Hutzinger, O., Choudhry, G.G., Chittim, B.G., Johnston, L. E., 1985, Formation of polychlorinated dibenzofurans and dioxins during combustion, electrical equipment fires and PCB incineration., Environ. Health Perspect., **60**, pp. 3–9.

[41] Tuppurainen, K., Halonen, I., Ruokoj, P., Tarhanen, J., and Ruuskanen, J., 1998, Formation of PCDDs and PCDFs in Municipal Waste Incineration and its Inhibition Mechanism: A review, Chemosphere, **36**(7), pp. 1493–1511.

[42] Lomnicki, S., and Dellinger, B., 2003, A Detailed Mechanism of the Surface-Mediated Formation of PCDD/F from the Oxidation of 2-Chlorophenol on a CuO/Silica Surface, J. Phys. Chem. A, **107**(22), pp. 4387–4395.

[43] Everaert, K., and Baeyens, J., 2002, The formation and emission of dioxins in large scale thermal processes., Chemosphere, **46**(3), pp. 439–48.

[44] Stieglitz, L., Zwick, G., Beck, J., Roth, W., and Vogg, H., 1989, On the de-novo synthesis of PCDD/PCDF on fly ash of municipal waste incinerators, Chemosphere, **18**(1-6), pp. 1219–1226.

[45] Gullett, B. K., Bruce, K. R., Beach, L. O., and Drago, A. M., 1992, Mechanistic Steps in the Production of PCDD and PCDF during Waste Combustion, Chemosphere, **25**, pp. 1387–1392.

[46] Raghunathan, K., and Gullett, B. K., 1996, Role of Sulfur in Reducing PCDD and PCDF Formation, Environ. Sci. Technol., **30**(6), pp. 1827–1834.

[47] Hunsinger, H., Seifert, H., and Jay, K., 2007, Reduction of PCDD/F Formation in MSWI by a Process-Integrated SO 2 Cycle, Environ. Eng. Sci., **24**(8), pp. 1145–1159.

[48] Amand, L.-E., and Kassman, H., 2013, Decreased PCDD/F formation when co-firing a waste fuel and biomass in a CFB boiler by addition of sulphates or municipal sewage sludge., Waste Manag., (2).

[49] Wikström, E., Ryan, S., Touati, A., and Gullet, B. K., 2003, Key parameters for de novo formation of polychlorinated dibenzo-p-dioxins and dibenzofurans., Environ. Sci. Technol., **37**(9), pp. 1962–70.

[50] Hutzinger, O., Choudhry, G. G., Chittim, B. G., and Johnston, L. E., 1985, Formation of polychlorinated dibenzofurans and dioxins during combustion, electrical equipment fires and PCB incineration., Environ. Health Perspect., **60**, pp. 3–9.

[51] Dickson, L. C., Lenoir, D., Hutzinger, O., Chemistry, E., and Republic, F., 1992, Quantitative Comparison of de Novo and Precursor Formation of Polychlorinated Dibenzo-p-dioxins under Simulated Municipal Solid Waste Incinerator Postcombustion Conditions, Environ. Sci. Technol., (26), pp. 1822–1828.

[52] Öberg, T., Bergbäck, B., and Filipsson, M., 2008, Catalytic effects by metal oxides on the formation and degradation of chlorinated aromatic compounds in fly ash., Chemosphere, **71**(6), pp. 1135–43.

[53] Choudhry, G. G., and Hutzinger, O., 1982, Mechanistic aspects of the thermal formation of halogenated organic compounds including polychlorinated dibenzo-p-dioxins. Part V: Hypotheses and summary, Toxicol. Environ. Chem., **5**(3-4), pp. 295–309.

[54] Stanmore, B. ., 2004, The formation of dioxins in combustion systems, Combust. Flame, **136**(3), pp. 398–427.

[55] Vehlow, J., Bergfeldt, B., and Hunsinger, H., 2006, PCDD/F and related compounds in solid residues from municipal solid waste incineration - a literature review, Waste Manag. Res., **24**(5), pp. 404–420.

[56] Gullet, B. K., 1990, The Effect of Metal Catalysts on the Formation of Polychlorinated Dibenzo-p-dioxin and Polychlorinated Dibenzofuran Precursor, Chemosphere, **20**(10-12), pp. 1945–1952.

[57] Kulkarni, P. S., Crespo, J. G., and Afonso, C. M., 2008, Dioxins sources and current remediation technologies--a review., Environ. Int., **34**(1), pp. 139–53.

[58] Lassesson, H., and Steenari, B.-M., 2013, Speciation of Copper in Ash from a Fluidized-Bed Boiler Fired with Municipal Solid Waste, Energy & Fuels, **27**(7), pp. 3891–3897.

[59] Fujimori, T., Takaoka, M., Kato, K., Oshita, K., and Takeda, N., 2008, Observing copper chloride during dioxin formation using dispersive XAFS, X-ray Spectrom., **37**, pp. 210–214.

[60] Nakayama, J., and Miyake, A., 2012, Catalytic effect of copper(II) oxide on oxidation of cellulosic biomass, J. Therm. Anal. Calorim., **110**(1), pp. 321–327.

[61] Wikström, E., Tysklind, M., and Marklund, S., 1999, Influence of Variation in Combustion Conditions on the Primary Formation of Chlorinated Organic Micropollutants during Municipal Solid Waste Combustion, Environ. Sci. Technol., **33**(23), pp. 4263–4269.

[62] Cains, P., 1997, Prediction of PCDD and PCDF emissions from municipal solid waste (MSW) incinerators, Chemosphere, **34**(1), pp. 51–69.

[63] Gullett, B. . K., Dunn, J. . E., Bae, S.-K. K., and Raghunathan, K., 1998, Effects of combustion parameters on polychlorinated dibenzodioxin and dibenzofuran homologue profiles from municipal waste and coal co-combustion, Waste Manag., **18**(6-8), pp. 473–483.

[64] Fangmark, I., Stromberg, B., Berge, N., and Rappet, C., 1994, Influence of Postcombustion Temperature Profiles on the Formation of PCDDs , PCDFs , PCBzs , and PCBs in a Pilot Incinerator, Environ. Sci. Technol, (4), pp. 624–629.

[65] Dickson, L. C., Lenoir, D., and Hutzinger, O., 1992, Quantitative Comparison of de Novo and Precursor Formation of Polychlorinated Dibenzo-p-dioxins under Simulated Municipal Solid Waste Incinerator Postcombustion Conditions, Environ. Sci. Technol., (26), pp. 1822–1828.

[66] Hunsinger, H., Kreisz, S., and Siefert, H., 1998, PCDD / F Behavior in Wet Scrubbing Systems of Waste Incineration Plants, Chemosphere, **37**(9-12), pp. 2293–2297.

[67] Chang, M. B., and Lin, J. J., 2001, Memory effect on the dioxin emissions from municipal waste incinerator in Taiwan, Chemosphere, **45**(8), pp. 1151–1157.

[68] Kolluri, R., and Altwicker, E., 1994, The Effect of the Electric Field on the Formation of PCDD in Electrostatic Precipitators, Hazard. Waste Hazard. Mater., **11**(1), pp. 145–156.

[69] Pekárek, V., Puncochár, M., Bures, M., Grabic, R., and Fiserová, E., 2007, Effects of sulfur dioxide, hydrogen peroxide and sulfuric acid on the de novo synthesis of PCDD/F and PCB under model laboratory conditions., Chemosphere, **66**(10), pp. 1947–54.

[70] Ke, S., Jianhua, Y., Xiaodong, L., Shengyong, L., Yinglei, W., and Muxing, F., 2010, Inhibition of de novo synthesis of PCDD/Fs by SO2 in a model system., Chemosphere, **78**(10), pp. 1230–5.

[71] Ryan, S. P., Li, X., Gullett, B. K., Lee, C. W., Clayton, M., and Touati, A., 2006, Experimental Study on the Effect of SO2 on PCDD / F Emissions: Determination of the Importance of Gas-Phase versus Solid-Phase Reactions in PCDD / F Formation, Environ. Sci. Technol., **40**(22), pp. 7040–7047.

[72] Ogawa, H., Orita, N., Horaguchi, M., Suzumi, T., Okada, M., and Yasuda, S., 1996, Dioxin reduction by sulfur component addition, Science (80-.)., **32**(1), pp. 151–157.

[73] Spiegel, M., Zahs, A., and Grabke, H. J., 2003, Fundamental aspects of chlorine induced corrosion in power plants, Mater. High Temp., **20**(2), pp. 153–159.

[74] Aho, M., 2001, Reduction of chlorine deposition in FB boilers with aluminium-containing additives, Fuel, **80**(13), pp. 1943–1951.

[75] Wolf, K. J., Mu, M., Hilpert, K., and Singheiser, L., 2004, Alkali Sorption in Second-Generation Pressurized Fluidized-Bed Combustion, Energy & Fuels, **18**, pp. 1841–1850.

[76] Backman, R., Khalil, R. a., Todorovic, D., Skreiberg, Ø., Becidan, M., Goile, F., Skreiberg, A., and Sørum, L., 2013, The effect of peat ash addition to demolition wood on the formation of alkali, lead and zinc compounds at staged combustion conditions, Fuel Process. Technol., **105**, pp. 20–27.

[77] Becidan, M., Houshfar, E., Khalil, R. A., Skreiberg, Ø., Løv, T., and Sørum, L., 2011, Optimal Mixtures To Reduce the Formation of Corrosive Compounds during Straw Combustion : A Thermodynamic Analysis, Energy & Fuels, **25**, pp. 3223–3234.

[78] Aho, M., Paakkinen, K., and Taipale, R., 2013, Destruction of alkali chlorides using sulphur and ferric sulphate during grate combustion of corn stover and wood chip blends, Fuel, **103**, pp. 562–569.

[79] Kassman, H., Pettersson, J., Steenari, B.-M., and Åmand, L.-E., 2013, Two strategies to reduce gaseous KCl and chlorine in deposits during biomass combustion — injection of ammonium sulphate and co-combustion with peat, Fuel Process. Technol., **105**, pp. 170–180.

[80] Aho, M., and Ferrer, E., 2005, Importance of coal ash composition in protecting the boiler against chlorine deposition during combustion of chlorine-rich biomass, Fuel, **84**(2-3), pp. 201–212.

[81] Kassman, H., Broström, M., Berg, M., and Åmand, L.-E., 2011, Measures to reduce chlorine in deposits: Application in a large-scale circulating fluidised bed boiler firing biomass, Fuel, **90**(4), pp. 1325–1334.

[82] Aho, M., Vainikka, P., Taipale, R., and Yrjas, P., 2008, Effective new chemicals to prevent corrosion due to chlorine in power plant superheaters, Fuel, **87**(6), pp. 647–654.

[83] Wu, H., Jespersen, J. B., Frandsen, F. J., Glarborg, P., Aho, M., Paakkinen, K., and Taipale, R., 2013, Modeling of Ferric Sulfate Decomposition and Sulfation of Potassium Chloride During Grate-Firing of Biomass, Am. Inst. Chem. Eng., **59**(11), pp. 4314–4324.

[84] Li, B., Sun, Z., Li, Z., Aldén, M., Jakobsen, J. G., Hansen, S., and Glarborg, P., 2013, Post-flame gas-phase sulfation of potassium chloride, Combust. Flame, **160**(5), pp. 959–969.

[85] Kassman, H., Bäfver, L., and Åmand, L.-E., 2010, The importance of SO2 and SO3 for sulphation of gaseous KCl – An experimental investigation in a biomass fired CFB boiler, Combust. Flame, **157**(9), pp. 1649–1657.

[86] Pyykönen, J., and Jokiniemi, J., 2003, Modelling alkali chloride superheater deposition and its implications, Fuel Process. Technol., **80**, pp. 225–262.

[87] Saastamoinen, J. J., and Shimizu, T., 2007, Attrition-Enhanced Sulfur Capture by Limestone Particles in Fluidized Beds, Ind. Eng. Chem. Res., **46**(4), pp. 1079–1090.

[88] Vainikka, P., Lindberg, D., Moilanen, a., Ollila, H., Tiainen, M., Silvennoinen, J., and Hupa, M., 2013, Trace elements found in the fuel and in-furnace fine particles collected from 80MW BFB combusting solid recovered fuel, Fuel Process. Technol., **105**, pp. 202–211.

[89] Vesanto, P., Hiltunen, M., Moilanen, A., Kaartinen, T., Laine-ylijoki, J., and Sipilä, K., 2007, Kierrätyspolttoaineiden ominaisuudet ja käyttö, VTT Publications, Espoo.

[90] Kelly, J. D., and Hedengren, J. D., 2013, A steady-state detection (SSD) algorithm to detect non-stationary drifts in processes, J. Process Control, **23**(3), pp. 326–331.

[91] Nickel Use in Society [Online]. Available: http://www.nickelinstitute.org/NickelUseInSociety/MaterialsSelectionAndUse/Ni-ContainingMaterialsProperties/NickelChemicals.aspx.

[92] Thoma, H., Hauschulz, G., and Hutzinger, O., 1987, PVC-induced chlorine-bromine exchange in the pyrolysis of polybrominated diphenyl ethers, -biphenyls, -dibenzodioxins and dibenzofurans, Chemosphere, **16**(1), pp. 297–307.

[93] Söderström, G., and Marklund, S., 2004, Formation of PBCDD and PBCDF during flue gas cooling., Environ. Sci. Technol., **38**(3), pp. 825–830.

[94] Schüler, D., and Jager, J., 2004, Formation of chlorinated and brominated dioxins and other organohalogen compounds at the pilot incineration plant VERONA., Chemosphere, **54**(1), pp. 49–59.

[95] Vassilev, S. V., Baxter, D., Andersen, L. K., and Vassileva, C. G., 2013, An overview of the composition and application of biomass ash. Part 1. Phase–mineral and chemical composition and classification, Fuel, **105**, pp. 40–76.

[96] Vainikka, P., Enestam, S., Silvennoinen, J., Taipale, R., Yrjas, P., Frantsi, A., Hannula, J., and Hupa, M., 2011, Bromine as an ash forming element in a fluidised bed boiler combusting solid recovered fuel, Fuel, **90**(3), pp. 1101–1112.

[97] Sarkar, A., Vishwakarma, S., Banichul, H., Mishra, K. K., and Roy, S. S., 2012, A Comprehensive Analysis of the Particle Size and Shape of Fly Ash from Different Fields of ESP of a Super Thermal Power Plant, Energy Sources, Part A Recover. Util. Environ. Eff., **34**(5), pp. 385–395.

[98] Klysubun, W., Sombunchoo, P., Deenan, W., and Kongmark, C., 2012, Performance and status of beamline BL8 at SLRI for X-ray absorption spectroscopy., J. Synchrotron Radiat., **19**(Pt 6), pp. 930–6.

[99] Ravel, B., and Newville, M., 2005, ATHENA, ARTEMIS, HEPHAESTUS: data analysis for X-ray absorption spectroscopy using IFEFFIT., J. Synchrotron Radiat., **12**(Pt 4), pp. 537–41.

[100] Weng, T.-C., Waldo, G. S., and Penner-Hahn, J. E., 2005, A method for normalization of X-ray absorption spectra., J. Synchrotron Radiat., **12**(Pt 4), pp. 506–10.

[101] Tian, S., Yu, M., Wang, W., Wang, Q., and Wu, Z., 2009, Investigating the speciation of copper in secondary fly ash by X-ray absorption spectroscopy., Environ. Sci. Technol., **43**(24), pp. 9084–8.

[102] Fujimori, T., and Takaoka, M., 2009, Direct chlorination of carbon by copper chloride in a thermal process., Environ. Sci. Technol., **43**(7), pp. 2241–6.

[103] Hsiao, M. C., Wang, H. P., Chang, J.-E., and Peng, C. Y., 2006, Tracking of copper species in incineration fly ashes, J. Hazard. Mater., **138**(3), pp. 539–542.

[104] Hsiao, M. C., Wang, H. P., Wei, Y. L., Chang, J. E., and Jou, C. J., 2002, Speciation of copper in the incineration fly ash of a municipal solid waste., J. Hazard. Mater., **91**(1-3), pp. 301–7.

[105] Lundholm, K., Nordin, A., and Backman, R., 2007, Trace element speciation in combustion processes—Review and compilations of thermodynamic data, Fuel Process. Technol., **88**(11-12), pp. 1061–1070.

[106] Hupa, M., 2012, Thermodynamic Modeling of Combustion Processes – Applications and Limitations, Chemical Thermodynamics in Furnaces a joint symposium and course for combustion specialists and metallurgists.

[107] Lindberg, D., Backman, R., Chartrand, P., and Hupa, M., 2011, Towards a comprehensive thermodynamic database for ash-forming elements in biomass and waste combustion — Current situation and future developments, Fuel Process. Technol., **105**, pp. 129–141.

[108] Konttinen, J., Backman, R., Hupa, M., Moilanen, A., and Kurkela, E., 2013, Trace element behavior in the fluidized bed gasification of solid recovered fuels – A thermodynamic study, Fuel, **106**, pp. 621–631.

[109] Koukkari, P., Pentillä, K., and Karema, H., 2009, New Dynamics for kiln chemistry, Advance Gibbs Energy Methods for Functional Materials and Processes ChemSheet 1999-2009, P. Koukkari, ed., Helsinki, pp. 117–123.

[110] Aurell, J., Fick, J., Haglund, P., and Marklund, S., 2009, Effects of sulfur on PCDD/F formation under stable and transient combustion conditions during MSW incineration., Chemosphere, **76**(6), pp. 767–773.

[111] Talonen, T., 2008, Chemical Equilibria of Heavy Metals in Waste Incineration: Comparison of Thermodynamic Databases, Åbo University.

[112] Sandelin, K., and Backman, R., 1999, A Simple Two-Reactor Method for Predicting Distribution of Trace Elements in Combustion Systems, Environ. Sci. Technol., **33**(24), pp. 4508–4513.

[113] Yan, R., Gauthier, D., Flamant, G., and Badie, J. ., 1999, Thermodynamic study of the behaviour of minor coal elements and their affinities to sulphur during coal combustion, Fuel, **78**(15), pp. 1817–1829.

[114] Furimsky, E., and Zheng, L., 2003, Quantification of chlorine and alkali emissions from fluid bed combustion of coal by equilibrium calculations, Fuel Process. Technol., **81**(1), pp. 7–21.

[115] Poole, D., Argent, B. B., Sharifi, V. N., and Swithenbank, J., 2008, Prediction of the distribution of alkali and trace elements between the condensed and gaseous phases in a municipal solid waste incinerator, Fuel, **87**(7), pp. 1318–1333.

[116] Kouvo, P., and Backman, R., 2003, Estimation of trace element release and accumulation in the sand bed during bubbling fluidised bed co-combustion of biomass, peat, and refuse-derived fuels, Fuel, **82**(7), pp. 741–753.

[117] Öhman, M., Nordin, A., Skrifvars, B.-J., Backman, R., and Hupa, M., 2000, Bed Agglomeration Characteristics during Fluidized Bed Combustion of Biomass Fuels, Energy & Fuels, **14**(1), pp. 169–178.

[118] Zevenhoven-Onderwater, M., Blomquist, J.-P., Skrifvars, B.-J., Backman, R., and Hupa, M., 2000, The prediction of behaviour of ashes from five different solid fuels in fluidised bed combustion, Fuel, **79**(11), pp. 1353–1361.

[119] Pedersen, A. J., Frandsen, F. J., Riber, C., Astrup, T., Thomsen, S. N., Lundtorp, K., and Mortensen, L. F., 2009, A Full-scale Study on the Partitioning of Trace Elements in Municipal Solid Waste IncinerationsEffects of Firing Different Waste Types †, pp. 3475–3489.

[120] Lundholm, K., Boström, D., Nordin, A., and Shchukarev, A., 2007, Fate of Cu, Cr, and As during combustion of impregnated wood with and without peat additive., Environ. Sci. Technol., **41**(18), pp. 6534–40.

[121] Ménard, Y., Asthana, a., Patisson, F., Sessiecq, P., and Ablitzer, D., 2006, Thermodynamic Study of Heavy Metals Behaviour During Municipal Waste Incineration, Process Saf. Environ. Prot., **84**(4), pp. 290–296.

[122] Hack, K., ed., 2008, The SGTE casebook Thermodynamics at work, Woodhead Publishing Limited, Cambridge.

[123] Koukkari, P., 2009, Advanced Gibbs Energy Methods for Functional Materials and Processes – ChemSheet 1999–2009.

[124] Kong, X., Zhong, W., Du, W., and Qian, F., 2013, Three Stage Equilibrium Model for Coal Gasification in Entrained Flow Gasifiers Based on Aspen Plus, Chinese J. Chem. Eng., **21**(1), pp. 79–84.

[125] Francois, J., Abdelouahed, L., Mauviel, G., Patisson, F., Mirgaux, O., Rogaume, C., Rogaume, Y., Feidt, M., and Dufour, a., 2013, Detailed process modeling of a wood gasification combined heat and power plant, Biomass and Bioenergy, **51**, pp. 68–82.

[126] Bale, C. W., 2012, Macro Processing Manual - FactSage 6.3.

[127] Zhou, H., Jensen, P. A., and Frandsen, F. J., 2007, Dynamic mechanistic model of superheater deposit growth and shedding in a biomass fired grate boiler, Fuel, **86**(10-11), pp. 1519–1533.

[128] Miller, J. C., and Miller, J. N., 1993, Statistics for Analytical Chemistry, Ellis Horwood Limited, West Sussex.

[129] Wold, S., and Sjostrom, M., 2001, PLS-regression : a basic tool of chemometrics, pp. 109–130.

[130] Wise, B. M., Gallagher, N. B., and Windig, W., Chemometrics Tutorial for PLS _ Toolbox and Solo.

[131] Christensen, K. a., Stenholm, M., and Livbjerg, H., 1998, The formation of submicron aerosol particles, HCl and SO2 in straw-fired boilers, J. Aerosol Sci., **29**(4), pp. 421–444.

[132] Brunner, T., 2006, Aerosol and coarse fly ashes in fixed-bed biomass combustion, Graz.

[133] Aho, M., Yrjas, P., Taipale, R., Hupa, M., and Silvennoinen, J., 2010, Reduction of superheater corrosion by co-firing risky biomass with sewage sludge, Fuel, **89**(9), pp. 2376–2386.

[134] Jiménez, S., and Ballester, J., 2005, Effect of co-firing on the properties of submicron aerosols from biomass combustion, Proc. Combust. Inst., **30**(2), pp. 2965–2972.

[135] Zevenhoven, M., Yrjas, P., Skrifvars, B.-J., and Hupa, M., 2012, Characterization of Ash-Forming Matter in Various Solid Fuels by Selective Leaching and Its Implications for Fluidized-Bed Combustion, Energy & Fuels, **26**(10), pp. 6366–6386.

[136] Chi, K. H., and Chang, M. B., 2005, Evaluation of PCDD/F congener partition in vapor/solid phases of waste incinerator flue gases., Environ. Sci. Technol., **39**(20), pp. 8023–31.

[137] Kim, S. C., Jeon, S. H., Jung, I. R., Kim, K. H., Kwon, M. H., Kim, J. H., Yi, J. H., Kim, S. J., You, J. C., and Jung, D. H., 2001, Removal efficiencies of PCDDs/PCDFs by air pollution control devices in municipal solid waste incinerators., Chemosphere, **43**(4-7), pp. 773–6.

[138] Littarru, P., 2006, Repartition of PCDD and PCDF in the emissions of municipal solid waste incinerators between the particulate and volatile phases., Waste Manag., **26**(8), pp. 861–8.

[139] Guerriero, E., Guarnieri, A., Mosca, S., Rossetti, G., and Rotatori, M., 2009, PCDD/Fs removal efficiency by electrostatic precipitator and wetfine scrubber in an iron ore sintering plant., J. Hazard. Mater., **172**(2-3), pp. 1498–504.

[140] Becker, B., 2003, Gas-/Partikelwechselwirkung chlorierter Aromaten bei der Rauchgasreinigung von Müllverbrennungsanlagen, Universitat Stuttgart.

[141] Shao, Y., Xu, C. (Charles), Zhu, J., Preto, F., Wang, J., Tourigny, G., Badour, C., and Li, H., 2012, Ash and chlorine deposition during co-combustion of lignite and a chlorine-rich Canadian peat in a fluidized bed – Effects of blending ratio, moisture content and sulfur addition, Fuel, **95**, pp. 25–34.

[142] Yokohama, N., Otaka, H., Minato, I., and Nakata, M., 2008, Evaluation of gas-particle partition of dioxins in flue gas I: evaluation of gasification behavior of polychlorinated dibenzo-p-dioxins and polychlorinated dibenzofurans in fly ash by thermal treatment., J. Hazard. Mater., **153**(1-2), pp. 395–403.

[143] Shiomitsu, T., Hirayama, A., Iwasaki, T., Akashi, T., and Fujisawa, Y., 2001, Volatilization and Decomposition of Dioxin from Fly Ash, Engineering, **85**(85), pp. 3–5.

[144] Lundin, L., and Marklund, S., 2008, Distribution of mono to octa-chlorinated PCDD/Fs in fly ash from a municipal solid-waste incinerator., Environ. Sci. Technol., **42**(4), pp. 1245–1250.

[145] Eitzer, B. D., and Hites, R. a., 1988, Vapor pressures of chlorinated dioxins and dibenzofurans, Environ. Sci. Technol., **22**(11), pp. 1362–1364.

[146] Johansson, L. S., Leckner, B., Tullin, C., Åmand, L., and Davidsson, K., 2008, Properties of Particles in the Fly Ash of a Biofuel-Fired Circulating Fluidized Bed (CFB) Boiler, (12), pp. 3005–3015.

[147] Sandelin, K., and Backman, R., 2001, Trace Elements in Two Pulverized Coal-Fired Power Stations, Environ. Sci. Technol., **35**(5), pp. 826–834.

[148] Gullett, B. K., Bruce, K. R., and Beach, L., 1992, Effect of Sulfur Dioxide on the Formation Mechanism of Polychlorinated Dibenzodioxin and Dibenzofuran in Municipal Waste Combustors, **1**(10), pp. 1938–1943.

[149] Harriot, P., and Markussen, J., 1992, Kinetics of Sorbent Regeneration in the Copper Oxide Process for Flue Gas Cleanup, Ind. Eng. Chem. Reseach, **31**(1987), pp. 373–379.

[150] Schüler, D., and Jager, J., 2004, Formation of chlorinated and brominated dioxins and other organohalogen compounds at the pilot incineration plant VERONA., Chemosphere, **54**(1), pp. 49–59.

[151] Obernberger, I., Fly ash and aerosol formation in biomass combustion processes – an introduction Ingwald Obernberger, **43**(316).

[152] Mikkanen, P., 2000, Fly ash particle formation in kraft recovery boilers, Espoo.

[153] Eggersdorfer, M. L., Kadau, D., Herrmann, H. J., and Pratsinis, S. E., 2011, Multiparticle sintering dynamics: from fractal-like aggregates to compact structures., Langmuir, **27**(10), pp. 6358–67.

[154] Skrifvars, B.-J., Yrjas, P., Kinni, J., Siefen, P., and Hupa, M., 2005, The Fouling Behavior of Rice Husk Ash in Fluidized-Bed Combustion. 1. Fuel Characteristics, Energy & Fuels, **19**(4), pp. 1503–1511.

[155] Pommer, L., Öhman, M., Boström, D., Burvall, J., Backman, R., Olofsson, I., and Nordin, A., 2009, Mechanisms Behind the Positive Effects on Bed Agglomeration and Deposit Formation Combusting Forest Residue with Peat Additives in Fluidized Beds, Energy & Fuels, **23**(9), pp. 4245–4253.

[156] Lu, S.-Y., Du, Y., Yan, J.-H., Li, X.-D., Ni, M.-J., and Cen, K.-F., 2012, Dioxins and their fingerprint in size-classified fly ash fractions from municipal solid waste incinerators in China-Mechanical grate and fluidized bed units, J. Air Waste Manag. Assoc., **62**(6), pp. 717–724.

[157] Söderström, G., and Marklund, S., 2004, Formation of PBCDD and PBCDF during flue gas cooling., Environ. Sci. Technol., **38**(3), pp. 825–30.

[158] Söderström, G., and Marklund, S., 2002, PBCDD and PBCDF from incineration of waste-containing brominated flame retardants., Environ. Sci. Technol., **36**(9), pp. 1959–64.

Paper I

Towards controlling PCDD/F production in a multi-fuel fired BFB boiler using two sulfur addition strategies. Part I: Experimental campaign and results

In: Fuel 134, pp. 677-687

Fuel 134 (2014) 677–687

Contents lists available at ScienceDirect

Fuel

journal homepage: www.elsevier.com/locate/fuel

Towards controlling PCDD/F production in a multi-fuel fired BFB boiler using two sulfur addition strategies. Part I: Experimental campaign and results

Cyril Jose E. Bajamundi [a,b,*], Pasi Vainikka [a], Merja Hedman [c], Irina Hyytiäinen [c], Jaani Silvennoinen [c], Teemu Heinanen [d], Raili Taipale [a], Jukka Konttinen [b]

[a] VTT Technical Research Centre of Finland, Koivurannantie 1 PL 1603, 40 101 Jyväskylä, Finland
[b] Department of Chemistry, Renewable Natural Resources and Chemistry of Living Environment, University of Jyväskylä, POB 35, FI-40014 Jyväskylä, Finland
[c] Valmet Power, Lentokentänkatu 11, FI-33101 Tampere, Finland
[d] Stora Enso Newsprint and Book Paper, Anjalankoski Mills, FI 46900 Anjalankoski, Finland

HIGHLIGHTS

- We have shown that anti-corrosion measures (S-pellet addition and peat co-combustion) can affect PCDD/F production.
- We have reduced the production of PCDD/F in the BFB boiler by up to 53% through S-pellet addition.
- We have established that the ESP can lower PCDD/F concentration in the flue gas by up to 76%.

ARTICLE INFO

Article history:
Received 10 February 2014
Received in revised form 17 April 2014
Accepted 13 May 2014
Available online 4 June 2014

Keywords:
PCDD/F
De novo
Copper
Sulfur addition
Electrostatic precipitator

ABSTRACT

Levels of PCDD/F production in a 140 MW_{th} bubbling fluidized bed boiler were measured. The boiler uses solid recovered fuel, bark and sludge. Homologue distribution patterns suggest the *de novo* mechanism is the main pathway for the generation of dioxin and furans in the post combustion zones of the boiler. Two modes of sulfur addition were tested to induce the deactivation of Cu which has been identified as the prime catalyst of this mechanism. First, S-pellet promoted Cu sulfation as supported by aerosol sampling data and resulted in a decrease in PCDD/F levels. The second approach was adding sulfur through peat; this resulted in an increase in PCDD/F concentration. Factors such as high Cu content in the SRF-peat-sludge fuel mixture and reduced volatilization of Cu may have contributed to the said increase. For all test cases, phase redistribution of PCDD/F was observed in the electrostatic precipitator favoring more gaseous PCDD/F at the outlet. The homologue distribution pattern did not change in the flue gas path, suggesting that further synthesis and/or chlorination in the stream were minimized. There is however evidence for subsequent reactions happening in the ESP fly ash. The homologue distribution pattern in the latter was different from that of the flue gas, and more highly chlorinated PCDD/Fs were present. Furthermore, the ratio of PCDD and PCDF was different from that of the samples in the flue gas path.

1. Introduction

As the world population grows the amount of waste grows as well; thus waste management continues to be a priority around the globe. In the European Union (EU), the 2008 Directive on Waste Management sets the order of priority on waste prevention and management as follows: prevention, preparing for re-use, recycling, other recovery, e.g. energy recovery, and disposal [1]. But with increasing cost and environmental issues related to disposal, energy recovery becomes a strategic choice. In fact in Finland, the fraction of waste converted to energy rose from 9.6% in 2001 to 24.9% in 2011; while the fraction of waste sent to landfill declined from 61.1% to 40.2% during the same period [2].

Waste-to-energy (WtE) reduces landfill waste by up to 20 fold by volume, leaving only sterile residues. However due to poor public understanding WtE facilities are still seen as *dioxin factories* [3]. This perception remains even with efficient post combustion cleaning strategies and strict regulations. In EU member states an

* Corresponding author at: VTT Technical Research Centre of Finland, Koivurannantie 1 PL 1603, 40 101 Jyväskylä, Finland. Tel.: +358 20 722 2574; fax: +358 20 722 2720.
E-mail address: cyril.bajamundi@vtt.fi (C.J.E. Bajamundi).

http://dx.doi.org/10.1016/j.fuel.2014.05.034
0016-2361/

emission limit of 0.1 ng/Nm^3 (O_2 content 6%) on polychlorinated dibenzo-p-dioxins (PCDDs) and dibenzofuran (PCDFs) are strictly imposed by the Waste Incineration Directive (WID) [4]. The limit is applicable to stationary and mobile technical equipment partially or fully utilizing waste as fuel and converting it to energy via thermal processes, e.g. combustion, gasification, and pyrolysis. WID is enacted to avoid trans-boundary emission movements from states with less stringent environmental standards, and for the protection of the public and environment.

PCDD/Fs are planar, aromatic, and chlorinated organic compounds. In a dioxin molecule two oxygen atoms bond the two benzene rings while for a furan a single oxygen atom bonds the two rings (Fig. 1). Dioxins and furans with the same number of chlorine atoms constitute a homologue group or isomers. Tetra- to octachlorinated homologues are considered in calculating the toxicity equivalence quantity or TEQ [5]. Common sources of PCDD/Fs are side reactions from chemical synthesis, thermal processes, photochemical reactions, and naturally occurring enzymatic reactions under the influence of peroxides [6].

1.1. Formation mechanisms

Theoretical investigations on the synthesis of PCDD/Fs gained ground in the years following 1982 after an industrial accident released these compounds in an area over 2.8 km^2 [7]. Pyrosynthesis or precursor formation was first suggested as a formation mechanism; it occurs between 300 and 600 °C. This gas phase mechanism requires chemically similar intermediates (e.g. chlorobenzene, chlorophenols and polychlorinated biphenyls [8]) to undergo self-condensation (coupling of molecules or radical intermediates), cyclization of intermediates [9,10], and chlorination/dechlorination reactions. The last step is remarkably enhanced on a Cu(II)O surface either via Eley–Rideal or Langmuir–Hinshelwood mechanism [11]. Precursor formation commonly yields a signature ratio of $\Sigma_{PCDF}/\Sigma_{PCDD} < 1$ [12].

In parallel a *de novo* mechanism was also under investigation; early experiments showed that this happens in the temperature range of 200 to 400 °C [13], is a heterogeneous reaction, catalyzed by metals in the incineration fly ash [14,15], is thought to occur in the post combustion zones of WtE facilities. *De novo* mechanism requires carbon molecules contained in fly ashes to react with oxygen and chlorine, and has a characteristic signature of $\Sigma_{PCDF}/\Sigma_{PCDD} > 1$ [13,16]. The availability of chlorine is important and can either be sourced from the carbon matrix of partially combusted fuel such as soot [17], or produced from the metal-catalyzed Deacon reaction of $HCl_{(g)}$ and $O_{2(g)}$ (see reaction (1)) [18].

$$2HCl_{(g)} + 1/2O_{2(g)} \rightleftharpoons Cl_{2(g)} + H_2O_{(g)} \quad (1)$$

Gullet showed that Cu (as CuO) promoted the increase in the concentration of tetra- to octachlorinated homologues. It was also reported that a strong peak of formation occurs at 400 °C for all the PCDD congeners [18,19]. Copper aids in cleaving the carbon matrices in the ash and shuttles Cl for the matrix's chlorination. Likewise, Cu can be continuously chlorinated and dechlorinated, converting $HCl_{(g)}$ to $Cl_{2(g)}$ via reaction (1) [20].

In the 1990s studies on the influence of combustion [21–23] and post-combustion conditions [24,25] reinforced the role that poor combustion efficiency plays in PCDD/F production. Poor combustion is conducive for forming chemically similar precursors that eventually react to form PCDD/Fs. In addition, understanding of the dioxin's behavior in the gas cleaning equipment was developed. Memory effects due to the absorption-desorption of dioxins and furans were reported [26]; this can increase the concentration of PCDD/F after the wet scrubber. The effect of corona discharge in the electrostatic precipitator (ESP) on PCDD formation was explored. Corona discharge in the ESP can cause an increase of O and OH which in turn may increase the concentration of chlorophenoxyl radicals [27].

1.2. Inhibition by sulfur

Sulfur present as SO_2 depletes the Cl_2 levels through the homogeneous gas phase reaction [28]

$$Cl_{2(g)} + SO_{2(g)} + H_2O_{(g)} \rightleftharpoons 2HCl_{(g)} + SO_{3(g)} \quad (2)$$

Raghunathan et al. noted that during SO_2 injection the exit HCl concentration is considerably higher than during times when injection was halted. They also proposed that SO_2 can heterogeneously poison $CuCl_2$ [29], a *de novo* catalyst, via the reaction

$$SO_{2(g)} + CuCl_{2(s)} + H_2O_{(s)} + 1/2O_{2(g)} \rightarrow CuSO_{4(s)} + 2HCl_{(g)} \quad (3)$$

The Gibbs free energies of these three reactions are shown in Fig. 2. The negative values suggest the possibility of an inhibition mechanism at 200–400 °C; however for the Deacon reaction, kinetic information is also important to assess its occurrence [28].

Ogawa et al. investigated the PCDD/Fs inhibition rates during addition of gaseous SO_2, coal high in sulfur, and coal with a sulfur agent; they concluded that the mode of addition affects the dioxin inhibition [30]. Hunsinger et al. performed a pilot plant campaign to assess the optimum conditions to support PCDD/F inhibition via S addition in their TAMARA municipal solid waste incinerator [31]. Their results emphasize two important process conditions for successful utilization of S as a potential inhibitor:

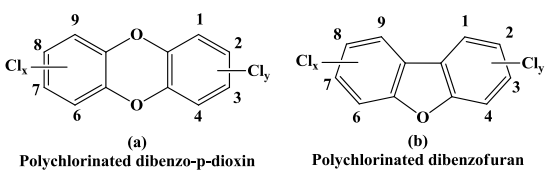

Fig. 1. Molecular structures of PCDD/F showing the position for chlorination. There are 75 PCDD and 135 PCDF congeners distinguished by the position and number of chlorine atoms attached to the benzene ring [9].

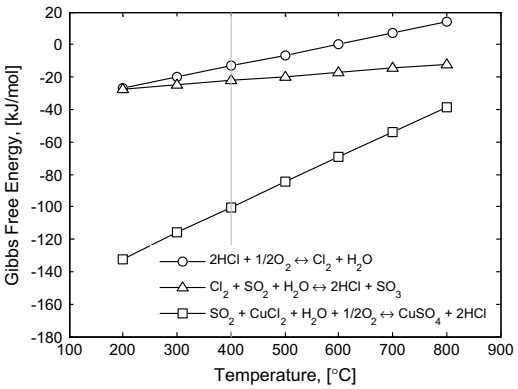

Fig. 2. Gibbs free energy values for reactions (1)–(3) calculated by FactSage 6.3. The line separates the temperature windows for the pyrosynthesis and the *de novo* formation mechanism.

1. Only maintaining a sufficient concentration of SO_2 (relative to HCl) in the flue gas will lower PCDD/F formation. Thus they proposed a recycling technique for the sulfur to remain in the system while avoiding excessive use of additives.
2. The ratio of HCl: SO_2 (both measured as mg/Nm^3) should be 1:1.

In addition, good combustion practices (GCP) have been adopted to ensure minimization of PCDD/F production. In the EU, the following GCP are imposed [4]:

1. Total organic carbon, TOC, content of the slag and bottom ashes should be less than 3%.
2. The combustion gas should be raised, after injection of the combustion air, to a temperature of 850 °C and be maintained there for at least 2 s.
3. Continuous measurement of CO, total dust, TOC, HCl, HF, NOx and SO_2.
4. At least two measurements per year of heavy metals, dioxins and furans; or one measurement at least every three months to be carried out for the first 12 months of the operation.

1.3. Goal of the study

This study aims to examine the levels of PCDD/F production in a bubbling fluidized bed boiler (BFB) utilizing solid recovered fuel (SRF), bark, and sludge. The facility is subject to the emissions limits set by the current WID [4]. Since the current WID is focused on limiting PCDD/F emissions alone, brominated (PBDD/F) and brominated-chlorinated (PXDD/F) varieties are not considered.

The test plan consisted of three cases. The first test (Case 1) is a reference case, and the succeeding tests examine the inhibitory effects to PCDD/F production when sulfur is introduced as sulfur pellets (Case 2) or sourced from peat (Case 3). These two sulfur sources are also countermeasures used in combustion systems to reduce chlorine induced corrosion by converting alkali chlorides to alkali sulfates [32–35].

To see the effect of S addition to the process, the concentrations of HCl and SO_2 at the post combustion region were monitored using FTIR. Aerosol sampling was done to examine the behavior of Cu and major ash forming elements. These behaviors can reveal the nature of the volatility and possible forms of these elements during this test.

The homologue distribution (fingerprint) of dioxin and furan was collected around the electrostatic precipitator to (a) identify the prevailing production mechanism in the post-combustion zones, (b) evaluate further production or phase redistribution at the flue gas path of electrostatic precipitator (ESP), and (c) fingerprint the PCDD/F in the ESP fly ashes and in the flue gas path.

Results presented in this paper will be analyzed further and validated in the succeeding parts of this three part study series. The ultimate aim of the study series is to propose a suitable combustion strategy focused on mitigating PCDD/F production in the BFB facility.

2. Materials and methods

2.1. The bubbling fluidized bed boiler and fuels

The study is limited to the boiler and the electrostatic precipitator; therefore the levels reported in this work cannot be considered as the actual PCDD/F emissions of the facility. The boiler is described in detail in another article [36], however the boiler has had a boiler area upgrade allowing operation at a capacity of 140 MW_{th} [37]. During the test campaign the boiler was operating at a mean load of 90 MW_{th}. Possible hotspots for PCDD/F formation are the economizers and the preheater. Flue gases enter the economizer on average at ~430 °C and exit at 340 °C, while at the air preheater the flue gases enter on average at ~260 °C and leave at ~185 °C.

The ESP consists of two parallel lines in the flue gas flow direction, both with two sequential fields being maintained at approximately 185–190 °C during the test runs, see Fig. 3b. This temperature setting was fixed to decrease the likelihood of generating more dioxins and furans in the ESP.

The process data extracted from the boiler's instrumentation are shown in Fig. 4. Together with a steady-state detection (SDD) algorithm developed by Kelly and Hedengren, we used these process data to assess whether the BFB was running at steady state. The SSD algorithm calculates the probability of being steady or at least stationary over a time interval by performing a residual Student's *t*-test using the estimated mean of the process signal without any drift and the estimated standard deviation of the underlying white-noise driving force [38].

The BFB facility uses Scandinavian spruce bark, dried paper mill sludge and solid recovered fuel (SRF). The bark comes from the debarking process of the paper mill adjacent to the boiler and the sludge is from the wastewater treatment facility of the same mill. This sludge is rich in calcium from paper fillers and coating used during the paper manufacturing. The wastewater treatment facility uses around 30–40 kg of iron(III)sulfate per ton of dry sludge as flocculant and aluminum(III) sulfate for pH control [39].

The SRF used in the study is collected from offices, wholesale businesses, and small – middle scale industries in southern Finland [40]. PVC based packaging plastics have been excluded during the collection and preparation of the SRF. In the SRF plant, materials are homogenized to 50–100 mm particle size and magnetic materials are separated, SRF is transported to the BFB in wrapped bales or fluffs [39].

The proportions, in percentage energy share, of the fuels fired are given in Table 1. Fuel mixtures containing SRF – Bark for Case 1 and 2, and SRF– Peat for Case 3 are fed to the boiler through the chutes in the left and right walls. Sludge is fed separately to the boiler from the thermal drying plant via pneumatic transport lines.

Each test case run lasted for 6 h; however for Case 2 the sulfur addition started the night before the actual test run to ensure that the system had been saturated with sulfur prior to the actual data collection. This is to follow the recommendation that only maintained level of S in the boiler is effective to combat dioxin and furan production [31].

The properties and the composition of the fuels fired in the boiler are found in Table 2. Because SRF has a large energy share, the majority of the elements found in the fuel mixture can be traced from it. This is true for example for minor components, sodium, potassium and chlorine, and for trace components copper, zinc and lead. Variation in the composition of the fuel mixture can also be traced directly to the SRF, with possible exceptions of Si and Al, since these elements are abundant in the peat. For the trace components, variability is high for Cr, Cu, Ni and Sb, as clearly seen in the values in the same table. This variation can be traced to the sources of these elements in the actual collected waste used to prepare the SRF. To name a few, Cu can come from brass, plastic catalyst and colorant, and copper wire, Cr can come from the impregnating agent found in CCA wood, Sb from fire retardant additives [39] and Ni can come from discarded electronics and additives in paint and plastics [41].

The concentration of Br in the fuel is low compared to Cl. Thus the amount of PBDD/F or PXDD/F that can be produced may be less compared to PCDD/F. Large PBDD/F formation in thermal treatment processes has been reported in the literature; however these studies have either used fuels with equal molar amounts of Br and Cl [42], or fixed proportion of the halogens in the fuel to reach a

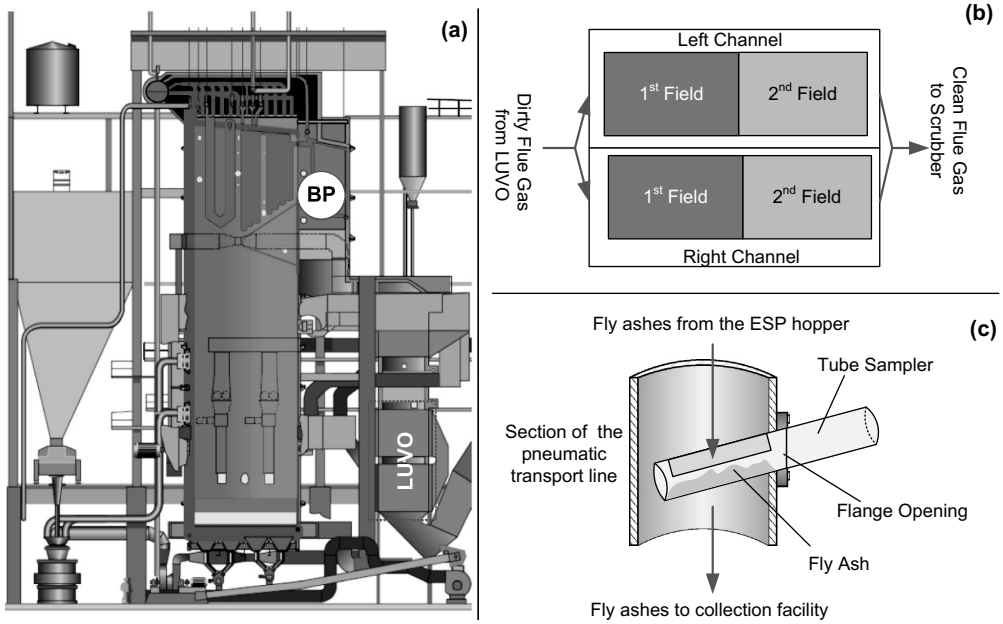

Fig. 3. (a) Schematic diagram of the bubbling fluidized bed boiler showing the location of the back pass (BP) where aerosol samplings were taken and the LUVO or air preheaters. (b) Flow of flue gas in the ESP channels and consequent fields. (c) Schematic for fly ash collection in the pneumatic transport line below the ESP hopper using a tube sampler.

Table 1
Fuel proportion and S-pellet addition in the study. Note that SRF-Bark or SRF-Peat comprises the fuel mixture described in Table 2.

Case	%Energy share				S-pellet added?
	SRF	Bark	Sludge	Peat	
1	50	44	6	0	No
2	50	44	6	0	Yes[a]
3	60	0	6	34	No

[a] Ratio of mass flow rate (kg/s) S-pellet/fuel is around 0.001.

required gas phase concentration [43], or performed test at pyrolytic conditions [44]. None of these proportions or conditions is applicable in this study.

In addition, chemical fractionation was performed to estimate the mode of occurrence of Na, K, Al and Si in the pure fuel. Increasingly aggressive solvents were used to leach out these elements, (a) H_2O for alkali sulfates, carbonates, and chlorides, (b) acetic acid (HOAc) for organically bound fractions, (c) HCl for carbonates and sulfates of alkaline earth and other metals [34]. The rest are silicates and minerals. The analysis was done by an accredited laboratory. However the advanced role of this procedure in this study is not emphasized [45] and the results are only used for the purpose noted above.

2.2. Aerosol sampling

Aerosol samples were collected from the right wall of the backpacks zone indicated by BP in Fig. 3 using the Dekati Low Pressure Impactor (DLPI). Each sampling interval runs for 40 min and the schedule is shown in Fig. 4. The impactor deposits were digested with water or strong acid for five days and subjected to ultrasonic mixing prior to extraction. The concentrations of water soluble Na, K and Ca, were measured using ICP-MS. For Cl, SO_4 and Br ion

Table 2
Properties of fuel mixture and sludge used in the study. Analyses were carried out according to the appropriate CEN/Ts, ASTM and ISO methods.

Parameter/Component	Fuel mixture			Sludge
	Case 1	Case 2	Case 3	
Gross heating value (MJ/kg, d)	23.02	21.78	19.59	20.2
Net heating value (MJ/kg, d)	21.51	20.35	18.38	18.920
Net heating value (MJ/kg, a.r.)	9.84	8.45	8.99	4.29
Moisture content (wt.%, a.r.)	48.7	52.2	45.1	68.5
Major components (wt.%, d.)				
C	52.5	51.2	46.0	49.3
H	7	6.6	5.6	5.9
N	0.63	0.56	0.76	1.81
S	0.12	0.21	0.41	0.5
O (calculated)	36.04	37.26	37.64	38.54
Minor components (mg/kg, d)				
Cl	3300	2900	2800	200
Na	1800	1700	3300	2300
K	1500	1700	4600	970
Ca	18,500	18,400	15,100	14,100
Mg	1000	1500	1700	840
P	430	390	290	1800
Al	3900	3000	11,100	5700
Si	4100	8600	47,300	11,400
Fe	1200	1700	6300	830
Trace components (mg/kg, d)				
Mn	200	280	120	1100
Zn	200	170	260	82
Br	10	10	20	30
Cr	17	56	340	7.3
Cu	26	26	670	13
Ni	3.8	11	150	1.9
Sb	5.9	4	140	0.5
Cd	0.24	0.24	0.46	0.25
Co	2.7	0.43	4.8	0.5
Pb	43	48	32	3.2
Sn	6.2	18	4.7	0.56
V	2.9	3.5	12	1.8

chromatography was used, and for the acid soluble copper ICP-MS was employed. A detailed discussion on the schematic and subsequent analysis of aerosol samples was provided earlier [36]. For this work, the aerosol concentration of Ca, Na, K, Cl, and S (represented as sulfate) and Br are from the water soluble fractions while that of Cu is from the acid soluble fraction.

2.3. ESP fly ash sampling and analyses

The fly ash was collected in the pneumatic transport lines below the fields of the ESP using a tube sampler made up of a steel pipe; see Fig. 3b and c. For each test case, five sampling periods lasting for about 4 min, sufficient for the sampler to be filled, were performed. Each sample was cooled before being bagged into a clean and sealed container. During the experimental runs, the volume of the fly ash collected in the 1st field of the ESP is four times that collected in the 2nd field. The composite sample for each test case was prepared according to the following procedure:

First, for each channel, 4 parts by volume of ashes collected from the 1st field and 1 part by volume of ashes collected from the 2nd field were mixed (dubbed as channel-mixture). Then equal mass portions of channel-mixtures from the left and right channels were combined (dubbed as sampling-mixture). Finally, five equal mass portions of sampling-mixtures were then combined to comprise the composite fly ash sample for each test case.

Analysis of PCDD/F concentration in the ESP fly ash was done by Eurofins GfA Lab Service GmbH in Germany. This laboratory uses an internal method and is accredited to perform this kind of test. The concentration of Cu and S was analyzed by Labtium Ltd. in Espoo, Finland using the XRF technique.

2.4. Dioxin/furan measurements in the flue gas path

Sampling and analysis of dioxin and furan in the flue gas path were done by Pöyry Oy, an accredited laboratory in Finland. Sample collection, clean up, extraction and measurements are governed by the CSN EN 1948: Stationary source emissions – determination mass concentration of PCDDs/PCDFs and dioxin like PCBs Part 1–3. Sampling locations are situated before and after the electrostatic precipitator in order to determine the dioxin/furan in-boiler production and assess if further production takes place in the ESP. For toxicity purposes only the homologues with four or more chlorine atoms are considered; thus only these homologues are reported in this study. All concentrations are based on I-TEQ at a 6% O_2 (101.3 kPa and 273 K) dilution factor.

3. Results

3.1. Boiler condition

Fig. 4 shows the operating conditions of the boiler during the tests. The probability that the process is running at a steady state was calculated using the steady-state detection (SDD) developed by Kelly et al. The term steady state implies that the process is operating around some stable point or within some stationary region where it must be assumed that the accumulation or rate-of-change of material, energy, and momentum is statistically insignificant [38]. A probability of 0.90 or greater indicates that the process is at a steady state. The probabilities for the process data used for this analysis (see Fig. 4) are all within the cut-off indicating that the BFB is running at a steady state or at least stationary during each test case.

3.2. Levels of SO_2 and HCl in the backpass

Sulfur addition increased the SO_2 concentration in the flue gas (Fig. 5) from 23 ± 8 mg/Nm^3 for Case 1 to 400 ± 80 mg/Nm^3 and

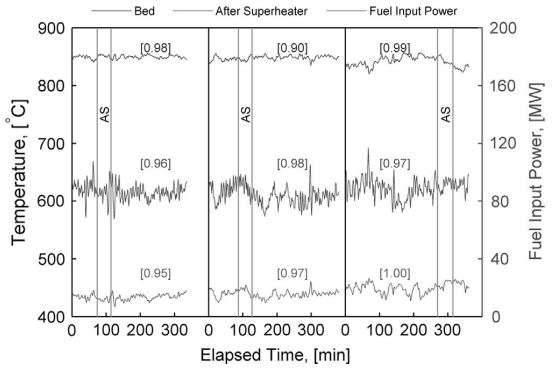

Fig. 4. Process data extracted from the boiler's instrumentation. Fuel input power does not include the power input from the sludge. AS indicates when aerosol sampling was taken. The numbers inside the square bracket indicate the probability that the process is at steady state using a steady-state detection algorithm [38].

463 ± 100 mg/Nm^3 for Cases 2 and 3, respectively. The SO_2 concentration was stable for Case 1 and 2, but in Case 3 a slight increase was noted from 3:00 pm onwards. The latter can be the result of variations in the S content of the peat. In terms of stability, the use of sulfur pellets is better as compared to peat. In the long run, the stability of the SO_2 concentration is important for effectively reducing the PCDD/F production [31].

The concentration of HCl in the flue gas likewise increased from 210 ± 22 mg/Nm^3 to 302 ± 30 mg/Nm^3 for S-pellet addition and to 325 ± 29 mg/Nm^3 for peat co-combustion. Such an increase happened even though the concentration of Cl in the fuel decreased (Table 2). This observation is similar to what Raghunathan and

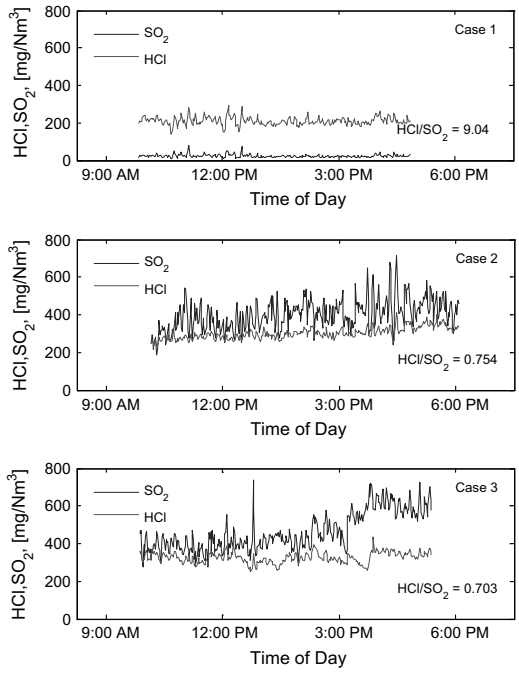

Fig. 5. Levels of SO_2 and HCl in the backpass for the three test cases as measured by the FTIR.

co-workers observed [28] and suggests of a possible occurrence of reaction 2 which decreases the amount of $Cl_{2(g)}$ in the flue gas.

The required HCl/SO_2 ratio of 1/1 [31] was not reached. However the ratios for Cases 2 and 3 are near, at 0.745 and 0.703 respectively (see annotated values in Fig. 5). The ratio suggests over addition of sulfur to the BFB; this was made to ensure sufficient amount of S is available for sulfation and saturation of S in boiler deposits.

3.3. Aerosols

For all the impactor results, fine particles found in the region of $d_p < 1.6$ μm were once in vapor form and due to supersaturation in the gas phase they had undergone homogeneous nucleation and coagulation. Particles found in the region of $d_p > 1.6$ μm represent coarse particles that are mostly non-volatile fragments of the fuel and/or entrained particles [46,47].

3.3.1. Main aerosol forming elements

For Case 1 the aerosols are mostly Na, K and Cl, with slight amounts of SO_4 (Fig. 6). In the fine particle mode, the molar ratio Cl/(Na + K) = 0.95 indicates that the alkalis present are mostly alkali chloride with some alkali sulfate. This is typical of boilers firing the same fuels [34] without the aid of anti-corrosion additives. The coarse particle fraction showed a significant amount of water soluble Ca, possibly as $CaSO_4$. The formation of $CaCl_2$ is minimized since some Na and K are also present in this fraction.

In Case 2 the fine particle fraction is composed of Na, K, and Cl with more SO_4 present. The molar ratio Cl/(Na + K) = 0.61 indicates that more of the alkalis present can now be found as alkali sulfates. The sulfation of the alkalis can proceed via the reaction (M is the alkali) [32,33,48]:

$$2MCl_{(g)} + SO_{3(g)} + H_2O_{(g)} \rightarrow 2HCl_{(g)} + M_2SO_{4(s)} \quad (4)$$

The required SO_3 in reaction (4) could have come directly from the oxidation of sulfur from the fuel or from reaction (2). The latter is possible because of the increase in HCl resulting in co-production of SO_3(see Fig. 5).

Sulfation requires sufficient time and results in particle growth [32,49]. Kassman and co-worker report growth in fine particle size from 0.1 μm to 0.4 μm in a reference case test for S- addition [50]. Such growth is seen when Case 1 and 2 are compared, as the peak concentration shifted from 0.09 to 0.26 μm to 0.26–0.6 μm. The increase of SO_4 and peak shift suggest successful alkali sulfation.

For Case 3, the size distribution is still bi-modal but the peak in the coarse particle range is now higher than in the fine particle range. In the coarse particle range, significant amounts of Ca and Cl are present with few alkalis. This suggests the presence of $CaCl_2$, $CaSO_4$ and some alkali chlorides or sulfates. In the fine particle range, the total amount of Na and K (0.91 mmol/Nm^3) is almost half of that in the two other cases (1.56 mmol/Nm^3 for Case 1 and 1.72 mmol/Nm^3 for Case 2); even though the concentration of Na and K for Case 3 is almost twice that in the two other cases, see Table 1. Three probable reasons can explain this observation: First, the difference in the mode of Na and K in the fuel mixture used in Case 3 relative to the two other cases. Second, sulfation via reaction (4) might have occurred because of the presence of SO_4 in the aerosol, with SO_3 being sourced again from reaction (2). Third, chemisorption of alkali aluminosilicates which converts gaseous alkali chloride to water-insoluble alkali-aluminosilicate [33] via the reaction

$$2MCl_{(g)} + Al_2O_3 \cdot xSiO_{2(s)} + H_2O_{(g)} \rightarrow M_2O \cdot Al_2O_3 \cdot xSiO_{2(s)} + 2HCl_{(g)} \quad (5)$$

The chemical fractionation results (Fig. 8) suggest that the decrease of alkalis in the aerosols for Case 3 is most likely the result of the mode of occurrence of Na and K in the fuel. With peat substituting bark in the fuel mixture for Case 3, the total amount of alkalis increased. However these alkalis are less "reactive" and are bound to the aluminosilicates in the peat [51] which lowers the amount of Na and K in the flue gas. The SO_4 in the aerosol could likewise be explained by reaction (4). Through this line of reasoning, the contribution of chemisorption is limited.

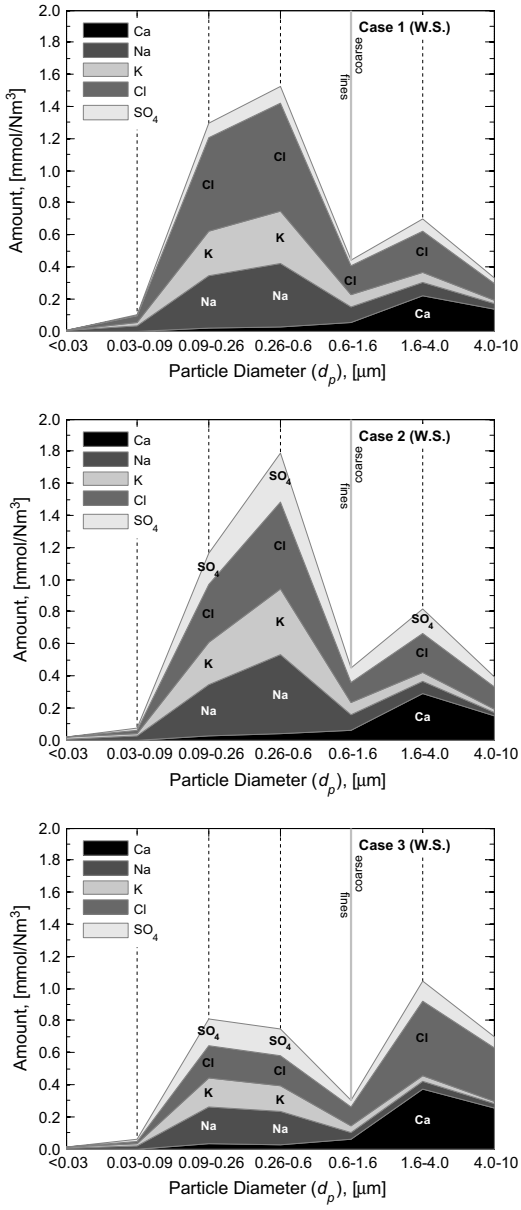

Fig. 6. Composition of select water soluble ash and aerosol forming elements collected at the backpass of the BFB boiler.

3.3.2. Copper and Bromine in the aerosol

For all the test cases, copper in the fine particle range suggests volatilization of this element. Cases 1 and 2 have cumulative

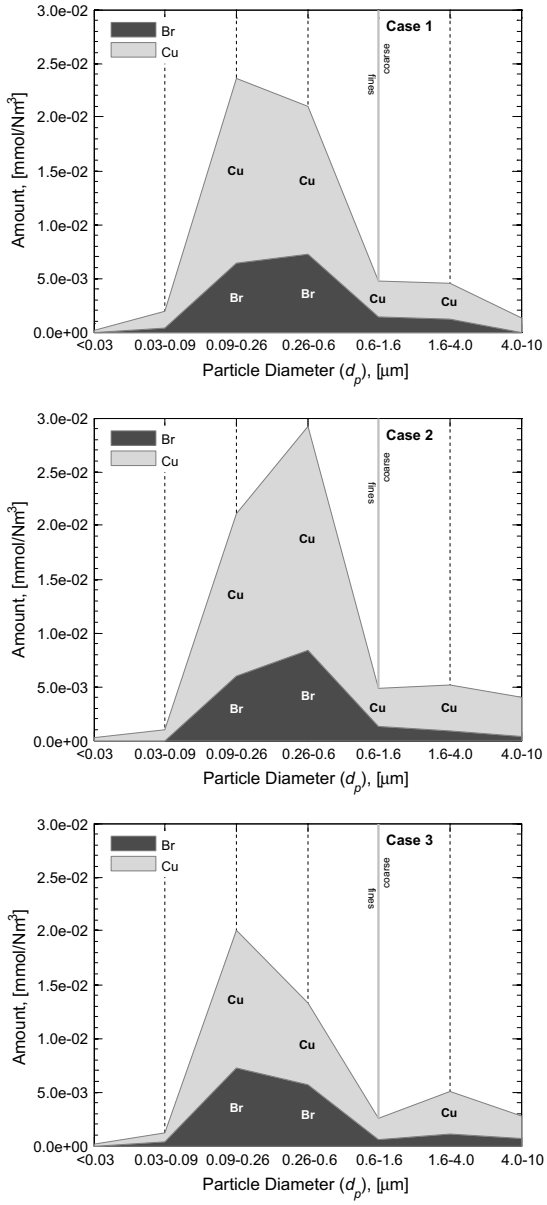

Fig. 7. Concentration of Cu and Br in the aerosols collected at the backpass. Data for copper are based on acid soluble fraction, while Br comes from water soluble fraction.

concentrations of 0.036 mmol/Nm^3 and 0.041 mmol/Nm^3 of Cu respectively. However, Case 3 exhibits the least amount Cu in the said range although the concentration of Cu in the fuel is high. For this case, copper might have been present in a less volatile form (e.g. metallic copper and solid oxides) and have remained in the coarse fly ashes or part of the fragments of the fuel being entrained in the flue gas.

A shift in the peak in the fine particle range from Case 1 to 2 suggests the possibility of $CuSO_4$ formation. Copper existing as

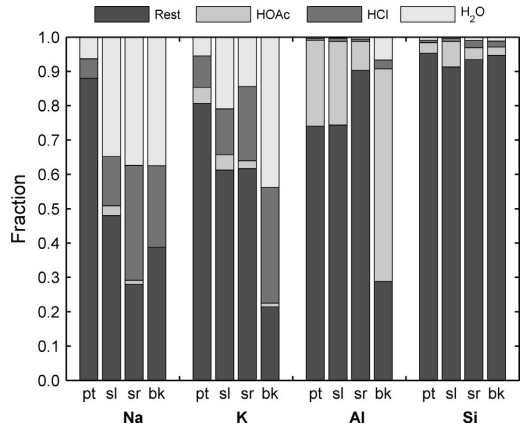

Fig. 8. Chemical fractionation of the pure fuels used in the tests – peat(pt), sludge(sl), SRF (sr) and bark (bk).

$CuCl_{(g)}$ or $CuCl_{2(s)}$ could be sulfated via reaction (4) and (3) respectively. In addition, free $Cl_{2(g)}$ can react with $CuO_{(s)}$ forming a product that can also be sulfated via the two step reaction postulated by Ryan et al. [52]:

$$2CuO_{(s)} + Cl_{2(g)} \rightleftharpoons 2CuOCl_{(s)} \quad (6)$$

$$2CuOCl_{(s)} + 0.5O_{2(g)} + 2SO_{3(g)} + H_2O_{(g)} \rightarrow 2CuSO_{4(s)} + 2HCl_{(g)} \quad (7)$$

Takaoka et al. have reported the presence of similar forms of copper oxychloride species using advanced X-ray techniques [53]; this supports the possibility of $CuO_{(s)}$ sulfation.

Sulfation is further supported by the increase in the S concentration in the ESP fly ash from 1.44 mg/kg to 2.03 mg/kg for Case 1 and 2 respectively (Table 3). These two values can easily be compared since the dilution effect of having too much ash is not very significant between these two cases.

Bromine is mostly found in the fine particle fraction and could have existed possibly as (K, Na)$Br_{(g)}$ and $CuBr_{3(g)}$ [37,39]. When Br is present it can compete with Cl for available Cu, which reduces the amount of active *de novo* catalyst such as $CuCl_2$. With respect to PCDD/F formation, it is clear that $CuCl_2$ is an important catalyst either for direct chlorination or as a provider of Cl_2 [42]. On the other hand the catalytic effects of Cu-Br compounds in PCDD/F formation have not been intensively investigated [43].

3.4. PCDD and PCDF production and removal

3.4.1. Total concentrations at different sampling points

The total concentration of PCDD/F, around the ESP, is found in Fig. 9. At the ESP inlet, the concentration of PCDD/F is 0.786 ng/Nm^3 for Case 1. Adding sulfur pellets (Case 2) reduced the

Table 3
Concentration of selected elements in the fly ash.

Element	Concentration (mg/kg a.r.)		
	Case 1	Case 2	Case 3
K	2.05	2.05	1.69
Al	10.06	8.26	7.09
Si	17.58	19.73	22.39
Cl	1.61	0.60	0.40
S	1.44	2.03	1.09
Cu	0.26	0.23	0.18

concentration to 0.363 ng/Nm^3 while co-firing of peat (Case 3) increased the concentration to 1.345 ng/Nm^3. The PCDD/F production did not follow the concentration of Cl in the fuel.

After the ESP, the concentration of PCDD/F for Case 2 is the lowest at 0.133 ng/Nm^3, while Case 1 and 3 have 0.369 ng/Nm^3 and 0.313 ng/Nm^3, respectively. These values show that the ESP is effective in reducing the concentration of these compounds in the flue gas path. But phase redistribution has occurred along the flue gas path; PCDD/F are particle bound in the inlet and they leave the ESP in the gaseous phase (especially furan). This particle to gas phase redistribution is typical in many ESPs [54–57].

As for the ESP fly ash, the concentration in the Case 1 is highest compared to the levels for Cases 2 and 3, which are almost comparable. For Case 1, poor sulfation of Cu may have prolonged the existence of active Cu species and have led to successive chlorination and/or synthesis. This can happen even if the temperature is below the optimum temperature window [58]. For Case 2, additional chlorination may have occurred but because of effective Cu sulfation, the PCDD/F levels in the fly ash remained low. Meanwhile, the low concentration in Case 3 could simply be the result of dilution. While we cannot exactly quantify the total amount of fly ash for each test, the particle loading data from the aerosol sampling may support this dilution hypothesis (see Fig. 12). Case 3 has the highest particle loading in the coarse size range and indicates that there is more fly ash during this case. A high tendency of peat to produce fly ashes when fired has been reported in the literature [63].

3.4.2. Homologue distribution in the flue gas path

PCDD/F homologue distribution can give information on the dominant mechanism of PCDD/F formation and help explain the trends noted above. For all the test cases the ratio $\Sigma_{PCDF}/\Sigma_{PCDD} > 1$ (see Fig. 10); this points to the *de novo* mechanism as the dominant means of production [13,16]. The conditions from the backpass to the LUVO are conducive for this mechanism; the flue gas is cooling to the right temperature window, the residence time requirement is met (order of seconds, 2.9 s at 340 °C [16]) and the deposition of carbon rich ash can occur.

Dioxin and furan concentrations are highest for the lighter homologues, penta-chlorinated dibenzo-p-dioxins (5D) and penta-chlorinated dibenzofuran (5F). The phase distribution favors species to be bound to particles. This suggests that the key ingredients for this in-flight *de novo* synthesis are present in the active fly ash.

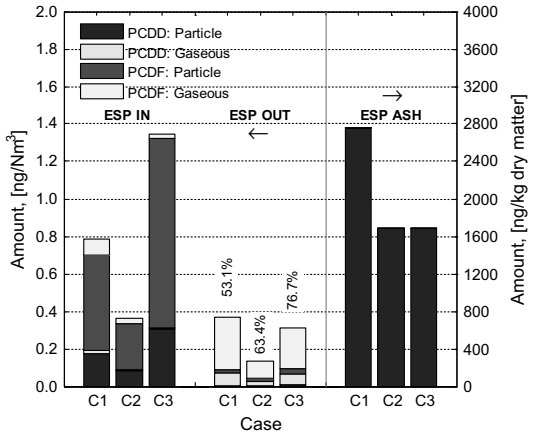

Fig. 9. Total levels of PCDD/F in the flue gas path (ESP IN and OUT) and ESP fly ash. The values above the bars for ESP OUT are the percentage removals of PCDD/F in the flue gas path.

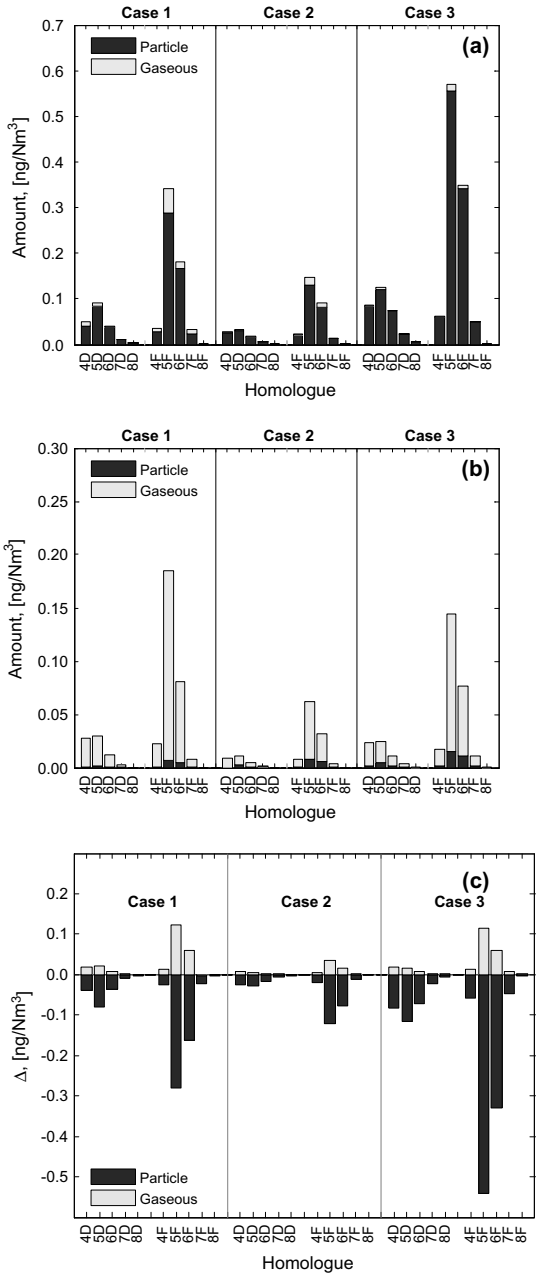

Fig. 10. Flue gas path homologue distribution patterns of toxic PCDD/F in (a) ESP IN, (b) ESP OUT and (c) changes in particle bound and gaseous concentration of PCDD/F or the removal homologue distribution.

The difference between the levels of production between Cases 1 and 2 can be explained by the deactivation of the key *de novo* catalyst, Cu. With the introduction of S-pellets, effective conversion of copper oxides and chlorides to sulfates may have been possible, as supported by the aerosol data in Fig. 7. Metal sulfates, unlike metal

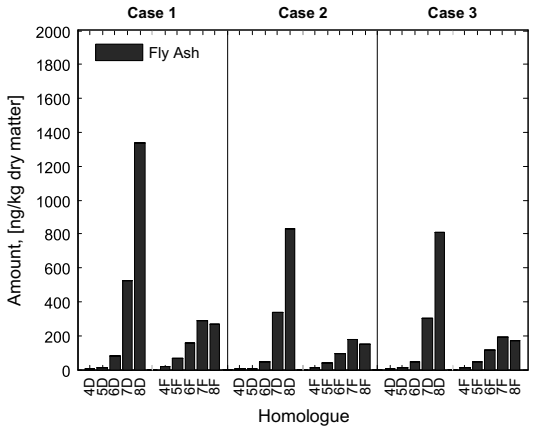

Fig. 11. ESP fly ash homologue distribution patterns of toxic PCDD/F.

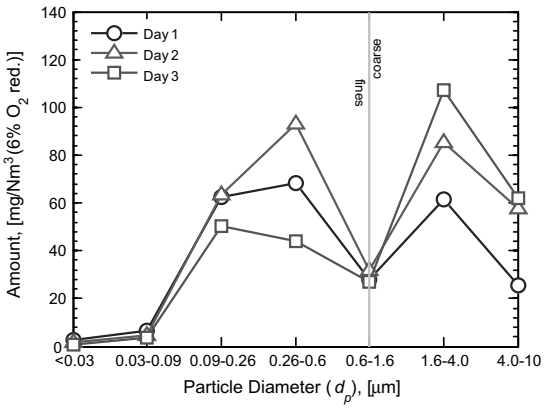

Fig. 12. Particle loading at different size fractions in the backpass from the impactor measurements.

chlorides or oxides, are not likely to promote the formation of PCDD/F [52]. In addition, the availability of free $Cl_{2(g)}$, an active ingredient for PCDD/F formation, may have decreased in Case 2 as discussed in Section 3.2.

The high concentration of PCDD/F for Case 3 is a result of high ash loading in the flue gas and low Cu volatilization. These two situations enhanced the possibility for Cu (in the form of oxide and oxychloride [53]) to remain in the ash and act as catalyst for cracking carbon matrices to form structurally related material [9]. Cu may also have easily aided in the shuttling of $O_{2(g)}$ and $Cl_{2(g)}$ to the active fly ash surface, thus adding to its effectiveness as catalyst for chlorination. In addition, particles can serve as effective and porous support where Cu, Cl, and partially burned or unburned carbon can adsorb. These observations benefit the in-flight PCDD/F production via *de novo* mechanism.

For all the test cases the homologue distribution patterns of PCDD/F in the outlet of the ESP are almost similar to patterns at the ESP inlet; dioxin and furan concentration peaks are seen at the lighter homologues, penta-chlorinated dibenzo-p-dioxins (5D) and penta-chlorinated dibenzofuran (5F), respectively. This is an indication that the succeeding reaction or chlorination may not have occurred in the ESP flue gas path. The ESP was operated at a temperature 10 °C below the temperature window for *de novo* synthesis [13,16,56] preventing subsequent reactions in the flue gas path.

Also the phase distribution of PCDD/F at the ESP flue gas path outlet now favors gaseous dioxins and furans. Changes in the concentrations of PCDD/F homologues between the two phases are found in Fig. 10c. The gas phase removal is negative, indicating vaporization or repartitioning of PCDD/F from the particle to the gas phase [51,54]. Vaporization can be affected by temperature [59], particle density and size distribution [60,61].

The increase in the gaseous furans is higher than that of dioxins. Factors affecting these are (a) original amount – there are more furans than dioxins to begin with, therefore if both are vaporized the change in furan should be higher, (b) the vapor pressure of furans is slightly higher than that of dioxins. For instance at 25 °C the vapor pressure of 1,2,3,4-tetrachloro dibenzofuran is 1.223×10^{-4} Pa while that for 2,3,7,8-tetrachloro dibenzo-p-dioxin is 1.044×10^{-4} Pa [62].

3.4.3. Homologue distribution in the ESP fly ash

In comparison to the homologue distribution in Fig. 10, the distribution for the ESP fly ash peaks at higher chlorinated dioxins and furans, see Fig. 11. Heavier homologues, octa-chlorinated dibenzo-p-dioxins (8D) and hepta-chlorinated dibenzofuran (7F), are dominant. In addition the $\Sigma_{PCDF}/\Sigma_{PCDD} < 1$, indicating subsequent chlorination or production in the fly ash. This implies that particle bound PCDD/F and catalysts such as copper and chlorine found in carbon matrices are still active. These reactions however may require longer time and thus have not contributed additional PCDD/Fs in the flue gas path. Furthermore, aging of the sample may also have contributed to this shift in the distribution patterns.

The next part of this series will use equilibrium thermodynamic modeling to explain the behavior of the aerosol samples mentioned above and will analyze the speciation of Cu. This will be used to understand the chemistries governing the test cases. This understanding may help explain the levels of PCDD/F measured and presented here.

4. Conclusions

The *de novo* mechanism is the dominant means of production of PCDD/F in the multi-fuel fired BFB facility. This mechanism is catalyzed by Cu. Aerosol samples showed that sulfur pellets were able to effectively convert copper chlorides or oxides to sulfates thus reducing the production of PCDD/F. On the other hand, during co-firing of peat, Cu was less volatile and ash loading in the flue gas increased; this led to a significant increase in PCDD/F.

In the flue gas path, most of the PCDD/F leaving the post combustion zones is particle bound. Phase redistribution or volatilization occurred in the ESP and resulted in an increase in gaseous PCDD/F leaving the device. However this phase redistribution did not affect the overall decrease of the PCDD/F concentration in the flue gas traversing the ESP.

There is evidence pointing to some reactions in the ESP fly ash because the homologue distribution pattern is different from the pattern in the flue gas path and the ratio of furans and dioxins is different. The trend in the PCDD/F concentration in the ash has been affected by dilution and the amount of active Cu in the ash.

At this point of the study, the addition of sulfur pellets is more advantageous in PCDD/F production abatement because of the reasons discussed above. However we are not yet discarding the possibility of peat as an efficient PCDD/F abatement technique; for one reason, Cu in Case 3 was way too high. The nature of SRF is very dynamic, thus the variability in Cu concentration may be high.

Acknowledgement

We are thankful to the OSER project, Metso Power, Foster Wheeler, the European Regional Development Fund, and RECOMBIO project TREN/FP7EN/239530/for the resources shared for this study. We appreciate Stora Enso Oyj for sharing the data presented in this paper. is gratefully acknowledged. Likewise we acknowledge Marko Räsänen and Juho Kauppinen for the collection of aerosol samples, Muhammad Nasrullah for carefully collecting and preparing the fuel samples for analysis, and Martti Aho for the helpful discussion on particle loading from the aerosol sampling.

References

[1] Directive 2008/98/EC of the European parliament and the council of 19 November 2008 on waste and repealing certain Directives. Off J Eur 2008:3–30.
[2] Statistics Finland/waste statistics FEI (SYKE). Municipal solid waste in Finland 1997–2011 n.d.
[3] Buekens A, Cen K. Waste incineration, PVC, and dioxins. J Mater Cycles Waste Manag 2011;13:190–7.
[4] Directive 2003/76/EC of the European parliament and the council of December 4, 2000 on the incineration of waste. Off J Eur Communities 2000: L 332/91–111.
[5] EnvironmentAustralia. Incineration and Dioxins review of formation processes, consultancy report prepared by environmental and safety services for environment Australia. Canberra: 1999.
[6] Wielgosin G. The reduction of dioxin emissions from the processes of heat and power generation. J Air Waste Manage Assoc 2011;61:511–26.
[7] Kulkarni PS, Crespo JG, Afonso CM. Dioxins sources and current remediation technologies–a review. Environ Int 2008;34:139–53.
[8] Hutzinger O, Choudhry GG, Chittim BG, Johnston LE. Formation of polychlorinated dibenzofurans and dioxins during combustion, electrical equipment fires and PCB incineration. Environ Health Perspect 1985;60:3–9.
[9] Altarawneh M, Dlugogorski BZ, Kennedy EM, Mackie JC. Mechanisms for formation, chlorination, dechlorination and destruction of polychlorinated dibenzo-p-dioxins and dibenzofurans (PCDD/Fs). Prog Energy Combust Sci 2009;35:245–74.
[10] Tuppurainen K, Halonen I, Ruokoj P, Tarhanen J, Ruuskanen J. Formation of PCDDs and PCDFs in municipal waste incineration and its inhibition mechanism: a review. Chemosphere 1998;36:1493–511.
[11] Lomnicki S, Dellinger B. A detailed mechanism of the surface-mediated formation of PCDD/F from the oxidation of 2-chlorophenol on a CuO/Silica surface. J Phys Chem A 2003;107:4387–95.
[12] Dickson LC, Lenoir D, Hutzinger O, Chemistry E, Republic F. Quantitative comparison of de novo and precursor formation of polychlorinated dibenzo-p-dioxins under simulated municipal solid waste incinerator postcombustion conditions. Environ Sci Technol 1992:1822–8.
[13] Everaert K, Baeyens J. The formation and emission of dioxins in large scale thermal processes. Chemosphere 2002;46:439–48.
[14] Choudhry GG, Hutzinger O. Mechanistic aspects of the thermal formation of halogenated organic compounds including polychlorinated dibenzo-p-dioxins. Part V: hypotheses and summary. Toxicol Environ Chem 1982;5:295–309.
[15] Stieglitz L, Zwick G, Beck J, Roth W, Vogg H. On the de-novo synthesis of PCDD/PCDF on fly ash of municipal waste incinerators. Chemosphere 1989;18:1219–26.
[16] Stanmore B. The formation of dioxins in combustion systems. Combust Flame 2004;136:398–427.
[17] Vehlow J, Bergfeldt B, Hunsinger H. PCDD/F and related compounds in solid residues from municipal solid waste incineration – a literature review. Waste Manag Res 2006;24:404–20.
[18] Gullet BK. The effect of metal catalysts on the formation of polychlorinated dibenzo-p-dioxin and polychlorinated dibenzofuran precursor. Chemosphere 1900;20:1945–52.
[19] Gullett BK, Bruce KR, Beach LO, Drago AM. Mechanistic steps in the production of PCDD and PCDF during waste combustion. Chemosphere 1992;25:1387–92.
[20] Bruce KR, Beach LO, Gullett BK. The role of gas-phase Cl2 in the formation of PCDD/PCDF during waste combustion. Waste Manag 1991;11:97–102.
[21] Wikström E, Tysklind M, Marklund S. Influence of variation in combustion conditions on the primary formation of chlorinated organic micropollutants during municipal solid waste combustion. Environ Sci Technol 1999;33:4263–9.
[22] Cains P. Prediction of PCDD and PCDF emissions from municipal solid waste (MSW) incinerators. Chemosphere 1997;34:51–69.
[23] Gullett BK, Bae S-KK, Raghunathan K. Effects of combustion parameters on polychlorinated dibenzodioxin and dibenzofuran homologue profiles from municipal waste and coal co-combustion. Waste Manag 1998;18:473–83.
[24] Fangmark I, Stromberg B, Berge N, Rappet C. Influence of postcombustion temperature profiles on the formation of PCDDs, PCDFs, PCBzs, and PCBs in a pilot incinerator. Environ Sci Technol 1994;24:624–9.
[25] Dickson LC, Lenoir D, Hutzinger O. Quantitative comparison of de novo and precursor formation of polychlorinated dibenzo-p-dioxins under simulated municipal solid waste incinerator postcombustion conditions. Environ Sci Technol 1992:1822–8.
[26] Hunsinger H, Kreisz S, Siefert H. PCDD/F behavior in wet scrubbing systems of waste incineration plants. Chemosphere 1998;37:2293–7.
[27] Kolluri R, Altwicker E. The effect of the electric field on the formation of PCDD in electrostatic precipitators. Hazard Waste Hazard Mater 1994;11:145–56.
[28] Raghunathan K, Gullett BK. Role of sulfur in reducing PCDD and PCDF formation. Environ Sci Technol 1996;30:1827–34.
[29] Pekárek V, Puncochár M, Bures M, Grabic R, Fiserová E. Effects of sulfur dioxide, hydrogen peroxide and sulfuric acid on the de novo synthesis of PCDD/F and PCB under model laboratory conditions. Chemosphere 2007;66:1947–54.
[30] Ogawa H, Orita N, Horaguchi M, Suzumi T, Okada M, Yasuda S. Dioxin reduction by sulfur component addition. Science 1996;32:151–7.
[31] Hunsinger H, Seifert H, Jay K. Reduction of PCDD/F formation in MSWI by a process-integrated SO_2 cycle. Environ Eng Sci 2007;24:1145–59.
[32] Aho M, Paakkinen K, Taipale R. Destruction of alkali chlorides using sulphur and ferric sulphate during grate combustion of corn stover and wood chip blends. Fuel 2013;103:562–9.
[33] Becidan M, Houshfar E, Khalil RA, Skreiberg Ø, Løv T, Sørum L. Optimal mixtures to reduce the formation of corrosive compounds during straw combustion: a thermodynamic analysis. Energy & Fuels 2011;25:3223–34.
[34] Vainio E, Yrjas P, Zevenhoven M, Brink A, Laurén T, Hupa M, et al. The fate of chlorine, sulfur, and potassium during co-combustion of bark, sludge, and solid recovered fuel in an industrial scale BFB boiler. Fuel Process Technol 2013;105:59–68.
[35] Backman R, Khalil RA, Todorovic D, Skreiberg Ø, Becidan M, Goile F, et al. The effect of peat ash addition to demolition wood on the formation of alkali, lead and zinc compounds at staged combustion conditions. Fuel Process Technol 2013;105:20–7.
[36] Vainikka P, Enestam S, Silvennoinen J, Taipale R, Yrjas P, Frantsi A, et al. Bromine as an ash forming element in a fluidised bed boiler combusting solid recovered fuel. Fuel 2011;90:1101–12.
[37] Vainikka P, Bankiewicz D, Frantsi A, Silvennoinen J, Hannula J, Yrjas P, et al. High temperature corrosion of boiler waterwalls induced by chlorides and bromides. Part 1: occurrence of the corrosive ash forming elements in a fluidised bed boiler co-firing solid recovered fuel. Fuel 2011;90:2055–63.
[38] Kelly JD, Hedengren JD. A steady-state detection (SSD) algorithm to detect non-stationary drifts in processes. J Process Control 2013;23:326–31.
[39] Vainikka P, Lindberg D, Moilanen A, Ollila H, Tiainen M, Silvennoinen J, et al. Trace elements found in the fuel and in-furnace fine particles collected from 80 MW BFB combusting solid recovered fuel. Fuel Process Technol 2013;105:202–11.
[40] Vesanto P, Hiltunen M, Moilanen A, Kaartinen T, Laine-ylijoki J, Sipilä K. Kierrätyspolttoaineiden ominaisuudet ja käyttö. Espoo: VTT Publications; 2007.
[41] Nickel Use in Society n.d.
[42] Söderström G, Marklund S. Formation of PBCDD and PBCDF during flue gas cooling. Environ Sci Technol 2004;38:825–30.
[43] Schüler D, Jager J. Formation of chlorinated and brominated dioxins and other organohalogen compounds at the pilot incineration plant VERONA. Chemosphere 2004;54:49–59.
[44] Thoma H, Hauschulz G, Hutzinger O. PVC-induced chlorine-bromine exchange in the pyrolysis of polybrominated diphenyl ethers, -biphenyls, -dibenzodioxins and dibenzofurans. Chemosphere 1987;16:297–307.
[45] Vassilev SV, Baxter D, Andersen LK, Vassileva CG. An overview of the composition and application of biomass ash. Part 1. Phase–mineral and chemical composition and classification. Fuel 2013;105:40–76.
[46] Christensen KA, Stenholm M, Livbjerg H. The formation of submicron aerosol particles, HCl and SO_2 in straw-fired boilers. J Aerosol Sci 1998;29:421–44.
[47] Brunner T. Aerosol and coarse fly ashes in fixed-bed biomass combustion. 1st ed. Graz: Inst. for Resource Efficient and Sustainable Systems, Graz Univ. of Technology; 2006.
[48] Aho M, Yrjas P, Taipale R, Hupa M, Silvennoinen J. Reduction of superheater corrosion by co-firing risky biomass with sewage sludge. Fuel 2010;89:2376–86.
[49] Jiménez S, Ballester J. Effect of co-firing on the properties of submicron aerosols from biomass combustion. Proc Combust Inst 2005;30:2965–72.
[50] Kassman H, Bäfver L, Åmand L-E. The importance of SO_2 and SO_3 for sulphation of gaseous KCl – An experimental investigation in a biomass fired CFB boiler. Combust Flame 2010;157:1649–57.
[51] Zevenhoven M, Yrjas P, Skrifvars B-J, Hupa M. Characterization of ash-forming matter in various solid fuels by selective Leaching and its implications for fluidized-bed combustion. Energy Fuels 2012;26:6366–86.
[52] Ryan SP, Li X, Gullett BK, Lee CW, Clayton M, Touati A. Experimental study on the effect of SO_2 on PCDD/F emissions: determination of the importance of gas-phase versus solid-phase reactions in PCDD/F formation. Environ Sci Technol 2006;40:7040–7.
[53] Takaoka M, Shiono A, Nishimura K, Yamamoto T, Uruga T, Takeda N, et al. Dynamic change of copper in fly ash during de novo synthesis of dioxins. Environ Sci Technol 2005;39:5878–84.
[54] Chi KH, Chang MB. Evaluation of PCDD/F congener partition in vapor/solid phases of waste incinerator flue gases. Environ Sci Technol 2005;39:8023–31.

[55] Kim SC, Jeon SH, Jung IR, Kim KH, Kwon MH, Kim JH, et al. Removal efficiencies of PCDDs/PCDFs by air pollution control devices in municipal solid waste incinerators. Chemosphere 2001;43:773–6.
[56] Littarru P. Repartition of PCDD and PCDF in the emissions of municipal solid waste incinerators between the particulate and volatile phases. Waste Manag 2006;26:861–8.
[57] Guerriero E, Guarnieri A, Mosca S, Rossetti G, Rotatori M. PCDD/Fs removal efficiency by electrostatic precipitator and wetfine scrubber in an iron ore sintering plant. J Hazard Mater 2009;172:1498–504.
[58] Becker B. Gas-/Partikelwechselwirkung chlorierter Aromaten bei der Rauchgasreinigung von Müllverbrennungsanlagen. Universitat Stuttgart, 2003.
[59] Yokohama N, Otaka H, Minato I, Nakata M. Evaluation of gas-particle partition of dioxins in flue gas I: evaluation of gasification behavior of polychlorinated dibenzo-p-dioxins and polychlorinated dibenzofurans in fly ash by thermal treatment. J Hazard Mater 2008;153:395–403.
[60] Shiomitsu T, Hirayama A, Iwasaki T, Akashi T, Fujisawa Y. Volatilization and decomposition of dioxin from fly ash. Engineering 2001;85:3–5.
[61] Lundin L, Marklund S. Distribution of mono to octa-chlorinated PCDD/Fs in fly ash from a municipal solid-waste incinerator. Environ Sci Technol 2008;42:1245–50.
[62] Eitzer BD, Hites RA. Vapor pressures of chlorinated dioxins and dibenzofurans. Environ Sci Technol 1988;22:1362–4.
[63] Shao Y, Xu C, Zhu J, Preto F, Wang J, Tourigny G, et al. Ash and chlorine deposition during co-combustion of lignite and a chlorine-rich Canadian peat in a fluidized bed – Effects of blending ratio, moisture content and sulfur addition. Fuel 2012;95:25–34.

Paper II

Towards controlling PCDD/F production in a multi-fuel fired BFB boiler using two sulfur addition strategies. Part II: Thermodynamic analysis

In: Fuel 134, pp. 688-697

Fuel xxx (2014) xxx–xxx

Contents lists available at ScienceDirect

Fuel

journal homepage: www.elsevier.com/locate/fuel

Towards controlling PCDD/F production in a multi-fuel fired BFB boiler using two sulfur addition strategies. Part II: Thermodynamic analysis

Cyril Jose E. Bajamundi [a,b,*], Pasi Vainikka [a], Merja Hedman [c], Jukka Konttinen [b]

[a] VTT Technical Research Centre of Finland, Koivurannantie 1 PL 1603, FI-40101 Jyväskylä, Finland
[b] Department of Chemistry, Renewable Natural Resources and Chemistry of Living Environment, University of Jyväskylä, POB 35, FI-40014, Finland
[c] Valmet Power, Lentokentänkatu 11, FI-33101 Tampere, Finland

HIGHLIGHTS

- We have developed a method to perform thermodynamic modeling for a 140 MW_{th} BFB boiler using Excel and FactSage macros.
- We have demonstrated that the speciation of Cu is correlated to the PCDD/F production.
- We have shown that peat co-firing can aid PCDD/F abatement if Cu content in the fuel mixture is low.

ARTICLE INFO

Article history:
Received 10 February 2014
Received in revised form 17 April 2014
Accepted 13 May 2014
Available online xxxx

Keywords:
Staged equilibrium modeling
FactSage
PCDD/F
Cu speciation
Sulfur addition

ABSTRACT

A staged equilibrium process model was developed for a bubbling fluidized bed boiler firing SRF, bark and sludge. The model was used to study the influence of sulfur addition strategies (S-pellet additive and peat co-firing) on the behavior of copper, bromine, and alkalis. Aerosol samples collected from the backpass of the boiler were used to validate the chemistry predicted by the model. The model revealed that Cu existed as $Cu_2S_{(s3)}$ in the reducing zone, and $CuCl_{(g)}$ (for all test cases) and $CuO_{(s)}$ (during peat co-firing) in the oxidation zones. $CuBr_{3(g)}$ was also present after the introduction of tertiary air. However the model failed to predict the formation of $CuSO_4$, an important passive species of Cu necessary for PCDD/F abatement. The modes of occurrence of Cu were classified as either active or passive with respect to *de novo* synthesis and an active/passive species molar ratio (APR) was introduced. APR showed high correlation with the PCDD/F production levels. Sensitivity analysis revealed that excessive Cu in the fuel mixture decreased the volatility of the element due to the formation of $CuO_{(s)}$. Simulation for peat co-firing with low Cu content showed that PCDD/F concentration is decreased and is comparable to that of S-pellet addition. Sensitivity analysis revealed that increasing the energy share of sludge can likewise lower PCDD/F production.

1. Introduction

In the first part of this study series, sulfur addition strategies influenced the production of dioxin and furan in a bubbling fluidized bed boiler firing SRF–bark–sludge (Case 1) [1]. Adding S-pellet to the fuel mixture (Case 2) decreased the PCDD/F production, while firing SRF–peat–sludge (Case 3) led to an increase. The homologue distribution pointed to a *de novo* mechanism as the formation pathway of these compounds. Cu is the main catalyst for this mechanism. Aerosol data showed that the volatility and speciation of Cu are different for the two cases. When S-pellet was added, Cu may have been sulfated to form copper sulfate and been less likely to participate in the *de novo* formation. During peat co-firing, Cu has limited volatility and may have remained in its active form in the fly ash. These observation help explained the differences in PCDD/F production for the sulfur addition strategies tested.

For this part of the study series, a thermodynamic equilibrium calculation and details of the *de novo* mechanism are used to explain the results obtained earlier. An empirical model is developed to determine if the elevated concentration of Cu had significant effect on PCDD/F formation when firing SRF–peat–sludge. In addition, a sensitivity analysis on the variation in energy share of sludge for Case 2 is tested.

* Corresponding author at: VTT Technical Research Centre of Finland, Koivurannantie 1 PL 1603, FI-40101 Jyväskylä, Finland. Tel.: +358 20 722 2574; fax: +358 20 722 2720.
E-mail address: cyril.bajamundi@vtt.fi (C.J.E. Bajamundi).

http://dx.doi.org/10.1016/j.fuel.2014.05.033
0016-2361/

Please cite this article in press as: Bajamundi CJE et al. Towards controlling PCDD/F production in a multi-fuel fired BFB boiler using two sulfur addition strategies. Part II: Thermodynamic analysis. Fuel (2014), http://dx.doi.org/10.1016/j.fuel.2014.05.033

1.1. Chemical equilibrium modeling

Chemical equilibrium calculations have been used to analyze systems such as combustion [2–4], gasification [5], cement kiln chemistry [6] and several others [7]. The flexibility of the computation approach and the rapid growth in computing power enabled systematic calculation of multi-phase multi-component equilibrium systems. Equilibrium calculations give accurate results in high temperature applications because the assumptions of the calculation are met. On the other hand, the applicability of thermodynamic equilibrium modeling can be limited by local temperature gradients, physical processes such as adsorption and capillary condensation, non-ideal mixing behavior between different ash forming elements and the mode of occurrence of components in the fuel which dictates its release or retention rate [20,38]. However, clever and carefully designed methodologies can produce valuable information about overall stabilities and speciation trends [10].

In the field of combustion, applications include the study of the behavior of fuel components during combustion [8], multi-fuel combustion strategies [9,10], alkali chemistry related to combustion [11,12], bed agglomeration [13–15] and the fate of trace elements [16–19]. However in practice, the role of reaction kinetics is equally important. This makes simulations of large-scale systems challenging when using straightforward global equilibrium calculation alone.

Dividing large processes into simpler subsystems or stages may add value to the calculation. Sandelin and Backman used this approach to analyze the behavior of trace elements in a coal-fired power plant [20]. They concluded that their modeling results agree with full scale measurements and the overall chemistry was predicted with satisfaction. Similarly Erikson and Hack used this approach to study production of metallurgical-grade silicon in an electric arc furnace. They reasoned that because the flows of two reacting substances are countercurrent, the local mass balances need not be identical to the overall mass balances. Also, the temperatures at different levels in the furnace are not controlled from the outside, but mainly determined by the heat exchange and the reactions taking place inside [21].

Staged equilibrium calculation can be done on several platforms. For example, ChemSheet combines MS Excel with the multi-phase multi-component calculation capability of FactSage [22]. Aspen Plus is also available and has been widely used in the field of chemical engineering [23,24].

This work uses the macro processing module of FactSage. Since the macros are already available in the FactSage distribution, additional software is no longer required. Macro commands enable the user to run the subprogram *Equilib* in the background and execute commands stored in a macro [25]. Although macros are advanced features of FactSage, little programming background is required.

The main motivation for the use of this platform is to take advantage of the integrated database and computing facility in FactSage, and to develop an Excel-based user interface as a process model for the boiler used in this study.

In a bubbling fluidized bed boiler (BFB) several key zones can be identified, each with unique local prevailing conditions (Fig. 1). The first is the zone above the bed (the splash zone). The atmosphere is reducing because the air to fuel ratio (λ) is less than unity. The fuel is gasified and volatile fractions are released. Non-volatile fragments can be retained in the bed and leave the boiler as bottom ash.

Then, secondary air is injected several meters above the splash zone. The reason for the staging of air is to minimize excessively hot zones where NO_x formation may occur. At this zone, the atmosphere is oxidizing with λ around the range 1.1–1.3. The temperature is highest and majority of the fuels are combusted.

Next, tertiary air is introduced below the bullnose for complete oxidation. Further downstream, the flue gas transfers heat in the superheaters resulting in a decrease in flue gas temperature. The flue gas becomes supersaturated with aerosol-forming elements, such as Na, K, Cl, leading to condensation and deposition. Then the flue gas travels to the colder post combustion zones, where other heat exchange devices cool it to around 200 °C.

This illustrates that the mass, prevailing conditions and flue gas composition are changing at the zones mentioned. These features can be incorporated to the thermodynamic model using staged equilibrium calculation.

1.2. Copper – the de novo catalyst

Copper is the most important catalyst responsible for the synthesis of PCDD/F in incineration systems [26–29]. In the BFB, Cu undergoes several chemical transformations such as sulfidation in the splash zone, oxidation in the O_2-rich stages, and chlorination in the cold zones of the boiler. The non-volatile fraction of Cu in the fuel leaves the boiler as part of the bottom ash, mostly as Cu^0, Cu^I or Cu^{II} [30]. The rest of the Cu is volatilized or entrained in flue gas and, depending on speciation, Cu can be a catalyst for the *de novo* reaction.

Using in situ X-ray absorption techniques, Takaoka and coworker observed the transformation of Cu from 200 °C to 400 °C

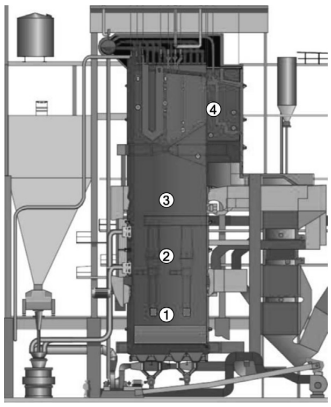

Location	Description	T_{gas}, [°C]	λ	Code
1	Just above the bed, splash zone	846 ± 4	0.600	846Rd
2	Downstream from the secondary air to just before the tertiary air.	906 ± 14	1.300	906Ox
3	Downstream from the tertiary to just below the bullnose	852 ± 4	1.379	852Ox
4	Back Pass	510 ± 9	1.379	510BP

Fig. 1. Key locations in the boiler used for the modeling and the local conditions at these locations. Aerosol sampling was made in the backpass or 4.

Please cite this article in press as: Bajamundi CJE et al. Towards controlling PCDD/F production in a multi-fuel fired BFB boiler using two sulfur addition strategies. Part II: Thermodynamic analysis. Fuel (2014), http://dx.doi.org/10.1016/j.fuel.2014.05.033

and the production of PCDD/F [31–33]. At 200 °C, the majority of copper exists as Cu^{I} or Cu^{0}. The rate of chlorination reaction of carbon is so slow and few dioxins are formed. At around 300–400 °C Cu undergoes oxidation and chlorination-forming oxychlorides. Additional HCl, Cl_2, KCl present in the surrounding gas may react with oxychlorides to form $CuCl_2$ or $CuCl_2{\cdot}2H_2O$. Cupric species can then chlorinate carbon in the ash and form dioxin/furan or compounds of similar structures. In parallel, oxychlorides and O_2 react to form copper oxide. CuO aides in the cleavage of carbon matrices in the ash and can enhance carbon gasification [34], a necessary step in PCDD/F formation.

Copper on the other hand is said to be poisoned when it reacts with $SO_{3(g)}$ forming $CuSO_{4(s)}$, possibly via the reaction [35]:

$$2CuOCl_{(s)} + 0.5O_{2(g)} + 2SO_{3(g)} + H_2O_{(g)} \rightarrow 2CuSO_{4(s)} + 2HCl_{(g)} \quad (1)$$

or via sulfation of active Cu species in the ash [36]:

$$2CuCl + SO_2 + 2O_2 \rightarrow CuSO_{4(s)} + CuCl_2 \quad (2)$$

These studies show that Cu is an active *de novo* catalyst when it is present as chloride (Cu–Cl), oxide (Cu–O) and oxychloride (Cu–O–Cl), while $CuSO_4$ is inactive or passive. Fig. 2 summarizes the reactions mention above.

1.3. Objective of the study

The main objective of this study is to examine how the variation of Cu concentration in the SRF–peat–sludge mixture can affect PCDD/F production. This is necessary because the amount of Cu during peat co-firing was high compared to the reference and S-pellet addition test [1].

To accomplish this, a process model for the bubbling fluidized bed boiler is developed using staged equilibrium calculation. The model is qualitatively validated against the results of the aerosol measurements, to see if it can explain the behavior of the ash-forming elements established earlier [1].

Then an empirical equation is developed using the speciation of copper extracted from the model and the detailed mechanism presented in Section 1.2. This is tested for correlation with the PCDD/F concentration measured in the ESP inlet. Using this correlation, the Cu concentration during SRF–peat–bark firing is reduced to predict PCDD/F production.

In addition, a sensitivity analysis on the effect of varying the energy share of sludge to PCDD/F production will be made.

2. Experimental methods

2.1. Key locations in the bubbling fluidized bed boiler

The boiler used in this study is described in detail in [37] and in the first part of this work [1]. The key locations and local prevailing conditions are found in Fig. 1. The temperature and λ are average values for the three test cases. Each location has a designated equilibrium stage in the staged equilibrium process model.

2.2. Fuel mix and additives

This facility fires Scandinavian spruce bark from the debarking process of the adjacent paper mill, dried sludge also from the same mill and solid recovered fuel collected in Southern Finland. Table 1 summarizes the fuel proportions and additive dosage used in the three test cases. Additional details are found in [1].

2.3. Aerosol and PCDD/F sampling

Aerosol sampling was done in the backpass (510BP) using a Dekati Low Pressure Impactor (DLPI). Pertinent discussions on the method, sample treatments and tests used have been presented earlier [1].

PCDD/F measurements were made around the electrostatic precipitator [1]. However this part focuses only on samples collected at the ESP inlet (Table 3). These are assumed to be the total production of PCDD/F in the boiler.

3. Model implementation

The process model uses Microsoft Excel and FactSage 6.3.1; and the structure of data flow is shown in Fig. 3. The Excel worksheet contains all the local conditions, the mass and composition of the

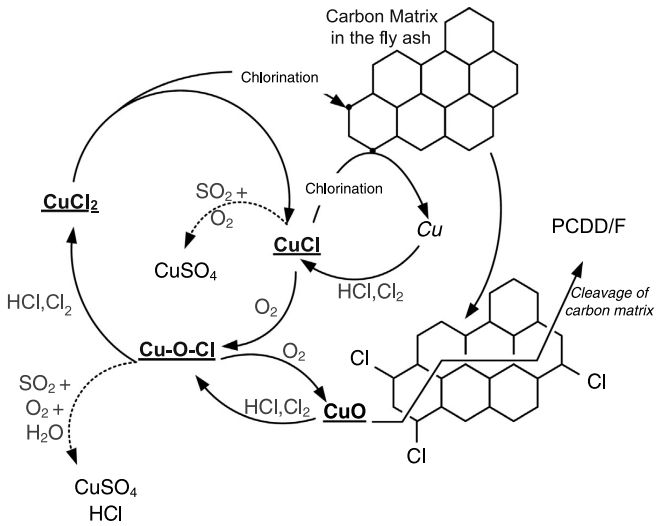

Fig. 2. Reactions of copper and the production of PCDD/F. Regular arrows represent active pathways towards PCDD/F production, while broken arrows represent poisoning. The main oxychlorination cycle is adopted from [32] and the poisoning reactions are from [35,36].

Please cite this article in press as: Bajamundi CJE et al. Towards controlling PCDD/F production in a multi-fuel fired BFB boiler using two sulfur addition strategies. Part II: Thermodynamic analysis. Fuel (2014), http://dx.doi.org/10.1016/j.fuel.2014.05.033

Table 1
Fuel proportion and S-pellet addition in the study.

Cases	% Energy share				S-pellet added?	Description
	SRF	Bark	Sludge	Peat		
1	50	44	6	0	No	Normal fuel mix
2	50	44	6	0	Yes[a]	Normal fuel mix + addition of S-pellet
3	60	0	6	34	No	Fuel substitution from bark to peat. Peat serves as fuel and source of sulfur

[a] Ratio of mass flow rate (kg/s) S-pellet/fuel is around 0.001.

Table 2
Coarse particle loading measured by DLPI and the entrained condensed phase in 846Rd and 510BP. The coarse particle loading corresponds to aerosols within the size range of 1.6–10 μm.

Cases	Coarse particle loading	Entrained condensed phase in 846Rd	Fly ash in 510BP	% Increase in condensed phase between 846Rd to 510BP
	(mg/N m^3)	(g/kg fuel fed)	(g/kg fuel fed)	
1	87.1	17.12	23.15	35.21
2	142.8	18.36	26.12	42.21
3	168.9	60.87	67.30	10.58

Table 3
APR evaluated at 852Ox and 510BP and the production of PCDD/F in the ESP inlet. R^2 is the square of the Pearson product moment correlation coefficient evaluated through data points PCDD/F at ESP inlet and APR.

Cases	PCDD/F at ESP inlet (ng/N m^3)	APR (unitless)	
		852Ox	510BP
1	0.786	37.459	8.481
2	0.363	7.764	5.497
3	1.345	80.270	74.151
R^2	0.99	0.84	

input/output streams for each stage (or equilibrium reactor). The worksheet also stores all equilibrium calculation results, and calculates the mass balance in the reactor network. A command button in the worksheet can launch a batch file that prompts the macro facility of FactSage to accept the process information, launch the *Equilib* subprogram, initialize and perform equilibrium calculation, and finally return the calculation results back to the interface. Data are exchanged from Excel to FactSage and vice versa via Object Linking and Embedding (OLEn).

The process model is made up of four stages, each representing a certain region in the BFB, see Fig. 1. Each stage is an adiabatic system operated at atmospheric pressure.

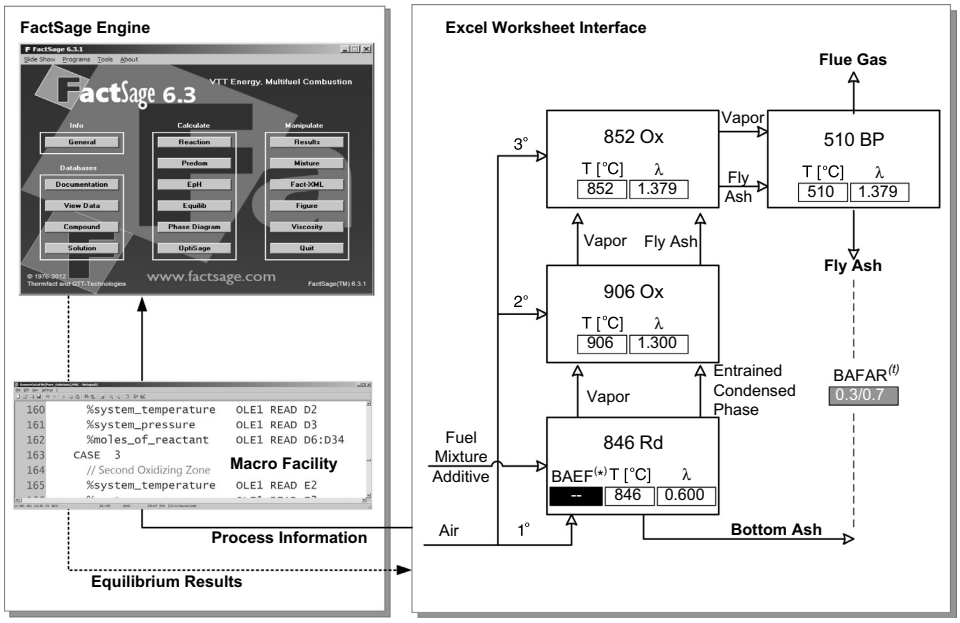

Fig. 3. Data flow structure between FactSage's equilibrium calculation engine and the staged equilibrium process model in Excel. The local temperature and air/fuel ratio, λ, are shown in the box inside each equilibrium reactor. (*) Denotes an adjustable parameter while (t) denotes a target parameter.

Please cite this article in press as: Bajamundi CJE et al. Towards controlling PCDD/F production in a multi-fuel fired BFB boiler using two sulfur addition strategies. Part II: Thermodynamic analysis. Fuel (2014), http://dx.doi.org/10.1016/j.fuel.2014.05.033

The first stage, 846Rd, represents the splash zone. 846Rd takes in all the fuel mixture (plus the additive for Case 2) and the primary air. After performing equilibrium calculation, a fraction of the condensed phase (pure and solid solutions) is entrained together with the vapor to the next reactor, with the remainder being drawn out as bottom ash. The amount of entrained-condensed phase is controlled by the adjustable parameter BAEF which is applied equally to all the condensed phase constituents (or species) formed in 846Rd.

The presence of this stage offers an advantage over global equilibrium calculations. 846Rd allows the removal of some fractions of elements that are expected to be enriched in the bottom ash. For example, Lundholm et al. reported that around 40–70% of Cu was retained in the bottom ash when burning chromate copper arsenate (CCA)-preserved wood with and without the addition of peat [17]. This changed the amount of copper downstream of the boiler. 846Rd meets this expectation and allows the partitioning of the element to be estimated. In the model, an element can partition between the bottom ash, fly ash, and flue gas stream.

The next stage, 906Ox, the first oxidation stage, takes in the secondary air and the vapor plus the entrained condensed phase from 846Rd. After equilibrium has been calculated, all of the vapor and condensed phase (now called fly ash) are passed to the 3rd stage as input. 906Ox simulates what happens to the components of the fuel mixture as they move from a reducing to an oxidizing atmosphere.

The third stage, 852Ox, the second oxidation stage, takes in the tertiary air and the results of the calculation in 906Ox. The air to fuel ratio at this stage is 1.379 and represents the final λ for the boiler during the test cases.

The last stage, 510BP, represents the backpass and accepts all the masses from 852Ox. This is the coldest among the four and is assumed to govern the total amount of fly ashes produced for each test case. This stage has two output streams: flue gas and fly ash.

Once the total amount of fly ash has been calculated, the bottom/fly ash ratio, BAFAR, is evaluated and compared against the target value of 0.3/0.7. The macro uses a simple bisection algorithm to meet the target BAFAR by iterating the adjustable parameter BAEF. The actual value of BAFAR is not exactly known because of the difficulty of measuring the flow of the bottom and fly ash for the test cases. The current value is based on historical estimates collected from the plant.

The thermodynamic database includes 181 gaseous and 337 pure solid species from the FactPS, FToxid, FTsalt and FTpulp database. Solution species from FToxid and FTsalt are likewise included. For each case and equilibrium stage, preliminary runs and post calculations of activities are made to ensure that no pure species that should be included in the thermodynamic database are left out in the simulation. Nitrogen is assumed to exist as $N_{2(g)}$ [38], and the mass and activity limits are 1 nanogram and 1×10^{-3} respectively.

4. Results

4.1. Coarse particle loading

The coarse size fraction measured in the backpass indicates that Case 3 gave the highest amount of coarse particle loading, while Case 1 registered the least [1].

The amount of particles entrained in 846Rd follows this trend (see Table 2). The model estimates that the amount of particles entrained for Case 1 (17.12 g/kg fuel fed) and Case 2 (18.36 g/kg fuel fed) are nearly equal. This is expected because the fuel mixtures for these two cases are similar. In both cases, the change in amount of the condensed phase between 846Rd to 510BP is large, at 35.21% and 42.21% respectively. This suggests that the fly ashes are not fragments of the original fuel but are formed from the condensation of some species in the flue gas.

Case 3 has the highest amount of condensed phase entrained in 846Rd, 60.87 g/kg fuel fed. However it has the lowest change in the amount of condensed phase between 846Rd to 510BP, 10.58%. This indicates that majority of the fly ash is from the splash zone. These observations are consistent with reports on peat co-combustion combustion [15,39,40]. Peat is rich in aluminosilicates and other ash forming compounds. Nonvolatile fuel fragments are usually formed in the lower part of the boiler and are entrained in the fluidizing air.

4.2. Main aerosol forming elements

Aerosol samples collected from the backpass show that Na and K have been sulfated when S-pellet is added to the reference fuel mixture [1]. Sulfation of alkalis usually occurs at a temperature range of 650–1000 °C [41]. Sulfation is accompanied by an increase in the peak of the fine particle fraction of the aerosol sampling to a slightly higher particle size range [42].

The partitioning of aerosol-forming elements calculated for the subsystem 846Rd–852Ox (SS) and the whole system 846Rd–510BP (WS) is shown in Fig. 4. For SS, partitioning of Na and K in the fly ash increased from Case 1 to Case 2. For Case 1, the alkalis are mostly present in the flue gas as KCl and NaCl; some are present

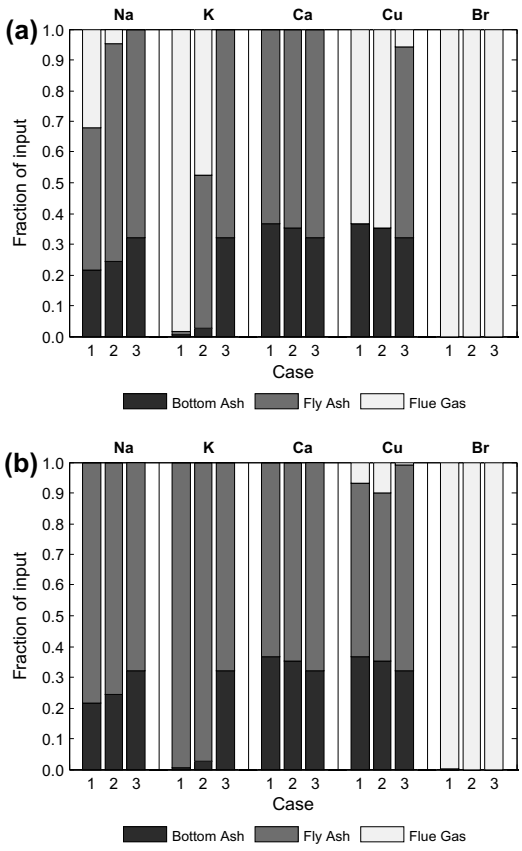

Fig. 4. Partitioning of aerosol forming elements in the bottom ash, fly ash and flue gas at (a) 852Ox and (b) 510BP.

Please cite this article in press as: Bajamundi CJE et al. Towards controlling PCDD/F production in a multi-fuel fired BFB boiler using two sulfur addition strategies. Part II: Thermodynamic analysis. Fuel (2014), http://dx.doi.org/10.1016/j.fuel.2014.05.033

as sulfates. For Case 2, Na_2SO_4 and K_2SO_4 were formed together with $KAlSi_2O_6$ and $NaAlSiO_4$. This supports the occurrence of sulfation detected in the experiments. Alkali-aluminosilicate is the results of the two folds increase in Si content of the fuel mixture for Case 2. However, the partitioning evaluated for WS failed to show the experimental observations. The alkalis are mostly present as solid compounds (salts and silicates). It is difficult to assess that sulfation happened at 510BP because the temperature is below the range of alkali sulfation noted above.

For Case 3 around 30% of the alkalis in the fuel partitioned to the bottom ash. This was true for SS and WS. For all the stages, 98% of Na and K was present as $KAlSi_2O_6$ and $NaAlSi_3O_8$ respectively. This agrees with the results of (1) chemical fractionation that shows that majority of the alkalis are "less reactive" and (2) aerosol samples that suggests alkalis are less volatile during SRF–peat–sludge combustion [1].

Calcium found in the DLPI was mostly in the coarse particle fraction [1]. This suggests that few gaseous Ca species formed during the tests. In the model, Ca partitioned between the bottom and fly ash alone. For all cases, gaseous species of calcium were not detected.

The results above show that the subsystem 846Rd–852Ox (SS) can more closely predict the results of the aerosol measurements. On the other hand, 846Rd–510BP (WS) overestimates condensation of the alkalis in the backpass. The current model cannot handle the influence of kinetics and other transport limitations at 510 °C (temperature of 510BP). That is the reason for the overestimation.

In the current model, no attempt was made to account for these kinetic and transport limitations, we assume that reactions after the introduction of the tertiary air may have been frozen [41] due to the phenomena cited above and the properties of such a "frozen" system was reflected in the aerosol samples.

4.3. Copper and bromine

Cu and Br in the aerosols were mostly found in the fine particle fraction, <0.03–1.6 μm. This indicates the presence of gaseous Cu

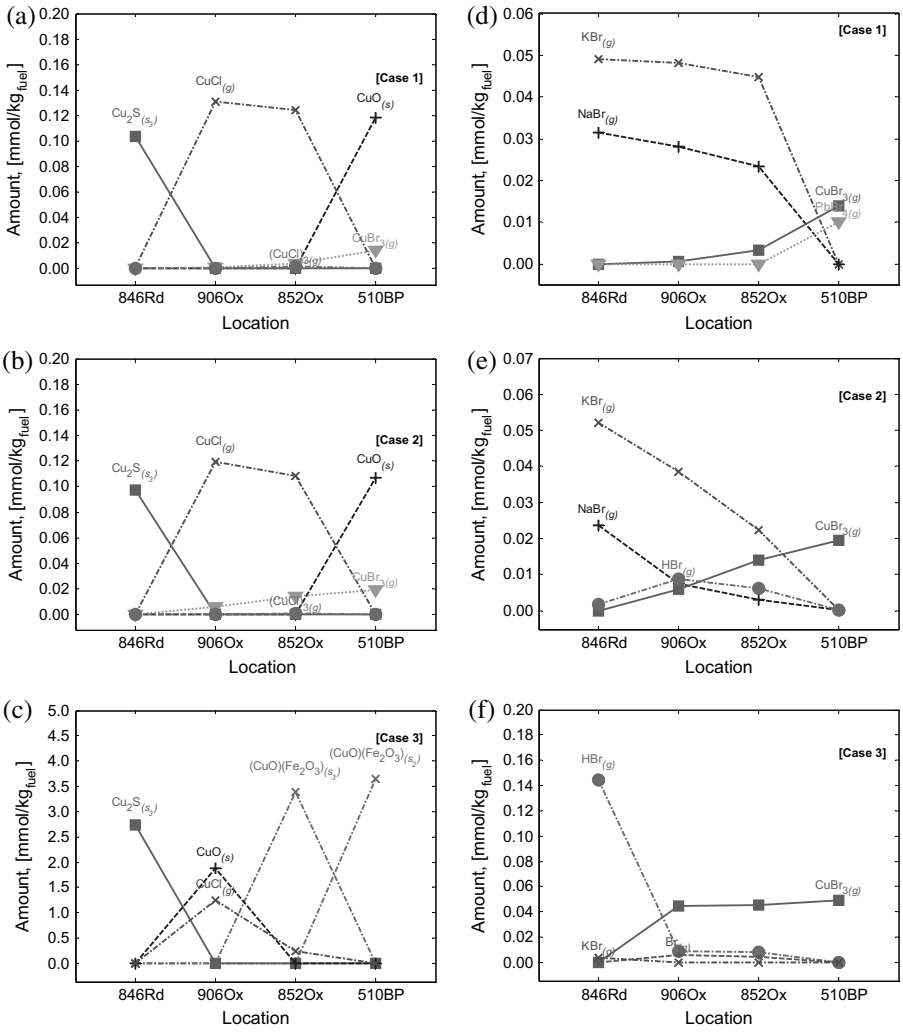

Fig. 5. Top species of Cu (a–c) and Br (d–f) at different stages in the BFB boiler as predicted by the staged equilibrium process model.

Please cite this article in press as: Bajamundi CJE et al. Towards controlling PCDD/F production in a multi-fuel fired BFB boiler using two sulfur addition strategies. Part II: Thermodynamic analysis. Fuel (2014), http://dx.doi.org/10.1016/j.fuel.2014.05.033

and Br species for all the test cases. It was also established that Cu was least volatile for Case 3 [1].

Similar to the main aerosol forming element, the partitioning of Cu and Br evaluated for WS overestimated condensation (Fig. 4b). On the other hand, SS shows the expected partitioning of Cu and Br. In Fig. 4a, the amount of Cu existing in the flue gas fraction is small in Case 3 as compared to that of Cases 1 and 2, supporting the findings of the aerosol sampling. Meanwhile, the majority of the Br partitioned to the flue gas.

Analysis of speciation of these two elements reveals their dominant mode of occurrence at a given stage in the boiler. First, Cu exists as $Cu_2S_{(s3)}$ at the reducing zone and becomes $CuCl_{(g)}$ (for Cases 1–3) and $CuO_{(s)}$ (for Case 3 alone) as it transitions from 846Rd to 906Ox. The formation of $CuO_{(s)}$ after secondary air injection is unique to Case 3 and explains the apparent decrease in volatility of copper as measured by the DLPI.

Most of the bromine exists as $KBr_{(g)}$ and $NaBr_{(g)}$ in the splash zone for Cases 1 and 2, while $HBr_{(g)}$ for Case 3. The latter is explained by the poor reactivity of the alkalis in Case 3. At 906Ox and 852Ox the amount of alkali chlorides decreased to favor formation of other gaseous bromine species: $CuBr_3$ for Case 1, $HBr_{(g)}$ and $CuBr_{3(g)}$ for Case 2 and $Br_{(g)}$ and $CuBr_{3(g)}$ for Case 3. As flue gas cools Br competes with Cl for Cu to form $CuBr_{3\ (g)}$. In Fig. 5(a) and (b), the concentration $CuCl_{(g)}$ decreases as $CuBr_{3(g)}$ are formed in 852Ox.

4.4. $CuSO_4$ formation

Formation $CuSO_4$ was not detected even at 510Ox where the temperature is lower than the decomposition temperature of $CuSO_4$ (572–678 °C) [42]. The presence of significant amounts of Ca in the fuel mixture led to the capture of most of the sulfur in the system. This is because the formation $CaSO_4$ is more thermodynamically favorable than $CuSO_4$. At 825 °C the phase stability diagram in Fig. 6(a) indicates that the partial pressure of SO_2 should be greater than 0.1 to support the formation of copper sulfate as $(CuO)(CuSO_4)_{(s)}$. The levels required for this formation may not be practical or feasible for the current boiler set-up. On the other hand Fig. 6(b) predicts that at 510 °C formation of $CuSO_4$ is feasible even at slightly lower concentrations of SO_2. Overestimation of $CaSO_4$ formation using the current modeling approach may explain why formation of $CuSO_4$ was not detected by the model.

Harriot et al. and Gullet et al. have shown that adsorption of sulfur compound on copper surfaces is possible leading to the subsequent formation of $CuSO_4$ [42,43]. However their studies also reveal that the formation of $CuSO_4$ requires longer residence time – in the order of minutes – and is therefore kinetically governed.

5. Discussions

5.1. Active and passive species of Cu

Since the limitations of the model in predicting the formation of $CuSO_4$ is recognized, an analysis on the speciation of copper is presented in this section. In Fig. 2, chlorides, oxide, and oxychlorides of Cu are active catalysts in the formation of PCDD/F. Their role can either be as chlorinating agent, as a catalyst in the cleavage of carbon matrices, or both. Meanwhile, $CuSO_4$ is the deactivated form of the *de novo* catalyst. In addition, Section 4.3 showed that the formation of Cu–Br compounds offers competition to Cl for available Cu thus reducing the formation of copper chloride. Compared to Cu–Cl, an accepted mechanism for the catalytic role of Cu–Br species focused in the formation of PCDD/F alone is not yet available [44,45].

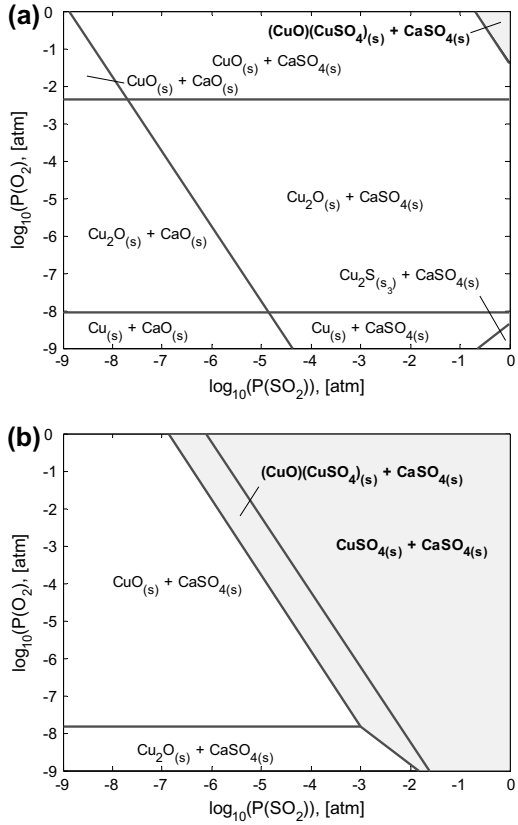

Fig. 6. Phase stability diagram of Cu–Ca–S–O system at (a) 825 °C and (b) 510 °C at 1 atm pressure, $0 < Ca/(Cu + Ca) < 1$. Diagrams are generated in FactSage 6.3.1. The shaded region corresponds to a concentration favorable for $CuSO_4$ formation.

With these observations, we can define the empirical molar active/passive species ratio (APR) as:

$$\mathrm{APR} = \left[\frac{(\mathrm{Cu{-}Cl}) + (\mathrm{Cu{-}O}) + (\mathrm{Cu{-}O{-}Cl}) + \mathrm{Cu}}{\mathrm{CuSO_4} + (\mathrm{Cu{-}Br}) + \mathrm{Cu}}\right] \quad (3)$$

$CuSO_4$ is still included to indicate that it is part of the passive form of copper with respect to the *de novo* reaction. Metallic copper is present both in the numerator and denominator because it can be chlorinated to become CuCl (active) or as the left-over product of the chlorination (passive) of the carbon matrix.

This ratio is evaluated from the results at 852Ox and 510BP. APR was not evaluated in 846Rd because of the reducing condition at this stage which is different from the oxygen-rich atmosphere of the post combustion zone. Similarly APR was not evaluated in 906Ox because this is still far from the post combustion conditions and the oxidant (air) introduction is not yet complete.

5.2. APR and the PCDD/F production level

The APR evaluated at 852Ox and 510BP is found in Table 3. Both APRs have correlation with the PCDD/F levels measured in the ESP inlet [1]. The correlation coefficient is higher for the APR evaluated at 852Ox. This is explained by the earlier observations that 852Ox

Please cite this article in press as: Bajamundi CJE et al. Towards controlling PCDD/F production in a multi-fuel fired BFB boiler using two sulfur addition strategies. Part II: Thermodynamic analysis. Fuel (2014), http://dx.doi.org/10.1016/j.fuel.2014.05.033

gives a better picture of what is happening in the backpass as compared to 510BP.

APR increases with PCDD/F at the ESP inlet. This agrees with the nature of the *de novo* mechanism. More active copper species should result in increased PCDD/F formation.

5.3. Peat–SRF–sludge with low Cu content

For this sensitivity analysis, the concentration of Cu for the fuel mixture is reduced from 670 mg/kg to 26 mg/kg dry solids. The latter is the concentration of Cu in the fuel mixture for Case 1. The concentration of the rest of elements in the fuel is similar to Case 3.

Fig. 7(a) compares the partitioning of the alkalis, Ca, Cu, and Br for the scenario being studied (Case 3*) and the two original cases (Cases 1 and 3). A decrease of Cu concentration in the fuel does not affect the alkalis, Ca and Br. On the other hand there was a remarkable increase in volatile Cu for Case 3*. Cu is present as $Cu_2S_{(s)}$ in the reducing zone and becomes $CuCl_{(g)}$ as it transitions to the first oxidizing zone, as the gas cools $CuBr_{3(g)}$ and $(CuO)(Fe_2O_3)_{(s2)}$ are formed. However $CuO_{(s)}$ did not form at 906Ox as it did in Case 3.

For the peat co-firing with low Cu content the APR at 852Ox is 2.195 mol/mol. This APR corresponds to the PCDD/F concentration estimate of 0.303 ± 0.013 ng/N m^3. This level is near the value reported for Case 2, indicating that the peat addition strategy may also help in PCDD/F abatement under the strict premise that the concentration of Cu in the fuel is kept as low as possible.

5.4. SRF–bark–sludge + S-pellet (Case 2) at varying sludge energy share

Low concentration of several trace elements in the sludge may produce dilution effects when the portion of sludge in the fuel mixture is increased. For this part, the energy share of sludge is varied according to the proportions in Table 4; note that the SRF/bark energy share ratio is maintained.

The partitioning of key elements for this sensitivity analysis is shown in Fig. 8(a). Variation of sludge energy share did not affect the partitioning of Cu and Br and Ca; this is because the speciation of these elements did not vary significantly at the proportions evaluated. On the other hand Na and K exhibited changes in partitioning. As sludge energy share increases, Al and Si concentration increase as well, leading to the enrichment of Na in the bottom ash due to the formation of $NaAlSiO_4$. This resulted in the increase

Table 4
Energy share simulated at varying sludge energy share and constant SRF/bark energy share ratio.

Cases	SRF	Bark	Sludge	S-pellet
2L	51.60	45.40	3	YES
2	50.00	44.00	6	YES
2H	46.81	41.19	12	YES

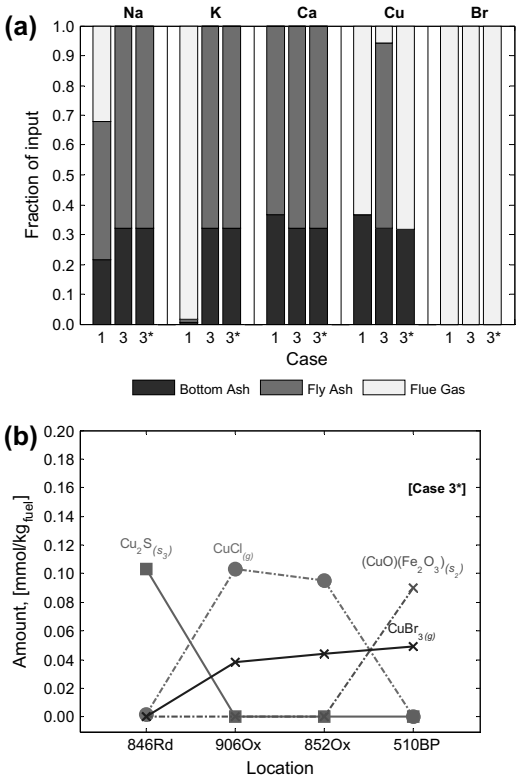

Fig. 7. (a) Partitioning of aerosol forming elements in the bottom ash, fly ash and flue gas at 852Ox showing Cases 1, 3 and 3*. (b) Top species of copper for peat–SRF–sludge combustion and reduced Cu concentration.

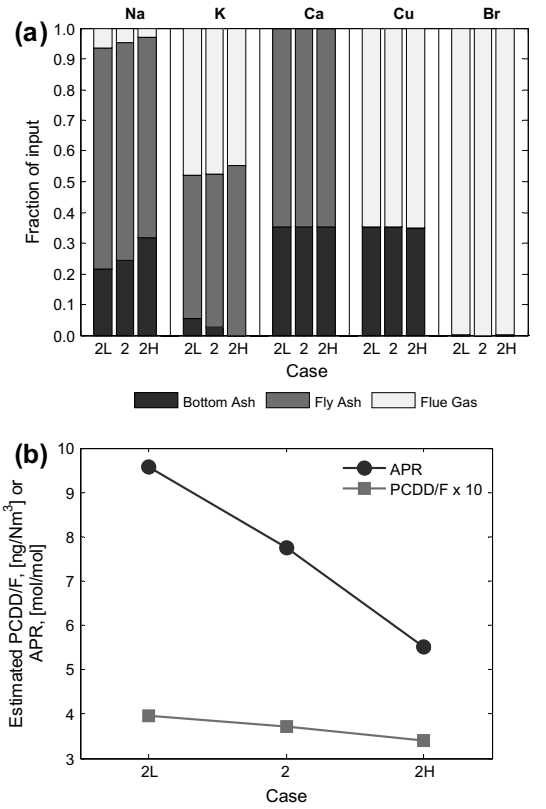

Fig. 8. Effects of varying sludge energy share (a) partitioning of aerosol forming elements in the bottom ash, fly ash and flue gas at 852Ox and (b) variation of APR and the estimated PCDD/F. All plots are from the 852Ox stage.

Please cite this article in press as: Bajamundi CJE et al. Towards controlling PCDD/F production in a multi-fuel fired BFB boiler using two sulfur addition strategies. Part II: Thermodynamic analysis. Fuel (2014), http://dx.doi.org/10.1016/j.fuel.2014.05.033

of available Cl for K, causing this alkali to be slightly more volatile at the splash zone.

K is captured by Si and Al in the succeeding stages. This could explain why even if K is volatile in the splash zone for Case 2H, the fraction of K in the gas phase (flue gas) is slightly smaller. Alkali capture during sludge co-combustion has been reported in the literature [46].

The partitioning of Cu did not change with sludge share, though its concentration has been reduced due to dilution. Also, since Br concentration is higher in the sludge [1], increasing the sludge share led to the passivation of Cu because more $CuBr_{3(g)}$ is formed. These observations led to the decrease of APR and eventually the PCDD/F concentration – see Fig. 8(b). In actual practice, S in sludge may also help enhance $CuSO_4$ formation and further reduce PCDD/F production [47].

This sensitivity analysis presents a possible situation where both alkali chloride deposition at the superheaters and PCDD/F production are reduced due to the synergistic effects of low trace element concentration, alkali capture of Si and Al from the sludge, and sulfation.

At this point of the study, both S-pellet addition and peat-SRF-sludge co-firing are seen as possible PCDD/F abatement strategies, provided that the amount of Cu in the latter strategy is kept as minimal as possible. In actual practice, peat–SRF–sludge co-firing may still be inferior with S-pellet addition because of the high share of SRF and variability of the concentrations of trace elements in the SRF. In the third and last part of this study, the formation of $CuSO_4$ will be experimentally investigated using advanced X-ray absorption techniques to settle which strategy can lead to more successful sulfation, and decide which of the strategies is superior.

6. Conclusion

By segmenting the BFB boiler into several stages, each representing a local governing condition, a staged equilibrium process model has been developed using the macro facility in FactSage plus an interface in Excel. The main justification for this approach is the possible existence of local equilibria at different parts of the boiler. A single global equilibrium calculation may not suffice when local governing conditions and mass balance vary from one section of the boiler to another.

The behavior of aerosol-forming elements (Na, K and Ca) collected at the backpass is better understood by examining the results of the subsystem 846Rd–852Ox (SS) as compared to 846Rd–510BP (WS). This indicates that after the addition of the tertiary air succeeding reactions of these elements may have been "frozen".

Furthermore, the behavior of Cu and Br in the aerosol sample can also be explained by the results of SS. Interactions of Cu–Br promoted the formation of volatile $CuBr_{3(g)}$ which competes with chlorine for available Cu. For Case 3 the volatility of Cu is lowest because of the formation of $CuO_{(s)}$. However, the model failed to predict the formation of $CuSO_{4(s)}$ which is the passive form of Cu critical to PCDD/F reduction.

An empirical ratio APR was introduced and correlated to the levels of PCDD/F measured at the ESP inlet. Correlation was found to be satisfactory for 852Ox, so it was used in the sensitivity analysis.

By reducing Cu in the fuel mixture, Case 3* estimates the PCDD/F level to be 0.303 ± 0.013 ng/N m^3. This shows that the abundance of Cu in Case 3 is contributed to the elevated PCDD/F levels measured. Furthermore the sensitivity analysis reveals that excessive Cu in the fuel favors the formation of $CuO_{(s)}$, a key *de novo* catalyst.

Synergistic effects of increasing sludge share and sulfur pellet addition can promote abatement of PCDD/F production and alkali capture. This can be explained by trace element dilution, alkali capture of Si and Al from the sludge, and additional S available for sulfation reactions. However the concentration of Ca in the sludge should be carefully noted. Excessive Ca in the system may react with the additional S and lead to the undesirable formation of $CaSO_4$.

Acknowledgments

We are thankful to the OSER project, Valmet Power, Foster Wheeler, the European Regional Development Fund, and RECOM-BIO Project TREN/FP7EN/239530/ for the resources they shared for this study. Stora Enso Oyj is gratefully acknowledged for sharing the data presented in this paper. Likewise we wish to thank Martti Mäkipää for the helpful discussion on the basic features of FactSage. The help of the VTT Mentoring program facilitated by Janne Kärki is also acknowledged. Jouni Hämäläinen is also acknowledged helping acquire FactSage.

References

[1] Bajamundi CJE, Vainikka P, Hedman M, Hyytiäinen I, Silvennoinen J, Heinanen T, et al. Towards controlling PCDD/F production in a multi-fuel fired BFB boiler using two sulfur addition strategies. Part I: experimental campaign and results. Manuscr Submit to FUEL Publ n.d.
[2] Lundholm K, Nordin A, Backman R. Trace element speciation in combustion processes—review and compilations of thermodynamic data. Fuel Process Technol 2007;88:1061–70.
[3] Hupa M. Thermodynamic modeling of combustion processes – applications and limitations. Chem. thermodyn. furn. a jt. symp. course combust. spec. metall.; 2012.
[4] Lindberg D, Backman R, Chartrand P, Hupa M. Towards a comprehensive thermodynamic database for ash-forming elements in biomass and waste combustion — current situation and future developments. Fuel Process Technol 2011;105:129–41.
[5] Konttinen J, Backman R, Hupa M, Moilanen A, Kurkela E. Trace element behavior in the fluidized bed gasification of solid recovered fuels – a thermodynamic study. Fuel 2013;106:621–31.
[6] Koukkari P, Pentillä K, Karema H. New Dynamics for kiln chemistry. In: Koukkari P, editor. Adv. Gibbs energy methods funct. mater. process. ChemSheet 1999–2009, Helsinki; 2009. p. 117–23.
[7] Hack K, editor. The SGTE casebook thermodynamics at work. Cambridge: Woodhead Publishing Limited; 2008.
[8] Yan R, Gauthier D, Flamant G, Badie J. Thermodynamic study of the behavior of minor coal elements and their affinities to sulfur during coal combustion. Fuel 1999;78:1817–29.
[9] Becidan M, Houshfar E, Khalil RA, Skreiberg Ø, Løv T, Sørum L. Optimal mixtures to reduce the formation of corrosive compounds during straw combustion: a thermodynamic analysis. Energy & Fuels 2011;25:3223–34.
[10] Becidan M, Sørum L, Lindberg D. Impact of Municipal Solid Waste (MSW) quality on the behavior of alkali metals and trace elements during combustion: a thermodynamic equilibrium analysis. Energy Fuels 2010;24:3446–55.
[11] Furimsky E, Zheng L. Quantification of chlorine and alkali emissions from fluid bed combustion of coal by equilibrium calculations. Fuel Process Technol 2003;81:7–21.
[12] Poole D, Argent BB, Sharifi VN, Swithenbank J. Prediction of the distribution of alkali and trace elements between the condensed and gaseous phases in a municipal solid waste incinerator. Fuel 2008;87:1318–33.
[13] Kouvo P, Backman R. Estimation of trace element release and accumulation in the sand bed during bubbling fluidized bed co-combustion of biomass, peat, and refuse-derived fuels. Fuel 2003;82:741–53.
[14] Öhman M, Nordin A, Skrifvars B-J, Backman R, Hupa M. Bed agglomeration characteristics during fluidized bed combustion of biomass fuels. Energy Fuels 2000;14:169–78.
[15] Zevenhoven-Onderwater M, Blomquist J-P, Skrifvars B-J, Backman R, Hupa M. The prediction of behavior of ashes from five different solid fuels in fluidized bed combustion. Fuel 2000;79:1353–61.
[16] Pedersen AJ, Frandsen FJ, Riber C, Astrup T, Thomsen SN, Lundtorp K, et al. A full-scale study on the partitioning of trace elements in municipal solid waste incinerations effects of firing different waste types†. Energy & Fuel 2009;23:3475–89.
[17] Lundholm K, Boström D, Nordin A, Shchukarev A. Fate of Cu, Cr, and As during combustion of impregnated wood with and without peat additive. Environ Sci Technol 2007;41:6534–40.
[18] Sørum L, Frandsen FJ, Hustad JE. On the fate of heavy metals in municipal solid waste combustion part I: devolatilisation of heavy metals on the grate. Fuel 2003;82:2273–83.

Please cite this article in press as: Bajamundi CJE et al. Towards controlling PCDD/F production in a multi-fuel fired BFB boiler using two sulfur addition strategies. Part II: Thermodynamic analysis. Fuel (2014), http://dx.doi.org/10.1016/j.fuel.2014.05.033

[19] Ménard Y, Asthana A, Patisson F, Sessiecq P, Ablitzer D. Thermodynamic study of heavy metals behavior during municipal waste incineration. Process Saf Environ Prot 2006;84:290–6.
[20] Sandelin K, Backman R. A simple two-reactor method for predicting distribution of trace elements in combustion systems. Environ Sci Technol 1999;33:4508–13.
[21] Eriksson G, Hack K. Production of metallurgical-grade silicon in an electric arc furnace. In: Hack K, editor. SGTE caseb. thermodyn. work. Cambridge: Woodhead Publishing Limited; 2008. p. 415–24.
[22] Koukkari P. Advanced Gibbs energy methods for functional materials and processes – ChemSheet 1999–2009; 2009.
[23] Kong X, Zhong W, Du W, Qian F. Three stage equilibrium model for coal gasification in entrained flow gasifiers based on Aspen Plus. Chin J Chem Eng 2013;21:79–84.
[24] Francois J, Abdelouahed L, Mauviel G, Patisson F, Mirgaux O, Rogaume C, et al. Detailed process modeling of a wood gasification combined heat and power plant. Biomass Bioenergy 2013;51:68–82.
[25] Bale CW. Macro processing manual – FactSage 6.3. Thermfact/CRCT (Montreal, Canada) and GTT-Technologies (Aachen, Germany); 2012.
[26] Gullet BK. The effect of metal catalysts on the formation of polychlorinated dibenzo-p-dioxin and polychlorinated dibenzofuran precursor. Chemosphere 1900;20:1945–52.
[27] Kulkarni PS, Crespo JG, Afonso CM. Dioxins sources and current remediation technologies–a review. Environ Int 2008;34:139–53.
[28] Stanmore B. The formation of dioxins in combustion systems. Combust Flame 2004;136:398–427.
[29] Altarawneh M, Dlugogorski BZ, Kennedy EM, Mackie JC. Mechanisms for formation, chlorination, dechlorination and destruction of polychlorinated dibenzo-p-dioxins and dibenzofurans (PCDD/Fs). Prog Energy Combust Sci 2009;35:245–74.
[30] Lassesson H, Steenari B-M. Speciation of copper in ash from a fluidized-bed boiler fired with municipal solid waste. Energy Fuels 2013;27:3891–7.
[31] Fujimori T, Tanino Y, Takaoka M, Morisawa S. Chlorination mechanism of carbon during dioxin formation using Cl–K near-edge X-ray-absorption fine structure. Anal Sci 2010;26:1119–25.
[32] Takaoka M, Shiono A, Nishimura K, Yamamoto T, Uruga T, Takeda N, et al. Dynamic change of copper in fly ash during *de novo* synthesis of dioxins. Environ Sci Technol 2005;39:5878–84.
[33] Fujimori T, Takaoka M, Kato K, Oshita K, Takeda N. Observing copper chloride during dioxin formation using dispersive XAFS. X-Ray Spectrom 2008;37:210–4.
[34] Nakayama J, Miyake A. Catalytic effect of copper(II) oxide on oxidation of cellulosic biomass. J Therm Anal Calorim 2012;110:321–7.
[35] Ryan SP, Li X, Gullett BK, Lee CW, Clayton M, Touati A. Experimental study on the effect of SO_2 on PCDD/F emissions: determination of the importance of gas-phase versus solid-phase reactions in PCDD/F formation. Environ Sci Technol 2006;40:7040–7.
[36] Ke S, Jianhua Y, Xiaodong L, Shengyong L, Yinglei W, Muxing F. Inhibition of *de novo* synthesis of PCDD/Fs by SO_2 in a model system. Chemosphere 2010;78:1230–5.
[37] Vainikka P, Enestam S, Silvennoinen J, Taipale R, Yrjas P, Frantsi A, et al. Bromine as an ash forming element in a fluidized bed boiler combusting solid recovered fuel. Fuel 2011;90:1101–12.
[38] Bankiewicz D, Vainikka P, Lindberg D, Frantsi A, Silvennoinen J, Yrjas P, et al. High temperature corrosion of boiler waterwalls induced by chlorides and bromides – part 2: lab-scale corrosion tests and thermodynamic equilibrium modeling of ash and gaseous species. Fuel 2012;94:240–50.
[39] Zevenhoven M, Yrjas P, Skrifvars B-J, Hupa M. Characterization of ash-forming matter in various solid fuels by selective leaching and its implications for fluidized-bed combustion. Energy Fuels 2012;26:6366–86.
[40] Johansson LS, Leckner B, Tullin C, Åmand L, Davidsson K. Properties of particles in the fly ash of a biofuel-fired Circulating Fluidized Bed (CFB) boiler. Energy & Fuels 2008;22:3005–15.
[41] Sandelin K, Backman R. Trace elements in two pulverized coal-fired power stations. Environ Sci Technol 2001;35:826–34.
[42] Gullett BK, Bruce KR, Beach L. Effect of sulfur dioxide on the formation mechanism of polychlorinated dibenzodioxin and dibenzofuran in municipal waste combustors. Environ. Sci. Technol. 1992;26(1):1938–43.
[43] Harriot P, Markussen J. Kinetics of sorbent regeneration in the copper oxide process for flue gas cleanup. Ind Eng Chem Res 1992;31:373–9.
[44] Söderström G, Marklund S. Formation of PBCDD and PBCDF during flue gas cooling. Environ Sci Technol 2004;38:825–30.
[45] Schüler D, Jager J. Formation of chlorinated and brominated dioxins and other organohalogen compounds at the pilot incineration plant VERONA. Chemosphere 2004;54:49–59.
[46] Vainio E, Yrjas P, Zevenhoven M, Brink A, Laurén T, Hupa M, et al. The fate of chlorine, sulfur, and potassium during co-combustion of bark, sludge, and solid recovered fuel in an industrial scale BFB boiler. Fuel Process Technol 2013;105:59–68.
[47] Amand L-E, Kassman H. Decreased PCDD/F formation when co-firing a waste fuel and biomass in a CFB boiler by addition of sulfates or municipal sewage sludge. Waste Manage 2013.

Please cite this article in press as: Bajamundi CJE et al. Towards controlling PCDD/F production in a multi-fuel fired BFB boiler using two sulfur addition strategies. Part II: Thermodynamic analysis. Fuel (2014), http://dx.doi.org/10.1016/j.fuel.2014.05.033

Paper III

Towards controlling PCDD/F production in a multi-fuel fired BFB boiler using two sulfur addition strategies. Part III: Cu speciation in the fly ash

In: Fuel 132, pp. 178- 186

Fuel 132 (2014) 178–186

Contents lists available at ScienceDirect

Fuel

journal homepage: www.elsevier.com/locate/fuel

Towards controlling PCDD/F production in a multi-fuel fired BFB boiler using two sulfur addition strategies. Part III: Cu speciation in the fly ash

Cyril Jose E. Bajamundi [a,b,*], Pasi Vainikka [a], Irina Hyytiäinen [c], Kirsi Korpijärvi [a], Manu Lahtinen [d], Wantana Klysubun [e], Jukka Konttinen [b]

[a] VTT Technical Research Centre of Finland, Koivurannantie 1 PL 1603, 40 101 Jyväskylä, Finland
[b] Department of Chemistry, Laboratories of Renewable Natural Resources and Chemistry of Living Environment, POB 35, FI-40014 University of Jyväskylä, Finland
[c] Valmet Power, Lentokentänkatu 11, FI-33101 Tampere, Finland
[d] Department of Chemistry, Laboratories of Inorganic and Analytical Chemistry, POB 35, FI-40014 University of Jyväskylä, Finland
[e] Synchrotron Light Research Institute, 111 University Avenue, Muang, Nakhon Ratchasima 30000, Thailand

HIGHLIGHTS

- We showed that fly ashes in the two ESP fields have different formation history.
- We detected the formation of $CuSO_4$ in the combustion system under study.
- We showed that the active/passive ratio of Cu species affects PCDD/F production.

ARTICLE INFO

Article history:
Received 10 February 2014
Received in revised form 17 April 2014
Accepted 22 April 2014
Available online 11 May 2014

Keywords:
PCDD/F
de novo
Copper speciation
Sulfur addition
XANES

ABSTRACT

PCDD/F abatement strategies – sulfur pellet addition and peat co-combustion – were tested for a BFB boiler facility utilizing SRF-bark-sludge as fuel. In this paper chemical and physical analyses of electrostatic precipitator (ESP) fly ashes were used to explain the differences in the performance of these strategies. These analyses revealed a difference between the coarse and fine fly ashes collected in the ESP. Chemical analysis of the fine fly ashes revealed high concentration of easily volatilized elements while the SEM micrographs showed that fine ash are composed of clusters of spherical particles, thereby leading to a conclusion that fine ashes were originally in a gas phase in the high temperature zones of the boiler. Variation in the distribution of active and passive forms of Cu in fly ashes was revealed using X-ray absorption spectroscopy (XANES mode). It was also found that peat co-combustion led to increased formation of Cu oxides that may act as active catalysts in *de novo* synthesis. Furthermore, XANES revealed the formation of $CuSO_4$ for all the test cases. By applying the empirical ratio between mole fractions of the active and passive species of Cu, the role of Cu speciation to PCDD/F production was emphasized. It is concluded that sulfur pellet addition is more effective than peat addition as a PCDD/F abatement strategy for the BFB facility understudy.

1. Introduction

Polychlorinated dibenzo-p-dioxin and dibenzofuran (PCDD/F) is one of the most highly regulated of emissions in waste-to-energy plants. The current waste directive of European Parliament sets an emission ceiling of 0.1 ng/Nm ^{3} (O_2 content 6%) for all stationary and mobile technical equipment either fully or partially utilizing waste as a fuel, and converting it to energy via thermal process [1]. PCDD/F released to the atmosphere can be removed either via photodegradation or by deposition, but the ultimate sink is believed to be aquatic sediments and from there PCDD/F can bioaccumulate in fish and invertebrates [2]. Humans are exposed to bioaccumulated PCDD/F primarily from food, e.g. seafood, milk and meat, and some contaminated vegetables. It has also been found that the degradation of tetra- to octachloro congeners is minimal in a soil environment perhaps due to the compound's poor solubility in water [3]. It is therefore important that production and emission of PCDD/Fs is addressed and minimized at its point sources.

* Corresponding author at: VTT Technical Research Centre of Finland, Koivurannantie 1 PL 1603, 40 101 Jyväskylä, Finland. Tel.: +358 20 722 2574; fax: +358 20 722 2720.
E-mail address: cyril.bajamundi@vtt.fi (C.J.E. Bajamundi).

http://dx.doi.org/10.1016/j.fuel.2014.04.075
0016-2361/

This research series aims to address the objective above and examines the possibility of reducing PCDD/F production via sulfur addition [4,5]. Sulfur has been found to reduce PCDD/F production by converting active Cu oxide, oxychloride, and chloride species to $CuSO_4$ -the inactive state of copper in terms of *de novo* synthesis [6,7].

1.1. Earlier findings

The key features and findings presented in our previous studies [4,5] with PCDD/F abatement strategies are briefly summarized in this section. Addition of S-pellet (Case 2) and *S* from peat (Case 3) affect the production levels of PCDD/F in a 140 MW_{th} bubbling fluidized bed boiler (operated at a mean load of 90 MW_{th} during the experimental campaign) burning Scandinavian spruce bark, dried paper mill sludge and solid recovered fuel (SRF) (see Fig. 5a for the PCDD/F concentration measured). The behavior of the fine-particle forming elements collected at the second pass of the boiler suggests an effective sulfation of Na, K, and Cu when S-pellets were added to the fuel mixture. The amount of PCDD/F produced in the post combustions zones of the boiler is significantly reduced. However for Case 3, high concentration and poor volatilization of Cu and high particle loading in the flue gas enhanced production of dioxins and furans [4]. The homologue distribution or fingerprint of PCDD/F also revealed that the main production is via the *de novo* mechanism. This mechanism is dominant at a temperature window of 200–400 °C and is catalyzed by Cu associated with Cl and/or O [8]. In the second part of the study series [5], staged equilibrium process modeling was developed and used to study the behavior of Cu in the BFB system during the tests. The model showed the possible presence of a "frozen equilibrium" [9] wherein gas phase reactions are frozen by kinetic restriction and other transport phenomena as the flue gas is cooled in the colder post-combustion zone of the boiler. The model was able to explain the chemistry governing the behavior of the aerosol samples collected at the backpass of the BFB boiler. However the staged equilibrium model failed to predict the formation of $CuSO_4$ due to overestimation of $CaSO_4$ formation and the kinetically governed nature of Cu sulfation [10]. This limitation prompted the introduction of an empirical molar active/passive species ratio (APR). The APR estimates the ratio of the amount of active Cu species that can participate as a catalyst in *de novo* synthesis and the amount of passive Cu species that cannot contribute or offer competition for active Cu. The active/passive species ratio is defined previously as [5]:

$$\mathrm{APR} = \left[\frac{(\mathrm{Cu}-\mathrm{Cl}) + (\mathrm{Cu}-\mathrm{O}) + (\mathrm{Cu}-\mathrm{O}-\mathrm{Cl}) + \mathrm{Cu}}{\mathrm{CuSO_4} + (\mathrm{Cu}-\mathrm{Br}) + \mathrm{Cu}}\right] \quad (1)$$

The numerator contains active species of Cu participating in oxycholorination reaction pertinent to the production of PCDD/F via *de novo* synthesis. The denominator contains the deactivated species of Cu, $CuSO_4$ and Cu–Br species which can steal Cu from chlorine and/or oxygen thereby disabling Cu from participating in the *de novo* synthesis of chlorinated dioxins and furans. Metallic copper is present both in the numerator and the denominator because it can be chlorinated (CuCl; active) or it can be the left-over product of the chlorination of the carbon matrix by CuCl which may have reduced catalytic activity (passive). This empirical ratio, showed a high correlation with the PCDD/F production levels and was used in the sensitivity analysis part [5].

1.2. Speciation of copper

Several methods are currently available for the speciation of elements found in fly ashes, but due to the complex mixture of elements present in these ashes most of these methods are applicable only to specific element constituents and at a given concentration.

One popular method is sequential chemical leaching or fractionation, where increasingly aggressive solvent are used [11]. Starting with H_2O, alkali salts (sulfates, chlorides) are leached, followed by ammonium acetate where ion exchangeable fractions (organically associated elements, carbonates, and chlorides) are extracted. This is followed by acid leaching, using HCl to leach acid soluble carbonates and sulfates; the remaining solid residues are assumed to be silicates and silicate minerals [12]. There is however a risk that new artificial and stable mineral phases are formed, as well as sorption phenomena of elements on some stable phases in the system during successive leaching, causing the elements to remain in the solid residue [11]. Also leaching does not give definitive results but provides only scope for hypothesizing an element's speciation. Therefore this procedure is not applicable for the goals of this study. Since fractionation may significantly influence the speciation process, the use of non-destructive technique is necessary.

One common non-destructive technique is X-ray photoelectron spectroscopy (XPS). This technique probes the energy distribution of electrons ejected from solids via irradiation by X-rays and photoelectric effect. The electrons contain information regarding the chemical oxidation state, electronic structure and atomic composition of the analyte being studied [13]. For instance, XPS has been used for the speciation of *S* and P in coal fly ashes. *S* was found to be SO_4^{2-} and P was PO_4^{3-}, which explains the difference in their leaching behavior [14]. XPS can distinguish metallic Cu from $CuCl_2$ (halide), CuO (oxide) and $CuSO_4$ (sulfate). However with the detection limit of 1 wt.% of Cu, XPS requires a considerable length of time to accomplish speciation due to the low concentration of Cu in the fly ash.

To address these issues above, a sensitive element-specific and non-destructive technique based on X-ray absorption is used in this work. X-ray absorption spectroscopy (XAS) is a method for investigating the local structural environment of elements. XAS is divided into X-ray absorption near edge structure (XANES) analysis which provides information primarily about the oxidation state of the absorbing element and its local geometry, and X-ray absorption fine structure (EXAFS) analysis which provides information about atomic coordination (type and number of neighboring atoms and inter-atomic distance). The physical basis of XANES is the electronic transition from the core level to the valence states, while for EXAFS it is the scattering of the X-ray exited photoelectron by the surrounding atom [15]. XAS can be used to study non-crystalline materials. The method uses an intense and energy-tunable source of X-ray provided by synchrotrons [16]. XAS has been successfully used in several studies concerned with the speciation of Cu from combustion fly ashes [8,17–21]. For example, Fujimori et al. used XANES data to observe the behavior of $CuCl_2$ during dioxin formation in the fly ash [20] and showed that chlorination and gasification of carbon matrices are important steps for dioxin formation in fly ashes containing $CuCl_2$. Fujimori and Takaoka [19] used XANES to examine the formation of organo-Cl compounds by $CuCl_2$ in the thermal process and explained why the *de novo* mechanism is most active at the temperature range of 200–400 °C. Moreover, Takaoka et al. used linear combination fitting analysis of Cu K-edge XANES spectra to study the oxychlorination cycle of Cu. They were able to explain how CuO can shuttle Cl to the carbon matrices and form PCDD/F [8]. Although they were not focused directly on PCDD/F production, Hsiao and co-worker used XANES with XPS to explain the high leachability of copper on the ESP fly ash. They suggested that leaching maybe a result of $CuCl_2$ enriched on the fly ash surfaces [22]. Recently, XAS was used to study the behavior of Cu found in different ashes extracted from a BFB boiler e.g. bottom,

hopper, cyclone, and filter ashes. Results revealed the transformation Cu that may be helpful in the development of methods to recover it from MSW combustion ash [23].

1.3. The objective of the study

The objective of this study is to determine the speciation of Cu in the fly ash collected from the electrostatic precipitator of the waste-to-energy facility described earlier [4,5]. The results of the speciation will be used to validate the active/passive species ratio (Eq. 1) and its correlation to PCDD/F production. APR was originally calculated using the results of the equilibrium stage mimicking the zone after tertiary air addition [5]. In this study the same equation is applied under the assumption that the remnants of the interaction of Cu with O, Cl, S, and Br are to some extent preserved in the fine fraction of fly ashes collected at the ESP.

2. Materials and methods

The ESP is composed of 4 fields: two parallel channels with two consequent fields. Particle-laden flue gas from the air preheaters (LUVO) is divided into two channels and enters the first fields of the ESP. The clean flue gas leave the second fields and enters the scrubber, see Fig. 1a.

Fly ash samples were collected from the pneumatic transport lines below the fields of the right channel (Case 1) or left channel (Case 2 and 3) using a simple tube sampler made up of a steel pipe, see Fig. 1b. For each test case, five sampling periods lasting for about four minutes were performed. Each sample was cooled before being bagged into a clean and sealed container. However unlike in Part I [4] the fly ashes collected in the first and second fields were not combined. It was anticipated that the chemical and physical properties of these two ashes may be different [24]. The composite sample was made by combining equal mass portions of ash sample from each sampling period for each field. In total six composite samples were prepared and analyzed for this study – 3 samples from the first field, and 3 samples from the second field. By visual inspection the first field captures the coarse fly ashes while the second collects the much finer fly ashes. For all test runs, the ESP is being maintained at 190 °C.

The concentration of major ash forming and trace elements in the fly ash were determined using X-ray fluorescence spectroscopy (XRF) without prior treatment except for size reduction using a ceramic ball mill. Micrographs were also taken using a scanning electron microscope (SEM) to examine the morphology of fly ash samples. X-ray powder diffraction data was measured using PANalytical ŕPert PRO alpha 1 diffractometer in Bragg–Brentano geometry using Johansson monochromator to produce Cu Kα1 radiation (1.5406 Å; 45 kV, 30 mA). The diffraction intensities were recorded by an ŕCelerator detector using continuous scanning mode in 2-range of 4–100° with a step size of 0.017° and counting times of 800 s per step. Data processing and semi-quantitative search-match identification of the crystalline phases were made by ŕPert HighScore Plus v. 2.2d program using the ICDD-PDF4 + (release 2012) powder diffraction database reference retrieval source. The semi-quantitative information was acquired by the reference intensity ratio method (RIR) included in the program.

XANES spectra of the fly ash samples were collected at BL8 of the Synchrotron Light Research Institute in Thailand [25]. The photon energy of the synchrotron X-rays was scanned by a Ge(220) double crystal in the K-edge XANES region of copper. The photon energy was calibrated against the K-edge of Cu foil at 8979 ± 0.3 eV. Prior to analysis, all samples were finely ground and deposited in polyimide tape. Due to the low Cu concentration all fly ash samples were scanned in the fluorescence mode. The incident photon intensity, I_O, was monitored by a 10 cm ion chamber filled with Ar (76 mbar), while the fluorescence signal, I_F, was measured using a 13-element Ge detector. Absorption is given by I_F/I_O. On the other hand the K-edge XANES spectra of the pure standards (Cu foil, Cu_2O, CuCl, CuO, $CuCl_2$, $CuBr_2$, and $CuSO_4$) were collected using the transmission mode due to high Cu concentration. The intensity of the incident X-ray beam, I_O, and the transmitted X-ray beam, I_t, were monitored by a 10 cm long ion chamber (with Ar at 76 mbar) and a 40 cm long ion chamber (with Ar at 413 mbar) respectively. Absorption is defined as $\ln(I_O/I_t)$. Each XANES spectrum is an average of two or more scans.

Data analysis for the spectra was performed in ATHENA a XAS data processing software [26]. Spectra were normalized using the MBACK algorithm developed by Penner-Hahn and co-workers [27]. Linear combination fitting (LCF) was used to perform a semi-quantitative compositional analysis of the chemical species of Cu in the ESP fly ash. LCF assumes that the spectrum of a given sample is a linear combination of known spectra from "model compounds" or references. Since the chemical species in real fly ashes are hardly known very accurately, selecting the proper set

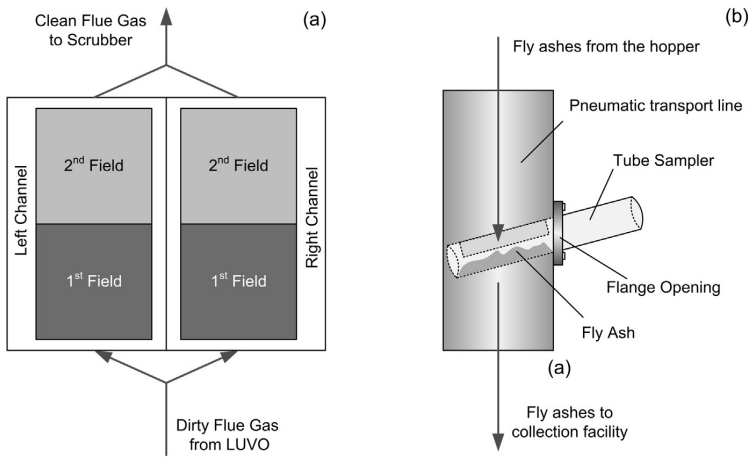

Fig. 1. (a) Flow of flue gas in the ESP channels and consequent fields. (b) Schematic for fly ash collection in the pneumatic transport line below the ESP hopper using a tube sampler.

of references is key to the robustness and validity of this analysis [8]. The selection of reference Cu compounds (see Table 3 and Fig. 3) was based on the thermodynamic modeling results in the second part of study [5] and similar studies on PCDD/F production using XAS as a method for Cu speciation [8,18–22]. This selection strategy limits the number of reference compounds used, so it is possible that other Cu compounds were present in the sample but were not accounted for. The fitting space is the normalized absorption $\mu(E)$ at the range of −20–30 eV around the absorption edge. The misfit (R – factor) is given by

$$R-\text{factor}=\frac{\sum[\text{data}-\text{fitted}]^2}{\sum \text{data}^2} \quad (2)$$

The coefficients obtained from linear combination fitting of the XANES spectra indicate mole percentage of the respective references used [8].

3. Results and discussions

3.1. Elemental analysis and morphology of the ESP fly ash

The concentration of major and trace elements in the ash samples are found in Table 1. In general the concentration of main ash forming elements Si, Ca, Al, and Fe, which are referred to as ash matrix forming elements [28], is higher in the samples collected in the first field as compared to the second field of the ESP. The first field of the ESP is designed to capture the coarse particles which are usually fragments or inert components of the fuel or fuel mixture being fired in the boiler [24]. This field is also designed to capture entrained bed materials.

The next group is the salt-forming group consisting of K, Cl, and S. The definition of "salt" is somewhat inaccurate, but here we refer to it to as low melting point water soluble fractions in contrast to the high melting point inert and insoluble oxides [29]. In general the concentration of the salts is higher in the second field which collects fine particle fractions of the fly ash entrained in the flue gas.

The fine ESP fly ash fraction is the end product of the complex process of aerosol formation and growth. In the post combustion zone of the BFB boiler, vapor species with a saturation ratio (S_∞) exceeding unity start to condense and eventually form particles. S_∞ is the partial pressure of the vapor in the flue gas over the saturation vapor pressure. These particles grow further by condensation on pre-existing particles or via chemical reactions. In addition, particles can collide with each other and form larger particles or coagulate [30]. Agglomerates formed from primary particles tend to partly coalesce together, from fractal-life aggregates to compact spherical structures, via the process called multiparticle sintering [31].

In both fields, the concentration of *K* in Case 1 and 2 are comparable, while Case 3 has the least. This trend is also true for Cl. These observations agree with earlier findings that the alkalis have poor "reactivity" and volatility during peat co-firing [4]. As a result *K* may have partitioned to the bottom ash [5]. Without the alkalis, the majority of Cl in the fuel formed $HCl_{(g)}$ and remained in the flue gas.

For the samples collected in the first field, the concentration of *S* for Case 2 is 1.84 times that of Case 1; this nearly corresponds to the increase in *S* content of the fuel mixture in Case 1 to Case 2 [4]. In the second field, the concentration of *S* for Case 2 is 1.43 times that of Case 1. These observations indicate the possibility that (1) *S* was non-volatile and stayed in the ash, or (2) *S* volatilized, reacted with Ca, alkalis and perhaps even Cu, and condensed back as part of the fly ash. The first is less likely to happen because $SO_{2(g)}$ measured at the backpass for Case 2 is almost 17.5 times that of Case 1 and the aerosol samples have shown indications that sulfation has occurred during S-pellet addition [4]. Meanwhile, in both fields *S* concentration for Case 3 is only 4/5 of *S* concentration in Case 1 even if the *S* in the fuel mixture for Case 3 is around 3.42 times that of Case 1 [4].

Lastly the trace element group (Cu, Zn, Cr, and Pb) exhibits a behavior of the salt-forming group. These elements are enriched in the fine fly ash particles collected in the second field as compared to the coarse particles of the first field. These elements volatilize and leave the fuel in the reducing zones of the boiler either as pure element, or sulfide, or chlorides, or oxides [32] and then condense in the post combustion zones of the boiler [33] and form fine particles in the fly ash. The presence of Cu in the fine fly ashes collected in the second field is important in understanding PCDD/Fs formation.

The morphology of the fly ashes collected in the first field is much coarser and larger relative to the ones collected in the second field (see Fig. 2). For the cases with SRF-bark-sludge (Case 1 and 2) the large particles are combination of spherical and unstructured morphologies. For SRF-sludge-peat firing (Case 3), large irregular shaped particles have been found together with some slightly smaller spherical particles. These irregularly shaped particles may have been fragments of the peat being used. There are reports in the literature that inert silicate-rich structures in fuels, though possibly subject to fragmentation, retain their morphology even after being subjected to the harsh combustion conditions [34].

On the other hand, the morphology of the fly ashes collected in the second field of the ESP is more homogeneous and composed of fine clusters of spherical particles. A higher degree of magnification reveals the detail of these clusters (Fig. 2e).

Table 1
Major and trace elements in the ESP fly ashes.

Element (mg/kg a.r.)	Field 1			Field 2		
	Case 1	Case 2	Case 3	Case 1	Case 2	Case 3
Si	111,000	108,000	164,000	69,000	78,000	101,000
Ca	210,000	224,000	158,000	274,000	249,000	200,000
Al	49,000	37,000	38,000	42,000	35,000	35,000
Fe	21,000	27,000	41,000	19,000	27,000	44,000
K	24,000	24,000	18,000	38,000	31,000	20,000
Cl	30,000	13,000	6000	90,000	23,000	19,000
S	44,000	81,000	36,000	72,000	103,000	61,000
P	6000	5800	3600	6800	7200	4200
Cu	3400	3700	2100	5700	4200	3200
Zn	4100	4300	2500	7700	5700	4400
Cr	380	380	310	480	370	520
Pb	530	510	320	1720	960	790

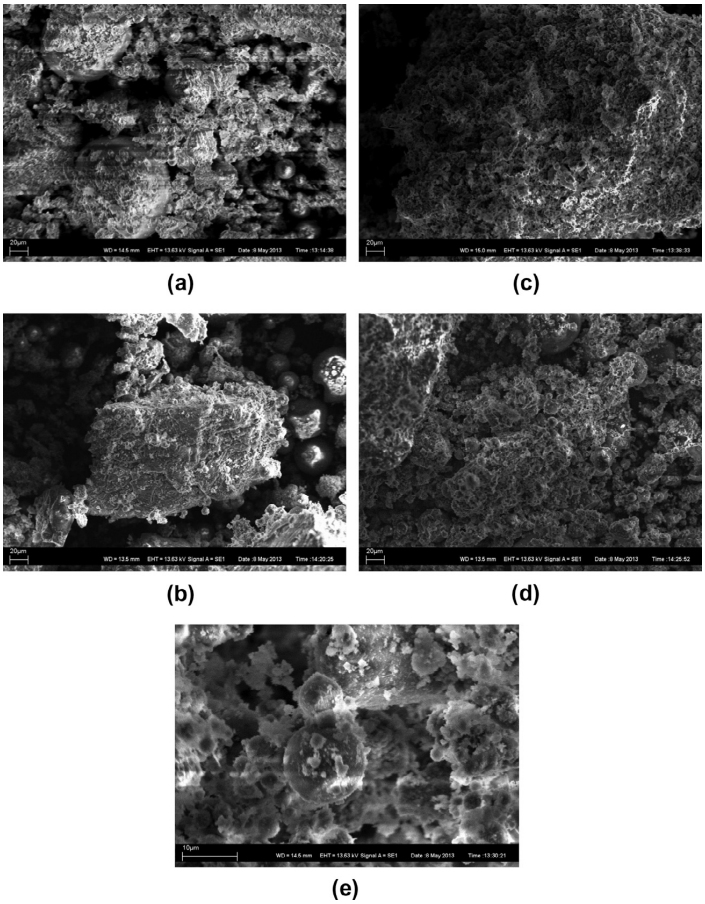

Fig. 2. SEM micrographs of the ESP fly ash. (a) and (b) are for the fly ashes collected at the first field, while (c) and (d) are from the second field. The first row is for the SRF-Bark-Sludge (Case 1 and 2) firing while the second row is for the case of SRF-Sludge-Peat firing (Case 3) and (e) is from Case 2 fly ash collected at the second field of the ESP. (a)–(d) are taken at 1000× magnification while (e) is taken at 6000× magnification.

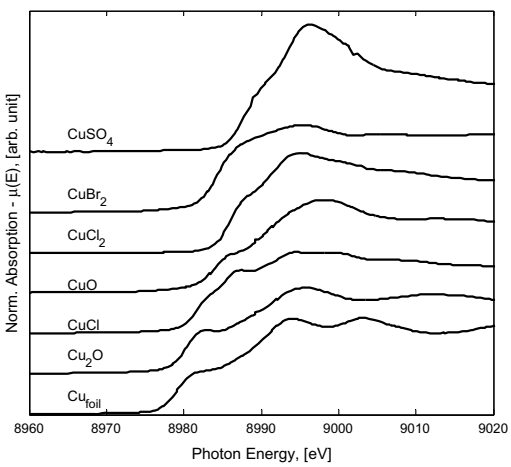

Fig. 3. Cu K-edge XANES spectra of the model or reference compounds used in LCF.

3.2. Crystalline compounds in the ESP fly ash

The relative mass fractions of phases identified by XRD are found in Table 2. Based on the semi-quantitative search-match analysis, the samples collected for both fields are composed primarily of SiO_2 (quartz), $CaSO_4$ (anhydrite), $CaCO_3$ (calcite), various alkali and alkaline earth metal containing tectoalumosilicates $(Na,Ca,K)Al(Si,Al)_3O_8$ (e.g. albeite, microcline, anorthite) and $Ca_2(Mg,Al)Al(Si,Al)O_7$ (e.g. gehlenite and melilite). Present in minor to trace amounts are phases like NaCl (halite), KCl (sylvite), $Ca(OH)_2$ (portlandite), MgO (periclase), Fe_2O_3 (hematite), Al (aluminum), and TiO_2 (rutile). However due to the complexity of the diffraction patterns, the presence or absence of trace amounts of K_2SO_4 (arcanite), Na_2SO_4 (thenardite) and/or $KNaSO_4$ (aphthitalite) cannot easily be ruled out.

In the same table, the species detected by the thermodynamic model are also indicated [5]. Not all phases detected by XRD are also detected by the model especially albite, gehlenite and microcline for Cases 1 and 2.

For all test cases, the mass fraction of quartz is higher for the samples from the first field as compared to the second field. The impact of peat co-firing to the fly ash is clearly demonstrated by

Table 2
Relative mass fraction of crystalline compounds identified by XRD and thermodynamic model. *x* means that the species has been detected in the condensed phase at the 3rd and/or 4th stage of the staged equilibrium model [5].

Phase	First field			Second field			Thermodynamic model		
	Case 1	Case 2	Case 3	Case 1	Case 2	Case 3	Case 1	Case 2	Case 3
SiO_2 (quartz)	22	29	38	8	16	25	x		x
$CaSO_4$ (anhydrite)	14	13	4	32	21	11	x	x	x
$CaCO_3$ (calcite)	7	4	3	24	10	8	x		
NaCl (halite)	1	1	1	7	3	2	x	x	
KCl (sylvite)	1	–	–	4	–	1	x	x	
$Ca(OH)_2$ (portlandite)	1	1	1	2	2	2			
MgO (periclase)	1	1	–	2	2	1	x	x	
Fe_2O_3 (hematite)	2	1	1	3	2	3	x		x
Al (metallic)	3	1	1	1	2	1			
$(Na,Ca,K)Al(Si,Al)_3O_8$ (albite)	18	23	21	2	24	23			x
$Ca_2(Mg,Al)Al(Si,Al)O_7$ (gehlenite)	8	6	4	13	13	9			
$(K,Na)AlSi_3O_8$ (microcline)	14	14	19	–	1	12			x
$K_2Ca_2(SO4)_3$ (langbeinite)	6	5	5	–	–	–			
TiO_2 (rutile)	2	1	2	2	4	2			

the increase of the relative mass fraction of quartz in the samples collected for Case 3. Furthermore, elevated fractions of $(K,Na)AlSi_3O_8$ (microcline) in samples for Case 3 supports poor reactivity and volatility of the alkalis during peat co-firing [4,5]. Microcline found in fly ashes are formed during combustion [35] or present as small fractions of original fuel such as peat [36]. This led to a decrease of NaCl (halite) and KCl (sylvite) on Case 3 (vs. Case 1) for samples collected at the second field.

Both sulfur addition strategy reduced halite and sylvite in the sample collected at the second field. For Case 2, this can be the result of sulfation of alkali chlorides. For Case 3, this can be the result of the presence of stable microcline in the fuel mixture which did not allow halite and sylvite to form [4,5]. In addition, the presence of $(Na,Ca,K)Al(Si,Al)_3O_8$ (albite) in the sample was also detected. Albite is formed from the capture of Na salts at around 576 °C by aluminosilicates and by subsequent crystallization [35].

Due to the presence of high amounts of Ca in the fuel mixture, especially for Cases 1 and 2, formation of $CaSO_4$ (anhydrite) was possible. In fact anhydrite is always present in appreciable amounts for all test cases and sampling locations. Anhydrite can be formed by sulfation of $CaO_{(s)}$ released from the organic fraction of the fuel [35].

These differences in chemical composition and morphology are indications that the histories of the fly ashes collected in the ESP fields are different. Ashes collected in the first field are composed primarily of large and relatively inert oxides originating from the fuel or from products of attrition or from fragmentation of bed material, while those that were collected at the second field can be traced from the condensation, heterogeneous nucleation or sintering of aerosol-forming elements.

3.3. Cu speciation via Cu K-edge XANES

The purpose of this experiment is twofold. First, to detect the presence of $CuSO_4$ which is the target compound and the main reason why sulfur was added to the fuel mixture being burned – see Part 1 of this study [4]. The second objective is the speciation of Cu and to assess whether the active/passive ratio, APR, defined above can still correlate with the levels of PCDD/F produced in the post combustion zones of the boiler. The comparison between the original and fitted spectra is found in Fig. 4 and the numerical results of LCF are found in Table 3.

Formation of $CuSO_4$ for all the test cases has been confirmed by the results of LCF. Even for the case where no *S* was added $CuSO_4$ formation was detected; this is probably the result of having sludge in the fuel mixture. In this study the concentration of *S* is

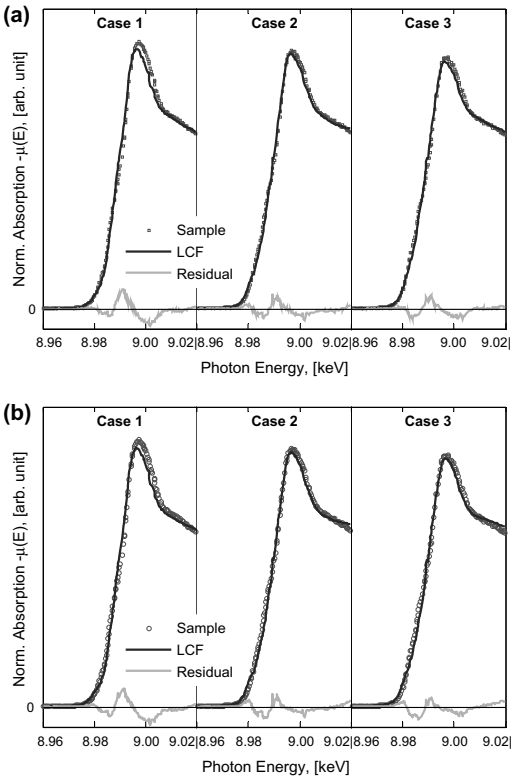

Fig. 4. Fly ash sample spectra and LCF results of Cu K-edge Xanes spectra and the residual. (a) Is for the samples from the first field and (b) is for the samples from the second field of the electrostatic precipitator.

0.5 wt% d.s. in the sludge [4]. Addition of sludge during combustion of SRF has been reported to also contribute in the inhibition of PCDD/F formation as it can also be a sulfur rich source [37]. The additional *S* may aid the poisoning of active Cu compounds. In the second ESP field, adding S-pellet led to a higher $CuSO_4$ mole fraction relative to peat co-combustion, which exhibited the smallest fraction. Other studies using the same technique have also detected $CuSO_4$ in the fine particles collected in a BFB fired with MSW [23].

Table 3
Result of the linear combination fitting of ESP fly ashes.

Standards	First field			Second field		
	Case 1	Case 2	Case 3	Case 1	Case 2	Case 3
Cu_2O	0.021 ± 0.042	0.057 ± 0.031	0.163 ± 0.039	0.000 ± 0.053	0.000 ± 0.035	0.065 ± 0.036
$CuBr_2$	0.000 ± 0.048	0.000 ± 0.040	0.000 ± 0.052	0.000 ± 0.060	0.000 ± 0.039	0.000 ± 0.041
$CuCl_2$	0.120 ± 0.055	0.000 ± 0.039	0.000 ± 0.050	0.219 ± 0.068	0.037 ± 0.044	0.120 ± 0.046
CuCl	0.118 ± 0.044	0.201 ± 0.046	0.227 ± 0.059	0.040 ± 0.057	0.115 ± 0.037	0.164 ± 0.038
CuO	0.230 ± 0.044	0.307 ± 0.038	0.212 ± 0.048	0.300 ± 0.059	0.309 ± 0.039	0.266 ± 0.040
$CuSO_4$	0.273 ± 0.028	0.216 ± 0.020	0.116 ± 0.025	0.359 ± 0.035	0.359 ± 0.023	0.287 ± 0.023
Cu foil	0.239 ± 0.108	0.218 ± 0.093	0.282 ± 0.117	0.082 ± 0.140	0.181 ± 0.090	0.098 ± 0.096
R – factor	0.0044	0.0019	0.0032	0.0064	0.0030	0.0037
Active[a]	0.728 ± 0.143	0.783 ± 0.121	0.884 ± 0.153	0.641 ± 0.184	0.642 ± 0.119	0.713 ± 0.125
Passive[b]	0.512 ± 0.121	0.434 ± 0.103	0.398 ± 0.130	0.441 ± 0.156	0.540 ± 0.101	0.385 ± 0.107
Active/passive Ratio	1.422 ± 0.437	1.804 ± 0.512	2.221 ± 0.824	1.454 ± 0.663	1.189 ± 0.313	1.852 ± 0.608

[a] [Cu_2O + $CuCl_2$ + CuCl + CuO + Cu].
[b] [$CuSO_4$ + $CuBr_2$ + Cu].

The fly ash collected at the first and second field for Case 1 registered high sum of $CuCl_2$ and CuCl mole fractions. Chlorinated copper is expected to be high in Case 1 because measures to induce or enhance sulfation have not yet been implemented. Gaseous $CuCl_2$ and CuCl leaving the furnace can condense in the post combustion zone and be collected in the fine particle fraction of the ESP fly ash. Eventually, the presence of Cu–Cl together with Cu–O species may further increase the degree of chlorination of the PCDD/F residing in the ESP fly ash. This explains why the degree of chlorination and concentration of PCDD/F in the ESP fly ash is the highest for Case 1 [4].

Likewise the high value of the combined mole fraction of Cu_2O and CuO in both fields also supports the observation that Cu was least volatile for Case 3 [4,5]. LCF reveals that the combined mole fraction of these two compounds in the second field is around 0.331 for Case 3, higher than the 0.300 and 0.309 for Cases 1 and 2 respectively. Cu_2O and CuO are nonvolatile species of copper under typical BFB boiler conditions where the temperature rarely exceeds 1000 °C.

The values of the APR are found in the last row of Table 3 and are plotted against the PCDD/F levels measured at the ESP inlet in Fig. 5a. There is no correlation between the APR evaluated in the first field and the PCDD/F concentration. On the other hand APR evaluated in the second level is linearly correlated with the PCDD/F levels. This observation is expected since the histories of these two fly ashes are different, as discussed above. The empirical equation was originally developed to take into account the transformation of Cu species existing in the vapor and in the condensed phases in the boiler [5]. Since fly ashes in the first field do not possess this history, the equation's applicability is limited in contrast to the fly ashes collected from the second field. It may also be irrelevant to evaluate APR in the fly ashes from the first field since large fly ash particles have been shown to contain less PCDD/F with respect to the finer ones [38].

In the second part of this study the APR evaluated at the equilibrium reactor mimicking the region just after tertiary air addition (T = 852 °C, λ = 1.379, coded as 852Ox), was able to explain the behavior of aerosol-forming elements and correlated with the PCDD/F levels measured at the ESP inlet [5]. In Fig. 5b the APR for the second field is plotted against the APR evaluated at 850Ox. The values of APR at 850Ox are higher than that of APR for the second field; however there still exists some degree of linear correlation between the two. The difference in magnitude is due to factors such as the limitation of the thermodynamic equilibrium modeling and the fact that the conditions at 852Ox are very different from those of the ESP. Therefore, while the active/passive species ratio is highly empirical and might be very specific to the conditions prevailing in this study, APR highlights the role of the modes of occurrences of Cu on PCDD/F production.

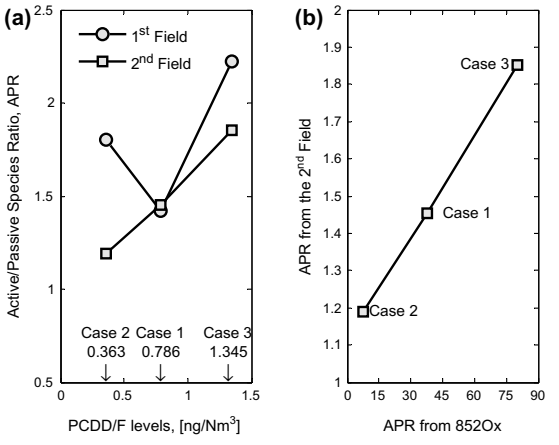

Fig. 5. (a) Correlation between the calculated APR vs. PCDD/F levels measured at the ESP inlet. (b) Comparison between the APR evaluated the 852Ox [5] and second ESP field.

4. Conclusion

X-ray fluorescence data showed that salt-forming and the trace elements (including Cu) are abundant in the fine particle fly ash fractions collected in the second field of the ESP. Conversely ash matrix forming elements are abundant in the coarse fly ashes from the first field of the ESP. This observation is further supported by the results of the XRD and the SEM micrographs taken from the fly ashes. These dissimilarities are due to the difference in the formation histories of these two ashes. Coarse fly ashes are products of attrition and fragmentation of the non-volatilized fuel components and bed material while fine fly ashes are formed from secondary gas/solid reaction (e.g. alkali aluminosilicate capture, sulfation) and salts that have been in the gas phase in the boiler and have condensed and agglomerated while traveling with the cooling flue gases.

Based on XANES analysis, the Cu–Cl species were found in the ESP ash when sulfur was not added. This is key in understanding the differences in PCDD/F levels in Case 1 and 2. Even though the amounts of Cu in the fuel in these two cases are practically equal, the presence of more Cu–Cl species in Case 1 led to a slightly higher PCDD/F concentration, relative to Case 2. This has implications also in the possible additional chlorination of particle-bound

PCDD/Fs of the ESP fly ashes. The combined presence of Cu–Cl and Cu–O promoted subsequent chlorination of PCDD/F in the ESP fly ash in Case 1; the homologue distribution favors octachlorinated dioxin and pentachlorinated furans, and the concentration of PCDD/F in the ESP fly ash is highest [4].

As for Case 3, linear combination fitting of XANES spectra showed the significant presence of Cu–O and in the fine ESP fly ashes suggesting that Cu was indeed the least volatile and that it could have effectively shuttled Cl to the carbon matrices which is required for the inflight *de novo* formation of PCDD/F. Moreover, the mole fraction of $CuSO_4$ fraction is smallest in Case 3 suggesting poor sulfation of Cu. These observations explains why Case 3 yields the highest PCDD/F level [4].

XANES analysis also corrects the limitations of the staged equilibrium models at low temperature conditions, as it was able to show that $CuSO_4$ did form.

These observations from the analysis of XANES spectra can point to the conclusion that even though the fine ESP fly ashes have travelled far enough from the furnace of the boiler, where the high temperatures favor key oxidation, chlorination, and sulfation reactions, remnants of these events are carried over to the ash collected at the ESP. This is probably because of the rate and transport limitations governing the colder zones of the boiler system.

The active/passive ratio evaluated from the fine ESP fly ashes highlights the role that the speciation of Cu plays in PCDD/F production. Having more active species ($Cu_2O + CuCl_2 + CuCl + CuO + Cu$) present in the post combustion zone could result in enhanced PCDD/F production. Inversely when the presence of passive forms of Cu ($CuSO_4 + CuBr_2 + Cu$) is high the abatement of PCDD/F is promoted.

Based on the results and objectives of this work it can be concluded that adding S-pellet to the fuel mixture is more suitable than peat co-firing because it accomplished the required extent of Cu sulfation. Furthermore, the increased particle loading in peat co-combustion may also be detrimental in PCDD/F abatement since this can house unburned organic carbon matrices – an important ingredient in *de novo* synthesis. In addition, keeping the concentration of Cu as low as possible is key to for PCDD/F abatement. This is because oxychlorination can happen and promote PCDD/F production if sulfur is unable to fully convert Cu–Cl and Cu–O species to $CuSO_4$.

Acknowledgements

We are thankful to the OSER project, Valmet Power (formerly Metso Power), Foster Wheeler, the European Regional Development Fund and the RECOMBIO project TREN/FP7EN/239530/ for the resources shared for this study. Stora Enso Oyj is gratefully acknowledged for sharing the data presented in this paper. Likewise we are thankful to the staff of BL8 at SLRI for helping in the collection of XANES data. Dr. Nurak Grisdanurak and Dr. Pummarin Khamdahsag are also acknowledged for providing the standards used in this experiment and Dr. Pongtanawat Khemthong for the help on the XAS data analysis. We are also very thankful to Dr. James Penner-Hahn for providing a copy the MBACK algorithm and explaining its usage and features; and to Dr. Bruce Ravel via the IFEFFIT mailing list for pointing out the key details of XAS analysis. Thanks to Matti Ranta-Korpi and Hannu Salo for the SEM micrographs.

References

[1] Directive 2008/98/EC of the European Parliament and the Council of 19 November 2008 on waste and repealing certain directives. Off J Eur; 2008,p. 3–30.
[2] Kulkarni PS, Crespo JG, Afonso CM. Dioxins sources and current remediation technologies–a review. Environ Int 2008;34:139–53.
[3] Orazio CE, Kapila S, Puri RK, Yanders AF. Persistence of chlorinated dioxins and furans in the soil environment. Chemosphere 1992;25:1469–74.
[4] Bajamundi CJE, Vainikka P, Hedman M, Hyytiäinen I, Silvennoinen J, Heinanen T, et al. Towards controlling PCDD/F production in a multi-fuel fired BFB boiler using two sulfur addition strategies. Part I: experimental campaign and results. Manuscr Submitt to FUEL Publ n.d.
[5] Bajamundi CJE, Vainikka P, Hedman M, Konttinen J. Towards controlling PCDD/F production in a multi–fuel fired BFB boiler using two sulfur addition strategies. Part II: thermodynamic analysis. Manuscr Submitt to FUEL Publ n.d.
[6] Hunsinger H, Seifert H, Jay K. Reduction of PCDD/F formation in MSWI by a process-integrated SO_2 cycle. Environ Eng Sci 2007;24:1145–59.
[7] Aurell J, Fick J, Haglund P, Marklund S. Effects of sulfur on PCDD/F formation under stable and transient combustion conditions during MSW incineration. Chemosphere 2009;76:767–73.
[8] Takaoka M, Shiono A, Nishimura K, Yamamoto T, Uruga T, Takeda N, et al. Dynamic change of copper in fly ash during de novo synthesis of dioxins. Environ Sci Technol 2005;39:5878–84.
[9] Sandelin K, Backman R. Trace elements in two pulverized coal-fired power stations. Environ Sci Technol 2001;35:826–34.
[10] Harriot P, Markussen J. Kinetics of sorbent regeneration in the copper oxide process for flue gas cleanup. Ind Eng Chem Res 1992;31:373–9.
[11] Vassilev SV, Baxter D, Andersen LK, Vassileva CG. An overview of the composition and application of biomass ash. Fuel 2013;105:19–39.
[12] Zevenhoven M, Yrjas P, Skrifvars B-J, Hupa M. Characterization of ash-forming matter in various solid fuels by selective leaching and its implications for fluidized-bed combustion. Energy Fuels 2012;26:6366–86.
[13] Chusuei C, Goodman DW. X-ray photoelectron spectrosopy. Encycl Phys Sci Technol 2002:921–38.
[14] Hirokawa K, Danzaki Y. Analytical application of XPS for surface characterization of coal fly ash and coal. Surf Interface Anal 1984;6:193–5.
[15] Penner-Hahn JE. X-ray absorption spectroscopy in coordination chemistry. Coord Chem Rev 1999;190–192:1101–23.
[16] Newville M. Fundamentals of XAFS 2004:1–41.
[17] Takaoka M, Fujimori T, Shiono A, Yamamoto T, Takeda N, Oshita K, et al. Formation of chlorinated aromatics in model fly ashes using various copper compounds. Chemosphere 2010;80:144–9.
[18] Tian S, Yu M, Wang W, Wang Q, Wu Z. Investigating the speciation of copper in secondary fly ash by X-ray absorption spectroscopy. Environ Sci Technol 2009;43:9084–8.
[19] Fujimori T, Takaoka M. Direct chlorination of carbon by copper chloride in a thermal process. Environ Sci Technol 2009;43:2241–6.
[20] Fujimori T, Takaoka M, Kato K, Oshita K, Takeda N. Observing copper chloride during dioxin formation using dispersive XAFS. X-ray Spectrom 2008;37:210–4.
[21] Hsiao MC, Wang HP, Wei YL, Chang JE, Jou CJ. Speciation of copper in the incineration fly ash of a municipal solid waste. J Hazard Mater 2002;91:301–7.
[22] Hsiao MC, Wang HP, Chang J-E, Peng CY. Tracking of copper species in incineration fly ashes. J Hazard Mater 2006;138:539–42.
[23] Lassesson H, Steenari B-M. Speciation of copper in ash from a fluidized-bed boiler fired with municipal solid waste. Energy Fuels 2013;27:3891–7.
[24] Sarkar A, Vishwakarma S, Banichul H, Mishra KK, Roy SS. A comprehensive analysis of the particle size and shape of fly ash from different fields of ESP of a super thermal power plant. Energy Sources, Part A Recov Util Environ Eff 2012;34:385–95.
[25] Klysubun W, Sombunchoo P, Deenan W, Kongmark C. Performance and status of beamline BL8 at SLRI for X-ray absorption spectroscopy. J Synchrotron Radiat 2012;19:930–6.
[26] Ravel B, Newville M. ATHENA, ARTEMIS, HEPHAESTUS: data analysis for X-ray absorption spectroscopy using IFEFFIT. J Synchrotron Radiat 2005;12:537–41.
[27] Weng T-C, Waldo GS, Penner-Hahn JE. A method for normalization of X-ray absorption spectra. J Synchrotron Radiat 2005;12:506–10.
[28] Obernberger I. Fly ash and aerosol formation in biomass combustion processes – an introduction Ingwald Obernberger n.d., 43.
[29] Backman R, Khalil RA, Todorovic D, Skreiberg Ø, Becidan M, Goile F, et al. The effect of peat ash addition to demolition wood on the formation of alkali, lead and zinc compounds at staged combustion conditions. Fuel Process Technol 2013;105:20–7.
[30] Mikkanen P. Fly ash particle formation in kraft recovery boilers. Springer; 2000.
[31] Eggersdorfer ML, Kadau D, Herrmann HJ, Pratsinis SE. Multiparticle sintering dynamics: from fractal-like aggregates to compact structures. Langmuir 2011;27:6358–67.
[32] Sørum L, Frandsen FJ, Hustad JE. On the fate of heavy metals in municipal solid waste combustion Part I: devolatilisation of heavy metals on the grate. Fuel 2003;82:2273–83.
[33] Enestam S, Mäkelä K, Backman R, Hupa M. Occurrence of zinc and lead in aerosols and deposits in the fluidized-bed combustion of recovered waste wood. Part 2: thermodynamic considerations. Energy Fuels 2011;25:1970–7.
[34] Skrifvars B-J, Yrjas P, Kinni J, Siefen P, Hupa M. The fouling behavior of rice husk ash in fluidized-bed combustion. 1. Fuel characteristics. Energy Fuels 2005;19:1503–11.
[35] Vassilev SV, Baxter D, Andersen LK, Vassileva CG. An overview of the composition and application of biomass ash. Part 1. Phase–mineral and chemical composition and classification. Fuel 2013;105:40–76.

[36] Pommer L, Öhman M, Boström D, Burvall J, Backman R, Olofsson I, et al. Mechanisms behind the positive effects on bed agglomeration and deposit formation combusting forest residue with peat additives in fluidized beds. Energy Fuels 2009;23:4245–53.
[37] Amand L-E, Kassman H. Decreased PCDD/F formation when co-firing a waste fuel and biomass in a CFB boiler by addition of sulphates or municipal sewage sludge. Waste Manag 2013.
[38] Lu S-Y, Du Y, Yan J-H, Li X-D, Ni M-J, Cen K-F. Dioxins and their fingerprint in size-classified fly ash fractions from municipal solid waste incinerators in China-Mechanical grate and fluidized bed units. J Air Waste Manag Assoc 2012;62:717–24.

Paper IV

Searching for a robust anti-corrosion measure to combust high SRF-energy-share fuel

Submitted to Fuel for publication
Manuscript no.: JFUE-D-14-02261

Searching for a robust anti-corrosion measure to combust high SRF-energy-share fuel

Cyril Jose E. Bajamundi [a, b,✉], Pasi Vainikka[a], Merja Hedman[c],

Jaani Silvennoinen[c], Teemu Heinanen[d], Raili Taipale[a], Jukka Konttinen[e]

[a.] VTT Technical Research Centre of Finland, Koivurannantie 1 PL 1603, 40 101 Jyväskylä, Finland

[b.] Department of Chemistry, Renewable Natural Resources and Chemistry of Living Environment, POB 35, FI-40014, University of Jyväskylä, Finland

[c.] Valmet Power, Lentokentänkatu 11, FI-33101, Tampere, Finland

[d.] Stora Enso Newsprint and Book Paper, Anjalankoski Mills, FI 46900 Anjalankoski, Finland

[e.] Tampere University of Technology, Department of Chemistry and Bioengineering, POB 541, FI-33101 Tampere, Finland

✉ Corresponding Author. Phone: +358 20 722 2574. Fax: +358 20 722 2720. E-mail: cyril.bajamundi@vtt.fi

Highlights

- We have demonstrated firing of 70 e-% SRF fuel mixture in a 140MW_{th} plant.
- We showed that sulfate injection is a robust anti-corrosion measure during high SRF e-share combustion.
- We used PLS regression to link the Cl conc. in deposits to the properties of the flue gas and aerosols.

Abstract

To meet the increasing volume of waste to be treated via energy recovery, high SRF-energy-share fuel is being fired in conventional waste-to-energy facilities. In this work, corrosion related risk during firing of 70 e-% share (target fuel) is studied and compared against the base case fuel containing 50 e-% share. Cl and S concentration is highest in the target fuel as a direct result of increasing the proportion of SRF in the fuel mixture. Br, Zn and Pb showed the same trend. Meanwhile, the concentration of Na, K, Al and Si are highly dependent on the type of the SRF fired. The corrosion risk of the base and target fuels are analyzed using the composition of the fine aerosol fraction and deposit samples measured near the vicinity of the superheater. Surprisingly aerosols for the target fuel are less risky – having less Cl and more S, than that of the base fuel. The effects of sulfur based additives – elemental sulfur and sulfate injection, and fuel substitution on superheater corrosion are likewise analyzed. All these methods can reduce the concentration of Cl in the aerosols, however it is concluded that sulfate injection is considered as a robust anti-corrosion measure. Sulfate injection is able to reduce Cl in the aerosols and deposits regardless of the quality of the fuel mixture. Robust anti-corrosion measures are important in ensuring the boiler performance during high SRF-energy share firing. An attempt of linking the quality of the deposits and the properties of the flue gas and aerosols around the superheater using partial least squares regression is also presented.

Keywords: SRF, waste-to-energy, corrosion, anti-corrosion measures

1 Introduction

On April of 2008 the Finnish Government approved the National Waste Plan for 2016 with the main aim of stabilizing the amount of municipal waste production and ensuring that the trend will be downwards by the year 2016. The specific target is to arrive at a situation where around 50% of all municipal waste is recycled as material, 30% is energy recovered and not more than 20% sent to landfilling [1]. By 2016, at least 70% of all construction and renovation waste will be used as material and energy sources. The plan estimates the required incineration capacity (incineration and co-incineration plants) for energy recovery to be between 700 000 and 750 000 tonnes. This is to be accomplished by increasing and promoting the use of non-recyclable waste as fuel in co-incineration plans, provided that such capacity is available in a given region or area (Section 4.3 of [1]).

The effect of this policy is clearly reflected in the historical data on the treatment of municipal waste (see Fig. 1) [2]. In 2012, 67% of the waste is energy-recovered or recycled, while 33% is still being sent to landfill. In the same year the amount of waste sent for energy recovery is 5.7 times that of 1997 and 1.9 times that of 2008 when the plan was approved.

1.1 Challenges

Co-combustion of waste derived fuels presents several operational challenges. Incompatibility of fuel components may lead to ash melting, slagging, severe bed agglomeration, and de-fluidization in fluidized bed boiler [3–5]. For example, addition of 5% refuse derived fuel (RDF) to coal substantially increased the deposition rate and the amount of melt found in deposits [4]. Co-firing of 30 wt.% grain waste, an agri-fuel, with wood fuel in a full-scale bubbling fluidized bed reactor led to heavy furnace-wall slagging due to increased potassium and phosphorous, which can similarly prevail during waste firing [5]. Formation of low melting eutectics is often the root cause of ash melting. Table 1 lists some of the common binary salt and oxide mixtures and their eutectic composition. The eutectic temperature of SiO_2 – Na_2O, KCl – NaCl and K_2CO_3 – KCl systems fall below typical bubbling fluidized bed boiler conditions.

Another issue related to waste co-firing is emission of heavy metals and organic pollutants. The main source of heavy metals is the commercial and industrial waste (C&IW) used as raw materials for producing the fuel. Vainikka et al. have studied some of the key trace elements found in the fuel of an 80MW BFB combusting solid recovered fuel (SRF) [6]. They concluded that these elements came mainly from additives, stabilizers, dyes, colorants and flame retardants used in the production of paper and plastics – which are the main components of the SRF [7]. After combustion these elements can end up in the bottom ash, fly ash and flue gas depending on their speciation and degree of volatilization [8–10]. One particular element of interest is

copper. Studies have shown that Cu is responsible for the production of dioxins and furans (PCDD/F) in the post combustion zones of waste-to-energy (WtE) systems [11,12]. PCDD/F is one of the organic pollutants that are strictly monitored in WtE systems, an emission limit of 0.1 ng/Nm^3 is set by the current European Waste Incineration Directive [13].

Co-combustion of waste derived fuels could also result to significant corrosion of heat exchange surfaces, especially the superheaters (SH). Corrosion follows the active oxidation mechanism [14], where alkali chlorides in superheater deposits act as key agents of corrosion [15–18]. Alkali chlorides may come from the fuel or be produced during the combustion of the fuel [19–22]. They react with the protective oxide scales e.g. Fe_2O_3 and Cr_2O_3, and produce $Cl_{2(g)}$. Chlorine can diffuse to the metal/scale interface and react with the metal to form solid metal chlorides ($MeCl_2$, Me = [Fe, Cr, Ni]), see S4 in Fig. 2. There it gets oxidized and gaseous metal chloride species are released. At typical superheater metal temperature, the vapor pressure of $FeCl_2$ is high enough to drive the vaporization of $FeCl_{2(g)}$, see S6 in Fig. 2. Volatile ferrous chloride diffuses to regions of high O_2 partial pressure and gets oxidized and releases $Cl_{2(g)}$ to begin the cycle anew. The net reaction for the metal, Me is described in R 1 and with little consumption of chlorides [14,23].

$$4Me_{(s)} + 3O_{2(g)} \rightarrow 2Me_2O_{3(s)} \qquad \text{R 1}$$

Minute amount of chlorine in the deposit is enough to initiate corrosion at typical superheater temperatures. For example a mixture of alkali sulfate and chloride containing 0.3 wt.% Cl has been shown to corrode 10CrMo9-10 and T91 steel grade [24].

Corrosion is further enhanced by the presence of molten phase on the surface of the steel. The rate of corrosion is faster for this case because (1) liquid phase reactions are faster than solid – solid reactions and (2) the liquid phase provides a electrolyte or pathway of ionic charge transfer, for the electrochemical attack [23]. The main source of these molten phases is low meting eutectics such as K_2SO_4–KCl, see Table 1.

Recently the presence of lead and zinc chlorides have been shown to increase the risk of corrosion at low metal temperature (230 – 450°C) during combustion of recovered waste wood; this makes the economizers susceptible to chlorine induced corrosion [25–27].

1.2 Destruction of alkali chlorides

Several methods are available for corrosion mitigation. Making sure that the waste derived fuel such as SRF is of good quality with low Cl content is the first line of defense. This can be done by ensuring minimal contamination of chlorinated plastics such as polyvinylchloride (PVC) and salt-containing food residues. However residual chlorine is always present in the SRF, thus in-situ solutions are still employed in actual operation.

One method to address Cl-induced corrosion is by alkali capture. The method prevents the formation of alkali chlorides by trapping the alkalis to the matrix of reactive aluminosilicates and aluminosilicate-containing additives such as kaolinite and bauxite [28]. The chemisorption process follows R 2,

$$2MCl + H_2O + Al_2O_3 \cdot xSiO_2 \rightarrow M_2O \cdot Al_2O_3 \cdot xSiO_2 + 2HCl \qquad \text{R 2}$$

where M = Na, K [29].

Peat ash addition has also been shown to significantly affect the chlorine content in the aerosols due to the interaction of K with the peat ash resulting in the reduced volatilization of the alkali [30]. Co-firing of peat can also lower the amount of alkali chlorides provided that the aluminosilicates present is "reactive". Sludge is also a possible alkali-capture agent [31].

Sulfation of alkali chlorides is another popular method to address chlorine induced corrosion in waste fired boilers [32,33]. Sulfation can happen in-flight or through intra-particle sulfation – a reaction between SO_2 and the alkali chlorides in the deposits. Both of these reactions produce $HCl_{(g)}$ via the reaction

$$2MCl_{(s)} + SO_{2(g)} + \frac{1}{2}O_2 + H_2O_{(g)} \rightarrow M_2SO_{4(s)} + 2HCl_{(g)} \qquad \text{R 3}$$

where M is Na or K [34].

R 3 can further be enhanced if the reactant SO_2 is substituted with SO_3. However in typical boiler conditions the partial pressure of SO_2 is much higher than SO_3. To supply the necessary SO_3, Aho et al. used ferric sulfate to carry out alkali sulfation in power plant boilers [32,35]. Thermal decomposition of ferric sulfate is estimated to produce 1.2 moles of SO_3 and 1.8 moles of SO_2 [36]. $Fe_2(SO_4)_{3(aq)}$ can easily be sprayed near the superheater region which guarantees high local SO_3 concentration to allow successful alkali sulfation. SO_3 reacts with the alkali chloride as follows:

$$2MCl_{(s)} + SO_{3(s)} + H_2O_{(g)} \rightarrow M_2SO_{4(s)} + 2HCl_{(g)} \qquad \text{R 4}$$

where M is Na or K [32]. The equilibrium constant for R 4 at 800°C is 2.997×10^4, a slight improvement from that of R 3 which 2.711×10^4.

Inflight sulfation using SO_2 and SO_3 is kinetically governed and follow a complex chemistry [36,37]. One manifestation of this condition is the growth in the peak size of the fine aerosol fractions collected during sulfur addition test [38].

Sulfation of alkali chlorides in the deposit or intra-particle sulfation is also possible. The mechanism and perils of this process is reviewed in [23] and is summarized below.

When all of the gaseous reactants required in R 3 are present the main product is alkali sulfate and $HCl_{(g)}$, see S1 in Fig. 2. HCl formation is possible especially if S1 happens near the flue gas and deposit interface [14] where O_2 partial pressure is high. A great deal of generated $HCl_{(g)}$ escapes the free gas stream [39], however

there will be a remainder that can diffuse to the metal/scale interface or be oxidized to form $Cl_{2(g)}$, see S3 in Fig. 2. A more problematic scenario occurs when intra-particle sulfation proceeds without H_2O and produce $Cl_{2(g)}$ directly, via S2 in Fig. 2 and governed by the reaction

$$2MCl_{(s)} + SO_{2(g)} + O_2 \longrightarrow M_2SO_{4(s)} + Cl_{2(g)} \qquad \text{R 5}$$

where M is Na or K. The generated chlorine can very easily push itself through the oxide layer by cracking, grain boundary grooving and fissuring [14]. Both S1 and S2 therefore increases the proximity of $HCl_{(g)}$ and/or $Cl_{2(g)}$ to the metal/scale interface ergo increasing the risk of Cl-induced corrosion. After sulfation, the corrosion mechanism is similar to that of the one described in section 1.1 [23].

Studies on the kinetics of intra-particle alkali sulfation reveal that the progress of this reaction follows Langmuir adsorption – reaction type and is dependent on flue gas temperature and the partial pressure of SO_2 [40,41] and O_2 [41]. The heterogeneous nature of intra-particle sulfation also suggests that transport limitations are also contributing to the actual rate of sulfation. Pyykönen and Jokiniemi examined the deposition of alkali chlorides in superheaters and concluded that the sulfation is localized in the periphery of the deposits and the extent of $NaCl_{(s,l)}$ sulfation is fairly low due to limited intra-particle flux of SO_2. However they emphasized that high levels of SO_2, even momentarily, can bring about high HCl levels in the deposits and thus increase the risk of Cl-induced corrosion [39,42].

Fig. 3 attempts to summarize the key interactions leading to ash melting and chlorine induced corrosion during waste firing/co-firing in typical BFB boilers. The interaction of (Na, K) – Cl and (Pb, Zn) – Cl promotes the deposition of risky forms of chlorine in the superheater and economizers. Meanwhile the interaction of the alkalis with Al and Si, depending on mode of occurrence, may help promote ash melting. Depending on the relative abundance of these elements, these non-favorable interactions can cause corrosion in the superheater and ash melting (mostly in the bed) to occur simultaneously or one at a time.

The presence of S can alter the chemistry inside the BFB boiler to favor the formation of alkali and trace-metal sulfates. This interaction reduces the risk of chlorine induced corrosion provided that the sulfation takes place in the proper phase. Sulfation of alkali chlorides allows the interaction H – Cl to happen. In a typical boiler, the concentration of $HCl_{(g)}$ in the flue gas around the superheater area rarely exceeds 1000 ppmv, thus the risk of severe gas phase corrosion attack is negligible [23]. Sulfation of Pb and Zn chlorides is also thermodynamically favorable, but due to severe kinetic restrictions the extent of reaction is low [43].

Meanwhile the presence of Ca in the BFB system may reduce the efficiency of alkali chloride sulfation and favor the production of $CaSO_{4(s)}$ [35]. Ca species can be sulfated as follows [44]

$$CaO_{(s)} + SO_{2(g)} + \frac{1}{2}O_{2(g)} \rightarrow CaSO_{4(s)} \qquad K_{eq,800^\circ C} = 9.031 \times 10^9$$ R 6

$$CaCO_{3(s)} + SO_{2(g)} + \frac{1}{2}O_{2(g)} \rightarrow CaSO_{4(s)} + CO_{2(g)} \; K_{eq,800^\circ C} = 2.019 \times 10^9$$ R 7

The equilibrium constant[1] at 800°C for R 6 and R 7 is higher than the sulfation of KCl described in R 3.

1.3 Objectives

Among the challenges mentioned above, chlorine induced corrosion is a principal restrictive constraint to the performance of waste-to-energy systems. This study aims to (1) understand corrosion risk associated from firing fuel mixtures with SRF e-% of up to 70% and (2) evaluate currently available corrosion mitigation measures to find a robust solution to counter said constraint. We define a robust solution as a procedure whose anti-corrosion performance is highly insensitive to the quality of the fuel being fired.

The study seeks to understand the impact of the quality and fuel blending to the quality of the fuel mixture being fired to the BFB. The work also investigates the relationship between the quality of superheater deposits and the conditions of the flue gas in the vicinity of the superheater.

[1] Estimated using FactSage® Reaction module at standard state conditions.

2 Experimental Section

2.1 Boiler and Test Scheme

The boiler in this study is a 140MW_{th} bubbling fluidized bed boiler located in Anjalankoski in South East Finland, see Fig. 4. The fuel mixture (except for sludge) enters the boiler through the left and right wall chutes. Sludge arrives to the boiler from the adjacent thermal drying plant via pneumatic transport lines. For additional boiler details the reader is referred to [45].

Fig. 5(a) shows the temperature profile of the BFB; all data are from the BFB's online instrumentation. Each location has a corresponding boxplot that shows the variation of temperature during the test in the said location. No outlier temperature was recorded.

Fig. 5(b) shows the boiler load and steam power during the duration of the study. The mean boiler load is 94 ± 3 MW and steam power is 80 ± 2 MW, giving a boiler efficiency of around 85%. The wet gas O_2 concentration is also shown in the figure with a mean of 8.82 ± 0.13% and corresponds to an air/fuel ratio of around 1.3.

Nine tests constitute this work, test points I to V are assessment phase tests while VI to IX are performance analysis tests. During the assessment stage we study the associated corrosion risk for firing the base case fuel of the BFB – Fuel 1 and the effect of three anti-corrosion measures: elemental S-addition (II), sulfate injection (III) and peat co-firing (IV). Elemental S addition is accomplished by adding S-pellet to the fuel mixture before being fired to the boiler. Sulfate injection uses aqueous solution of 43-47% diiron tris(sulfate) and sprayed just below the bullnose of the boiler, see Fig. 4. During V the amount of SRF is 60 e-%, an intermediate value between the base fuel and the target fuel. Promising anti-corrosion measures from the assessment stage are applied to the target fuel in the performance analysis test. The test scheme is summarized in Fig. 6.

The duration of the test vary from a minimum of 1.3 h (IV) to 8.5 h (V) because other parameters outside the scope of this study are also measured and required longer test time. There is a period prior to each test point allotted to allow the BFB to reach steady state condition. All the necessary data gathering presented in this work have been collected at a relatively constant time span and at steady state operation.

2.2 Fuel

Table 2 list the recipe of pure fuels used to prepare the fuel mixture. F1 to F3 are for the assessment phase and F4 is the target mixture for the performance analysis test. The ultimate analysis of the pure fuel used in the study is in Table 3. Test point V used sludge 1 and SRF 1 because it was performed a week earlier compared to the rest of the test.

The gross calorific value (mean = 21 ± 0.7 MW/kg, d) and the concentration of C, H, O in the pure fuels do not vary significantly. Thus a change in the fuel proportion does not significantly impact the calorific value of the fuel mixture being fired to the BFB.

Variation of minor and trace components is high. The range of the coefficient of variation (standard deviation/mean) for the concentration of minor element is 0.41 – 1.51 while for the trace element 0.75 – 2.34. For the minor elements, the concentration of Cl, Ca, Mg and Ti is highest in SRF relative to the other fuels. The concentration of S, Na, Al and Si is comparable for the sludge and SRF. Peat and bark have low concentrations of minor elements compared to the other two fuels. For the trace elements, the concentration of Zn, Sn, Sb, As, Pb, Cr, Co, Cu, Ni and V is highest in the SRF. In the fuel mixture, increasing the proportion of SRF increases the concentration of these elements.

2.3 Sampling Techniques

To examine the risk of corrosion to the SH we collected flue gas composition and condition, aerosol composition, and deposits near the vicinity of the secondary superheater, indicated by point 2 in Fig. 4. During the performance stage, additional aerosol samples were made at the back pass (point 3 in Fig. 4) to assess for possible risk of corrosion in the economizer and air preheater. Corrosion at these heat exchange surfaces is associated to lead and zinc chloride deposition.

Gas properties and composition were collected using GASMET Fourier transform infrared spectroscopy. Aerosol sampling was made using Dekati Low Pressure Impactor (DLPI), each sampling lasts for 40 min. The impactor deposits were digested with water for five days and subjected to ultrasonic mixing prior to extraction. A detailed discussion on the schematic and subsequent analysis of aerosol samples is found in [45].

Deposits were collected using an air-cooled probe (38 mm diameter, 1.9 m long with 1.4 m in contact with the flue gases) and equipped with a detachable metal ring. The temperature of metal ring facing the wind side is held at around 500°C. Deposits were sampled at three locations along the circumference: on the side facing the flow (wind), 30 – 40° (side) and 180° (lee). The deposits were placed on copper tape strip and sent

to SEM/EDS for analysis. Each sampling lasted for 2 h. Additional features of the sampling procedure is found in [5].

2.4 Relating flue gas conditions and risk of corrosion

The quality of the flue gas arriving in the superheater has a significant impact on the risk of corrosion. Modeling of the arrival of corrosive species to critical heat exchange areas such as the superheater is in various state of development. Zhou et al. divides the ash deposition models as: empirical indices models, mechanistic models, and computational fluid dynamics (CFD) models [46]. The objective of these models is to examine the importance of a given parameter e.g. temperature to a certain response. However, process data from large scale combustion systems are often plentiful and collinear. Collinearity makes the use of process data as predictors challenging for classical multiple linear regression (MLR); because MLR requires a full rank for the matrix of predictor variables [47].

To solve the issue of multi-collinearity, partial least squares (PLS) regression is used to relate flue gas conditions and the quality of the SH deposits. PLS regression is a method that generalizes MLR and is particularly useful in dealing with collinear predictors. The goals of PLS regression and MLR are similar, that is to predict the response, **Y** given a set of predictors, **X**. We summarize below the properties of key matrices required in PLS regression listed in [48]. A more detailed and exhaustive explanation on the method is found in this reference.

PLS regression searches for a set of "new" and fewer variables called x-scores (**T**) which are linear combinations of the original variables,

$$T = XW^* \qquad \text{R 8}$$

where $\mathbf{W}^*$ are the weights. The weights provide information about the importance of a predictor to a given score. X-scores are good predictors of **Y**, such that

$$Y = TC' + F \qquad \text{R 9}$$

where **C** is the matrix of weights of the linear model for **Y** and **F** is the residual of the model. Combining R 8 and R 9 yields an equation analogous to MLR.

$$Y = XW^*C' + F = XB + F \qquad \text{R 10}$$

where **B** is the "PLS regression coefficient". C is used to calculate the model of Y or the Y-scores (**U**), such that

$$Y = UC' + G \qquad \text{R 11}$$

where **G** is the residual.

In essence x-scores are model of **X** (R 8) and simultaneously predictors of **Y** (R 10). X-scores are chosen such that the first x-score (t_1) contains the highest covariance with the first y-score (u_1), the second x-score (t_2) has the highest covariance with the second y-score (u_2) and so on. The number of scores or factors required to model the response is evaluated using cross validation. The rule of thumb is to only choose additional factors if the Root Mean Square Error of Cross-Validation (RMSECV) improves by at least 2% and to choose as few factors as possible [49]. We implemented PLS regression using the PLS_Toolbox installed in Matlab 2014a [49].

3 Results

In this chapter we first present the results and implications of the data collected during the assessment stage. Thereafter the performance stage follows.

3.1 Concentration of key components in the resulting fuel mix

Fig. 7 shows the mean concentration of key fuel components of the fuel mixture fired during the tests. Sulfur content is lowest for F1; partial and full substitution of bark by peat/SRF increase the S content in F2 & F3. The target fuel, F4 also has high S concentration. Chlorine concentration is highest in the target fuel, a direct result of increasing the proportion of the SRF in the fuel mixture.

Na, K, Al and Si registered high concentration in F3 which is probably the result of increased concentration of these elements in the type of SRF used – SRF 1, see Table 2 and Table 3. Calcium concentration is highest in F4. As for the Br, Zn and Pb their concentration is highest for F4, this is a result of increasing the energy share of the SRF.

In general, moving from the base fuel to the target fuel recipe increases the concentration of chlorine and trace elements in the fuel mixture. There is also an increase in S which may help lessen the risk of corrosion. But this increase in S may be countered by corresponding increase of Ca concentration in the target fuel.

3.2 Aerosols arriving in the superheater

For all the impactor results, fine particles found in the region of $d_p < 1.6$ micron were once in vapor form and due to supersaturation in the gas phase have undergone homogeneous nucleation and coagulation. Particles

found in the region of d_p > 1.6 micron represent coarse particles that are mostly non-volatile fragments of the fuel and/or entrained particles [50,51].

3.2.1 Effect of peat substitution

Aerosol samples collected for firing F1 and F3 are shown in Fig. 8. Both exhibits a bimodal particle size distribution, though for firing F1, the peak of the fine particle is more pronounced compared to the coarse particle. For F3, the peak height is almost equal for both size fractions. The peak in the coarse particle may have come from fragments of the peat used. The presence of Si in the coarse fraction of Fig. 8(b) may support this claim.

The elements comprising the fine aerosol fraction are similar, namely K, Na, Cl and SO_4. However, the concentration of these K, Na and Cl is higher for firing F1. The mode of occurrence of the alkalis may be "less reactive" during firing of F3 and could have resulted in the decrease of K, Na and Cl.

3.2.2 Assessment of anti-corrosion measures to aerosol quality

To assess the performance of the anti-corrosion measures, we take the sum of the concentration of Na+K, Cl and SO_4 in the fine particle fraction of the DLPI samples and plot them in Fig. 9. We have chosen only these elements because of their central role in active corrosion and mitigation (see Fig. 3). Pb and Zn were not included because the measured concentration is low and have low condensation temperature.

The aerosol in I is rich Cl and the proportion of Na+K and Cl is almost near that of the alkali chloride – MCl. Upon addition of elemental sulfur the fraction of Cl is decreased to more than half (see the dashed arrow connecting points I and II in Fig. 9) and is accompanied by an increase in the proportion of SO_4. Although not shown here, the peak of the fine particle fraction shifted from 0.09 – 0.26 μm to 0.26 – 0.60 μm - an indication of alkali chloride sulfation [38].

When the sulfate solution is injected, III, the aerosol is virtually free of Cl. Na+K and SO_4 dominate the fine aerosol fraction (see the solid arrow connecting points I and III in Fig. 9). The peak of the fine particle is at 0.26 – 0.60 μm and there is enough SO_4 to ensure the formation of $(Na, K)_2SO_4$. The risk of fire side corrosion is much lower for III compared to I and II based on the aerosol composition data.

When peat is added in the fuel mixture to partially substitute bark (Fuel 2 and IV), the proportion of the elements of interest is not very far from those collected during I. When bark is not used in the fuel mixture (Fuel 3 and V) the proportion of Cl in the aerosol is reduced. However, this decrease is not solely attributable to the absence of bark but more likely to the difference in the quality of the SRF used. Test point V is using

an SRF with a Cl content of 3700 mg/kg, d., which is almost half of the Cl content of the SRF for the other tests (see Table 3). For both IV and V, the peak in the fine particle fraction has remained in the 0.09 – 0.26 μm range. These observations suggest that peat co-firing is not a robust method to combat Cl-induced corrosion. The concentration of Cl in the resulting aerosol is more tied to the quality of the SRF than to the corrosion mitigating power of peat.

3.3 Flue gas

Variation in the fuel mixture and application of corrosion mitigating measures do not significantly vary the parameters listed in Table 4 except of the SO_2, HCl and CO concentration.

Test point I registered the least concentration of SO_2 in the flue gas. Without the necessary SO_2 alkali chlorides persist and are detected in the aerosol samples, see Fig. 8(a). At this condition the risk of corrosion is high.

Upon the addition of S-pellets (II) a tenfold increase in SO_2 concentration is measured, with a corresponding increase in HCl concentration (~1.2×). These observations and in conjunction with the changes in the quality of the aerosols noted earlier suggest the progress of R 3 and/or R 4.

Sulfate injection (III) resulted to an increase in SO_2 concentration (~3.4×), with an accompanying increase in HCl concentration comparable to II, ~1.18×. Together with the aerosol results, these observations suggest that sulfate injection is able to wipe out alkali chloride via R 3 and/or R 4. However, the contribution of R 4 is more significant for III compared to II because sulfate was injected in the strategic position, ensuring high local concentration of SO_3 just below the bullnose, see point 2 in Fig. 4.

When peat partially substituted bark (IV) SO_2 concentration is similar to III, but the increase in HCl concentration is lower than II and III. The Cl concentration is least for F2 - the fuel fired in IV, but this is not seen as the primary reason for a small increase measured for HCl. Aerosol data in Fig. 9 suggest that the conversion of (Na,K)Cl to $(Na,K)_2SO_4$, which produces HCl, did not happen appreciably during IV compared to II and III.

Total substitution of bark with peat/SRF (V, fuel F3) likewise increased SO_2 concentration, by c.a. 6×, with an increase in HCl concentration (~1.19×). HCl could have been produced via R 3 or at the lower part of the BFB, i.e. splash zone. The latter is also likely because Na, K might have been bound with the Al, Si in F3 making them *less* reactive. Without reactive alkalis, Cl preferred to interact with H forming HCl.

We simulated the combustion during III, IV and V in FactSage 6.4 to estimate the fraction of Cl_{fuel} that formed HCl in the splash zone. In Fig. 10, test points IV and V both have Cl_{fuel} to HCl conversion higher

than 0.6; with V having higher conversion than IV. However for III, Cl_{fuel} to HCl conversion is below 0.6. This supports the earlier claim that the increase in HCl measured for III is a result of successful alkali sulfation via R 3 and more importantly R 4; while HCl measured during V is the result of H – Cl interaction in the lower part of the BFB.

3.4 Quality of the Deposits

Table 5 shows the concentration of select components of the deposits. Among the components listed Ca and S registered the highest concentration; this indicates abundance of $CaSO_4$ in the deposits. The concentration of Cl and Fe (may also be occasionally come from the ring itself) has high variation during the assessment stage, with coefficient of variation or c.v. of 0.99 and 1.52 respectively. For Na and K the variation is low, with c.v. of 0.35 for both elements.

The concentration of Cl is consistently lowest during sulfate injection (III), on average 0.1 wt.%. The test for sulfur addition (II) and peat co-firing (V) both registered an average Cl concentration of 0.4 wt.%. These three tests are all significantly lower than the base case test (I) with an average Cl concentration of 6.1 wt.%. The average is taken from the concentration of the element in the wind, side and lee positions.

In the fine particle fraction of the aerosols, the Cl content is virtually zero during III but we detect the presence of Cl in the deposits. This suggests that other size fractions and factors can contribute to chlorine deposition.

Test point III registered the highest concentration of Fe in the deposit, 5.4 wt.%, six times its concentration during I. This result is consistent with the decomposition of $Fe_2(SO_4)_{3(aq)}$ which produces Fe_2O_3 [36]. Due to the proximity of sulfate injection to the superheater, the oxide can later be deposited in the superheater region. The risk associated to ash melting is low even at this condition. Using the composition at the wind position, thermodynamic equilibrium calculation estimates the molten fraction of the deposit to be below 1% in the temperature range 500 – 800°C. Risk of ash melting is low because the deposit has plenty of $CaSO_4$ (T_{melt} = 1459 °C).

3.5 Assessment Phase Output

The aerosol composition, flue gas condition, and deposit analysis suggest that sulfate injection is able to significantly reduce the risk of Cl-induced corrosion. With sulfate injection, a strategic location can be chosen to ensure maximum effect of the additive. Sulfate injection yields the lowest Cl concentration in the deposit and in the fine particle fraction.

Peat co-firing and elemental S addition can also able to bring down the concentration of Cl in the aerosol and in deposits. However, since the performance of peat co-firing is dependent on the nature of the SRF being combusted, we see this strategy as less robust compared to S-pellet addition.

In the performance analysis stage, elemental S addition and sulfate injection are tested. Test points VI and VIII fire the target fuel alone, while VII and IX are for S addition and sulfate injection test respectively. VI serves as reference test for VII, while VIII is the reference for IX.

3.6 Combustion of the target fuel – Performance Stage

The composition of the aerosols before the superheater during firing of the target fuel (F4 and VI) is shown in Fig. 11(a). Even though Cl is highest in F4, the risk of corrosion when firing this fuel is not enhanced. In fact in Fig. 9, the fraction of Cl in the Na+K / SO_4 / Cl system decreases from the base fuel (I) to the target fuel (VI and VIII). In addition, the average concentration of Cl in the deposits is 5.1 wt.% for VI and VIII, lower than the 6.1 wt.% measured for I.

A possible explanation for these measurements is the increase in S_{fuel} from F1 to F4. The flue gas concentration of SO_2 in VI and VIII are 2.5× and 4.5× that of I respectively, which may provide the necessary sulfur to achieve alkali sulfation even without the additives. Due to increased Zn and Pb in F4, it is also probable that some Cl's formed zinc and/or lead chlorides [52] which partly lowers the amount of condensable Cl in the superheater region.

Elemental S addition to the target fuel (VII) improves the quality of the aerosols and deposits. In the aerosols, the fraction of Cl is lowered similar to II (see Fig. 9). The flue gas registered the highest SO_2 concentration (see Table 4) with an accompanying increase in HCl concentration. However the Cl content in the deposit is on average 1.4 wt.%, c.a. 26% of its reference test (VI).

Sulfate injection during combustion of the target fuel (IX) yields an aerosol with composition similar to III. The aerosol is virtually free of Cl and the deposit has an average Cl concentration of 0.1 wt.% which is c.a. 2.6% of its reference case (VIII). Similar to III, the deposit is also rich in Fe with mean concentration of 7 wt.%.

For all test in the performance analysis phase, Ca and S have the highest concentration in the deposits.

The aerosol at the back pass (point 3 in Fig. 4) collected during IX is composed mainly of Na, K and SO_4. Trace elements Pb and Zn are present at very low concentration; see Fig. 11(b).

These results suggest that elemental S and sulfate injection are both robust means of reducing the corrosion risk associated to combustion of high SRF share fuel mixture. Even though there are variations in the quality of the SRF used between I, II, III and VI-IX, both procedures were able to provide consistent trends in

aerosol and deposit composition as well as flue gas conditions. However in terms of ensuring that the superheater deposit is Cl free, the performance of sulfate injection is more superior than sulfur addition.

4 Discussions

The fuel composition and anti-corrosion measures tested are able to affect the composition of the aerosols and the deposits. However, the concentration of the Cl in the deposit is never totally reduced to zero even if the concentration of alkali chlorides in the aerosols is virtually negligible. In order to know what other factors should be considered to effectively understand Cl deposition we examined the relationship of flue gas and fine aerosol properties and the concentration of Cl in the deposit collected before the superheater (point 2 in Fig. 4).

Partial least squares regression is used to examine the contribution of the 14 variables found in the abscissa of Fig. 12. We used PLS regression model, because we have no systematic way of including or excluding variable/s to create a set of non-collinear estimators. The predictive power of this model is not expected to be high due to the limited number of test point and extrapolation of results is not advised.

$\%\Delta T_{fg}$ is the percent decrease in flue gas temperature traversing the superheaters; H_2O, O_2, SO_2 and HCl are concentration of components of the flue gas (see Table 4); and the rest are concentration of the components of the aerosol. Since the units of these variables vary we first performed mean centering. The mean centered data forms the matrix of predictors, **X** and the wind side Cl-concentration is the response, **Y**. MLR is not attempted because the rank of **X** is only 7 and several variables have shown significant collinearity.

Cross validation step suggests the use of three components or x-scores in the PLS regression model. Using a 3-component PLS regression model, the calculated R^2 is 0.94. The first component of the regression captures 82.29% of the variance and the weight of the original variables in this component is found in Fig. 12.

The decrease in the temperature of the flue gas traversing the superheaters, and the Cl and Br content in the aerosol have high positive effects to Cl-deposition. The effect of temperature and Cl is easily understood - an increase in Cl in the aerosol plus high flue gas temperature decrease due to heat transfer result in enhanced saturation of Cl species around the superheater which then enhances Cl-deposition. On the other hand, the effect of Br is still unclear and warrants further investigation. One hypothesis is the formation of BrCl [53,54]. Formation of bromine chloride is thermodynamically feasible at typical boiler conditions however, it is less stable compared to other chloride salts (see Fig. 13). Na and K also contribute positively to Cl-deposition via formation of alkali chlorides. Ca and Al are also positively affecting Cl-deposition via

formation of chlorides or capturing the sulfates by forming aluminum or calcium sulfate instead of alkali sulfates.

Meanwhile, O_2, SO_2 and HCl reduce Cl-deposition through alkali sulfation. O_2 and SO_2 are reactants to R 3 and R 4 which produces HCl. HCl is not expected to condense in the superheater thus reducing Cl-deposition. These three species are also reactants in the intra-particle sulfation of the alkali chlorides. Intra-particle sulfation localized in the periphery of the deposits results in the loss of Cl to the flue gas as HCl [39], albeit some Cl can still diffuse towards the metal. Integrating the intra-particle sulfation kinetics proposed by Sengeløv et al. [41] for the time interval of 2 h and with the properties of the flue gas (temp., O_2 and SO_2) in Table 4 for VII and IX, we estimate a conversion value of 0.042 and 0.019 for the alkali chloride during elemental S addition and sulfate injection respectively. This conversion values translate to more HCl production during VII since its deposit contains more alkali chlorides compared to the deposit in IX (see Table 5). Some of the HCl can be oxidized (Weldon process) to form Cl_2 (see Fig. 2). If the Cl species diffuse towards the metal/scale interface active corrosion may be enhanced during VII.

The concentrations of SO_4 and Pb in the aerosol also have negative weights in the 1st component of the PLS regression model. Having more SO_4 in the aerosol increases the likelihood that R 3 and/or R 4 took place and the amount of condensable Cl is reduced. The presence of Pb in the water-soluble aerosol samples may indicate the presence of $PbCl_2$ which reduce the amount of condensable Cl in the superheater region. Zn meanwhile has low effect on Cl deposition because the formation of ZnO is more favored than $ZnCl_2$ (see Fig. 13). These interpretation agrees with Enestam's estimates that in the superheater region Pb is predominantly $PbCl_{2(g)}$ while Zn can exist mostly as $ZnO_{(s)}$ and some as $ZnCl_{2(g)}$ [52].

5 Conclusion

In this two stage study, we have shown that chlorine-induced corrosion is present during firing of a fuel mixture containing 50, 60 and 70 e-% share SRF. The quality of the fuel mixture, in terms of its composition, is affected by the proportion of the pure fuels used. Increase in SRF share increases Cl and trace elements in the fuel.

In the assessment stage, sulfur addition and sulfate injection exhibited robust performance against the agents of active corrosion by partially or fully reducing the concentration of alkali chlorides. Peat co-firing can also reduce alkali chlorides but its action is dependent on the quality of the fuel mixture used.

During firing of the target fuel (70 e-% share of SRF), sulfur addition and sulfate injection are able to lower the concentration of alkali chlorides in the aerosol and deposits at the superheater. However, sulfate injection

ensures that the concentration of Cl in the aerosol and deposits is minimal. With these observations we conclude that sulfate injection is a robust strategy to combat Cl-induced corrosion of the superheater.

The quality of the flue gas and the aerosol has a strong impact on the quality of deposits. During firing of high e-% share SRF, Cl content of the aerosol has the highest positive impact on Cl deposition. Therefore, any corrosion mitigating measure must be able to reduce Cl concentration in the aerosols to as minimum as technically and economically possible.

6 Acknowledgement

We are thankful to the OSER project, Valmet Power, Foster Wheeler, the European Regional Development Fund, and RECOMBIO project TREN/FP7EN/239530/ for the resources shared for this study. We appreciate Stora Enso Oyj for sharing the data presented in this paper. Likewise we acknowledge Marko Räsänen and Juho Kauppinen for the collection of aerosol samples, Muhammad Nasrullah for carefully collecting and preparing the fuel samples for analysis.

References

[1] Towards a recycling society – The National Waste Plan for 2016. Helsinki: Ministry of the Environment; 2009.

[2] Official Statistics of Finland (OSF): Waste statistics [e-publication]. ISSN=2323-5314. 2012. Helsinki: Statistics Finland n.d.

[3] Dunnu G, Maier J, Scheffknecht G. Ash fusibility and compositional data of solid recovered fuels. Fuel 2010;89:1534–40.

[4] Kupka T, Mancini M, Irmer M, Weber R. Investigation of ash deposit formation during co-firing of coal with sewage sludge, saw-dust and refuse derived fuel. Fuel 2008;87:2824–37.

[5] Silvennoinen J, Hedman M. Co-firing of agricultural fuels in a full-scale fluidized bed boiler. Fuel Process Technol 2013;105:11–9.

[6] Vainikka P, Lindberg D, Moilanen A, Ollila H, Tiainen M, Silvennoinen J, et al. Trace elements found in the fuel and in-furnace fine particles collected from 80MW BFB combusting solid recovered fuel. Fuel Process Technol 2013;105:202–11.

[7] Nasrullah M, Vainikka P, Hannula J, Hurme M, Kärki J. Mass, energy and material balances of SRF production process. Part 1: SRF produced from commercial and industrial waste. Waste Manag 2014:http://www.ncbi.nlm.nih.gov/pubmed/24735992.

[8] Sørum L, Frandsen FJ, Hustad JE. On the fate of heavy metals in municipal solid waste combustion Part I: devolatilisation of heavy metals on the grate. Fuel 2003;82:2273–83.

[9] Toledo JM, Corella J, Corella LM. The partitioning of heavy metals in incineration of sludges and waste in a bubbling fluidized bed 2. Interpretation of results with a conceptual model. J Hazard Mater 2005;126:158–68.

[10] Miller BB, Kandiyoti R, Dugwell DR. Trace Element Emissions from Co-combustion of Secondary Fuels with Coal : A Comparison of Bench-Scale Experimental Data with Predictions of a Thermodynamic Equilibrium Model. Energy & Fuels 2002:956–63.

[11] Takaoka M, Shiono A, Nishimura K, Yamamoto T, Uruga T, Takeda N, et al. Dynamic change of copper in fly ash during de novo synthesis of dioxins. Environ Sci Technol 2005;39:5878–84.

[12] Fujimori T, Tanino Y, Takaoka M, Morisawa S. Chlorination mechanism of carbon during dioxin formation using Cl-K near-edge X-ray-absorption fine structure. Anal Sci 2010;26:1119–25.

[13] Directive 2008/98/EC of the European Parliament and the Council of 19 November 2008 on waste and repealing certain Directives. Off J Eur 2008:3–30.

[14] Grabke HJ, Reese E, Spiegel M. The Effects of Chloride, Hydrogen Chloride and Sulfur Dioxide in the Oxidataion of Steels Below Deposits. Corros Sci 1995;37:1023–43.

[15] Becidan M, Sørum L, Lindberg D. Impact of Municipal Solid Waste (MSW) Quality on the Behavior of Alkali Metals and Trace Elements during Combustion: A Thermodynamic Equilibrium Analysis. Energy & Fuels 2010;24:3446–55.

[16] Becidan M, Sørum L, Frandsen F, Pedersen AJ. Corrosion in waste-fired boilers: A thermodynamic study. Fuel 2009;88:595–604.

[17] Jappe Frandsen F. Utilizing biomass and waste for power production—a decade of contributing to the understanding, interpretation and analysis of deposits and corrosion products. Fuel 2005;84:1277–94.

[18] Otsuka N. A thermodynamic approach on vapor-condensation of corrosive salts from flue gas on boiler tubes in waste incinerators. Corros Sci 2008;50:1627–36.

[19] Tillman DA, Dao D, Miller B. Chlorine in Solid Fuels Fired in Pulverized Fuel Biolers - Sources, Forms, Reactions and Consequences: a Literature Review. Energy & Fuels 2008;23:3379–91.

[20] Becidan M, Sørum L, Lindberg D. Impact of Municipal Solid Waste (MSW) Quality on the Behavior of Alkali Metals and Trace Elements during Combustion: A Thermodynamic Equilibrium Analysis. Energy & Fuels 2010;24:3446–55.

[21] Vainio E, Yrjas P, Zevenhoven M, Brink A, Laurén T, Hupa M, et al. The fate of chlorine, sulfur, and potassium during co-combustion of bark, sludge, and solid recovered fuel in an industrial scale BFB boiler. Fuel Process Technol 2013;105:59–68.

[22] Vainikka P, Bankiewicz D, Frantsi A, Silvennoinen J, Hannula J, Yrjas P, et al. High temperature corrosion of boiler waterwalls induced by chlorides and bromides. Part 1: Occurrence of the corrosive ash forming elements in a fluidised bed boiler co-firing solid recovered fuel. Fuel 2011;90:2055–63.

[23] Nielsen HP, Frandsen FJ, Dam-Johansen K, Baxter LL. The implications of chlorine-associated corrosion on the operation of biomass-fired boilers. Prog Energy Combust Sci 2000;26:283–98.

[24] Skrifvars B-J, Backman R, Hupa M, Salmenoja K, Vakkilainen E. Corrosion of superheater steel materials under alkali salt deposits Part 1: The effect of salt deposit composition and temperature. Corros Sci 2008;50:1274–82.

[25] Enestam S, Boman C, Niemi J, Bostr D, Backman R, Kari M. Occurrence of Zinc and Lead in Aerosols and Deposits in the Fluidized-Bed Combustion of Recovered Waste Wood . Part 1 : Samples from Boilers 2011:1396–404.

[26] Enestam S, Mäkelä K, Backman R, Hupa M. Occurrence of Zinc and Lead in Aerosols and Deposits in the Fluidized-Bed Combustion of Recovered Waste Wood. Part 2: Thermodynamic Considerations. Energy & Fuels 2011;25:1970–7.

[27] Bankiewicz D, Vainikka P, Lindberg D, Frantsi A, Silvennoinen J, Yrjas P, et al. High temperature corrosion of boiler waterwalls induced by chlorides and bromides – Part 2: Lab-scale corrosion tests and thermodynamic equilibrium modeling of ash and gaseous species. Fuel 2012;94:240–50.

[28] Aho M. Reduction of chlorine deposition in FB boilers with aluminium-containing additives. Fuel 2001;80:1943–51.

[29] Wolf KJ, Mu M, Hilpert K, Singheiser L. Alkali Sorption in Second-Generation Pressurized Fluidized-Bed Combustion. Energy & Fuels 2004;18:1841–50.

[30] Backman R, Khalil R a., Todorovic D, Skreiberg Ø, Becidan M, Goile F, et al. The effect of peat ash addition to demolition wood on the formation of alkali, lead and zinc compounds at staged combustion conditions. Fuel Process Technol 2013;105:20–7.

[31] Becidan M, Houshfar E, Khalil RA, Skreiberg Ø, Løv T, Sørum L. Optimal Mixtures To Reduce the Formation of Corrosive Compounds during Straw Combustion : A Thermodynamic Analysis. Energy & Fuels 2011;25:3223–34.

[32] Aho M, Paakkinen K, Taipale R. Destruction of alkali chlorides using sulphur and ferric sulphate during grate combustion of corn stover and wood chip blends. Fuel 2013;103:562–9.

[33] Kassman H, Pettersson J, Steenari B-M, Åmand L-E. Two strategies to reduce gaseous KCl and chlorine in deposits during biomass combustion — injection of ammonium sulphate and co-combustion with peat. Fuel Process Technol 2013;105:170–80.

[34] Aho M, Ferrer E. Importance of coal ash composition in protecting the boiler against chlorine deposition during combustion of chlorine-rich biomass. Fuel 2005;84:201–12.

[35] Aho M, Vainikka P, Taipale R, Yrjas P. Effective new chemicals to prevent corrosion due to chlorine in power plant superheaters. Fuel 2008;87:647–54.

[36] Wu H, Jespersen JB, Frandsen FJ, Glarborg P, Aho M, Paakkinen K, et al. Modeling of Ferric Sulfate Decomposition and Sulfation of Potassium Chloride During Grate-Firing of Biomass. Am Inst Chem Eng 2013;59:4314–24.

[37] Li B, Sun Z, Li Z, Aldén M, Jakobsen JG, Hansen S, et al. Post-flame gas-phase sulfation of potassium chloride. Combust Flame 2013;160:959–69.

[38] Kassman H, Bäfver L, Åmand L-E. The importance of SO2 and SO3 for sulphation of gaseous KCl – An experimental investigation in a biomass fired CFB boiler. Combust Flame 2010;157:1649–57.

[39] Pyykönen J, Jokiniemi J. Modelling alkali chloride superheater deposition and its implications. Fuel Process Technol 2003;80:225–62.

[40] Boonsongsup L, Iisa K, Frederick WJ. Kinetics of the Sulfation of NaCl at Combustion Conditions. Ind Eng Chem Reseach 1997;5885:4212–6.

[41] Sengeløv LW, Hansen TB, Bartolome C, Wu H, Pedersen KH, Frandsen FJ, et al. Sulfation of Condensed Potassium Chloride by SO2. Energy & Fuels 2013;27:3283–9.

[42] Matsuda H, Ozawa S, Naruse K, Ito K, Kojima Y, Yanase T. Kinetics of HCl emission from inorganic chlorides in simulated municipal wastes incineration conditions. Chem Eng Sci 2005;60:545–52.

[43] Jones F, Tran H, Lindberg D, Zhao L, Hupa M. Thermal Stability of Zinc Compounds. Energy & Fuels 2013;27:5663–9.

[44] Saastamoinen JJ, Shimizu T. Attrition-Enhanced Sulfur Capture by Limestone Particles in Fluidized Beds. Ind Eng Chem Res 2007;46:1079–90.

[45] Vainikka P, Enestam S, Silvennoinen J, Taipale R, Yrjas P, Frantsi A, et al. Bromine as an ash forming element in a fluidised bed boiler combusting solid recovered fuel. Fuel 2011;90:1101–12.

[46] Zhou H, Jensen PA, Frandsen FJ. Dynamic mechanistic model of superheater deposit growth and shedding in a biomass fired grate boiler. Fuel 2007;86:1519–33.

[47] Miller JC, Miller JN. Statistics for Analytical Chemistry. 3rd ed. West Sussex: Ellis Horwood Limited; 1993.

[48] Wold S, Sjostrom M. PLS-regression : a basic tool of chemometrics 2001:109–30.

[49] Wise BM, Gallagher NB, Windig W. Chemometrics Tutorial for PLS _ Toolbox and Solo. n.d.

[50] Christensen K a., Stenholm M, Livbjerg H. The formation of submicron aerosol particles, HCl and SO2 in straw-fired boilers. J Aerosol Sci 1998;29:421–44.

[51] Brunner T. Aerosol and coarse fly ashes in fixed-bed biomass combustion. 1st ed. Graz: 2006.

[52] Enestam S. Corrosivity of hot flue gases in the fluidized bed combustion of recovered waste wood. Åbo Akademi University, 2011.

[53] Söderström G, Marklund S. Formation of PBCDD and PBCDF during flue gas cooling. Environ Sci Technol 2004;38:825–30.

[54] Söderström G, Marklund S. PBCDD and PBCDF from incineration of waste-containing brominated flame retardants. Environ Sci Technol 2002;36:1959–64.

Figures

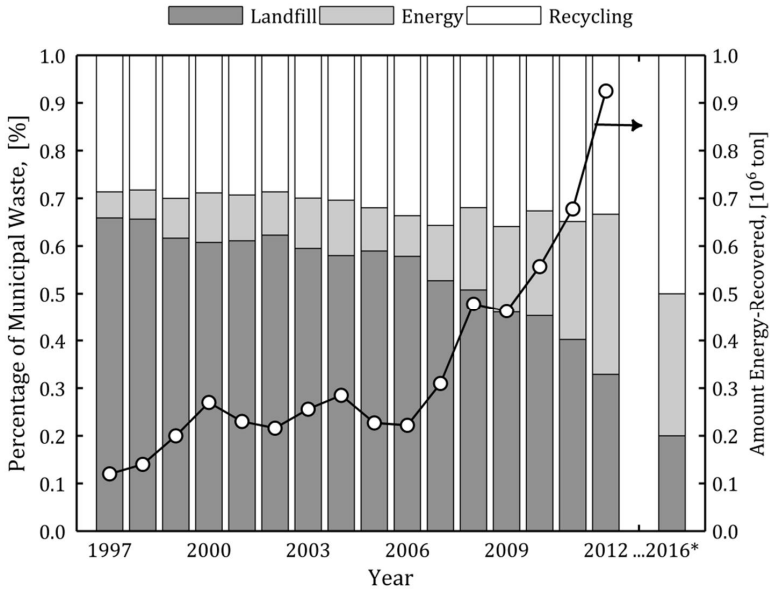

Fig. 1 Fifteen year history of treatment of municipal solid waste in Finland and the 2016 target [2].

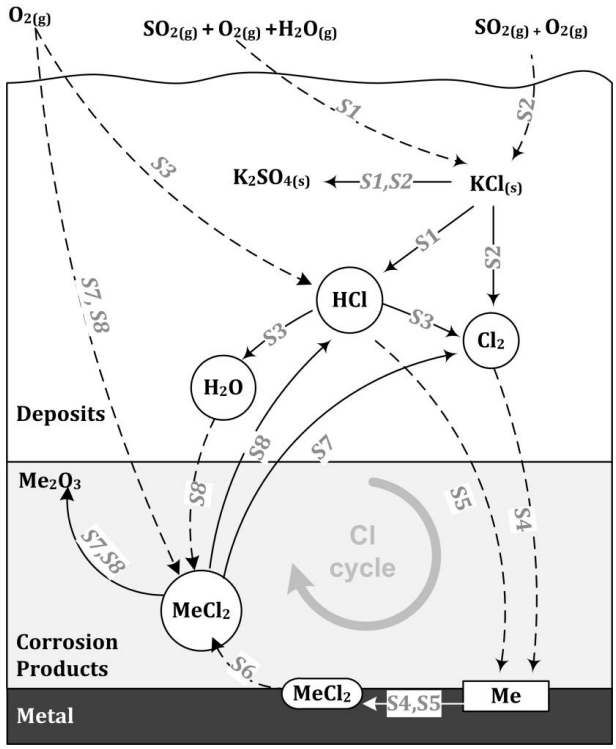

Fig. 2 Mechanism of intra-particle sulfation of KCl and the subsequent attack of the metal, adopted from the discussion in [23]. S1 and S2 are KCl sulfation described by R 3 and R 4. S3 is the oxidation of HCl. S4 and S5 is the inward diffusion of HCl and Cl to the metal/scale interface and subsequent metal chlorination. S6 is the vaporization of the metal chloride. S7 and S8 are the oxidation of the vaporized metal chloride producing oxide and H_2O, HCl and Cl_2.

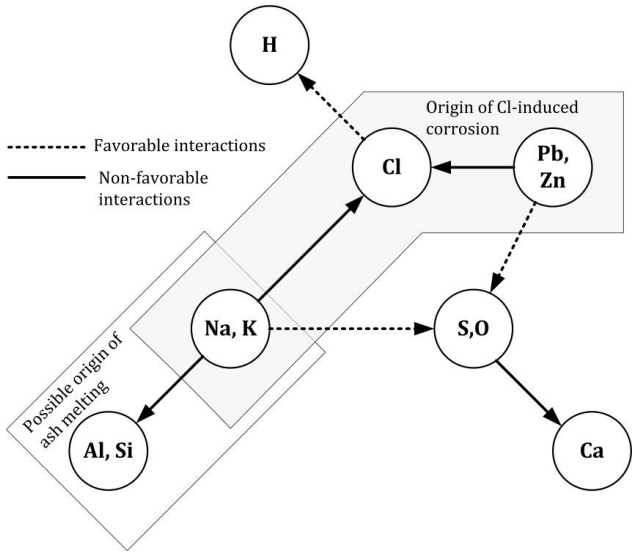

Fig. 3 Simplified interactions of key ash and aerosol forming and trace elements during waste firing in a BFB boiler. A nearly similar diagram appears in [18]. Favorable interactions reduce the availability of alkali chlorides in the superheater. Non-favorable interaction causes alkali chloride formation and/or ash melting.

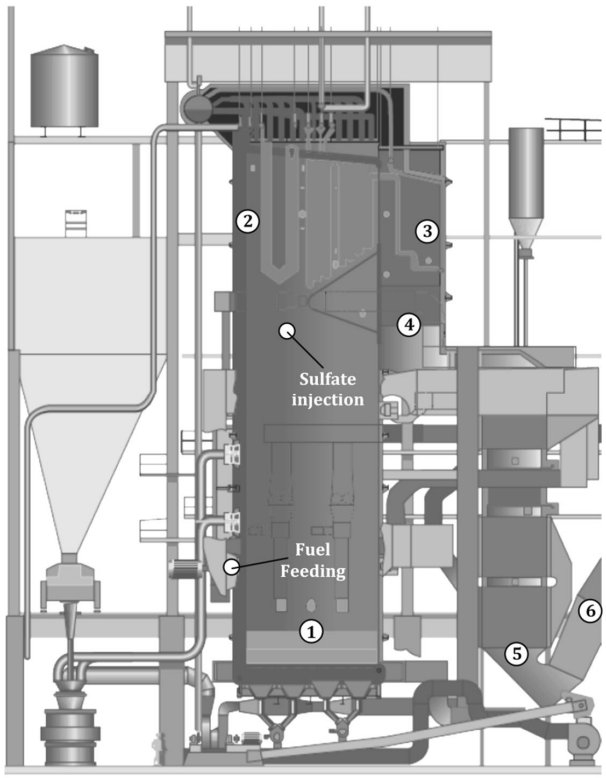

Fig. 4 Sketch of the bubbling fluidized bed boiler. Key locations: (1) Bed; (2) before the superheater; (3) after the superheater; (4) after the economizer; (5) after the LUVO; (6) before electrostatic precipitator.

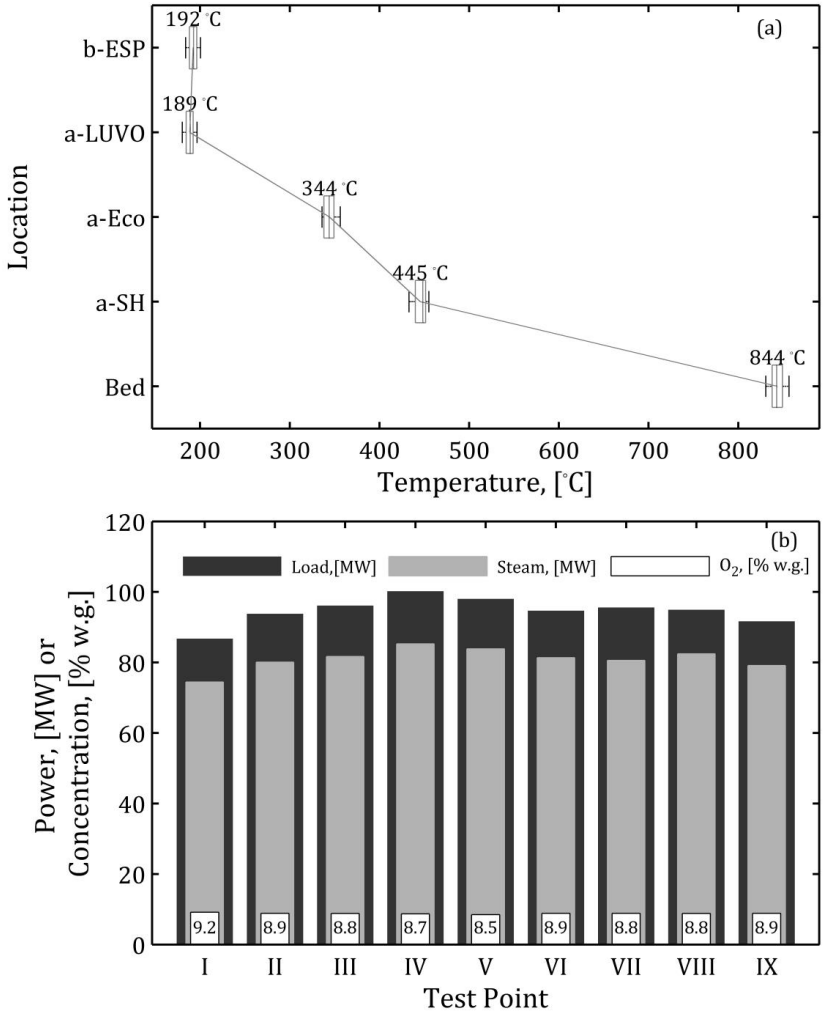

Fig. 5 (a) Boxplot of temperatures at key locations in the boiler: bed; after superheater, a-SH; after economizer, a-Eco; after LUVO, a-LUVO; before ESP, b-ESP. Mean temperature is annotated. (b) Fuel load, steam power and O_2 concentration in the wet flue gas.

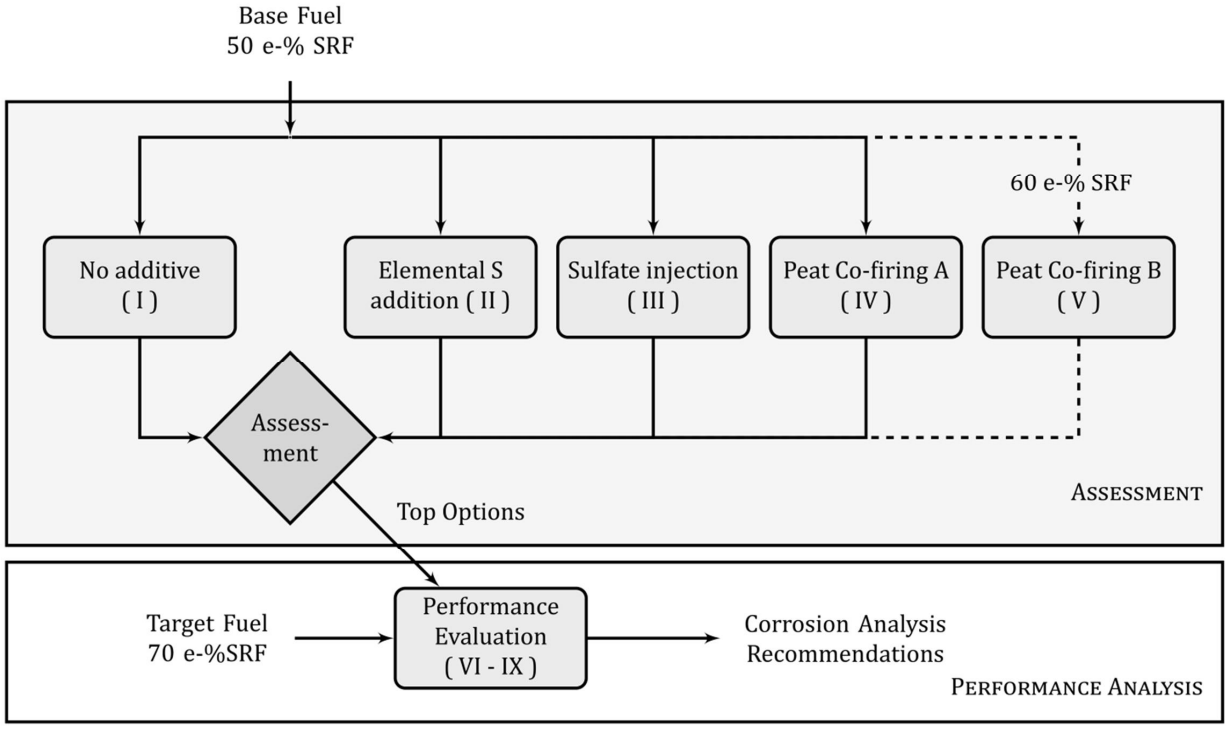

Fig. 6 Schema of tests.

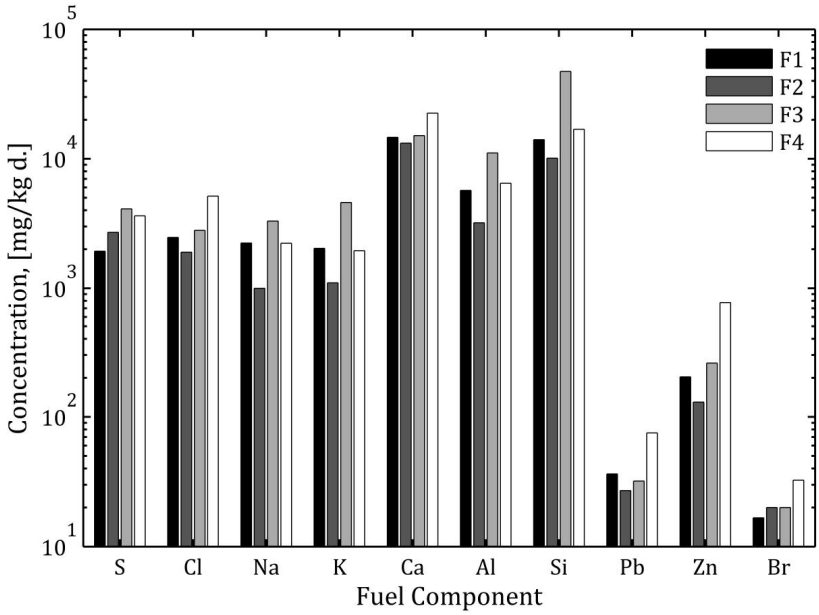

Fig. 7 Resulting concentration of key fuel components in the fuel mixture defined in Table 2.

(a)

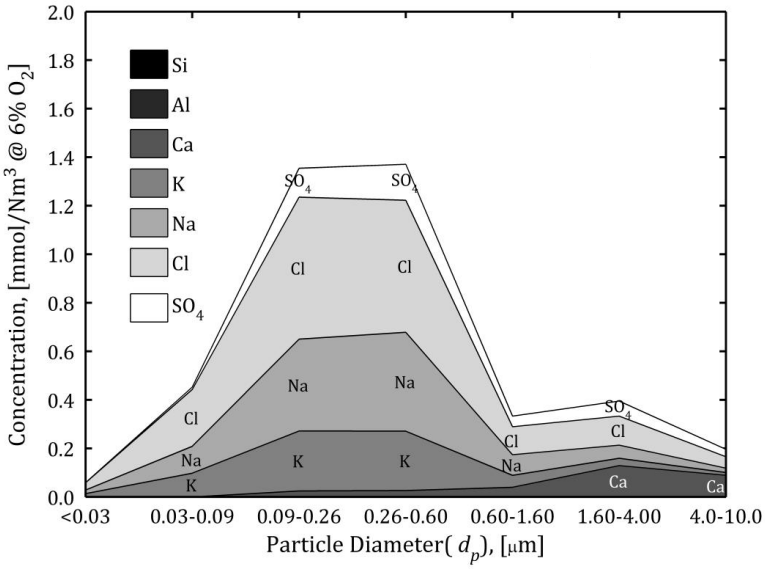

(b)

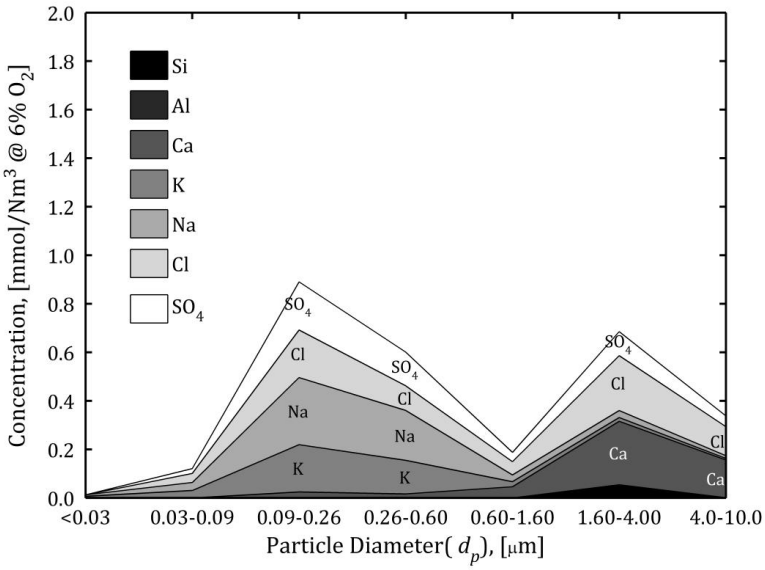

Fig. 8 Particle size distribution of aerosols collected before the SH during (a) Test point I and (b) Test point V.

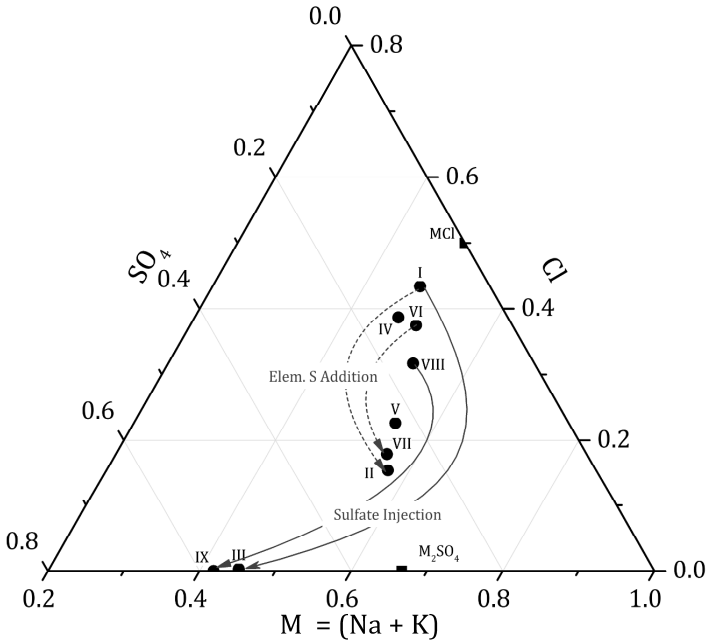

Fig. 9 Summary of composition of the fine particle fraction of the aerosols collected before the SH. Points are labelled according to test points.

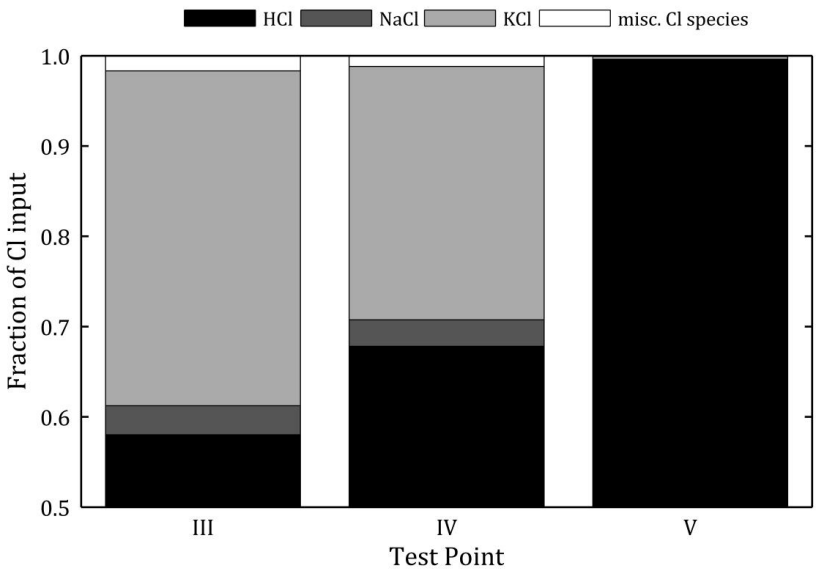

Fig. 10. Conversion of Cl to HCl, alkali chlorides and misc. Cl species estimated using FactSage 6.4 The temperature is 840°C and $\lambda = 0.6$, these are the average condition at the splash zone in the boiler.

(a)

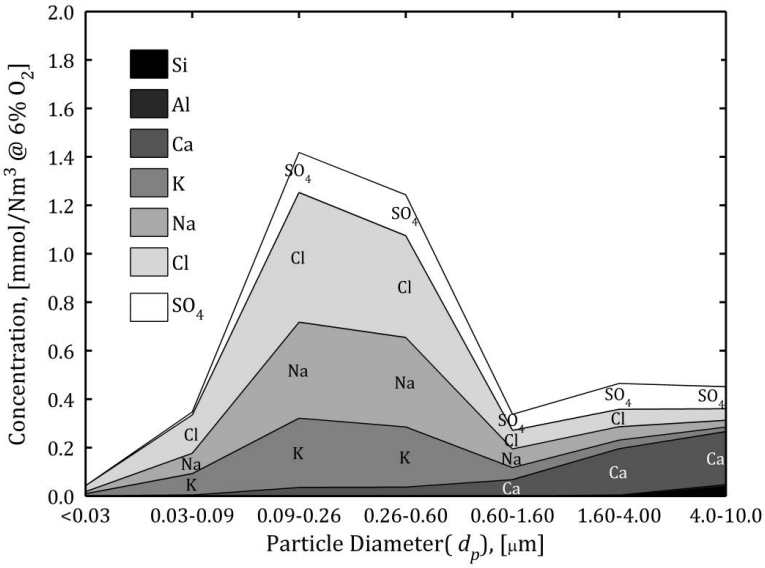

(b)

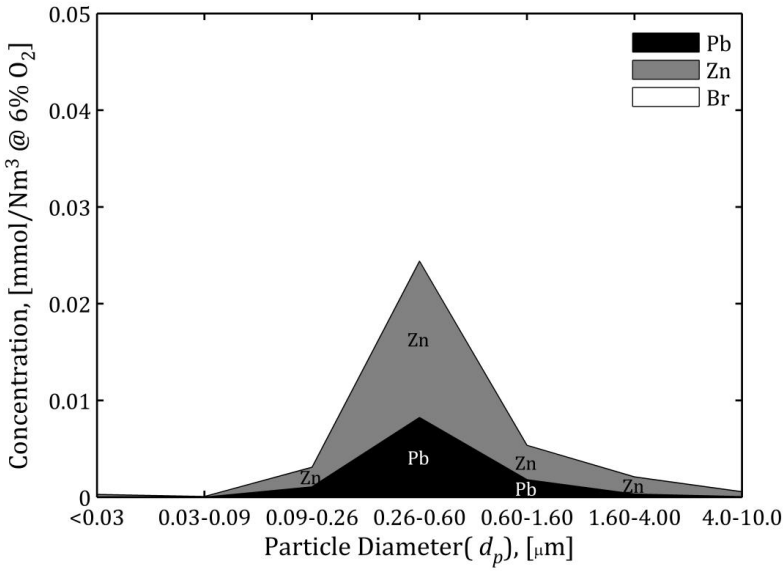

Fig. 11 Particle size distribution of (a) aerosols collected before the SH during firing of the target fuel (test point VI), and (b) trace elements after the SH during IX.

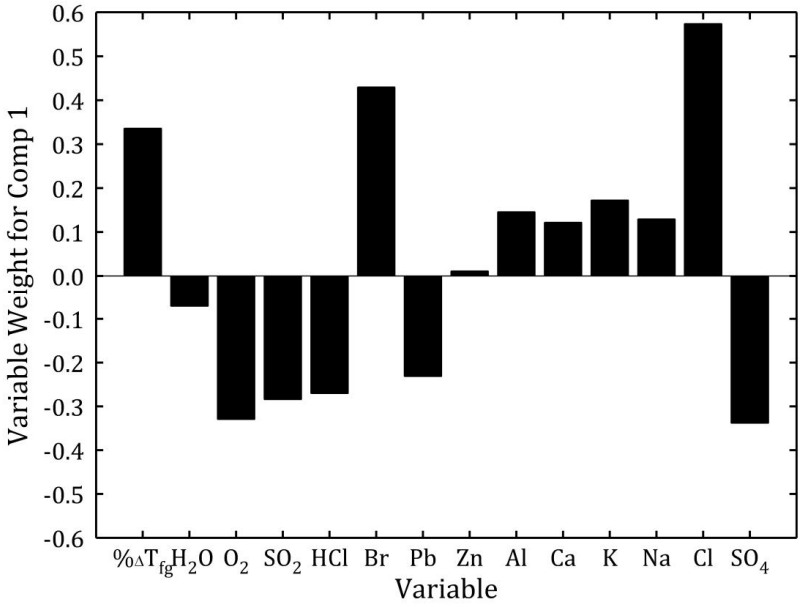

Fig. 12. Weights of variables tested to component 1 of the PLS regression model for the wind side superheater deposits.

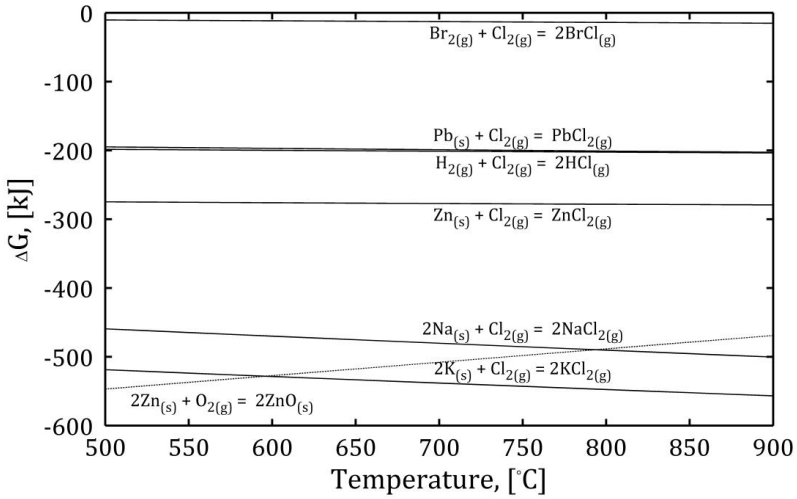

Fig. 13. Stability of chlorine containing compounds and ZnO. Calculated using FactSage 6.4® Reaction module at standard state conditions

Tables

Table 1 . Eutectic composition and temperature of binary salts and oxide systems estimated using FactSage 6.4.

System and Composition, [mol/mol]	Eutectic Temperature, [°C]
0.957 SiO_2 – 0.043 Al_2O_3	1594
0.613 SiO_2 – 0.387 CaO	1437
0.050 Al_2O_3 – 0.950 Na_2O	1132
0.741 SiO_2 – 0.259 Na_2O	793
0.260 K_2SO_4 – 0.74 KCl	690
0.506 KCl – 0.494 NaCl	657
0.376 K_2CO_3 – 0.624 KCl	631

Table 2. Fuel mixture showing the pure fuel components used and their corresponding energy share.

Fuel Components	**Energy Share, [%]**			
	F 1	**F 2**	**F 3**	**F 4**
SRF	50	50	60	70
Bark	44	10	-	24
Sludge	6	6	6	6
Peat	-	34	34	-
Test point	I, II, II, III	IV	V	VI - IX

Table 3 Properties of the *pure fuel*. Analyses were carried out according to appropriate CEN/Ts, ASTM and ISO methods.

Properties	Units	Fuel					
		Sludge 1[a,b]	Sludge 2[a,c]	SFR 1[b]	SFR 2[c]	Peat[d]	Bark[d]
Gross calorific value	MJ/kg, d	20.20	20.19	21.86	22.26	21.56	20.39
Net calorific value	MJ/kg, d	18.92	18.91	20.39	20.80	20.34	19.06
Ash content (815°C)	wt%, d	7.6	6.7	12.3	10.7	3.1	1.7
Ash content (550°C)	wt%, d	8.0	6.9	14.0	12.3	3.2	2.2
Volatile matter	wt%, d	73.5	74.8	75.0	75.8	69.6	77.9
Total moisture	wt%	68.5	67.9	45.5	45.0	49.8	63.5
Major Components	wt%, d						
C		49.3	49.3	50.6	50.6	54.3	51.8
H		5.9	5.9	6.8	6.8	5.6	6.1
N		1.81	1.81	0.61	0.74	1.16	<0.3
O (calculated)		34.5	35.6	27.5	29.1	35.6	39.6
Minor Components	mg/kg, d						
S		5000	4900	4700	4600	1800	200
Cl		200	160	3700	7000	250	90
Br		30	20	50	30	20	<10
Ca		14100	11100	24400	23600	3600	5600
Mg		840	620	2400	2900	830	630
Na		2300	1800	2300	2100	440	400
K		970	820	2100	1800	600	1600
P		1800	1600	440	160	340	430
Mn		1100	1200	110	84	62	260
Fe		830	630	4400	2300	2900	330
Al		5700	5400	7000	5400	2200	420
Si		11400	10400	17500	12300	5600	1500
Ti		91	78	1800	1800	94	32
Trace Elements	mg/kg, d						
Zn		82	63	180	230	9.6	65
Sn		0.56	0.63	11	26	<0.5	<0.5
Cd		0.25	0.21	0.3	0.76	0.09	0.24
Tl		<0.5	<0.5	<0.5	<0.5	<0.5	<0.5
Hg		0.26	0.49	0.08	0.1	<0.05	<0.05
Sb		<0.5	0.57	42	150	<0.5	<0.5
As		0.92	0.78	16	20	1.1	<0.5
Pb		3.2	2.8	42	68	2.9	0.59
Cr		7.3	5	51	53	3.2	3.2
Co		<0.5	<0.5	8.7	3.7	0.74	<0.5
Cu		13	9	80	3200	2.5	12
Ni		1.9	0.69	20	12	0.77	<0.5
V		1.8	1.4	13	11	2.7	<0.5

a. Wet sludge collected before the thermal drying plant.
b. Used for test point V.
c. Used for all test points except test point V.
d. Used for all test points.

Table 4 Properties of the flue gas in the superheater region. All data expect for temp after SH is from the FTIR. The coefficient of variation c.v. (standard deviation/mean) is also shown.

Property	Unit	Test Points										
		Assessment Stage						Performance Analysis Stage				
		I	II	III	IV	V	c.v.(I-V)	VI	VII	VIII	IX	c.v.(VI-IX)
Temperature before SH	°C	701	701	701	n.d.	634	*0.05*	739	739	751	751	*0.01*
Temperature after SH[a]	°C	441	449	455	433	438	*0.02*	440	448	453	451	*0.01*
H_2O	vol-%	17.0	17.3	17.5	14.7	16.0	*0.07*	17.4	16.7	17.5	19.9	*0.08*
O_2	vol-% dry	8.1	8.3	8.4	8.8	9.2	*0.05*	8.0	8.3	8.4	8.1	*0.02*
CO_2	vol-% 6%O_2 dry	6.0	5.9	5.8	5.9	5.7	*0.02*	6.1	6.1	6.1	6.2	*0.01*
CO	mg/Nm^3 6% O_2 dry	0.0	0.0	0.0	0.0	0.3	*2.24*	0.0	0.1	0.2	0.2	*0.85*
SO_2	mg/Nm^3 6% O_2 dry	54.8	598.9	185.1	185.0	333.6	*0.77*	138.2	758.0	247.0	480.6	*0.68*
HCl	mg/Nm^3 6% O_2 dry	175.7	225.8	208.2	185.5	210.1	*0.10*	198.5	278.6	226.8	313.0	*0.20*

n.d. : no data available

a.: From the BFB's online instrumentation

Table 5 Selected components of the deposits. No data is available for test point IV.

Component	Test Points							
	Assessment Stage				Performance Analysis Stage			
	I	II	III	V	VI	VII	VIII	IX
Wind, wt%								
Ca	22.0	18.7	17.1	11.8	26.2	20.2	22.7	13.4
S	11.9	11.3	14.6	8.9	12.4	13.7	12.7	15.5
Fe	1.0	0.5	5.3	3.1	0.9	0.7	1.2	8.5
Cl	4.5	0.7	0.2	0.2	3.1	1.9	2.1	0.2
Na	4.2	3.9	3.5	3.3	2.0	3.5	2.7	3.0
K	4.3	3.8	4.5	5.7	1.9	2.2	1.9	4.5
Side, wt%								
Ca	15.0	7.4	11.6	9.5	20.6	10.5	0.5	9.4
S	11.3	13.0	16.4	5.9	11.2	6.8	4.3	17.4
Fe	0.9	0.4	7.3	1.6	1.1	0.3	8.6	9.8
Cl	6.8	0.3	0.1	0.5	4.5	0.7	6.6	0.1
Na	2.4	8.3	5.2	3.9	2.5	4.8	0.2	3.9
K	3.6	10.6	7.0	9.6	3.7	8.8	1.6	6.8
Lee, wt%								
Ca	19.6	12.8	14.7	12.2	15.0	15.0	13.1	10.1
S	13.6	13.6	16.0	4.9	11.1	12.4	10.5	14.7
Fe	0.6	0.6	3.6	1.6	1.8	1.0	1.4	2.8
Cl	7.0	0.3	0.1	0.5	7.8	1.5	6.5	0.1
Na	4.5	6.9	6.0	4.1	6.2	5.6	6.5	4.9
K	6.4	9.1	5.2	6.6	7.0	7.0	7.8	4.7

Paper V

Physical properties of aerosols measured from a bubbling fluidized bed boiler

In: Fuel 139, pp. 144- 153

Fuel 139 (2015) 144–153

Contents lists available at ScienceDirect

Fuel

journal homepage: www.elsevier.com/locate/fuel

Physical properties of aerosol particles measured from a bubbling fluidized bed boiler

Heino Kuuluvainen [a,*], Panu Karjalainen [a], Cyril J.E. Bajamundi [b,c], Joni Maunula [d], Pasi Vainikka [c], Juha Roppo [d], Jorma Keskinen [a], Topi Rönkkö [a]

[a] Department of Physics, Tampere University of Technology, Tampere, Finland
[b] Department of Chemistry, University of Jyväskylä, Jyväskylä, Finland
[c] VTT Technical Research Center of Finland, Jyväskylä, Finland
[d] Valmet Power Oy, Tampere, Finland

HIGHLIGHTS

- The combustion process was studied by sampling the aerosol particles from the boiler.
- In the boiler, the particle size distribution was unimodal in the measurement range.
- Gas phase species formed a second smaller particle mode in the dilution.
- The larger mode particles were more dense.
- Ferric sulfate additive decreased the number and mass of the smaller mode particles.

ARTICLE INFO

Article history:
Received 7 April 2014
Received in revised form 15 August 2014
Accepted 19 August 2014
Available online 30 August 2014

Keywords:
Fluidized bed boiler
Aerosol
Nanoparticle
Real time measurement

ABSTRACT

Increased use of biomass and waste fuels, and the consequent corrosion problem have led to an increased need to study and monitor the combustion processes. This study presents an extensive physical characterization of aerosol particles measured from a bubbling fluidized bed boiler with different fuel mixtures and optional ferric sulfate feeding. The fuel mixtures included bark, sludge, peat and solid recovered fuel. Previously, the characterization of the particles analyzed from a fluidized bed reactor has mainly focused on chemical off-line analysis of collected impactor samples, large coarse mode particles or laboratory-scale reactors. In this study, the focus is in the particle size range from 3 to 500 nm, where mobility size distributions, effective density, morphology and electric net charge of particles were measured and analyzed. In the boiler, the particle size distribution in the measurement range was unimodal. Gas phase species formed a second smaller particle mode in the dilution. The number concentration of the smaller mode, peaking around 20 nm, was mostly dominating but variations were seen with respect to measurement location, fuel mixture and additive feeding. The effective density of these particles was approximately 1.4 g/cm^3. The larger mode, peaking around 80 nm, was found to be more stable and the effective density of these particles decreased as a function of particle size, being 3–4 g/cm^3 at the maximum. The results of this work suggest that the cores of these particles already exist in the boiler and partly consist of heavier lead and zinc compounds. The ferric sulfate feeding decreased the number and mass concentration of the smaller mode particles, which are formed in the sampling and dilution processes mainly from the gas phase alkali chlorides. These condensable species were also linked to the negative net charge of particles. This study deepens the understanding of the combustion process and the sampling of aerosol particles with an aspect of on-line monitoring.

1. Introduction

The utilization of biomass and waste in energy production has significantly increased in recent years. The main reasons for this development are global warming concerns and the need to reduce fossil fuel burning. In addition, new manners are being sought to treat different waste products cost-effectively and to avoid dumping them at landfill sites. Unfortunately, burning of biomass and waste incineration lead to various ash related problems in power plants [5,28,4,9,13]. So far, the most well-known problem is the

* Corresponding author.

http://dx.doi.org/10.1016/j.fuel.2014.08.048
0016-2361/

high temperature corrosion of the superheaters in a boiler, induced by alkali chloride deposition [30]. Also other elements found in fuels, such as bromine, have been indicated to have similar effects [34]. Altogether, the increased utilization of biomass fuels and different waste fuels has led to an increased need to study the combustion process and to develop fuel additives against corrosion.

The corrosion problem is based on the fact that most biomass fuels and waste fuels have a relatively high content of alkali metals and chlorine, but they contain clearly less sulfur than fossil fuels. In a boiler, alkali chlorides are found to be in the gas phase. They tend to condense on the boiler heat transfer surfaces and form complex alkali salts with iron and other elements in the heat transfer components. These salts are highly corrosive. However, it has been showed that, by spraying sulfate containing compound into the flue gas after the combustion is completed, the corrosion can effectively be reduced [11]. Consequently, before the flue gas reaches the superheater, alkali chlorides are effectively converted to alkali sulfates. These compounds are more stable and much less corrosive than alkali chlorides. Several reagents have been protected for the application with patents [3]. These compounds are $(NH_4)_2SO_4, NH_4HSO_4, H_2SO_4$ and $FeSO_4$. Also co-combustion with peat has been shown to reduce corrosion [18].

To study the effects of fuel additives and fuel components on corrosion, the instrumentation of the in situ measurements of gaseous alkali chlorides has been developed. Several methods capable of on-line analysis of metal species in industrial processes are extensively reviewed by Monkhouse [29]. A few applications have recently been developed to define the amount of KCl and NaCl in the hot flue gas channel, i.e. the in situ alkali chloride monitor, IACM, based on the differential optical absorption spectroscopy [8] and the CPFAAS (collinear photofragmentation and atomic absorption spectroscopy) method presented by Sorvajärvi et al. [33]. The advantages of these methods are that no gas preparation system is needed and measurements are performed in situ. However, the calibration of the instruments is not trivial and it should be performed in similar temperature conditions as the measurement. These sort of optical instruments are also fairly expensive.

In addition to the reagents mentioned earliettr, Aho et al. [2] showed that also aluminium sulfate and ferric sulfate, i.e. $Al_2(SO_4)_3$ and $Fe_2(SO_4)_3$ respectively, have similar tendency to prevent corrosion. In studying these alternatetive reagents, aerosol particle and fly ash measurements have had an important role. A specific sampling system enables the measurement of aerosol particles from the flue gas. After an air-cooled sampling probe and a two-step dilution, particles can be collected with a low pressure cascade impactor or led through an additional dilution to other aerosol measuring devices. Most of the studies based on this sampling system rely on the chemical off-line analysis of the collected impactor samples [2,34,35]. An electrical low pressure impactor, ELPI [19], has been used in these measurements to provide an aspect of on-line monitoring, but the instrument data has not been analyzed further.

In general, the physical properties of aerosol particles measured from flue gas and the formation processes of these aerosols have been widely studied since 1990s. In straw-fired boilers, the variety of experimental methods have been extensive, including low pressure impactors (LPI), scanning mobility particle sizers (SMPS) and electron microscopy [6,7,40]. The focus has been in sub-micron particles and understanding the formation of the particles [12]. In fluidized bed reactors burning waste and biomass, the research has focused on low pressure impactor measurements and electron microscopy of particles larger than one micron [23,36,13]. More recently, Lind et al. [24] and Sippula et al. [32] have been investigated the composition and the formation mechanisms of the aerosol particles measured from a laboratory scale fluidized bed reactor.

The main purpose of this study is to broaden the analysis of aerosol particles measured with the previously presented sampling system [2]. So far, the chemical composition of the flue gas particles measured from a full scale fluidized bed reactor has been studied in many different cases, but the physical properties, especially in the size range below 500 nm, have not been characterized at all. In this study, aerosol size distributions, the physical structure and the electric net charge of the particles are considered. The analysis is based on the measurements at a bubbling fluidized bed (BFB) boiler. An important aspect is how the ferric sulfate feeding affects the properties of aerosol particles. The final goal in that sense is the on-line monitoring of additive feeding processes. In addition to this possibility, this study aims at more profound understanding of the combustion process and the sampling of aerosol particles. To support the physical characterization and to connect the results to previous studies, also chemical off-line analysis of collected impactor samples is presented.

2. Experimental

2.1. BFB boiler and measurement locations

The experiments were carried out at the co-incineration plant of Anjala Paper Mill located in southern Finland during a two-week campaign. Detailed information on the plant and its history is given by Vainikka et al. [34]. Briefly, the plant started as a pulverized coal boiler but was converted to BFB boiler in 1995. The change enabled the utilization of solid recovered fuel (SRF) as a fuel component, and after 2006, the SRF share from all fuels was increased to 60%. The flue gas cleaning system includes an electrostatic precipitator (ESP) and a wet scrubber, from which the latter was installed in 1995. The ESP is designed to remove particulate emissions and the wet scrubber gaseous components. With this system, the plant could meet the EU Waste Incineration Directive (WID) emission limits [34].

The schematic of the BFB boiler is presented in Fig. 1. The furnace size is approximately $8 \times 8 \times 30$ m. Fuel is introduced to the furnace at the height of 3.5 m from the grate. The secondary air feeding takes place at 5.5 m and tertiary air feeding at 15 m from the grate. After the tertiary air addition, the air to fuel ratio is approximately 1.37. The flue gas temperature is at its highest 950 °C downstream from the secondary air feeding. In between the superheater tube blanks it is 740 °C and in the second pass under 400 °C. The economizers and air pre-heaters are located in the second pass.

In this study, the flue gas sample was taken either from the superheater area or from the second pass of the boiler. The temperatures at these locations in the boiler are 740 °C and 400 °C, respectively. The measurement locations were chosen in order to study the flue gas composition in the superheater and reveal the possible changes of the composition while moving downstream to the second pass. These objectives are directly connected to the corrosion problem caused by the wall deposition of different compounds.

2.2. Fuels, fuel mixtures and fuel additives

The boiler is designed to handle firing fuel mixtures of SRF, Scandinavian spruce bark, and dried paper mill sludge. The SRF originates from southern Finland and has undergone homogenization to 50–100 mm particle size and magnetic separation. In addition, PVC based packaging plastics have been excluded during the collection and preparation. SRF is delivered to the facility in wrapped bales or fluffs. The bark comes from the debarking processes of the adjacent paper mill while the sludge comes from the waste water treatment facility of the same mill [34]. The fuel mixtures

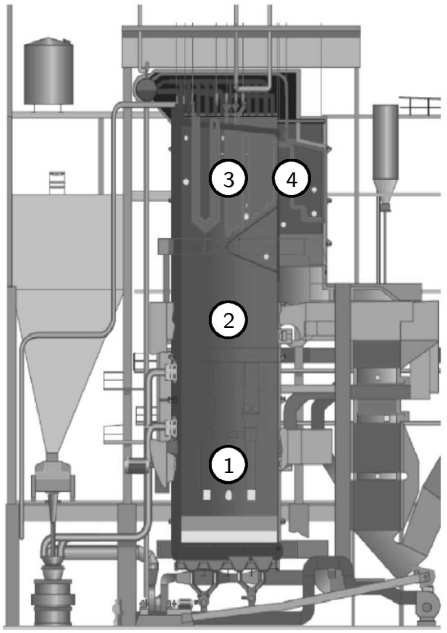

Fig. 1. Schematic of the BFB boiler at the co-incineration plant of Anjala Paper Mill: (1) secondary air feed, (2) tertiary air feed, (3) superheater and (4) 2nd pass. The schematic is reprinted with the permission of Valmet Corporation.

except sludge are introduced through fuel openings in the left and right walls of the boiler. Meanwhile the sludge is transported via pneumatic transport line from the thermal drying plant. In addition to the normal operation of the plant, also peat was used in the experiments of this work. It was typical Finnish peat with a sulfur content of 0.2%. The peat was introduced to the boiler together with the bark.

In this study, the fuel is a mixture of SRF, bark, sludge and peat. The proportions of individual fuels are shown in Table 1. The amount of SRF varied from 50% to 70% and the amount of bark from 0% to 44%. The peat was used in two fuel mixtures having a peat share of 34%. Furthermore, all the mixtures included 6% of sludge. The properties of the fuel mixtures are seen in Table 2. Analyses were carried out according to standardized CEN/TS, ASTM and ISO methods for biomass and SRF.

As fuel additive, aqueous solution of ferric sulfate was used. The solution of 43–47% diiron tris (sulfate) was sprayed just below the bullnose in the front, right and left walls of the boiler. In addition, also the effect of solid sulfur pellets mixed to the fuel was tested, but practically no difference compared to reference was seen. Thus, this study focuses on the ferric sulfate feeding. The effect of sulfate additive feeding on the properties of fuel mixtures and ash forming compounds is seen in Table 2 as an example for Fuel 2.

The measurement campaign included 18 steady point experiments. A single steady point experiment means a certain combination of fuel mixture and additive feeding including the reference with no additive feeding. During a steady point experiment these factors were kept constant and the burning process in the boiler was relatively stable. The elapsed time of the steady point experiments varied from one and a half hours up to nine hours depending on the measurements. The parameters of the combustion are seen in Table 2 for steady point experiments with different fuel mixtures. Unfortunately, the SO_2 concentration for the steady point with additive feeding is not available. At this point, it should be pointed out that the SO_2 concentrations are measured in the boiler and, after the wet scrubber, they are close to zero.

Table 1
The compositions of the fuel mixtures used in the experiments.

	SRF (%)	Bark (%)	Sludge (%)	Peat (%)
Fuel 1	50	44	6	–
Fuel 2	70	24	6	–
Fuel 3	50	10	6	34
Fuel 4	60	–	6	34

2.3. Sampling system and measurement setup

Fig. 2 shows a schematic diagram of the sampling system and the measurement setup. The sampling system, which has been used in several previous studies [2,34,35], is marked with a dashed line. A detailed description of the system is provided by Vainikka et al. [35]. In short, the system consists of an air-cooled sampling probe, two ejector diluters and two cyclones with a 10 μm cut-size. With respect to the results and discussion of this study, it is important to describe the dilution process in the sample flow. At first, the sample is sucked in the probe and immediately diluted within a 200 mm long gas permeable tube diluter with an inner diameter of 8.8 mm. At this stage, the sample is cooled by 250 °C in less than 0.2 s mainly due to the cooling effect of the diluting nitrogen gas. The target dilution ratio in this first stage of dilution is 8. The second stage of dilution is after the probe an ejector diluter with a dilution ratio 3. After this, the sample flow is divided into two parts. One part of the sample flows to a Dekati low pressure impactor (DLPI), which is a part of the previously used setup and it is used to collect impactor samples for the chemical analysis and weighing. The other part continues through another ejector diluter, i.e. the third stage of dilution with a dilution ratio 11, to all the aerosol instruments.

In Fig. 2, the part outside the dashed line describes the measurement setup used to characterize the physical properties of particles. It consists of two parallel scanning mobility particle sizers (SMPS), a TEM collector and an ELPI, with which the sample can be led straight to the inlet or through a differential particle sizer (DMA). The latter case enables a measurement of monodisperse aerosol and different particle sizes with the ELPI.

In general, the primary dilution conducted by the permeable tube diluter is to be expected to affect particle population due to the nucleation and condensation of initially gaseous compounds. Instead, based on the study of Giechaskiel et al. [10], the ejector diluters can be assumed to affect only the particle concentration, not other parameters or characteristics of particle population. For instance, ejector type diluters have been used in several studies focused on electric charge of combustion originated particles [25,21,22].

2.4. Aerosol measurements and data processing

Two parallel SMPS's with different size ranges measured the particle mobility size distributions. The Nano-SMPS consisted of a Nano-DMA (TSI Model 3085) and a CPC (TSI Model 3025) having a size range of 3–65 nm, and the Long-SMPS of a Long-DMA (TSI Model 3071) and a CPC (TSI Model 3775) having a size range of 10–422 nm. In general, the SMPS [38] enables the measurement of an aerosol size distribution with a high size resolution. If the SMPS is compared to the ELPI, it measures smaller particles and is also more accurate with particle sizes below 20 nm. With respect to time resolution, the SMPS is slower. In these measurements, the time resolution of both the SMPS's, i.e. the time between two consecutive size distributions, was 150 s. Compared to the duration of

Table 2
The properties of the fuel mixtures and the parameters of the combustion process for chosen steady point experiments defined by the fuel mixture and possible sulfate additive feeding.

	Fuel 1	Fuel 2	Fuel 3	Fuel 4	Fuel 2 + sulfate
Moisture (wt%)	47.3	46.4	42.2	44.0	43.2
Ash (wt%)	6.8	7.8	6.8	18.4	10.2
In dry solids (wt%)					
C	52.3	50.9	56.0	18.4	10.2
H	6.9	6.5	7.3	5.6	6.1
N	0.70	0.75	0.80	0.81	0.84
O	32.8	33.0	33.9	28.3	33.7
S	0.14	0.39	0.28	0.41	0.37
Cl	0.31	0.66	0.18	0.27	0.30
Ash forming compounds (mg/kg)					
Na	1826	1866	1075	3191	2207
K	1475	1530	1112	4379	2089
Ca	18312	19754	13360	14962	20552
Combustion parameters					
O_2 (%)	7.2	7.0	7.5	7.7	6.5
H_2O (%)	18.2	17.5	14.7	16	19.9
CO_2 (%)	8.4	8.5	8.3	8.0	8.7
CO (%)	0.6	0.2	0	0.3	0.3
SO_2 (ppm)	16.9	118	88.4	159.4	–
NO_x (ppm)	138.7	152.1	180.9	169.5	156.4

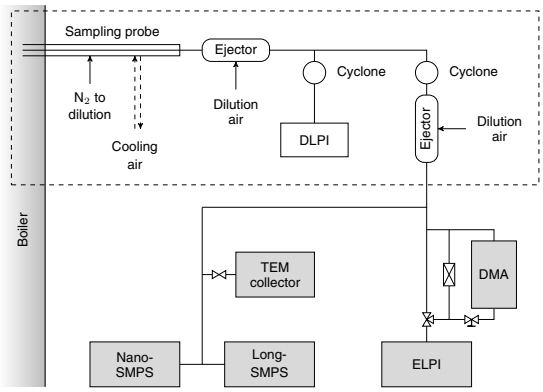

Fig. 2. A schematic diagram of the sampling system and the measurement setup. The sampling system and the previously used setup is marked with a dashed line.

the steady point experimets, this time resolution is very good. The first step in the data analysis performed for all the data was to combine two size distributions with different size ranges to a single size distribution. This was carried out by calculating a linearly weighted average for the size range 10–65 nm, so that the weight of the Nano-SMPS was 100% at the lower end and the weight of the Long-SMPS was 100% at the higher end. In addition, all the size distributions presented here are multiplied by the total dilution ratio. With this procedure, the distribution concentrations represent the number of particles existing in the boiler per standard cubic centimeter and the similarly understood potential of the flue gas to form particles in the dilution.

The ELPI was used in the experiments for two different purposes, i.e. the effective density measurement and the net charge measurement. The ELPI is an aerosol instrument that classifies particles in a cascade impactor according to their aerodynamic size. Particles are charged in a corona charger before entering the impactor and measured electrically with sensitive electrometers connected to the impactor stages. In these experiments, the ELPI was equipped with a filter stage [27] and an extra stage [39]. In addition, standard steel substrates were placed by porous substrates at the impactor stages in order to prevent particle bouncing in the case of different solid particle materials [20]. Impactor collection efficiency curves for this setup have been measured in the laboratory.

In the effective density measurement, the sample was led through an aerosol neutralizer and a Vienna-type DMA to the ELPI. By changing the voltage of the DMA, different particle electrical mobilities could be chosen from the sample aerosol. In this configuration, a single electrical mobility may not directly correspond to a single particle mobility size because of multiply charged particles. However, the probability of multiply charge particles with the same electrical mobility is very small for small particles, and, for larger particles, there are very few multiply charged particles with the same electrical mobility because of the clearly declining shape of the particle distribution over 100 nm. Consequently, the measurement and the data analysis could be performed by taking account only singly charge particles. The effective density measurement and calculation is based on the relation between the mobility diameter d_p and the aerodynamic diameter d_a of the particle [31]:

$$\rho_{eff} C_C(d_p) d_p^2 = \rho_0 C_C(d_a) d_a^2, \quad (1)$$

where C_C is the slip correction factor, ρ_0 is the unit density and ρ_{eff} the effective density. With the help of the known collection efficiency curves of the ELPI impactor and this relation, it is possible to calculate a theoretical ELPI current distribution for a certain mobility size and for a certain effective density. By setting the effective density as a free parameter and minimizing the difference between the theoretical currents and the measured currents, the effective density can be defined. Similar method has previously been used, for instance, in diesel exhaust measurements [37] and in the measurement of atmospheric aerosols [15].

To support the effective density analysis, the DLPI total mass size distributions were compared to the number size distributions measured with the SMPS. In this procedure, the density of the particles was set to be as a free parameter but constant as a function of particle size. The mass size distributions as a function of particle mobility size were then calculated from the number size distributions by assuming spherical particles and using the density parameter. At the same time, the DLPI mass size distributions could be converted to mass size distributions as a function of mobility size by using the same density parameter. The output of the DLPI is as a

function of aerodynamic size as it is in the ELPI. Finally, the differences between these mass size distributions were minimized and the density values defined. To distinguish this procedure from the effective density analysis, the term density parameter ρ is used here. It means the average density over the whole size distribution while assuming spherical particles.

The measurement indicating the net charge of the particles was carried out with the ELPI by setting off the corona charger of the instrument and comparing it to the reference signal measured with the charger. In the case without the charger, a polydisperse aerosol sample was measured straight from the sample line. Because the charger was set off, only the naturally charged particles in the sample were measured with the ELPI electrometers. By comparing this current distribution to the reference measured with the charger, the particle net charge distribution as a function of aerodynamic particle size was obtained. If half of the particles in a certain size range are negative and half of them positive, the net charge is zero and no signal is detected. However, if the balance is on either negative or positive side, a current signal is measured at the corresponding impactor stage.

Particle samples for the transmission electron microscope (TEM) analysis were collected on holey carbon coated copper grids. During the collection, the flow through the grid was one liter per minute, and the collection times varied between 10 and 750 s. The collection efficiency of the holey grids is not constant as a function of particle size. Different physical collection mechanisms dominating at different particle sizes lead to uneven collection of particles at wide size range but, however, all the particle sizes relevant to this study are represented. In addition to the TEM image analysis, also Energy-dispersive X-ray spectroscopy (EDS) analysis was conducted for the collected particles.

3. Results and discussion

3.1. Aerosol size distributions

In general, aerosol particles formed a two-modal size distribution in the covered mobility size range of 3–422 nm. Fig. 3 shows an example of a size distribution measured at the superheater. The distribution represents a single steady point and it is calculated as an average of several tens of measurements. Also the standard deviation of the data set is shown as a metric for the variation in the particle concentration. The smaller particle mode, referred as Mode 1, reaches its peak at around 20 nm. The variation in the concentration of this mode is notable. In contrast, the standard deviation is much smaller in the larger mode, referred as Mode 2. The peak of Mode 2 is slightly under 100 nm. The approximate positions of the peaks and the characteristics of the stabilities can be generalized to different steady points and both the measurement locations.

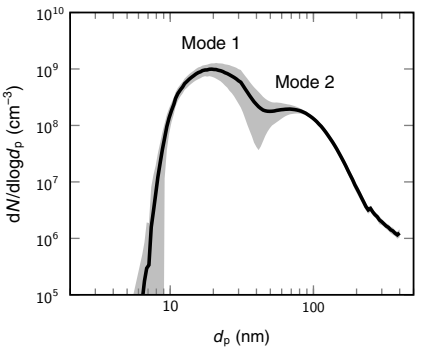

Fig. 3. An example of the particle size distributions measured at the superheater. The distribution is calculated as an average of several measurements and the gray area represents the standard deviation.

Particle size distributions with respect to fuel mixture are shown in Fig. 4a measured at the superheater and in Fig. 4b measured at the 2nd pass. At first, it is reasonable to look at some general features of the distributions between the two measurement locations. Mode 2, or at least the right hand side of it, which is not affected by the overlapping of Mode 1, seems to remain unchanged in the boiler while moving from the superheater to the 2nd pass. At the same time, changes of magnitude can be seen in the concentration of Mode 1. Also the mean particle size changes dramatically for some of the fuel mixtures. Consequently, the hypothesis would be that the particles of Mode 2 exist already in the boiler and the particles of Mode 1 are formed in the dilution from the condensable species existing in the boiler. In this respect, condensable species refer to the molecules having a relative low saturation vapor pressure and being able to either condense on existing particles in the dilution or form new particles through nucleation. The presented hypothesis can also be supported by several other facts later on.

According to the size distribution data (Fig. 4), the fuel mixtures can be divided into two groups: the fuel mixtures including peat and the fuel mixtures not including peat. The first group consists of Fuels 3 and 4, both having a peat share of 34%. The size distributions measured at the superheater are very similar for these two fuel mixtures. The only difference is seen at very small particle sizes where also the standard deviation is high. However, the difference to the other fuel mixtures is notable. The fuel mixtures including peat seem to have lower concentration in Mode 1 and smaller particle size in Mode 2 compared to other fuel mixtures measured at the superheater. At the 2nd pass, the difference in the concentration of Mode 1 is vice versa and Mode 2 remains unchanged. Unfortunately, there are no data available for Fuel 3 measured at the 2nd pass.

The other group, i.e. the fuel mixtures not including peat, consists of Fuels 1 and 2. The size distributions of these fuel mixtures show very high concentrations in Mode 1 at the superheater, but there is a huge decrease while moving to the 2nd pass. Also the mean particle size of these modes decreases. These results suggest a possible decrease in concentration of condensable species present in the flue gas around the superheater and the 2nd pass. Of course, the initial temperature in the boiler may affect to some extent the formation of Mode 1 particles in the dilution and thus the measured size distributions.

The loss of Mode 1 particles between the superheater and the 2nd pass can be explained by the presence or absence of alkali chloride salts, e.g. KCl and NaCl. Being in the gas phase in the boiler these salts often populate the lower particle size range of sample collected by the ELPI or DLPI. The temperature around the superheater surface in contact with the gas is enough to reach the dew point of these salts. The dew point of these salts is shown to be within the temperature range of the superheater environment [34].

For the fuel mixtures without peat, the flue gas arriving at the superheater is enriched with these alkali chloride species. The temperature around the superheater surface in contact with the gas is enough to reach the melting point of these salts. The melting points for KCl and NaCl are 770 °C and 801 °C, respectively. This phenomenon may help to explain why with Fuels 1 and 2, a huge loss of Mode 1 particles is seen while moving from the superheater to the 2nd pass.

Meanwhile for peat containing fuel mixtures, the loss of Mode 1 particles is minimal. To begin with, the flue gases from peat

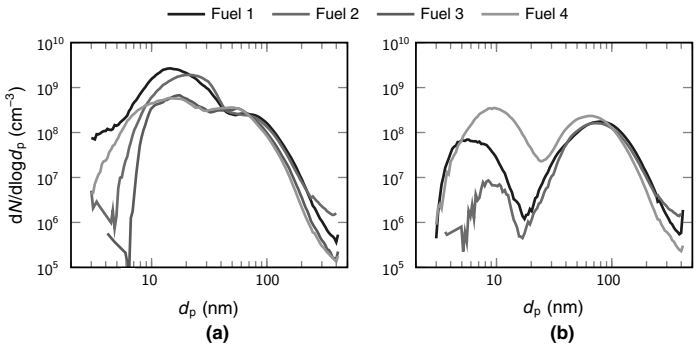

Fig. 4. Particle size distributions with respect to fuel mixture measured (a) at the superheater and (b) at the 2nd pass.

containing fuel mixtures may have less alkali chloride salts as they arrive in the superheater region, thus, minimizing the condensation and loss of Mode 1 particles. The alkali capture ability and the sulfur in peat are possible reasons why alkali chloride content in the flue gas arriving at the superheater is lower. The recent study by Kassman et al. [18] reported similar results.

The sulfur in peat may be released as SO_2 or SO_3 and attack alkali chlorides to form alkali sulfates and HCl via the following reactions:

$$2MCl(g) + SO_2(g) + H_2O + \frac{1}{2}O_2 \rightarrow M_2SO_4(s) + 2HCl(g) \quad (2)$$

$$2MCl(g) + SO_3(g) + H_2O(g) \rightarrow M_2SO_4(s) + 2HCl(g) \quad (3)$$

where M is the alkali [17]. In addition the alkali capture ability of peat will also produce HCl. Hydrogen chloride has lower dew point temperature thus is not expected to condense between the superheater and the 2nd pass.

Particle size distributions with respect to additive feeding are shown in Fig. 5. These distributions were measured for Fuel 2 at the superheater. It can be seen that additive feeding affects the concentration of both the distribution modes. Especially, the concentration of Mode 1 decreases with more than a magnitude. Similar effects were also seen with other fuel mixtures at the superheater. Thermal decomposition of ferric sulfate produces SO_3 according to the equation below [1].

$$Fe_2(SO_4)_3(s) \rightarrow 3SO_3(g) + Fe_2O_3(s) \quad (4)$$

When SO_3 meets alkali chlorides the reaction in Eq. (3) may then commence. SO_3 is more aggressive than SO_2 in destroying alkali chlorides and, as a result, the formation of alkali sulfate is almost warranted. This is exhibited by the composition of the aerosols shown in Fig. 6. The fraction of Cl in Mode 1 and 2 particles are almost eradicated during the sulfate addition. However, the reaction in Eq. (3) requires time for completion and particle growth is expected [14,16]. The reason for that is probably the longer residence time for particle growth in the sulfur case, as K_2SO_4 nucleates at a higher temperature than KCl [16]. This could explain the shift in the peak of Mode 1 and 2 particles shown in Fig. 5.

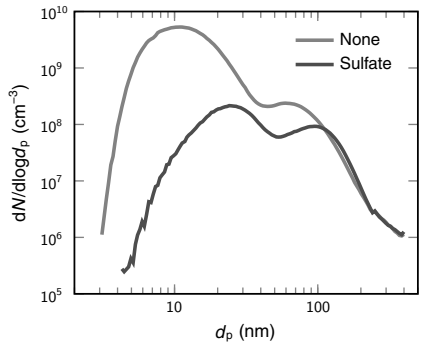

Fig. 5. Particle size distributions with respect to additive feeding for Fuel 2 measured at the superheater.

3.2. Physical structure of particles

The effective density measurements together with the TEM image analysis play an important role in understanding the physical structure of the particles. Fig. 7a shows the results of the density analysis with respect to additive feeding and Fig. 7b with respect to fuel mixture. Altogether, Mode 1 has a constant density 1.5 ± 0.3 g/cm^3 (standard deviation as error limits) and the density of Mode 2 particles is clearly higher but decreases as a function of particle size. These results support the idea of some condensable species forming new particles in the dilution and subsequent aerosol processes as coagulation affecting the composition and morphology of Mode 2 particles. According to the chemical analysis of DLPI samples, Mode 1 particles are found to be rich in K, Na, Cl and/or S depending on whether an appropriate additive and dose is introduced. The bulk densities of most probable compounds KCl, NaCl, K_2SO_4 and Na_2SO_4 are 1.99, 2.16, 2.66 and 2.66 g/cm^3, respectively. The measured effective density of Mode 1 particles is not far from these but still lower than any of the mentioned bulk densities. An explanation for this difference could be the porousness of the particle material or other additional chemical compounds. Because the total mass of Mode 1 particles is rather small, there may be some chemical compounds slightly affecting the density of the particles but not seen in the chemical analysis.

As seen in Fig. 7a, the ferric sulfate feeding results in slightly lower effective density values for the particles of Mode 1. With the sulfate feeding the density is on average only 1.24 ± 0.05 g/cm^3, while without any additive feeding it is 1.6 ± 0.3 g/cm^3. This result is contradictory to the assumption that the sulfate feeding would decrease the amount of alkali chlorides and increase the amount of more dense alkali sulfates in the particles. However, it should be remembered that the sulfate feeding significantly decreases the number concentration of Mode 1 particles and, thus, the role of trace elements and other possible chemical compounds may increase. In Mode 2, the effect of the additive feeding on the effective density is not seen. At the current size range below 200 nm, the density of Mode 2 is dominated by the density of

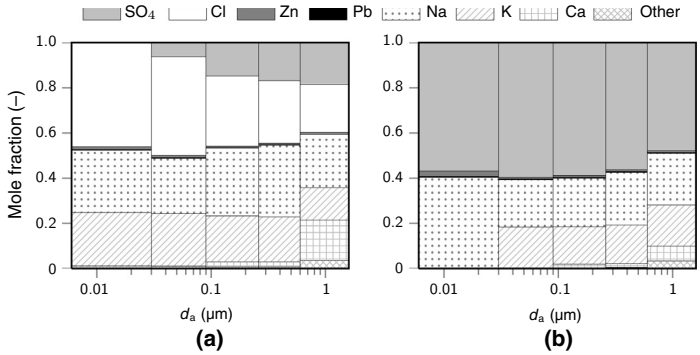

Fig. 6. Molar composition of collected particles as a function of particle aerodynamic size for Fuel 2 (a) without and (b) with ferric sulfate additive.

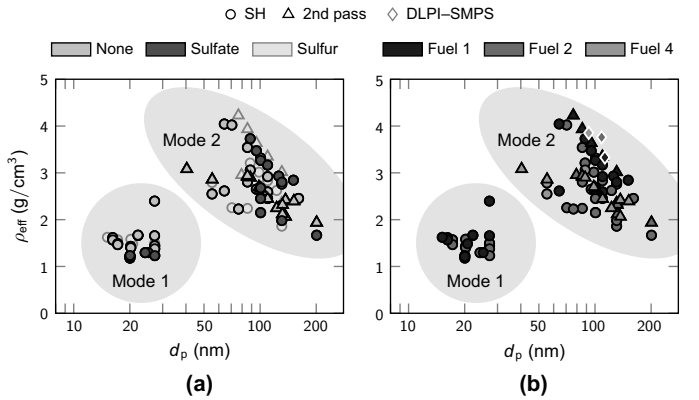

Fig. 7. Effective density of particles as a function of particle mobility size with respect to (a) additive feeding and (b) fuel mixture. Both the subfigures include the whole effective density data measured from the superheater and 2nd pass. Supporting data calculated from the DLPI–SMPS mass distribution comparison is also shown.

the particles presumably existing in the boiler and not by the density of condensable species. The relatively high density up to 4 g/cm^3 of Mode 2 particles or, at least, the core density of those particles cannot be explained by alkali chlorides and alkali sulfates. There should be some compounds with higher density present as heavy metal compounds, e.g. $PbCl_2$, $PbSO_4$ and $ZnSO_4$ with bulk densities 5.85, 6.29 and 3.54 g/cm^3, respectively. The effect of the solid sulfur feeding is not distinguished from the reference in any of the particle density results.

While the effective density of Mode 1 is affected by the additive feeding, the density of Mode 2 is mostly affected by the fuel mixture. This can be seen in Fig. 7b. For Fuels 1 and 4, the density values clearly decrease as a function of particle size and the measurement location seems to have very little effect on them. One possible reason for the decreasing density as a function of particle size is the morphology of the particles. If smaller particles are more spherical than larger particles, the larger particles also have lower effective density. Another possible explanation is the change in the chemical composition of the particles as a function of particle size. This could be caused by the condensation of condensable species and the coagulation of Mode 1 particles on the larger particles. The fact that the measurement location does not effect on the density of Mode 2 also supports the size distribution data, in which Mode 2 was observed to be independent on the measurement location (see Fig. 4). The densities of Mode 2 for Fuel 2 differ from the other fuel mixtures in the deviation of the data set. This can be explained by the very high SRF content in this fuel mixture and the realtive high amount of various heavy metal compounds in the fuel compared to other fuels used in these experiments.

The results of the DLPI–SMPS mass size distribution analysis strongly support the effective density analysis. The average densities for each fuel mixture are seen in Fig. 7b as a function of the mass size distribution GMD. Although these values are averaged over all the steady points with and without additive feeding, the standard deviations are below 0.4 for all the densities and these are in good agreement with other data points. Because in the mass size distribution analysis Mode 2 is dominating, also the densities and the GMDs are mostly representing the particles of Mode 2. Fig. 8 shows two examples of fitted mass size distributions for Fuel 1 without and with sulfate additive feeding. Note that the DLPI also measures the coarse particle mode which is seen approximately in the size range of 0.5–10 μm. However, this is excluded from the fitting analysis as well as the largest particle sizes measured by the SMPS. Comparing the mass size distributions without and with additive feeding, it is seen that the total mass is greater in the latter and Mode 2 strongly dominates in the mass size distribution. The main reason for this is the growth in particle size of Mode 2 particles. The mass median diameter of Mode 2 is 109 nm without additive and 128 nm with additive. In the mass size distribution without additive feeding (Fig. 8a), also Mode 1 is clearly seen. Evidently, this leads to a lower density value compared to the case of additive feeding because the particles of Mode 1 are less dense.

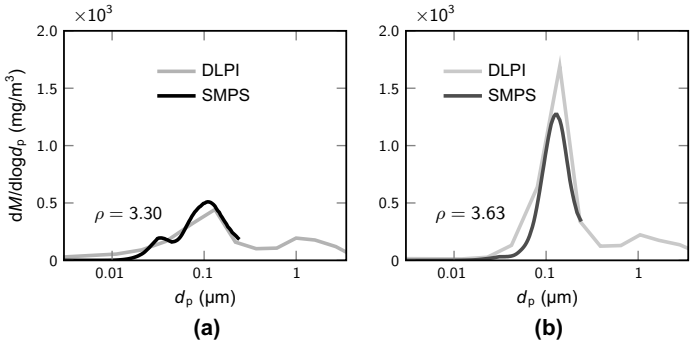

Fig. 8. Mass size distributions for Fuel 1 (a) without and (b) with sulfate additive feeding. Both the distributions calculated from the SMPS measurement and from the DLPI measurement are shown. Also the fitting parameter density ρ is presented for each case.

Another important aspect supporting the effective density analysis is the shape of the DLPI mass size distributions. In spite of the relative small size resolution, the right hand side of Mode 2 is very steep. This can be explained by the decrease in effective density as a function of particle mobility size. Larger particles are less dense and thus aerodynamically smaller.

An example TEM image of the collected particles is seen in Fig. 9. These particles were collected from the superheater during an experiment with Fuel 3. Considering only the general features of the TEM images, some of the findings presented in the size distribution analysis and in the effective density analysis can be supported. At first, there can be seen particles in the size range of both the particle modes. The distribution of the collected particles on the TEM grid may not match with the size distribution measurement because of the irregularities in the TEM sampling but both the modes are still represented. The smallest particles seem to be homogeneous and near-spherical. This is consistent with the fact that these particles would be formed in the dilution. Looking at the larger particles in Fig. 9, more heterogeneous structures are seen. Some agglomerates are seen, but the fractal structuring is not so prevailing that it would totally explain the decrease in the density of Mode 2 particles. However, there are also seen lighter material or smaller particles attached on some larger and darker Mode 2 particles. Thus, the change in the chemical composition would partly explain the decrease in the effective density.

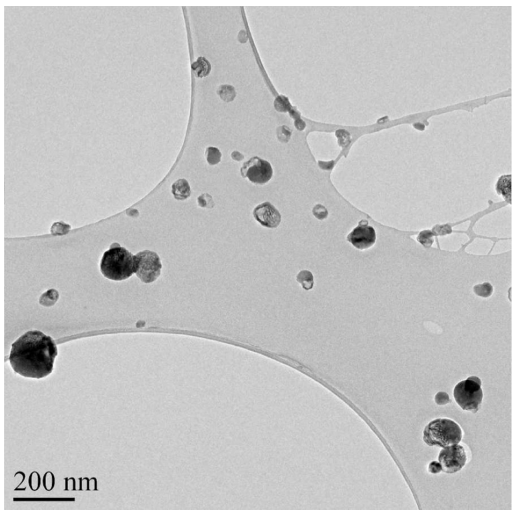

Fig. 9. A TEM image of the collected particles. The picture is taken before the electron beam has remarkably affected the particles and led to the evaporation of particle material.

Common for all the analyses performed in the electron microscope was that particles tend to evaporate in the vacuum conditions required by the microscope. This was especially seen when the energetic electron beam was focused on the particles. Several different elements were found in the EDS spectra including e.g. sulfur, sodium, potassium, silicon, calcium, oxygen and chlorine. Even if there are lots of uncertainties in the amount of these elements given by the analysis, some conclusion can be highlighted. For instance, chlorine was clearly seen in the samples taken without additive feeding but totally absent when sulfate additive feeding was on. The most common elements analyzed nearly from all the samples were potassium, sulfur and sodium. These observations are in line with the chemical analysis of the DLPI samples. Also lead and zinc were found in the larger particles. This supports the idea of Mode 2 particles consisting partly of more dense lead and zinc compounds. Unfortunately, the EDS analysis cannot be exploited quantitatively because of the beam sensitivity and evaporation of the samples.

3.3. Electric net charge of particles

An example of the electric net charge measurement with the ELPI as a function of particle size is seen in Fig. 10. The current distributions with and without the charger represent the instrument output. In normal operation, when the corona charger is turned on, the net charge of particles is defined by the charging efficiency of the ELPI [26]. This is called here as reference charge q_{ref} and is illustrated in Fig. 10c. The net charge of particles q_{net} measured straight from the sampling line is now presented in relation to this reference charge (Fig. 10d). Although this is only one example, it represents the general features of all the measurements. The current distribution measured without the charger is in the order of 100 fA per stage and, thus, clearly measurable. The relative net charge is in the order of 1% compared to the reference charge and it is changing as a function of particle size. Practically, the net charge is strongly dependent on particle size but the relation to the reference charge remains in the same order of magnitude in spite of the changing polarity. For example, the net charge at 134 nm is 0.11 elementary charges per particle and at 809 nm it is −1.16.

According to the results, the smallest fraction of particles, i.e. the particles under 50 nm in aerodynamic size, have negative net

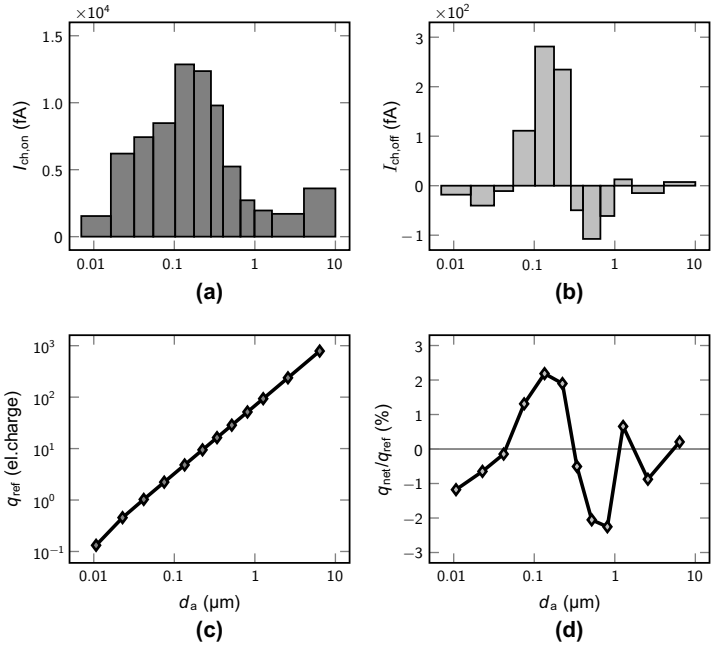

Fig. 10. An example of the net charge measurement with the ELPI as a function of particle size. The currents measured (a) with the charger and (b) without the charger are shown. The reference charge (c) q_{ref} produced by the charger is known and the net charge of the particles measured straight from the sampling line (d) q_{net} is obtained from the measurement. The latter is presented in relation to q_{ref}.

charge. This can evidently be connected to the size distribution data and Mode 1 particles. At the aerodynamic size range from 50 to 200 nm, the net charge is positive and above 200 nm it clearly drops again to the negative side. In this respect, the particles of Mode 2 mainly seem to have positive net charge. However, when the relatively high density of these particles and the difference of mobility size and aerodynamic size are taken into account, it can be said that the larger particles in Mode 2 probably have negative net charge. Altogether, the conclusion is that the condensation and formation of new particles in the dilution produce negative charge to the aerosol phase while the particles presumably existing in the boiler have positive net charge.

The main role of these net charge measurements and the presented results is to show that the particles are clearly charged and, thus, a lot of information can be obtained by investigating the electric charge. To give an example from another field of combustion, i.e. heavy duty diesel engines, Lähde et al. [21] observed that the charge of the emission particles is linked to driving parameters and exhaust gas after treatment. Measurements of the electric charge of flue gas particles have not been reported before. In this study, the changes in the net charge as a function particle size could be preliminary linked to the size distribution data, but this definitely is a field that should be studied more carefully in the future. The fractions of positively charged, negatively charged and neutral particles should be measured separately as a function of particle size. In addition, the effect of different fuels and fuel additives on these should be studied. The more detailed information on particle charge could lead to more profound understanding of the particle formation and growth in the boiler and in the dilution system. Charging might be affected by different nucleation mechanisms, temperature conditions and the chemistry of the condensable and gaseous species. All in all, extensive measurements and analysis are needed to fully understand the electrical properties of the particles measured from the boiler and, finally, to exploit the high possibilities of on-line monitoring of the combustion process by relatively simple electrical measurement devices and sampling.

4. Summary and conclusions

This study provides an extensive physical characterization of aerosol particles measured from a bubbling fluidized bed boiler. Previous studies have shown that, by collecting the particles sampled from the flue gas and analyzing their chemical composition, the effect of different fuels and fuel additives on the combustion process can be studied. This is important because of the corrosion problem caused by the increased use of biomass burning and waste fuels in energy production. The results of this work include information on the particle size distributions, morphology and effective density, and observations of the net charge of the particles.

In the boiler, the particle size distribution in the size range below 500 nm was unimodal. Gas phase species formed a second smaller particle mode in the dilution. The smaller mode, referred as Mode 1, dominated the number concentration size distribution measured at the superheater. The effective density occurred to be around 1.4 g/cm^3 and the shape of the particles was nearly spherical. The number size distribution and the effective density of the larger mode, referred as Mode 2, was found to be independent on the measurement location. The effective density values were rather high, from 3 to 4 g/cm^3 at the maximum, but clearly decreased as a function of particle size. This decrease can partly be explained by the irregular morphology of the particles, but also changes in the chemical composition are likely. The results indicate the presence of heavier lead and zinc compounds in the core of these particles. Combining all the information about these two modes, it can be concluded that Mode 1 is formed in the dilution,

and Mode 2, or at least the core of Mode 2, already exists in the boiler.

The use of ferric sulfate as fuel additive significantly decreased the number concentration of Mode 1 particles and, on the other hand, increased the mean particle size and the total mass of Mode 2 particles. This observation is consistent with the chemical off-line analysis of collected impactor samples and the previous knowledge [2]. When the amount of alkali chlorides decreases through sulfation in the flue gas, the formation of new particles in the dilution is not as aggressive, and the sulfates tend to form larger particles or condense on existing particles.

The particles were observed to have clearly measurable net charge. As a function of particle size, both polarities were seen, and most likely the negative net charge was related to the condensable species and particle formation in the dilution. The measurement of electrically charged particles is generally simple and fast. In this respect, the aerosol particles naturally charged in the combustion process, or formed as charged particles in the dilution, may be valuable. Together with the extensive information on the physical properties of the particles and understanding of the particle dynamics in the sampling system, this may lead to simple applications for on-line monitoring of combustion processes.

Acknowledgements

RECOMBIO Project TREN/FP7EN/239530 is gratefully ack nowledged.

References

[1] Aho M, Paakkinen K, Taipale R. Destruction of alkali chlorides using sulphur and ferric sulphate during grate combustion of corn stover and wood chip blends. Fuel 2013;103:562–9.
[2] Aho M, Vainikka P, Taipale R, Yrjas P. Effective new chemicals to prevent corrosion due to chlorine in power plant superheaters. Fuel 2008;87(6):647–54.
[3] Andersson C. A method for operating a heat production plant for burning chlorine-containing fuels. European patent no. EP 1354167; 2002.
[4] Baxter LL, Miles Jr TR, Miles TR, Jenkins BM, Milne T, et al. The behavior of inorganic material in biomass-fired power boilers: Field and laboratory experiences. Fuel Process Technol 1998;54(1–3):47–78.
[5] Bryers RW. Fireside slagging, fouling, and high-temperature corrosion of heat-transfer surface due to impurities in steam-raising fuels. Prog Energy Combust Sci 1996;22(1):29–120.
[6] Christensen K, Livbjerg H. A field study of submicron particles from the combustion of straw. Aerosol Sci Technol 1996;25(2):185–99.
[7] Christensen K, Stenholm M, Livbjerg H. The formation of submicron aerosol particles, hcl and so 2 in straw-fired boilers. J Aerosol Sci 1998;29(4):421–44.
[8] Forsberg C, Broström M, Backman R, Edvardsson E, Badiei S, Berg M, et al. Principle, calibration, and application of the in situ alkali chloride monitor. Rev Scient Instrum 2009;80(2).
[9] Frandsen F. Utilizing biomass and waste for power production – a decade of contributing to the understanding, interpretation and analysis of deposits and corrosion products. Fuel 2005;84(10):1277–94.
[10] Giechaskiel B, Ntziachristos L, Samaras Z. Effect of ejector dilutors on measurements of automotive exhaust gas aerosol size distributions. Meas Sci Technol 2009;20(4).
[11] Henderson P, Szakálos P, Pettersson R, Andersson C, Högberg J. Reducing superheater corrosion in wood-fired boilers. Mater Corros 2006;57(2):128–34.
[12] Hindiyarti L, Frandsen F, Livbjerg H, Glarborg P, Marshall P. An exploratory study of alkali sulfate aerosol formation during biomass combustion. Fuel 2008;87(8-9):1591–600.
[13] Hupa M. Ash-related issues in fluidized-bed combustion of biomasses: recent research highlights. Energy Fuels 2012;26(1):4–14.
[14] Jiménez S, Ballester J. Effect of co-firing on the properties of submicron aerosols from biomass combustion. Proc Combust Inst 2005;30(2):2965–72.
[15] Kannosto J, Virtanen A, Lemmetty M, Mäkelä JM, Keskinen J, Junninen H, et al. Mode resolved density of atmospheric aerosol particles. Atmos Chem Phys 2008;8(17):5327–37.
[16] Kassman H, Bäfver L, Åmand L-E. The importance of so2 and so3 for sulphation of gaseous kcl – an experimental investigation in a biomass fired cfb boiler. Combust Flame 2010;157(9):1649–57.
[17] Kassman H, Broström M, Berg M, Åmand L-E. Measures to reduce chlorine in deposits: application in a large-scale circulating fluidised bed boiler firing biomass. Fuel 2011;90(4):1325–34.
[18] Kassman H, Pettersson J, Steenari B-M, Åmand L-E. Two strategies to reduce gaseous KCl and chlorine in deposits during biomass combustion – injection of ammonium sulphate and co-combustion with peat. Fuel Process Technol 2013;105:170–80.
[19] Keskinen J, Pietarinen K, Lehtimäki M. Electrical low pressure impactor. J Aerosol Sci 1992;23(4):353–60.
[20] Kuuluvainen H, Arffman A, Saukko E, Virtanen A, Keskinen J. A new method for characterizing the bounce and charge transfer properties of nanoparticles. J Aerosol Sci 2013;55(0):104–15.
[21] Lähde T, Rönkkö T, Virtanen A, Schuck TJ, Pirjola L, Hämeri K, et al. Heavy duty diesel engine exhaust aerosol particle and ion measurements. Environ Sci Technol 2009;43(1):163–8.
[22] Lähde T, Rönkkö T, Virtanen A, Solla A, Kytö M, Söderström C, et al. Dependence between nonvolatile nucleation mode particle and soot number concentrations in an EGR equipped heavy-duty diesel engine exhaust. Environ Sci Technol 2010;44(8):3175–80.
[23] Latva-Somppi J, Moisio M, Kauppinen EI, Valmari T, Ahonen P, Tapper U, et al. Ash formation during fluidized-bed incineration of paper mill waste sludge. J Aerosol Sci 1998;29(4):461–80.
[24] Lind T, Kauppinen EI, Hokkinen J, Jokiniemi JK, Orjala M, Aurela M, et al. Effect of chlorine and sulfur on fine particle formation in pilot-scale cfbc of biomass. Energy Fuels 2006;20(1):61–8.
[25] Maricq M. On the electrical charge of motor vehicle exhaust particles. J Aerosol Sci 2006;37(7):858–74.
[26] Marjamäki M, Keskinen J, Chen D-R, Pui DYH. Performance evaluation of the electrical low-pressure impactor (ELPI). J Aerosol Sci 2000;31(2):249–61.
[27] Marjamäki M, Virtanen A, Moisio M, Keskinen J. Modification of electrical low pressure impactor for particles below 30 nm. J Aerosol Sci 1999;30(Supplement 1):S393–4.
[28] Miles TR, Miles Jr TR, Baxter LL, Bryers RW, Jenkins BM, Oden LL. Boiler deposits from firing biomass fuels. Biomass Bioenergy 1996;10(2–3):125–38.
[29] Monkhouse P. On-line spectroscopic and spectrometric methods for the determination of metal species in industrial processes. Prog Energy Combust Sci 2011;37(2):125–71.
[30] Nielsen HP, Frandsen FJ, Dam-Johansen K, Baxter LL. Implications of chlorine-associated corrosion on the operation of biomass-fired boilers. Prog Energy Combust Sci 2000;26(3):283–98.
[31] Ristimäki J, Virtanen A, Marjamäki M, Rostedt A, Keskinen J. On-line measurement of size distribution and effective density of submicron aerosol particles. J Aerosol Sci 2002;33(11):1541–57.
[32] Sippula O, Lind T, Jokiniemi J. Effects of chlorine and sulphur on particle formation in wood combustion performed in a laboratory scale reactor. Fuel 2008;87(12):2425–36.
[33] Sorvajärvi T, Saarela J, Toivonen J. Optical detection of potassium chloride vapor using collinear photofragmentation and atomic absorption spectroscopy. Opt Lett 2012;37(19):4011–3.
[34] Vainikka P, Enestam S, Silvennoinen J, Taipale R, Yrjas P, Frantsi A, et al. Bromine as an ash forming element in a fluidised bed boiler combusting solid recovered fuel. Fuel 2011;90(3):1101–12.
[35] Vainikka P, Silvennoinen J, Taipale R, Alphen CV, Moilanen A, Falcon R, et al. Halide aerosols in circulating fluidised bed co-combustion. Role of coal bound kaolin. Fuel Process Technol 2011;92(9):1738–49.
[36] Valmari T, Kauppinen EI, Kurkela J, Jokiniemi JK, Sfiris G, Revitzer H. Fly ash formation and deposition during fluidized bed combustion of willow. J Aerosol Sci 1998;29(4):445–59.
[37] Virtanen A, Ristimäki J, Keskinen J. Method for measuring effective density and fractal dimension of aerosol agglomerates. Aerosol Sci Technol 2004;38(5):437–46.
[38] Wang SC, Flagan RC. Scanning electrical mobility spectrometer. Aerosol Sci Technol 1990;13(2):230–40.
[39] Yli-Ojanperä J, Kannosto J, Marjamäki M, Keskinen J. Improving the nanoparticle resolution of the ELPI. Aerosol Air Quality Res 2010;10(4):360–6.
[40] Zeuthen J, Jensen P, Jensen J, Livbjerg H. Aerosol formation during the combustion of straw with addition of sorbents. Energy Fuels 2007;21(2):699–709.

Series title and number

VTT Science 85

Title	**Sulfur based abatement of PCDD/F and alkali chlorides production during fluidized bed combustion of solid recovered fuel**
Author(s)	Cyril Jose E. Bajamundi
Abstract	Waste-to-Energy (WtE) facilities have the potential to treat large volumes of waste generated by constantly growing communities. Due to the heterogeneous and dynamic nature of the composition of these wastes, several issues arise that work against the realization of this potential. This thesis seeks to address production of polychlorinated dibenzo-p-dioxins/ dibenzofuran (PCDD/F) and alkali chloride production in a 140 MWth bubbling fluidized boiler fired with fuel mixtures with advanced energy-share (50 to 70%) solid recovered fuel. Combustion of 50% solid recovered fuel (SRF) – 44% bark – 6% sludge results to an in-boiler PCDD/F production level of 0.7 ng/Nm^3; with the addition of S-pellets the production level is reduced to 0.3 ng/Nm^3; while co-combustion with peat increases production to 1.3 ng/Nm^3. Aerosol data from the backpass, thermodynamic modeling and x-ray absorption analysis of electrostatic precipitator (ESP) fly ash reveals that adding sulfur pellet could induce sulfation of Cu, a key catalyst in the de novo formation of PCDD/F. During peat co-combustion, high amounts of Cu (mostly coming from the SRF) poorly volatilized, have remained in the ash and could have easily aided the heterogeneous formation of PCDD/F in the post combustion zones on the boiler. The ESP on the other hand can reduce the concentration of PCDD/F in the flue gas path however phase redistribution of PCDD/F from solid to gas can occur. In the search for a robust anti-corrosion procedure, sulfate injection is found to be superior in ensuring that the superheater (SH) deposits have minimal Cl-content even during firing of 70% SRF – 24% bark – 6% sludge mixture. Sulfate injection can be introduced in a strategic location in the boiler to ensure inflight sulfation of corrosive alkali chlorides. Other strategies tested to minimize Cl-content in the deposits are peat co-combustion and sulfur-pellet addition. Peat co-combustion can lower the Cl-content both in the aerosol and superheater deposits, but its performance is highly dependent on the quality of the SRF; sulfur-pellet addition meanwhile can lower the concentration of Cl in the aerosol and SH deposit though to a lesser extent compared to sulfate injection. Through the use of sulfur based additive, PCDD/F and alkali chlorides production can be addressed, thus contributing to the realization of the potential of WtE facilities.
ISBN, ISSN	ISBN 978-951-38-8244-0 (Soft back ed.) ISBN 978-951-38-8245-7 (URL: http://www.vtt.fi/publications/index.jsp) ISSN-L 2242-119X ISSN 2242-119X (Print) ISSN 2242-1203 (Online)
Date	April 2015
Language	English, Finnish abstract
Pages	110 p. + app. 96 p.
Name of the project	
Commissioned by	
Keywords	PCDD/F, corrosion, elemental sulfur, sulfate, SRF, co-combustion
Publisher	VTT Technical Research Centre of Finland Ltd P.O. Box 1000, FI-02044 VTT, Finland, Tel. 020 722 111

Julkaisun sarja ja numero

VTT Science 85

Nimeke	**PCDD/F- ja alkalikloridi-yhdisteiden vähentäminen rikkiyhdisteiden avulla kierrätyspolttoaineen kerrosleijupolton yhteydessä**
Tekijä(t)	Cyril Jose E. Bajamundi
Tiivistelmä	Jätteitä polttavissa energiantuotantolaitoksissa voidaan hyödyntää suuria määriä yhdyskuntajätteitä. Yhdyskuntajätteen heterogeenisyys ja ongelmallinen kemiallinen koostumus tuo kuitenkin runsaasti haasteita hyötykäyttöön. Tässä väitöskirjatyössä tutkittiin polykloorattujen dibentso-p-dioksiinien/dibentsofuraanin (PCDD/F) sekä alkalikloridin muodostumista 140 MWth kerrosleijukattilassa käytettäessä polttoaineseoksia, joissa kiinteän kierrätyspolttoaineen energiaosuudet ovat korkeita (50–70 %). Polttoaineseos, jossa oli 50 % kiinteää kierrätyspolttoainetta, 44 % puun kuorta ja 6 % lietettä, tuotti savukaasuun PCDD/F- yhdisteitä noin 0,7 ng/Nm^3. Rikkipitoisten pellettien lisääminen alensi tuon pitoisuuden tasolle 0,3 ng/Nm^3, ja yhteispoltto turpeen kanssa nosti sen tasolle 1,3 ng/Nm^3. Savukaasulinjastosta mitattujen aerosolipitoisuuksien, sähkösuodattimelta kerätyn lentotuhkan röntgen absorptioanalyysin ja termodynaamisen mallinnuksen avulla havaittiin, että rikkipellettien lisääminen saattaa aiheuttaa kuparin sulfatoitumista. Kupari katalysoi voimakkaasti de novo-mekamismia (joka muodostaa PCDD/F-yhdisteita savukakavassa). Poltettaessa kierrätyspolttoainetta turpeen kanssa suuri osuus lähinnä kierrätyspolttoaineesta peräisin olevaa kuparia pysyy tuhkassa ja saattaa voimistaa PCDD/F:n heterogeenista muodostumista kattilan tulipesän jälkeisissä osissa (de novo). Sähkösuodattimen (ESP) avulla voidaan alentaa PCDD/F:n pitoisuuksia savukaasulinjan kiintofaasissa. On kuitenkin mahdollista, että PCDD/F:n yhdisteitä voi siirtyä kaasufaasiin, jolloin ne läpäisevät suodattimet. Sulfaatin injektio osoittautui parhaaksi tulistinkorroosiota ehkäiseväksi menetelmäksi. Kloorin kerrostuminen tulistimille saatiin hallintaan jopa 70 % kierrätyspolttoaineen, 24 % puunkuoren ja 6 % lietteen seoksella. Sulfaatti-injektio estää kloorikorroosion tietyillä tulipesän alueilla. Muut tutkitut vaihtoehdot kloorin kerrostumisen rajoittamiseksi ovat sekapoltto turpeen kanssa sekä rikkipellettien lisäys. Seospoltto turpeen kanssa voi vähentää sekä savukaasun aerosolien että tulistimen kerrostumien klooripitoisuutta, mutta alenema riippuu voimakkaasti kierrätyspolttoaineen laadusta. Rikkipellettien lisäys voi myös alentaa aerosolien ja tulistimen kerrostumien klooripitoisuutta mutta vähemmän tehokkaasti kuin sulfaatti-injektio. Rikkipohjaisten lisäaineiden käytöllä voidaan heikentää PCDD/F:n ja alkalikloridien muodostumista jätteenpolton yhteydessä ja samalla tehostaa jätteiden hyödyntämistä energiantuotannossa.
ISBN, ISSN	ISBN 978-951-38-8244-0 (nid.) ISBN 978-951-38-8245-7 (URL: http://www.vtt.fi/publications/index.jsp) ISSN-L 2242-119X ISSN 2242-119X (Painettu) ISSN 2242-1203 (Verkkojulkaisu)
Julkaisuaika	Huhtikuu 2015
Kieli	Englanti, suomenkielinen tiivistelmä
Sivumäärä	110 s. + liitt. 96 s.
Projektin nimi	
Rahoittajat	
Avainsanat	PCDD/F, korroosio, alkuainerikki, sulfaatti, kierrätyspolttoaine, seospoltto
Julkaisija	Teknologian tutkimuskeskus VTT Oy PL 1000, 02044 VTT, puh. 020 722 111

Sulfur based abatement of PCDD/F and alkali chlorides production during fluidized bed combustion of solid recovered fuel

Energy recovery from waste is one viable option for ensuring efficient waste management. It can reduce landfill waste by up to 20 fold by volume leaving only sterile residues. However, there are several issues that are against the realization of this potential. Waste-to-energy facilities are considered by some as "dioxin factories", and Cl in the waste could cause significant profit loss due to corrosion.
This work presents the production and abatement of polychlorinated dibenzo-p-dioxins/ dibenzofuran (PCDD/F) and alkali chlorides in a 140 MWth bubbling fluidized boiler fired with fuel mixtures containing a high energy-share of solid recovered fuel. Sulfur based additives induce sulfation of Cu and alkali salts. These additives can readily be applied in similar fluidized bed combustion and can therefore be a practicable solution to the issues discussed.

ISBN 978-951-38-8244-0 (Soft back ed.)
ISBN 978-951-38-8245-7 (URL: http://www.vtt.fi/publications/index.jsp)
ISSN-L 2242-119X
ISSN 2242-119X (Print)
ISSN 2242-1203 (Online)